ANTHROPOGENIC INFLUENCES ON THE SEDIMENTARY EVOLUTION OF THE COROMANDEL HARBOUR

A thesis

submitted partial fulfilment

of the requirements for the degree

of

Master of Science (Research) in Earth and Ocean Sciences

at

The University of Waikato

by

Alexander Hitchcock Harpur

THE UNIVERSITY OF
WAIKATO
Te Whare Wānanga o Waikato

2016

Abstract

The Coromandel Harbour is located on the eastern side of the Coromandel Peninsula, North Island, New Zealand. To date, sedimentological research conducted in the harbour has been confined to nearshore areas, with limited data existing for the subtidal regions of the harbour. The primary aim of this thesis is to identify whether and how various human activities in the catchment have altered harbour-wide, intertidal and subtidal, sedimentation rates and sediment geochemistry. A secondary aim is to identify the sedimentary evolution of the whole Coromandel Harbour over broad time scales (i.e. thousands of years).

Sedimentological data has been collected from 17 intertidal and subtidal sediment cores. Cores have been analysed for down-core changes in sediment texture, mineralogy, observational characteristics and geochemistry measured through portable X-ray fluorescence (pXRF). A facies model constructed from this data has been used to interpret the sedimentary development of the harbour. Pre-human and anthropogenic sediment accumulation rates (SARs) have been estimated using radiocarbon dating, qualitative pollen analysis and facies analysis. Anthropogenic heavy metals have been interpreted against pre-human baselines to identify influences on natural contaminant levels, with specific values compared with regional contaminant guidelines to assess ecological threats.

Deeply weathered soils developed in a subaerial environment somewhere between the last interglacial at c.120 ka and the extended last glacial maximum (eLGM) at 29 ka. These soils were overtopped by streambank and floodplain deposits at the eLGM to the onset of the mid-Holocene sea level rise at c.7500 cal yr B.P. As sea level rose, inundated eLGM and early estuarine sediments were initially pyritised in a stratified, restricted marine setting. Over time, sea level rose and the stratification of the harbour was destroyed, ceasing pyritisation. Streams began to rapidly aggrade at the harbour with the positive change in base level, giving early estuarine (c.7500-5000 cal yr B.P) subtidal SARs of ~0.31-0.45 mm/yr. As streams reached stable profiles, SARs decreased to generally conformable rates of 0.25-0.47 mm/yr in the intertidal regions and ~0.1-0.25 mm/yr in the subtidal regions during the pre-Polynesian phase (c.7500-700 cal yr B.P). Polynesian SARs (700-130 cal yr B.P) decreased to ~0.05-0.13 mm/yr. Whole European

(1820 A.D-present) SARs in the northern parts of the harbour are ~0.52-0.77 mm/yr and appear to be chiefly related to mining and deforestation. Recent European (1975 A.D-present) SARs are ~3.52-10.37 mm/yr in the southern parts of the harbour and are chiefly related to pine plantation erosion. A secondary depocentre for pine plantation sediments appears to be at the inlet where rates of ~4.98 mm/yr occur.

Only arsenic and mercury exist over Australian and New Zealand Environment and Conservation Council (ANZECC) Interim Sediment Quality Guidelines (ISQG) Low concentrations in anthropogenic sediments analysed. Maximum harbour-wide arsenic concentrations of up to 33.5 mg/kg that exceed the ISQG-Low value of 20 mg/kg are associated with mining related sediments near the Whangarahi Stream mouth. Maximum arsenic concentrations in pine plantation sediments is 22.3 mg/kg. Mercury may also exceed ISQG-Low/High values throughout all harbour sediments, though it is unclear whether mercury has been incorrectly measured by pXRF.

Acknowledgements

I must express the utmost gratitude to my chief supervisor Dr Beth Fox for providing me with crucial assistance and support throughout my MSc research. Your guidance has been greatly appreciated! Thanks are also given to my secondary supervisor, Dr Willem de Lange. Your assistance has provided me with a broader appreciation of coastal processes and brought a lot of focus to my research.

Thanks must be given to technical advisors (in no particular order): Dean Sandwell, Chris Morcom, Annette Rodgers, Janine Rhyburn, Warrick Prowie, Shaun Barker, Renat Radosinsky, Kirsty Vincent, and Annie Barker for all of their support, guidance and time spent inducting me into numerous laboratories. Thanks to Alan Hogg, Fiona Petchey and the rest of the team at the Waikato Radiocarbon Lab for helping me with my radiocarbon dating. Thanks to Chris Morcom and Dean Sandwell for ongoing assistance with vibracoring and field work. Thanks to Dr Xun Li, Dr Marcus Vandergoes and the rest of the crew at GNS for palynology training and ongoing assistance through this project.

I am very grateful for help Ian Boyce and the crew of the Golden Ridge Marine Farms who provided boating and technical expertise during the subtidal coring component of this research. Thanks to Darren Skene of Quaternary Resources who provided crucial practical assistance during subtidal coring. To my colleagues Taylor Brodie and Johan Watson, with whom I bribed into taking part in my fieldwork with an acknowledgement in my thesis, *thank you.* Thanks to Annette, Tim and Jarren King for your kind accommodation and introduction to the Coromandel community. Thanks to the Coromandel Harbourmaster, Stuart Crawley for assistance during intertidal coring. Thanks to Ashley Franklyn for introduction to the catchment geology and mining practices that occurred in the Coromandel Harbour catchment. Acknowledgements to the Coromandel Aero club and Coromandel Glass for land access to the intertidal flats.

My research has been supported by the following scholarship bodies: University of Waikato, Ngai Tahu and the Te Putea Tautoko (UoW). The analytical component of this research has been partly funded by the Waikato Regional

Council. Without this support, the breadth of research that has been conducted would have never been possible. I am very grateful for all of this support.

Thanks to Beth Fox, Leigh Harpur (mum) and Rosie Hughes for proofreading my chapters. I cannot express how much your support has helped me through the final stages of writing. Thank you to my friends and family for putting up with me over the last year, your support has been very helpful throughout this entire process. For anyone who I may have inadvertently missed from this list, thank you.

Table of Contents

List of Figures

List of Tables

Chapter 1

Introduction

This chapter first introduces the Coromandel Harbour and the nature of the sedimentological problem that this research will address. Secondly, thesis aims and objectives are identified.

1.1 Background

The Coromandel Harbour is thought to be currently infilling at rates greater than those observed in pre-human times. Hume & Dahm (1991) used limited sediment cores to identify elevated harbour sedimentation rates related to various Polynesian and European activities within the harbour catchment. They estimated that sedimentation rates since European settlement have been 10–40 times higher than prior to human habitation. Several studies have also identified elevated concentrations of heavy metals arsenic, zinc, lead and copper within the most recent sediments relative to the pre-human baseline (Coffee, 1992; Hume & Dahm, 1991; Aurecon, 2015). Rapid anthropogenic sedimentation threatens aquaculture, tourism and recreational activities in the harbour, infilling boating channels and disrupting hydrodynamics surrounding various aquaculture farms. Contamination of the surficial and shallow subsurface sediments poses threats to estuarine ecologies and aquaculture industries.

The Thames-Coromandel District Council has proposed dredging the Coromandel and Te Kouma wharf boating channels as a part of the Coromandel Harbour Facilities Project (TCDC, 2016). The project aims to increase aquaculture capabilities and develop the Auckland-Coromandel tourist ferry infrastructure to facilitate economic growth in the future. The bulk sedimentological research conducted in the harbour has been confined to limited studies of the intertidal and shallow subtidal areas of the estuary, leaving a knowledge gap surrounding broader harbour sediment dynamics, chemistry and accumulation rates (Coffee, 1992; Hume & Dahm, 1991; Aurecon, 2013). The lack of comprehensive data on sedimentation dynamics and sediment geochemistry restricts the ability of the Council to assess dredged channel management (i.e. how often channels will have

to be re-dredged) and ecological threats posed by resuspension of contaminated surface sediments.

The harbour-wide uncertainty relating to anthropogenic sedimentation processes necessitates a holistic sedimentological research project. This project aims to bridge the knowledge gaps identified above and provide a robust foundation of sedimentological data that can be used as a basis for future research on processes within the harbour.

1.2 Study area

The Coromandel Harbour is located on the western side of the Coromandel Peninsula, New Zealand (36 46 56S, 175 28 22E) (Fig. 1.1). The Coromandel Township lies to the north-east of the harbour and is primarily residential, though some industrial areas occur around its western margins. At present, the Coromandel Township has a population of around 1600 that can rise to 5,300 in summer months (TCDC, 2010).

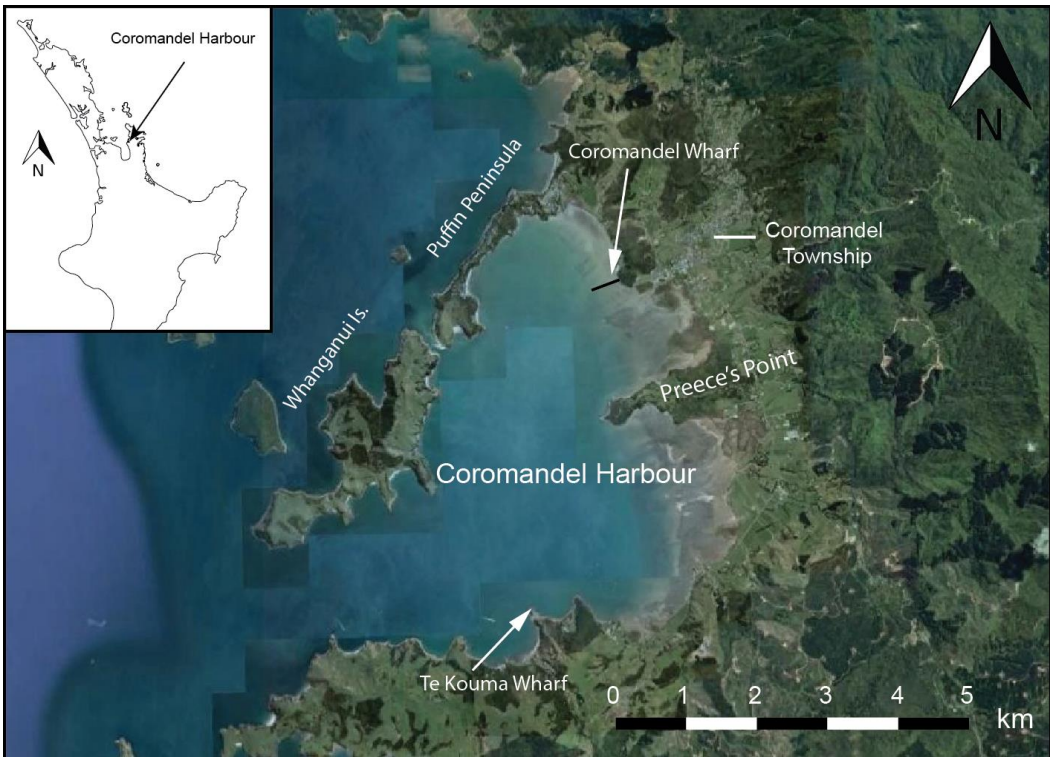

Fig. 1.1 - Location of Coromandel Harbour and Coromandel Township on the North Island of New Zealand. Image taken from Google Earth Pro.

The Coromandel Harbour is bounded to the east and south by the Coromandel Peninsula. The Coromandel Peninsula and Coromandel Ranges to the east extend ~120 km north-west from the Bay of Plenty and are characterised by steep topography and mountain ranges of up to 900 m above sea level. The elevated topography of the peninsula shelters the Firth of Thames and Coromandel Harbour from swell and easterly winds sourced from the Pacific Ocean to the east. The western margins of the harbour are bound by Puffin Peninsula and Whanganui Island, which shelter the estuary from north-west wind and swell from the Firth of Thames.

The harbour has a total high tide area of 23.6 km^2 and tidal range of 2.3 m (Mead & Moores, 2004). Tidal waters cycle through a primary inlet (Fig. 1.2 A-A') and a small, secondary inlet (Fig. 1.2 B-B'). The primary inlet is from here referred to as the 'primary inlet', and the secondary inlet termed the 'secondary inlet'. The harbour's total catchment area is 73.57 km^2, which is drained primarily by the Whangarahi Stream in the north and the Waiau Stream in the south (Fig. 1.2) (Land, Air, Water, 2016; DOC, n.d). Preeces Point divides the intertidal region of the harbour into a northern embayment (NEmb) and southern embayment (SEmb) (Fig. 1.2). Subtidal regions outside of the NEmb and SEmb are defined as the centre harbour.

Several mussel and oyster farms are located in the shallow subtidal to intertidal regions (Fig. 1.2). There are two main wharfs in the harbour: Coromandel Wharf in the north and the Te Kouma Boat Ramp in the south (Fig. 1.2). Coromandel Wharf is primarily used for recreational purposes, while the use of Te Kouma Boat Ramp is centred on aquaculture (e.g., mussel barge docking and loading).

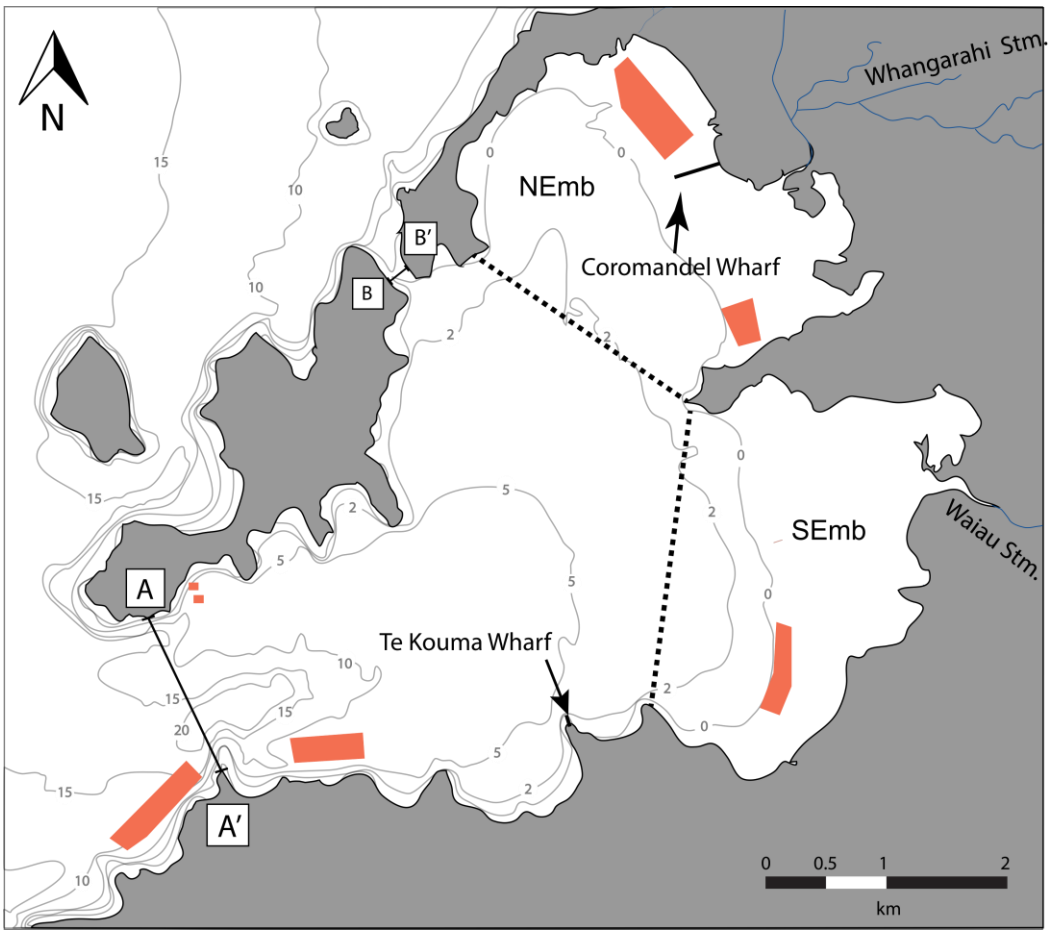

Fig. 1.2 - Bathymetry of the Coromandel Harbour including locations of the Coromandel Wharf and Te Kouma Boat Ramp. Aquaculture farms are noted in red. Dotted lines indicate the boundaries of the NEmb and SEmb. Depths expressed as depth below mean low water spring (MLWS). Bathymetry and locations of aquaculture farms taken from LINZ (2016) Chart NZ 533.

1.3 Research Aims and Objectives

The primary aim of this thesis is to identify whether and how various human activities in the catchment have altered harbour-wide sedimentation rates and sediment geochemistry. Previous studies have primarily focused upon identifying anthropogenic influence on surface sediments near the intertidal regions. At present, no research has been conducted into sedimentation and sediment geochemistry throughout the harbour over broad time scales (i.e. thousands of years). This research aims to address these knowledge gaps. The specific objectives of this research are to:

1) apply radiocarbon and pollen dating methods to estimate Holocene sedimentation rates within the harbour, placing emphasis on comparing sedimentation rates before and after human settlement;

2) identify catchment sources of anthropogenic sediments and highlight depocentres within the harbour;

3) assess the degree of heavy metal contamination in anthropogenic sediments and compare them to pre-human concentrations to gather contamination enrichment factors;

4) develop a stratigraphic model of harbour sediments to infer harbour-wide sediment dynamics and development through the Holocene. This model will also be used to identify pre-human sedimentation and sediment chemistry variability in the harbour. From this information, the degree of anthropogenic variability can be assessed against natural variability.

1.4 Thesis outline

Chapter Two presents a literature review primarily focussed on the environmental background of the Coromandel Harbour. The timing and environmental significance of anthropogenic settlements and activities in the harbour catchment are also discussed.

Chapter Three describes field methods, core collection and logging processes.

Chapter Four presents core logs and down-core geochemistry for each core analysed. This data is interpreted in Chapter Five.

Chapter Five uses grain size, thin section, and XRF analysis and interpretation to construct a facies analysis for the harbour.

Chapter Six uses multiproxy age data to calculate sedimentation rates. Sedimentation rates for pre-human, Polynesian and European periods are calculated. Spatial variability of these sediments throughout the harbour is identified.

Chapter Seven determines contamination enrichment in anthropogenic sediments relative to pre-human sediments. Contaminants in surface sediments are compared to regional sediment guidelines to assess current threats to estuarine ecologies.

Chapter Eight draws together the data and interpretations of previous chapter to present a reconstruction of environmental change in Coromandel Harbour since the early Holocene. Recent sedimentation rates and contaminant levels are discussed in the context of longer-term variability.

Finally, a conclusion chapter summarizes the findings of this thesis while also identifying potential for future research.

Chapter 2

Literature Review

This chapter reviews relevant literature to identify the present-day knowledge of the sedimentary evolution of the Coromandel Harbour. Firstly, the regional Coromandel Peninsula geology and Coromandel Harbour catchment geology are defined. Then, the Coromandel Harbour's climate and hydrodynamic setting are discussed to provide insight into possible implications on sedimentation. A time-line of the development of the Coromandel Harbour since the mid-Holocene is then presented, identifying potential sources of estuarine sediments. Lastly, regional and site specific research on sedimentation rates and heavy metal contamination are discussed.

2.1 Geology and Tectonic Setting

2.1.1 Regional geology

The Coromandel Peninsula and Coromandel Ranges are part of the Coromandel Volcanic Zone (CVZ), a remnant volcanic arc that was formed by Pacific–Australian plate subduction through the Early Miocene to Late Pliocene (18 Ma to 2.5 Ma) (Booden, Smith and Mauk, 2009). The CVZ is a horst structure that extends ~200 km NW from Te Puke to Great Barrier Island with widths of up to 40 km (Christie *et al.,* 2007). The CVZ is bound on its western margins by the Hauraki Rift system which downthrows to the east (Hochstein *et al.,* 1986; Booden *et al.,* 2012).

Basement material in the Coromandel Peninsula is comprised of indurated Mesozoic metagreywacke-argillite of the Manaia Hill and Tokatea Hill Groups (Skinner, 1967; Adams *et al.,* 1994). The Manaia Hill Group is a lithic volcanic greywacke, while the Tokatea Group is a feldspathic greywacke devoid of volcanic detritus (Skinner, 1967). Exposed sections of the basement are found mostly in the furthermost NW and SEmb reaches of the Coromandel Peninsula (Fig. 2.1) (Adams *et al.,* 1994).

Calc-alkaline CVZ volcanism from 18 Ma to 2.5 Ma unconformably overtopped the basement with igneous basalts, andesites to dacites and rhyolites, which dominate the present day topography of the Coromandel Peninsula (Fig. 2.1) (Bradshaw, 1991; Booden *et al.,* 2012; Christie *et al.,* 2007; Booden, Smith and Mauk, 2009). CVZ eruptives are categorised by Skinner (1986) into three groups: the Coromandel, Whitianga and Merrcury Basalt Groups (Booden, Smith and Mauk, 2009). Andesitic to dacitic Coromandel Group rocks were erupted in the Early to late Miocene, forming the continental volcanic arc system and the Coromandel Ranges on the western side of the Peninsula (Fig. 2.1) (Skinner, 1986; Adams *et al.,* 1994). Volcanism shifted to the east of the peninsula during the Late Miocene, with eruptives shifting to the rhyolitic Whitianga Group (Fig. 2.1). Late Miocene andesitic to basaltic Mercury Basalts were the final eruptives, and are found on the outermost NEmb regions of the Coromandel Peninsula and Mercury Islands (Fig. 2.1). CVZ volcanism was intermittent, with periods of quiescence and erosion occurring between eruptive intervals (Christie & Brathwaite, 2005). Fluvial erosion through the Cenozoic has carved valleys and formed alluvial plains throughout the peninsula. Eroded regional materials and CVZ and TVZ eruptives have subsequently infilled lowland depressions and river channels throughout the Quaternary (Fig. 2.1).

Regional faulting generally trends along the axis of the Peninsula and is associated with Mesozoic basement faults formed during the Cretaceous Rangitata Orogeny (Skinner, 1967; Bradshaw, 1991). The closest fault to the field area is the Hauraki Fault, which is not known to be active (McSaveney & Beetham, 2006) Uplift rates throughout the Coromandel are ~0.25 mm yr-1-0.3 mm yr-1 (Pillans, 1986 and Abrahamson, 1987 in Clement, 2011).

Extensive hydrothermal alteration during the Miocene mineralized economic concentrations of gold and silver throughout Coromandel Group andesites and dacites (including the Kuaotunu Subgroup, see subsection 2.1.2.1). Heavy metal elements arsenic (As), zinc (Zn), lead (Pb), copper (Cu) and mercury (Hg) were also mineralised in Coromandel Group rocks during this period (Hume & Dahm, 1991). Hydrothermal alteration of regional rock has resulted in a deeply weathered regolith on steep slopes throughout the Coromandel (Hume & Dahm, 1991). Land slips are common during rainfall events and significantly exacerbated

where vegetation cover has been removed (i.e. deforestation) (Bradshaw, 1991; Hume & Dahm, 1991).

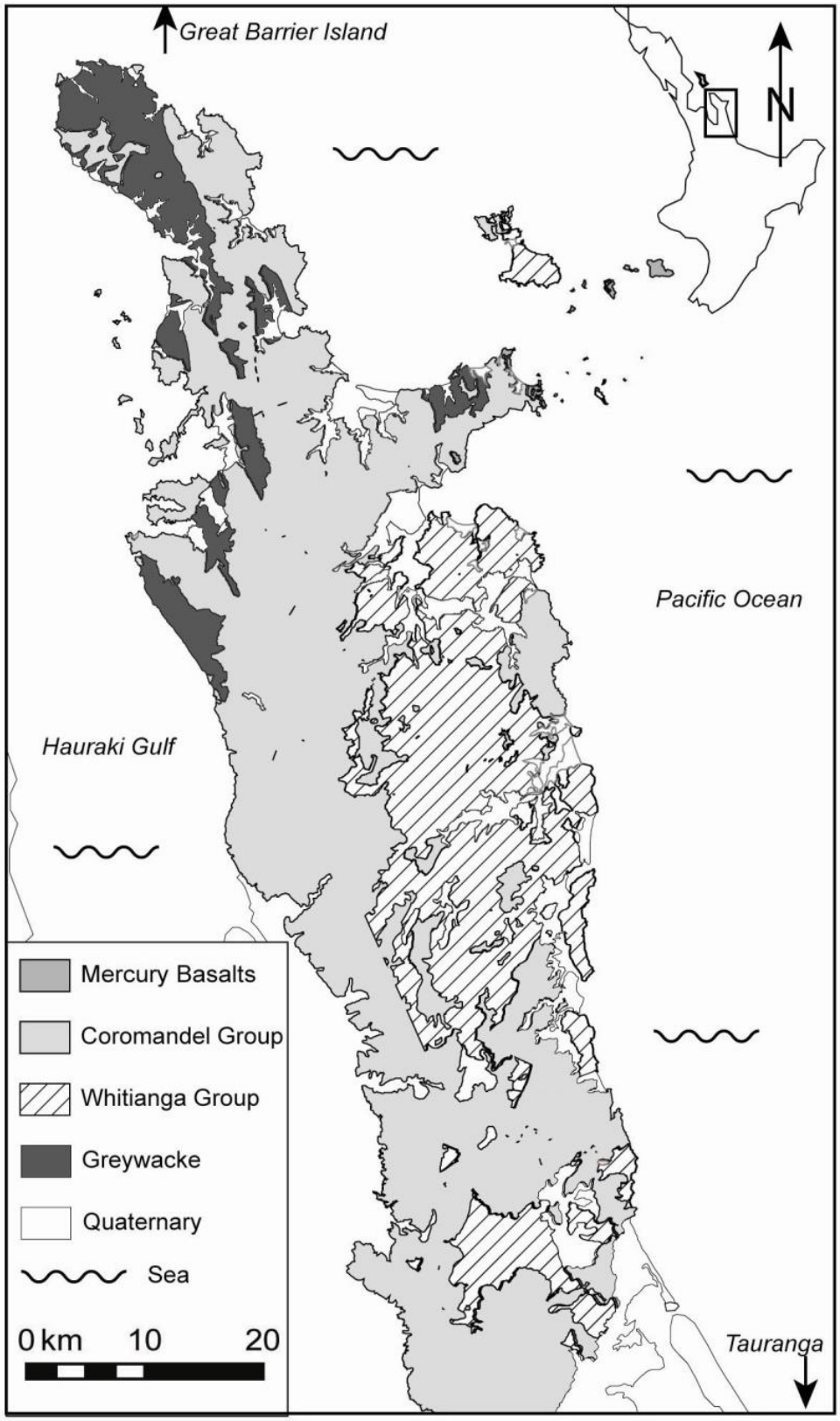

Fig. 2.1- Geology of the upper Coromandel Peninsula (From Booden *et al.*, 2009).

2.1.2 Catchment geology

Sediment entering Coromandel estuaries is primarily derived from catchment erosion (Mead & Moores, 2004). Therefore, catchment geology has significant implications for estuarine sedimentation throughout the Coromandel. Catchment geology also has significance for sediment chemistry, as the majority of heavy metals that enter Coromandel estuaries are sourced from hydrothermally altered catchment rocks (Hume & Dahm, 1991).

The Coromandel Harbour catchment consists of Neogene rocks of the Coromandel Group's Kuaotunu Subgroup and the Manaia Hill Group basement. The Kuaotunu Subgroup is found at the surface in all regions, while the Manaia Hill Group outcrops are located in the South and East (Fig. 2.2). Quaternary sediments have infilled river channels and lowland plains (Fig. 2.2). The catchment is dominated by steep to rugged terrain (Land, Air, Water, 2016).

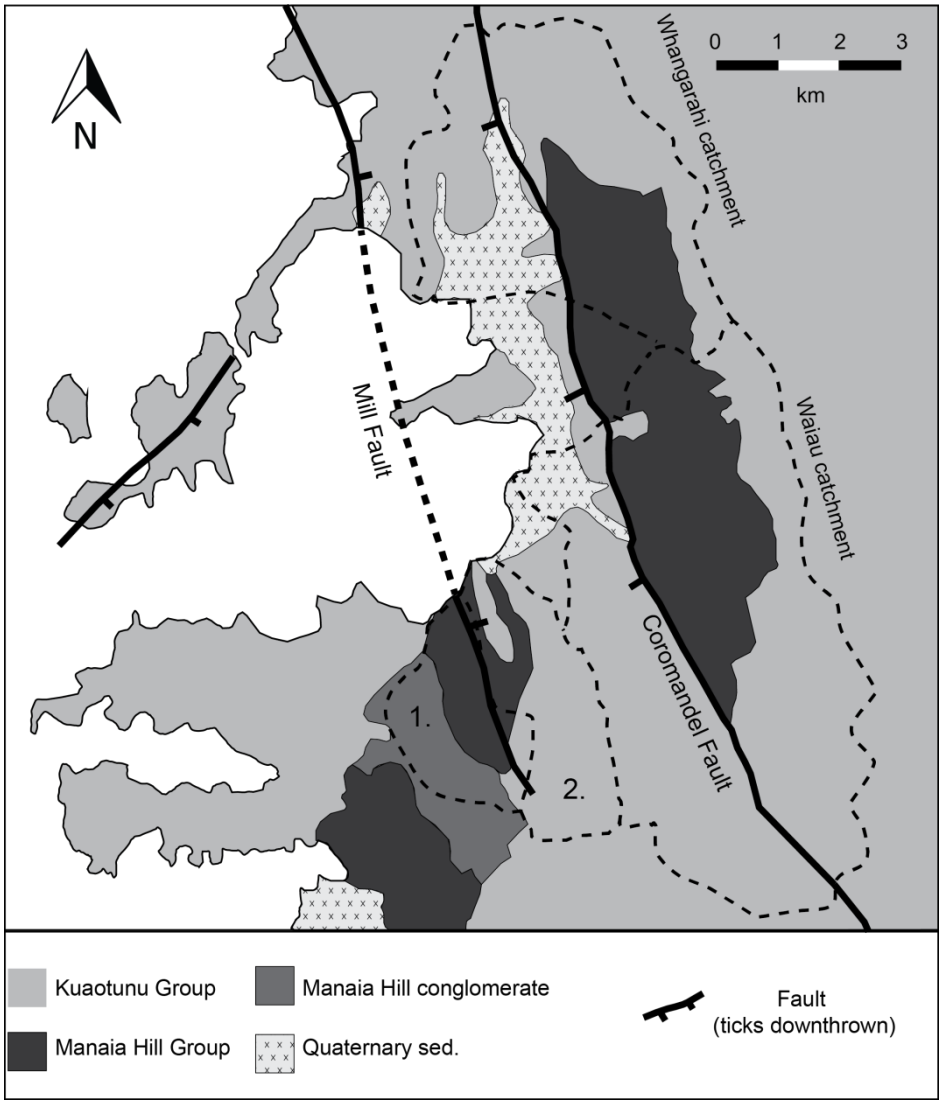

Fig. 2.2 – Geology of the Coromandel Harbour catchment including the catchment boundaries of the Whangarahi, Waiau, Awakanae (2.) and unnamed (1.) streams (dashed lines). Modified from LINZ Topo 50 and Edbrook (2001). NB. Some small faults and catchments of smaller streams have not been represented as they are not relevant to this research.

2.1.2.1 The Kuaotunu Subgroup

Within the catchment, Kuaotunu Subgroup occurs as deeply weathered hydrothermally altered andesites and dacites (Edbrooke, 2001). Tuff and conglomerate lithologies often overlie lava flows and intrusions, resulting in sensitive slip planes. Small rotational slips and soil creep are therefore common, with examples of 60 ha slips in the catchment (Edbrooke, 2001 McSaveney & Beetham, 2006). Kuaotunu rocks are typically phyric, comprising hornblende, orthopyroxene clinopyroxene, plagioclase and quartz (Adams *et al.*, 1994).

2.1.2.2 Manaia Hill Group

Folded Manaia Hill Group rocks outcrop to the west and south of the SEmb as indurated volcanic greywacke-sandstones and conglomerates. Manaia Hill group rocks occur as both weathered and un-weathered outcrops, and are generally unstable and prone to slip events and soil creep (Edbrooke, 2001). Mania Hill greywackes sampled in the catchment by Skinner (1967) comprised quartz and feldspar with accessory weathered biotite and hornblende. Skinner (1967) defined the Manaia Hill conglomerate (Fig. 2.2) as a combination of sub-rounded volcanic pebbles within a matrix of sub-angular quartz, plagioclase and orthoclase mineral grains. The Manaia Hill Group conglomerates have accessories minerals of biotite, epidote and muscovite.

2.1.2.3 Faults and tectonism

2.1.2.3.1 Faults

The Coromandel Fault is a high angle normal fault that runs NNW adjacent to the western margin of the Coromandel Harbour (Fig. 2.2). Upthrusting on the eastern side of the fault has exposed Manaia Hill Group rocks to the east of the harbour (Edbrooke, 2001). Mill Fault lies parallel to the Coromandel Fault to the west, down throwing to the east. The occurrence of Mill Fault through the harbour has not been outright identified though is often suggested in regional tectonic maps (Edbrooke, 2001; Christie *et al*, 2007) (Fig. 2.2). Both fault systems are inactive and unlikely to have had noteworthy impacts on Holocene sedimentation.

2.1.2.3.2 Tectonic uplift

No studies were found on subsidence and tectonism in the Coromandel Harbour. Abrahamson (1987) (in Clement, 2011) proposed uplift rates of 0.3 mm yr^{-1} along the western side of Coromandel Peninsula. Pillains (1986) gave uplift rates of ~0.25 mm/yr for the Coromandel Peninsula. It is unclear whether these rates can be applied to the Coromandel Harbour. Interpreting the evolution of the harbour with regard to unclear uplift rates would be difficult. Thus, this study will not consider regional tectonism further in its investigation of Holocene sedimentation.

2.2 Climate

2.2.1 Rainfall

The Coromandel Peninsula is characterised by high yearly rainfall. Average rainfall along the eastern side of the Peninsula ranges from 1200 mm/yr to 1800 mm/yr. Rainfall on the western side of the Peninsula ranges from 1600 mm/yr to 3200 mm/yr. Along the Coromandel ranges, rainfall is often in excess of 3000 mm/yr, sometimes even exceeding 4500 mm/yr (Chappell, n.d; Hume & Dahm, 1991). Severe rainfall and flooding is common through April–August, typically in response to westward moving ex-tropical cyclones. An example of such rainfall is illustrated by Cyclone Fergus which hit the area in 1996. During the storm, around 300 mm of rain fell over the Coromandel in a 24 hour period. High rainfall on the steep topography can generate significant runoff, induce flooding and transport eroded sediments to the harbour (Hume & Dahm, 1991).

2.2.2 Wind climate

There is limited availability of reliable wind velocity and direction data for the Coromandel Harbour area; however, some conclusions can be drawn from the surrounding topography. Elevated landmasses shelter the harbour from N, S and E winds. Dominant SW-W winds move into the harbour through the primary inlet, where SW-W winds of up to 45 km/h are not uncommon (Pers. Comm. Stuart Crawley, Coromandel Harbour Master; TCDC, 2016). The southern parts of the harbour are located at the end of the SW-W fetch and are therefore likely to have the greatest wind activity in the harbour (TCDC, 2016). Some SW-W winds will refract around Whanganui Island and enter the NEmb, where winds are typically weaker than those to the south (Fig. 2.3) (TCDC, 2016).

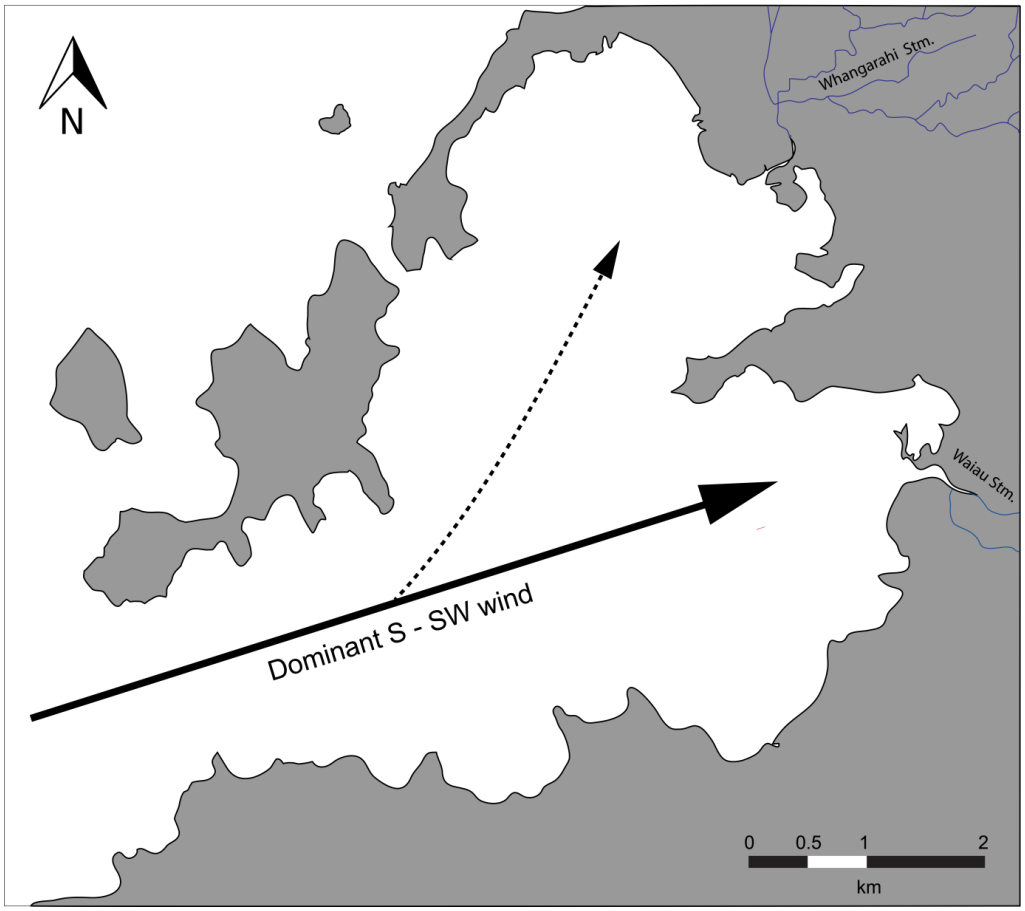

Fig. 2.3 – SW-W winds moving through the primary inlet into the harbour. Adapted from unpublished wind wave models presented in TCDC (2016).

2.3 Hydrodynamics

2.3.1 Estuary classification

The harbour is bracketed by volcanic headlands to the NW (Whanganui Island and Puffin Peninsula) and south (Te Kouma) (Fig. 1.2). Intertidal regions are broad, up to 1 km wide at low tide along the western margins of the harbour. Mangroves are common near intertidal stream channels. The harbour has an unusual morphology and does not fit squarely into a single specific estuary type under NIWA's Estuary Environment Classification (EEC). The harbour is elongate and has little fluvial input, characteristics of Category D–coastal embayments. However, the inlet is constricted and not open to the ocean under this classification. The harbour also has characteristics of category H–drowned valley, or ria, where the estuary has the structure of a narrow elongate basin and has characteristically deep (>10 m) subtidal areas. Expansive intertidal areas and unlikely stratification removes the harbour from this classification. As such, the

Coromandel Harbour has been generalised with a morphology between a coastal embayment and a ria.

2.3.2 Tidal influence

The harbour has a high tide area of 23.6 km^2 (Mead & Moores, 2004) with a mean spring tidal range of 2.7 m and a mean neap tidal range of 1.8 m (LINZ Nautical Almanac, n.d; TCDC, 2016). The primary tidal inlet is situated in the SW of the harbour with a high tide width of 1.38 km. The majority of tidal waters will move through the primary inlet. The primary inlet is expressed as a deepened channel. This may be a result of constricted tidal waters accelerating through the inlet over tidal cycles. A second 100 m wide inlet is situated between Puffin Peninsula and Whanganui Island and cycles tidal waters during high tide (Fig. 1.2). Review of google Earth time-lapse photography shows sediment plumes moving through this in inlet during tidal cycles. Areas near this second inlet may therefore be likely to be influenced by erosion and redeposition from tidal mixing. The Coromandel Harbour has a tidal prism of 47.7 × 10^6 m^3. This is a large tidal prism for the catchment size of the harbour, which suggests that the harbour will be well mixed by tidal waters (Jones, 2008).

2.3.3 Fluvial inputs

Fluvial input into the harbour is low, drawing from a total catchment of 73.57 km^2 (Mead & Moores, 2004). Two primary streams flow into the Coromandel Harbour: the Whangarahi Stream (draining into the NEmb) and the Waiau Stream (draining into the SEmb) (Fig. 2). Two smaller streams also drain into the southern margin of the harbour, though are not likely to be as significant in terms of sediment outwash as the two primary streams (Fig. 2) The Whangarahi Stream drains a 25 km^2 catchment and the Waiau Stream a 35 km^2 (Land, Air, Water, 2016; DOC, n.d). Both primary streams have rough to steep catchment topography (Land, Air, Water, 2016; DOC, n.d).

2.3.4 Wave climate

A dominant SW–W wind runs directly into the southern intertidal parts of the harbour (Fig. 2.3). Unpublished, preliminary wind wave modelling for the

Coromandel Harbour by the DHI presented in the Coromandel Harbour Facilities Project report (TCDC, 2016) suggests wind waves of up to 1 m may develop in the harbour from SW-S winds. Uncalibrated wind wave modelling in the harbour indicates that these winds will generate the largest wind waves (and thus wave mixing) occurring in centre of the harbour to the SEmb. SW-W winds do refract around Whanganui Is., moving into the NEmb, generating lower wind waves in the NEmb (TCDC, 2016). During field work, larger wave-related bedforms were observed in the SEmb intertidal region compared to the NEmb intertidal region. This appears to support this hypothesis.

2.3.5 Mixing processes

No further evidence has been found on mixing processes in the Coromandel Harbour. The degree of mixing in the harbour and dominant forcing of mixing is unclear. It is likely the harbour is primarily mixed by the tidal cycles and wind wave mixing in the NEmb and SEmb.

The harbour has a large tidal prism and what appears to be a constricted inlet. Thus, it is likely that tidal mixing will generate eddies through the water column that will remove any sort of bottom water salinity stratification.

2.4 Holocene Evolution of the Coromandel Harbour

2.4.1 Sea level rise

Following deglaciation from the extended last glacial maximum (LGM), sea level rapidly rose ~120 m across New Zealand's coastal margins (Hume & Dahm, 1991; Newnham *et al.,* 2007; Clement, Sloss & Fuller, 2010). Palaeo-valleys and depressions across the region were inundated and drowned as sea level rose to near to present-day mean sea level (PMSL), forming the initial pattern of New Zealand's present day estuaries. With sea level rise, palaeosols were inundated and overlain by marine sediments.

It is not clear when sea-level reached its present-day level in the Coromandel (Clement, 2011). By interpolating clear sea level rise trends in the proximal Northland-Auckland region and applying the Holocene sea level curve

constructed by Clement, Sloss & Fuller (2010), it can be inferred that sea level was around 5 m below PMSL at c.8500 cal yr B.P are rose to around its present day level within the Coromandel at around c.7500 cal yr B.P (Clement, 2011). Recent work on dating chenier plains (associated with sea level fluctuations) by Dougherty & Dickson (2012) has proposed that sea level on the western side of the Coromandel Peninsula was ~2 m higher than present at c.4000 cal yr B.P. Sea level dropped to the present day level between c.4000 cal yr B.P and c.1000 cal yr B.P, and has since remained relatively constant to the present day (Dougherty & Dickson, 2012).

2.4.2 Anthropogenic Influences in the Catchment

Hume & Dahm (1991) divide human activity in the Coromandel into four periods: pre-Polynesian, Polynesian, early European and recent European. These periods are defined by well-dated anthropogenic events. Each period has a distinct catchment erosion and estuarine sedimentation regime. Interpreting sedimentation rates based on these periods is common practise in New Zealand sediment accumulation rate (SAR) studies (Hume & Gibb, 1987; Hume & Dahm, 1991; Sheffield *et al.,* 1995; Mead & Moores, 2004). Here, these periods are defined and discussed in the Coromandel Harbour context.

2.4.2.1 Pre-Polynesian c.7500 cal yr B.P–700 cal yr B.P

Prior to human habitation, the Coromandel Peninsula was characterised by extensive native forest. Widespread vegetation cover sheltered well-developed soils, which resulted in low catchment erosion. Estuarine sedimentation was low and relatively steady (Hume & Dahm, 1991).

2.4.2.2 Polynesian 700 cal yr B.P–130 cal yr B.P (1820 A.D)

The first anthropogenic influence in the Coromandel Harbour catchment was that of Polynesian (Maori) settlement. Work on rat-gnawed seeds (rats were transported to the country on settlers boats) in the Coromandel Peninsula by Wilmshurst & Higham (2004) has dated Polynesian arrival in the area to no earlier than 700 cal yr B.P. Upon arrival, settlers used small-scale fires to clear land for agricultural purposes. Some large-scale accidental fires may have also

occurred (Hume & Dahm, 1991). The removal of vegetation cover and agricultural land practices exposed soils to amplified erosion (Mead & Moores, 2004), resulting in marginal increases in estuarine sedimentation (Hume & Dahm, 1991).

2.4.2.3 Early European 1820 A.D.–1910 A.D.

2.4.2.3.1 Deforestation and kauri gum digging

While Europeans had made voyages to the Coromandel by 1769 A.D, the first noteworthy European influence in the Coromandel Harbour catchment was the widespread deforestation from 1820 A.D–1910 A.D. Native kauri was felled for timber in significant volumes from the catchment and transported to the downstream through controlled flooding and release of driving dams (Hume & Dahm, 1991) (Fig. 2.4). Significant volumes of sediment would have passed through stream systems during these processes, with sediment sourced from the erosion of exposed weathered soils during felling and through mechanical streambank erosion during dam breaking.

Once in the harbour or along river banks, timber was transported to local saw mills for processing. One such saw mill was Frasers Sawmill, which was located in the lower region of the Waiau Stream catchment. During mill operation, saw dust and wastes were deposited into stream channels and waterways, and much of the detritus was likely to have ultimately moved into the harbour. No other historic kauri mills have been identified in the Coromandel Harbour catchment.

In conjunction with deforestation, Kauri gum digging was also widespread during this period. Kauri gum, historically an expensive varnish and commodity, was abundant throughout the soils of Coromandel's kauri forests. Large-scale land burn-offs were used to clear land for gum digging, further exposing soils to erosion.

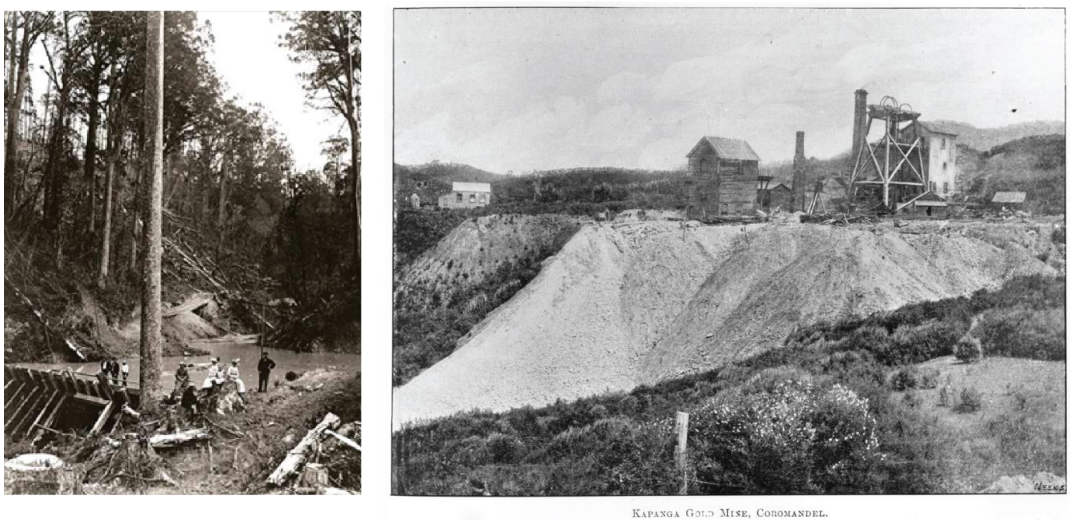

Fig. 2.4 - Left-A Coromandel Peninsula driving dam. Note the exposed soils and significant amounts of organic detritus in the background. Right–Kapanga gold mine in the upper Whangarahi Stream catchment. Driving dam photo courtesy of the Thames Historical Museum. Kapanga mine photo from the Sir George Grey Special Collections, Auckland Libraries, 7-A8897.

2.4.2.3.2 Gold mining

World-class deposits of gold were mined from Kuaotunu Subgroup rocks within the Coromandel Harbour catchment from 1850 A.D–1910 A.D Gold was mined alluvially (i.e. from stream channels) and from underground shafts, with mine wastes disposed of down banks and within stream channels (Fig. 2.4). Several stamper batteries within the Whangarahi Stream catchment (which drains to the NEmb) refined ore using crushing and cyanide methods, washing tailings into stream channels. These mine wastes are well known to be enriched in heavy metal elements (Hume & Dahm, 1991). Gold mining activity was located chiefly in the Whangarahi Stream catchment, and therefore we expect to find mine wastes primarily within the NEmb (Fig. 2.5).

Historic newspaper articles indicate that some gold dredging was attempted in the NEmb near the mouth of the Whangarahi Stream (Otago Daily Times, 1920). The extent of this activity is not well documented. The extent of how these activities have disrupted primary sedimentation in these areas is unclear.

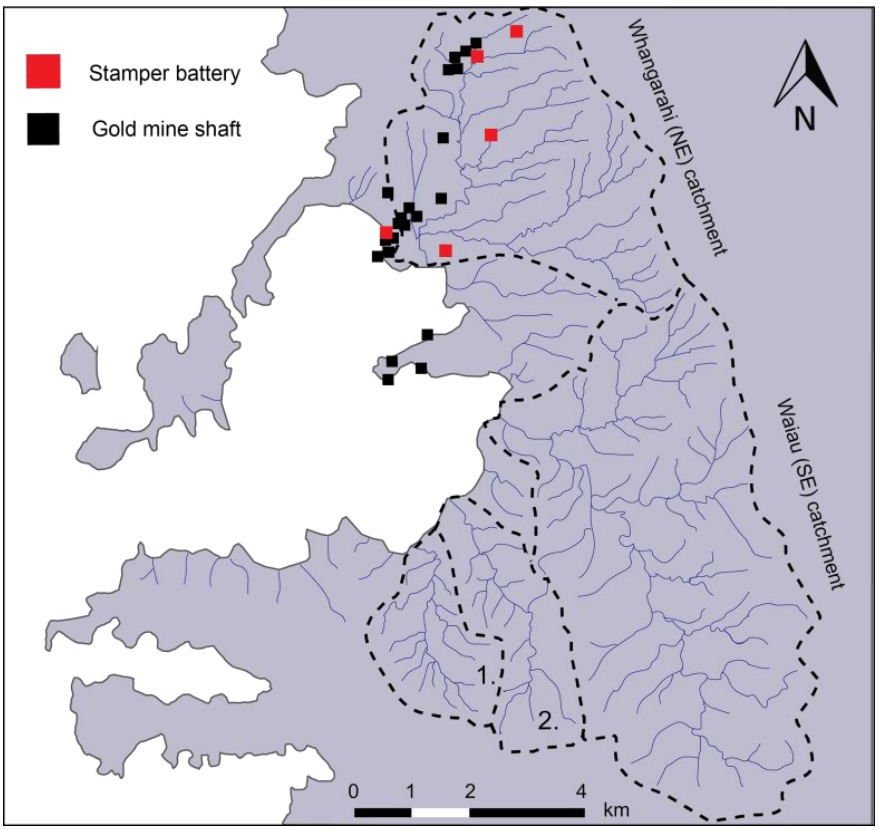

Fig. 2.5 – Locations of historic (1850 A.D–1910 A.D) gold mines and stamper batteries within the Coromandel Harbour catchment. The catchment boundaries of the Whangarahi, Waiau, Awakanae (2.) and unnamed (1.) streams are included for reference. Adapted from Moore & Ritchie (1996).

2.4.2.4 Recent European 1910 A.D.–present

Gold mining and deforestation activities had largely ceased by 1910 A.D, leaving much of the catchment un-vegetated. Land uses changed to farmland and secondary native forest, much of which is still seen throughout the area in the present day (Hume & Dahm, 1991).

2.4.2.4.1 Pine plantations

Pine plantations have been located on steep slopes in the SEmb catchment (Waiau, Awakanae and unnamed streams in Fig. 2.6) since ~1975 A.D (Hume & Dahm, 1991) (Fig. 2.6). Over 800 ha of pine plantations are currently located in the Semb catchment. Pine plantations are well understood to increase erosion rates, as cyclic harvesting exposes unconsolidated soils to mechanical erosion (e.g. abrasion from trees moving down slope), weathering, and land slip events (Marden, Rowan, & Phillips, 2006). Sediments derived from pine plantations are characteristically

high in woody detritus and are frequently reported to be rapidly infilling regional estuaries (Hume & Dahm, 1991; Sheffield *et al.*, 1995, Reeve, 2008). Severe pine plantation erosion and consequent organic rich debris flows have been noted throughout the Coromandel during storm events (McSaveney & Beetham, 2006).

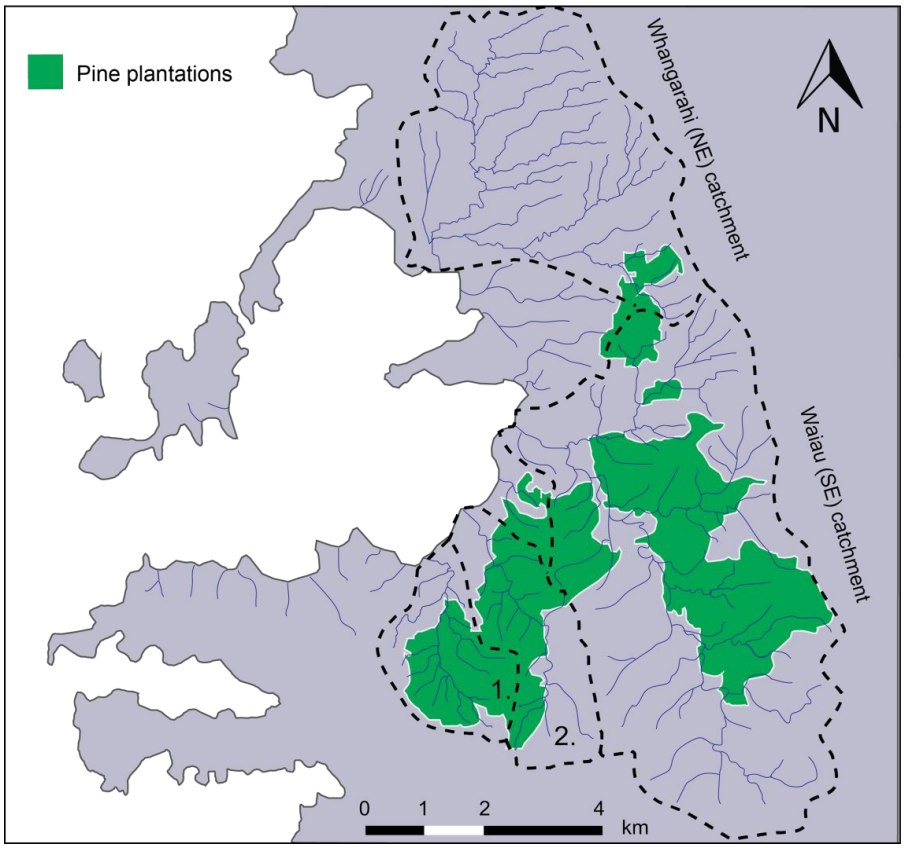

Fig. 2.6 – Present day location of pine plantations in the Coromandel Harbour catchment. The catchments of the boundaries of the Whangarahi, Waiau, Awakanae (2.) and unnamed (1.) streams are included for reference. Modified from Ministry for the Environment (2012) LUCAS New Zealand Land Use Map.

2.5 Sedimentation Accumulation Rates (SARs) in Coromandel Estuaries

The various Coromandel estuaries are expected to have undergone relatively similar anthropogenic catchment activities, and to have comparable anthropogenic estuarine sedimentation trends. Numerous studies have identified anthropogenic SARs across various Coromandel estuaries (Hume & Dahm, 1991; Sheffield *et al.*, 1995; Reeve, 2008). These SARs have been calculated using various methods including radiocarbon dating, palynology, ^{210}Pb dating, heavy metal analysis and

interpretation of unique anthropogenic sediment markers (Hume & Dahm, 1991; Sheffield *et al.*, 1995; Reeve, 2008). Here, previous studies are discussed to provide insight into the Coromandel Harbour's SAR dynamics. A table containing the summarized SAR data from each of these studies is first presented and subsequently developed upon in detail (Table 2.1).

Table 2.1– Summary of sedimentation rates within Coromandel estuaries. All data expressed in mm/yr-1. From Hume & Dahm (1991), Sheffield et al. (1995), Swales & Hume (1995), Mead & Moores (2004), Reeve (2008). Data from McGlone (1998) and Turner and Riddle (2001) have been sourced from Mead & Moores (2004) and are not developed upon further in this review.

Coromandel estuary	Pre-Polynesian	Polynesian	Early European	Recent European	Dating methods	Source
Coromandel Harbour (northern embayment)	0.02	0.07	0.82		^{14}C, pollen	Hume & Dahm (1992)
Coromandel Harbour (southern emabyment)	0.94	0.39 -0.57	1.01	11.7	^{14}C, pollen	Hume & Dahm (1992)
Tairua	N/A	N/A	N/A	6 (average)	Wooden floor marker bed	Hume & Gibb (1987)
Whangapoua Harbour	0.03 - 0.08	0.12 - 0.13	1.3 - 1.5	0.89 - 1.33	^{14}C, pollen	Hume & Dahm (1992)
Whangapoua Harbour	~0.16		~1		?	McGlone (1998) in Turner & Riddle (2001)
Whangamata Estuary	0.1	0.3	6.0 - 11		^{14}C, pollen	Sheffield *et al*. (1995)
Whitianga Estuary	N/A	N/A	21 - 30	5.0 - 9	^{210}Pb	Reeve (2008)
Wharekawa Estuary	0.09 - 0.12	N/A	~ 3.6 - 7.2	5.0 - 8.0	?	Swales & Hume (1995)
Firth of Thames (7.5 km from Waihou River mouth)	0.09	0.13	0.5		^{14}C, pollen	Hume & Dahm (1992)

2.5.1 Previous sedimentation studies

The majority of data concerning anthropogenic SARs in Coromandel estuaries come from Hume & Dahm (1991). In their report, the authors investigated changes in sedimentation rates by applying radiocarbon and pollen dating methods to core samples from the Coromandel Harbour, Whangapoua Estuary and the Firth of Thames. Radiocarbon dates were measured on shell material within cores. Changes in pollen assemblage associated with various anthropogenic activities within the catchments were used to infer dates from surficial sediments.

Later work by Sheffield *et al.* (1995) calculated SARs in the Whangamata Estuary, applying radiocarbon and pollen dating methods in the same manner as Hume & Dahm (1991). Reeve (2008) used ^{210}Pb dating to investigate European anthropogenic sedimentation in the Whitianga Estuary. The short half-life of ^{210}Pb makes it only applicable to sediments <150 years old. Thus, pre-Polynesian and Polynesian sedimentation rates could not be identified.

Here, the results of these reports are discussed with regard to the four anthropogenic periods defined by Hume & Dahm (1991).

2.5.1.1 Pre-Polynesian SARs

Hume & Dahm (1991) identified pre-Polynesian sediments with native pollen assemblages and generally fine-grained silt to sand sediments. Hume & Dahm report similarly low pre-Polynesian SAR of 0.02–0.12 mm/yr throughout all Coromandel estuaries studied. Some elevated outliers are observed near the outlets of streams, where natural SARs are high (Hume & Dahm, 1991) Sheffield *et al.* (1995) report similar pre-Polynesian SARs in the Whangamata of 0.1 mm/yr.

Low pre-Polynesian SARs are interpreted as primarily due to the extensive vegetation cover that restricted erosion of catchment geology (Hume & Dahm, 1991; Sheffield *et al.*, 1995). Storms are likely to have generated periodic erosion and sedimentation; however, due to the sampling resolution of the dating methods, the effects of these processes cannot be identified.

Interestingly, Hume & Dahm (1991) infer that pre-Polynesian sedimentation rates in several areas were highest immediately following the beginning of PMSL. However, they do not discuss this conclusion further.

2.5.1.2 Polynesian SARs

Polynesian sediments are characterised by a marked increase in bracken pollen, an indicator of forest disturbance induced by small-scale fires (Hume & Dahm, 1991). Hume & Dahm (1991) and Sheffield *et al.* (1995) both calculate Polynesian SARs as equal to or marginally greater than pre-Polynesian SARs, increasing to 0.07–0.57 mm/yr. The authors associate these rises in sedimentation with agricultural land clearance practices. In some cases Polynesian SARs decrease compared with pre-Polynesian SARs (Hume & Dahm, 1991). Possible reasons for this are not clear.

The influences of Polynesian activity on sedimentation are generally considered marginal relative to European influence (Hume & Dahm, 1991).

2.5.1.3 Early European SARs

The most significant changes to estuarine sedimentation in the Coromandel are related to European activities since ~1820 A.D. Early European sediments have high organic matter content elevated heavy metal concentrations relative to the deforestation and gold mining activities that occurred during this period (Hume & Dahm, 1991, Reeve, 2008). Early European sedimentation rates are calculated at between 0.82 mm/yr and 7.2 mm/yr, (Table 2.1) (Hume & Dahm 1991; Sheffield *et al.* 1995). Reeve (2008) presents early European deforestation-related sedimentation rates of up to 30 mm/yr in Whitianga Estuary. These rates are much greater than those observed in other Coromandel estuaries and may be related to the Whitianga Estuary's large catchment size (Reeve, 2008).

Hume & Dahm (1991) and Reeve (2008) note that recent European sediments are enriched in heavy metals relative to pre-human sediments, and associate this with outwash of historic mining wastes and erosion of metal-enriched soils. Hume &

Dahm (1991) use heavy metal enrichment to infer mining periods in the Coromandel Harbour. Reeve (2008) used heavy metal enrichment to validate SARs calculated using ^{210}Pb dates in the Whitianga Estuary, where elevated heavy metals were interpreted as a European stratigraphic marker.

2.5.1.4 Recent European SARs

Recent European sediments are distinguishable from early European sediments by a change in pollen assemblage to high compositions of pine pollen and a rise in native forest species (associated with replantation of secondary native forest). At some sites, (e.g. Coromandel Harbour), this sediment is appears to be derived from pine plantations in the catchment (Hume & Dahm, 1991; Sheffield, 1995; Reeve, 2008). A recent European SAR of 11.7 mm/yr has been collected from the SEmb of the Coromandel Harbour (Hume & Dahm, 1991). Hume & Dahm (1991) suggested that this may be an overestimate due to pine pollen being reworked by bioturbation into earlier sediment. Hume & Dahm (1991) also noted that European sediments are generally coarser than pre-European sediment, highlighting increased erosional energy in the catchment.

Sheffield *et al.* (1995) also noted a significant rise in sedimentation in the recent European period, and related this to pine plantation erosion throughout the catchment. In the Whangamata Estuary, recent European sedimentation rates may be up to 110 times greater than pre-Polynesian SARs. These sediments accumulated rapidly, and contain abundant pine pollen. Sheffield *et al.* (1995) suggested that this marked increase can be associated with the large scale of pine plantations in the Whangamata catchment.

Reeve (2008) calculated recent (since 1950 A.D) European SARs within the Whitianga Estuary of 5–9 mm/yr. While Reeve (2008) did not suggest a source for these sediments, it seems likely that this sediment is derived from the extensive pine plantations throughout the catchment. Pine plantations are the only significant land-use changes in the Whitianga catchment for the last 50 years.

It is clear that pine plantations are significantly influencing estuarine sedimentation rates in recent European periods in Coromandel estuaries. These sediments contain abundant pine pollen and are often coarse-grained. Given their characteristic properties, these sediments should be easily observable in Coromandel Harbour sediments, where pine plantations occur extensively in the catchments of the SEmb.

2.5.1.5 Non-conventional dating methods

Radioactive isotope and pollen dating methods are not always applicable in all sedimentary environments. Thus, researchers often have to apply novel methods to date sedimentary successions.

Hume, Fox, & Wilcock (1989) proposed the use of organochloride stratigraphic markers to place age constraints on recent European sediments. Dichlorodiphenyltrichloroethane (DDT), a pesticide that was used extensively on agricultural land from 1950 A.D–1970 A.D, does not occur in nature and can only be related to human activity. As the period of use of the pesticide is well defined, DDT provides a unique stratigraphic marker. Hume, Fox, & Wilcock (1989) analysed DDT and its breakdown components in sediments of the Manukau Harbour, Auckland, using pollen to validate the dating of the marker bed. Their preliminary study noted that earliest sediments deposited during the period of DDT use could be accurately identified through DDT measurements. Due to ongoing leaching of DDT from the catchment and bioturbation, they found that the upper boundary of DDT-contaminated sediments may not be distinguishable in estuarine sediments. The results do however validate the use of the organochloride as a marker for 1950 in New Zealand estuaries.

Another interesting method of interpreting age from anthropogenic sediments is presented by Hume & Gibb (1987), who associate occurrence of a wood-rich layer with early European deforestation and kauri milling within the Tairua catchment. The “wooden floor” consists of wood chips and organic detritus derived from kauri milling processes. Associating the wooden floor with mill waste outwash that were deposited in 1933, Hume & Gibb were able to calculate

net early European sedimentation rates of 6 mm/yr. These rates are slightly elevated compared to other Coromandel estuaries, though this may be due to the large, steep catchment and intensive early European land practices within the region. The rates do still broadly conform with other Coromandel Peninsula early European sedimentation rates calculated using conventional methods, thus validating the viability of the dating method.

As the use of DDT was widespread across the country, the stratigraphic marker may be observable in the Coromandel Harbour. The same can be said for the wooden floor marker bed, as kauri was extensively felled and milled in the catchment.

2.5.1.6 Applicability of dating methods

All of the studies discussed draw attention to the applicability of dating methods used to infer SARs, outlining possible means of dating error.

Pollen, DDT, "wooden floor" material and ^{210}Pb can easily be bioturbated through a sediment succession, which can result in sediments being interpreted as older than or younger than their true depositional age. These methods are therefore best applied in conjunction with other dating methods and careful interpretation of sediment character. For example, Hume & Dahm (1991) and Reeve (2008) used heavy metal analysis to correlate mining-related sediments with early European pollen dates. Hume & Dahm also correlated the appearance of abundant pine pollen with changes in sediment composition to highly organic and coarser sediments, and inferred that these changes were all related to the appearance of pine plantations in the catchment. Hume & Dahm (1991) acknowledged the possibility of bioturbation effects on pollen dates and applied a 10 cm margin of error for all pollen dates.

Radiocarbon dates from Coromandel estuaries have typically been measured on shell material. While shells can accumulate *in situ*, providing accurate sediment ages, they can also be reworked and re-deposited during erosion and storm events (Hume & Dahm, 1991; Sheffield *et al.*, 1995). Radiocarbon dates should be

interpreted carefully and compared with other dating and sedimentological data. Both Hume & Dahm (1991) and Sheffield *et al.* (1995) interpret radiocarbon dates alongside pollen dates, with Hume & Dahm (1991) additionally using heavy metal analysis.

2.5.1.7 Sedimentation rates summary

All of the SAR studies within Coromandel estuaries have found similar trends of changes in sedimentation rates for the periods identified, even if the absolute SARs themselves differ. Differences between SARs in different estuaries have been related to a number of variables, including catchment geography and size and catchment-specific anthropogenic activities.

Pre-Polynesian sedimentation rates are low in all estuaries studied. Typically, Polynesian settlement and catchment activity can be seen inducing small increases in sedimentation. In some cases, Polynesian sedimentation does not produce any increase at all. The most significant change in SAR has been since European arrival. Early European deforestation, kauri gum digging and mining all influenced SAR increases to varying extents in Coromandel estuaries. In general, early European sedimentation increased SARs by a factor of ~10–20 times pre-Polynesian SARs (excluding the Whitianga outlier). Where mining has been an influence, early European sediments can be elevated in heavy metals, a feature that can be used to identify mining-related sediments in estuarine sediment successions. The largest increases in sedimentation rates are seen in recent European sediments, and may be associated with pine plantations within catchments. Here, we see sedimentation rates increasing up to 40 times those of pre-Polynesian times. Some large estimates for SARs in this period may be overestimates due to the effects of bioturbation.

Sedimentation rates have typically been identified through radiometric dating and palynological studies. Novel methods of DDT and “wooden floor” dating have been identified, and are shown to have applicability in the Coromandel Harbour setting. Dating methods do not always provide accurate sediment dates, with bioturbation and erosion and re-depositional processes often generating errors.

Dating methods must therefore be used in conjunction with other dating proxies and sedimentological investigation, and applied with common sense to avoid erroneous age interpretations and anthropogenic SAR estimates.

2.6 Heavy Metals in the Coromandel Harbour

Heavy metals are well known to cause detrimental effects to estuarine ecologies (Yanko *et al.*, 1998; Cundy *et al.*, 2003). At present, several studies have identified anthropogenic heavy metals in near shore areas of the harbour at concentrations which may have negative implications on marine life (Coffey, 1992, PDP, 2012, Aurecon, 2013).

2.6.1 Heavy metal sources

Miocene to Pliocene hydrothermal alteration enriched Kuaotunu Subgroup andesites and dacites with heavy metals such as As, Zn, Pb, Cu, and Hg (Hume & Dahm, 1991). During pre-human and Polynesian phases, heavy metals that entered the Coromandel Harbour were chiefly sourced from natural weathering processes on these rocks (Hume & Dahm, 1991; Edbrooke, 2001; Craw & Chappell, 2000). The catchment had low erosion rates due to extensive vegetation during these phases (Hume & Dahm, 1991). This likely resulted in low levels of heavy metals entering the harbour.

During the early European phase (~1860 A.D–1910 A.D), the Kuaotunu Subgroup andesites and dacites were extensively mined for epithermal gold and silver deposits (Moore & Ritchie, 1996; Craw & Chappell, 2000). Vast volumes of mine waste rock were deposited in stream networks during mining operations (Moore & Ritchie, 1996; Craw & Chappell, 2000). Gold cyanidation and mercury amalgamation were used to extract gold at several stamper batteries throughout the NEmb catchment, with tailings deposited directly into stream networks (Hume & Dahm, 1991; Moore & Ritchie, 1996; Craw & Chappell, 2000; Aurecon, 2013). This exposed a significant amount of crushed Kuaotunu Subgroup rock to weathering and increased erosion, liberating elevated concentrations of heavy metals into stream networks and thus the harbour. Mine waste throughout the NEmb catchment may have continually leached heavy metals into stream

networks as acid mine drainage. Mine waste enters stream networks during runoff events or intercepts groundwater systems, which eventually enters the harbour (Aurecon, 2013). Mining activities took place chiefly in the NEmb catchment, and are assumed to have primarily influenced contamination in the NEmb intertidal regions (see 2.4.2.3.2) (Coffey, 1992, Hume & Dahm, 1991; PDP, 2012; Aurecon, 2013).

Amplified erosion of Kuaotunu Subgroup catchment rocks are likely to have been the primary sources of heavy metals to the harbour in European times (Aurecon, 2013). Some heavy metals are also likely to have entered the harbour from recent industrial activities in the catchment, such as construction, metal works and automotive industries, though the exact influence of these activities on sediment geochemistry is not known.

2.6.2 Previous studies

The majority of previous studies into heavy metals in the Coromandel Harbour have focused primarily on surficial sediments within the intertidal and shallow subtidal regions near the outlet of the Whangarahi Stream (Fig. 2.5). These areas have been of particular interest due to continual development and dredging around the Coromandel Wharf (Aurecon, 2013). The nearshore areas of the NEmb are also of environmental interest as they are considered to be most associated with mining outwash (Aurecon, 2013).

Numerous studies have analysed various suites of heavy metals near the Whangarahi Stream mouth (Coffey, 1992, Hume & Dahm, 1991; PDP, 2012; Aurecon, 2013). Aurecon (2013) compiled all of the data from these studies to compare heavy metal contamination in these areas with the Interim Sediment Quality Guidelines (ISQG) developed by the Australian and New Zealand Environment and Conservation Council (ANZECC) (Table 2.2) (ANZECC, 2000). ISQG-Low indicates contaminant concentrations that are very unlikely to have a negative effect on local ecologies. ISQG-High values are contaminant concentrations which are expected to adversely affect half of the exposed organisms (WRC, n.d.). The effects of contaminants on organisms at

concentrations between ISQG-High and ISQG-Low are not known, but are classed as moderate (WRC, n.d.).

Table 2.2-ANZECC (2000) ISQG for heavy metals and organochlorides (DDT) of interest in this study. Heavy metal concentrations presented in dry weight. DDT concentrations are presented in dry weight and are normalised to 1% organic carbon. Adapted from WRC, n.d.

Trace element or organic compound	ISQG-Low (mg/kg)	ISQG-High (mg/kg)
Arsenic (As)	20	70
Cadmium (Cd)	1.5	10
Chromium (Cr)	80	370
Copper (Cu)	65	270
Lead (Pb)	50	220
Mercury (Hg)	0.15	1
Zinc (Zn)	200	410
DDT	0.0016	0.046

Sediments around the Whangarahi stream mouth and Coromandel Wharf have concentrations of cobalt (Co), Cu, chromium (Cr), Pb, Zn and nickel (Ni) at concentrations lower than ISQG-low concentrations (Coffey, 1992, Hume & Dahm, 1991; PDP, 2012; Aurecon, 2013). Some arsenic values rise above the ISQG-Low value in several regions with concentrations of ~20–30 mg/kg (Coffey, 1992, PDP, 2012, Aurecon, 2013). PDP (2012) and Aurecon (2013) both found Hg levels above the ISQG-High values near the Coromandel Wharf with Hg concentrations ranging from 0.18 mg/kg to 3.1 mg/kg. Heavy metal contaminants in these sediments are assumed to be associated with mining activities and continual outwash of mine wastes into the harbour (Coffee, 1992; Hume & Dahm, 1991; PDP, 2012; Aurecon, 2013).

The report by Hume & Dahm (1991) is the only study to address heavy metal contaminants in other areas of the harbour. They analysed one anthropogenic core sample (through XRF) from the intertidal regions of the SEmb and report

concentrations of heavy metals Hg, Pb, As, Cu, Zn, Cr and Ni were lower than ISQG-Low values. Hume & Dahm (1991) note heavy metals in anthropogenic sediments as ~1-1.4 times greater than pre-Polynesian sediments, identifying that human influences have increased the amount of heavy metals moving into the harbour.

2.7 Present Sedimentary Knowledge Gaps in the Coromandel Harbour

Currently, no studies have identified sedimentation processes in the deep subtidal regions of the Harbour. Anthropogenic influences on SARs, sediment dynamics and sediment geochemistry in these areas remains unclear.

The oldest sediments identified in the harbour were by Hume & Dahm (1991), who suggested grey silty sediments in their cores to be up to mid-Holocene in age. These sediments were identified in the intertidal to shallow subtidal areas of the Coromandel Harbour, and thus little is known on harbour development in the subtidal harbour. No data exists on the evolution of the harbour prior to the Holocene. Thus, the broad sedimentary evolution (i.e. prior to mid-Holocene sea level rise through to the present day) of the harbour is also not clear.

2.8 Summary

The Coromandel Harbour catchment geology primarily consists of Miocene Kuaotunu Subgroup andesites and dacites with some Manaia Group metagreywacke-argillite basement occurring to the east and south of the harbour. Quaternary sediments infill lowland depressions and river channels. Soils and sediments derived from parent Kuaotunu Subgroup volcanics and Manaia Hill Group rocks are largely situated on steep and rugged topography and prone to land slips and erosion, especially during intense rainfall events.

The Coromandel Peninsula is characterised by high yearly rainfall and can experience intense rainfall events in relation to westward moving ex-tropical cyclones. Dominant winds are predominantly sourced from the W–SW, primarily

moving into the harbour through the primary inlet. Winds are greater in the southern parts of the harbour than the northern.

The Coromandel Harbour has a total high tide area of 23.5 km^2 and a mean spring tidal range of 2.7 m and a neap tidal range of 1.8 m. Intertidal regions are broad (up to 1 km wide) along the western margins of the harbour. Tides predominantly enter through the primary inlet. Fluvial inputs into the harbour drain from a total catchment of 73.6 km^2. Wind waves are most energetic in the SEmb and less energetic in the northern. The harbour is likely to be primarily mixed by tidal cycles and wind waves which are dominant in the SEmb and lesser in the NEmb.

The Coromandel Peninsula has had a diverse history of anthropogenic land uses that have all had varying impacts on estuarine sedimentation. Polynesian settlement and agricultural practices either induced no change or marginally increased estuarine SARs relative to pre-Polynesian SARs. Early European deforestation, kauri gum digging and mining increased sedimentation in Coromandel estuaries by a factor of ~5–20 times greater than pre-Polynesian SARs. Recent European SARs are up to 40 times greater than pre-Polynesian SARs, and are expected to be chiefly related to pine plantation erosion in Coromandel catchments.

Anthropogenic heavy metal contamination studies in the Coromandel Harbour have been primarily conducted at the mouth of the Whangarahi Stream, which is thought to be most influenced by mining sedimentation. In these areas, heavy metals As and Hg have been identified with concentrations greater then ISQG-Low values. Hg does also occur with values above ISQG-High values in a number of studies. Apart from the Whangarahi Stream mouth, heavy metal investigation in the subtidal region is limited and currently exists as a knowledge gap.

Chapter 3

Field methods and Core Processing

This chapter describes the rationale behind core locations and the methods of core collection and processing.

3.1 Core Locations and Collection

Cores were located along two transects from the outwash areas of the Whangarahi and Waiau Streams through to the harbour inlet (Fig. 3.1). The purpose of these transects was to identify any differences in terrigenous sedimentation sourced from the two streams and their respective catchments, as well as to understand spatial variability in sedimentation rates and sediment characteristics throughout the harbour. The transect that runs from the NEmb to the inlet is defined as the northern transect. The transect that runs from the SEmb to the primary inlet is defined as the southern transect. Several additional cores were placed off-transect to identify spatial sediment distribution in areas of the harbour not directly in outflow zones of the two fluvial inputs (e.g. Fig. 3.1. *CH10, CH9, 007*). These cores would allow for a full 3D identification of spatial and temporal variability in harbour sedimentation. Cores CH4 and CH3 are hereby defined as 'near-inlet' areas.

All cores were positioned away from stream channels and banks where primary sedimentation may have been altered by secondary reworking processes associated with stream meandering and migration. Intertidal cores were positioned in areas accessible through private or common land that could be cored in one tidal cycle. Subtidal cores were restricted to areas with at least 1 m water depth at high tide due to the draught of the vessel. Core locations are shown in Fig. 3.1.

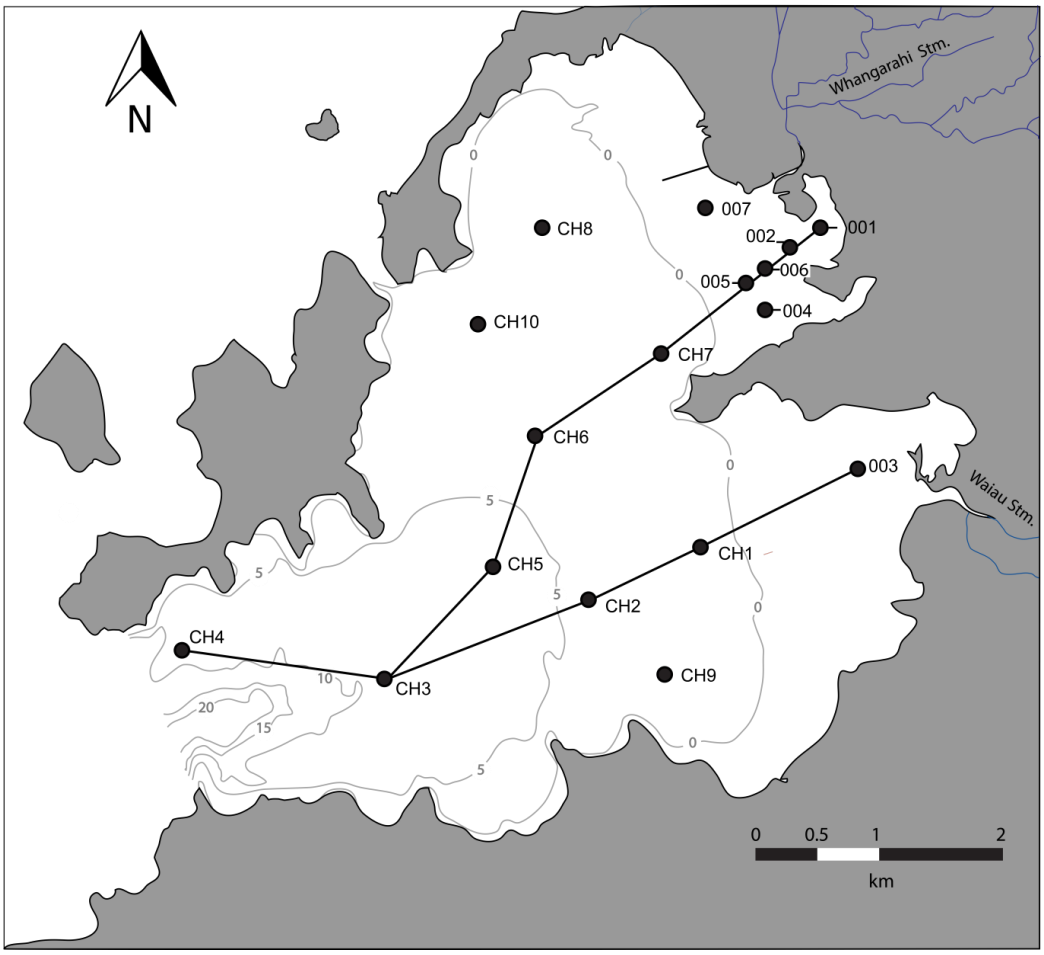

Fig. 3.1 - Core location and transect lines imposed upon a bathymetric map of the harbour. Cores preceded by the letters CH (Coromandel Harbour) indicate subtidal cores. The remaining cores were retrieved from intertidal regions. Depths are expressed as depth below mean low water spring (MLWS). Bathymetry taken from LINZ (2016) Chart NZ 533.

3.1.1 Core barrel selection

80 mm internal diameter PVC (polyvinyl chloride) core barrel was chosen over standard 76 mm internal diameter aluminium core barrel. Using PVC reduced the possibility of aluminium contaminants being introduced to the sediment cores during coring and core splitting procedures. Eliminating aluminium contamination is of significance as both metal geochemistry and magnetic susceptibility are used in this study. A larger internal diameter was also beneficial to analysis as a greater volume of sediment was retrieved with each core.

3.2 Intertidal Coring

Intertidal regions were cored during low tide with a generator powered vibracorer (Fig. 3.2).

Cores were driven down by the user's weight and the vibrational motion generated by the vibrating head unit. Following full penetration of the core, a plug was placed in the top of the core to retain negative pressure in the core barrel during retrieval. The core was extracted from the sediment using a tripod and winch system. Excess PVC at the top of the core was removed with a hacksaw and the total sediment recovery noted. Any space at the top of the barrel was plugged with foam to prevent movement of sediment within the barrel during transport and storage. Core barrels were labelled, cut into ~1 m lengths and capped prior to transportation. Core sections were placed in 4°C refrigerated storage no more than 48 hours after their retrieval.

Fig. 3.2 – Left – core being driven into the sediment using the handheld vibracorer. Right - core extraction using the tripod and winch system.

Intertidal coring took place over three field excursions during October to December, 2015. Intertidal core lengths ranged from 0.74 m to 2.4 m with an average core length of 1.72 m. Maximum core penetration was largely determined by loss of momentum following the repositioning of the fixed vibrating head unit, or by the interception of a coarse shell/gravel unit.

3.3 Subtidal Coring

Subtidal coring was undertake on-board the Triton (Fig. 3.3). A remote controlled towered vibracorer was implemented off the side of the vessel using a Hiab and winch system to gather cores of up to 4.75 m.

Fig. 3.3 - Towered vibracorer being positioned over the side of the Triton (left) and winched to the estuary floor using a HIAB crane at core location CH9.

Predetermined core locations were approached using an on-board GPS. Core barrels were pre-cut to length on board the Triton and fitted with aluminium core catchers. At each core location, a barrel was secured to the vibrating head unit. The vibracore tower was then lowered to sediment surface using a HIAB and winch system. Once at the sediment surface, the vibrating head unit was engaged, and the core barrel driven into the sediment. The vibracorer was powered for 20-30 seconds or until core penetration had ceased, indicated by a slackening in the rope attached to the vibrating head unit.

The tower and enclosed core barrel were then winched to the surface. A non-return valve at the top of the core along with the core catcher at the bottom of the barrel secured the sediment within the barrel during extraction. Once the tower had been placed on the deck, the core barrel was removed from the tower and both core penetration and total sediment recovery were noted. Sediment housed within the core-catcher was either placed at the bottom of the core or stored separately. A foam plug was placed at the top of the core to secure the sediment within the

barrel. The barrels were then labelled, capped and cut into 1 m sections. Cores were placed in 4°C refrigerated storage no more than 48 hours after retrieval.

Subtidal coring took place over the 26th and 27th of January, 2016 over two tidal cycles. Core lengths ranged from 2.8 m to 3.64 m with an average core length of 3.02 m. Core penetration was limited by the interception of a sand layer or a dense, compacted orange clay.

3.4 Core Processing and Logging

3.4.1 Core splitting

Core barrels were split lengthwise using either a hand saw or dedicated saw table. The exposed sediment surfaces of each half core were cleaned with a plastic card to remove sediment and contaminants spread down-core during the splitting process. Immediately after cleaning, cores were photographed and stratigraphically logged.

3.4.2 Visual core logging

Split cores were logged for variations in sediment texture, observable mineralogy, biogenic content, bioturbation, burrowing and colour. All sedimentological data collected through core logging were converted to stratigraphic columns using Adobe Illustrator CC 2015 software. Further data were added to these charts as the investigation progressed.

3.4.3 Spaced subsampling

Spaced subsamples were taken from the working halves of each core. Starting at the top of each core, 1 cm bands of sediment were taken at 5 cm intervals. Sediment was gathered from the centre of the core barrel where material was not expected to have been disturbed during the coring or core splitting processes.

Subsamples were weighed and dried at 60°C for 24 hours. Subsamples were then reweighed to gather moisture content. Dried subsamples were sieved to 2 mm, with the >2 mm fraction recorded for terrigenous/shell ratio, and the <2 mm

fraction placed into labelled sample bags. Additional samples were also gathered from intervals where higher resolution was desired. Dried <2 mm subsamples were used in subsequent physical and chemical analyses described in Chapters 5, 6 and 7.

3.5 Terminology

3.5.1 Core sample terminology

Specific samples collected from cores are often referred to in text (especially in Chapter 5). Throughout this report, samples have been described by the core number followed by the specific subsample from the same core. For example, CH1–12 refers to subsample 12 from core CH1. As subsamples have been collected every 5 cm from the surface, this subsample can be identified as being collected from a depth of 0.55 m.

3.5.2 Grain size terminology

Sediment grain size is described using the Wentworth Scale (Wentworth, 1922). A Wentworth grain size scale chart has been included in Appendix H for reference. Grain sizes are often abbreviated in this report as: VF=very fine, F=fine, M=medium, C=coarse, VC=very coarse followed by the type of sediment. For example, a M/C sand is a medium to coarse sand.

Chapter 4

Core Logs and Down-Core Data

This chapter presents core logs, down-core geochemical and magnetic susceptibility data for cores analysed. Several fence diagrams are also included. This data is interpreted in Chapter 5.

This chapter presents data that is applied in facies analysis in Chapter 5. Data includes core logs generated from visual observations, down-core geochemical and magnetic susceptibility and sediment fence diagrams. Note that high resolution PDF versions of these images are available in Appendix G.

4.1 Core Logs

Some cores have not been geochemically analysed or analysed for magnetic susceptibility, and therefore facies based upon geochemical or magnetic susceptibility characteristics cannot be associated to these cores. Areas such as this have been noted with a question mark (?). Note that core 007 has not been logged. This was because this core was considered to be influences by stream migration and secondary erosion and redeposition. Anthropogenic sediments in core 007 not interpreted for SAR study but are interpreted geochemically in further chapters.

4.1.1 Core log legend

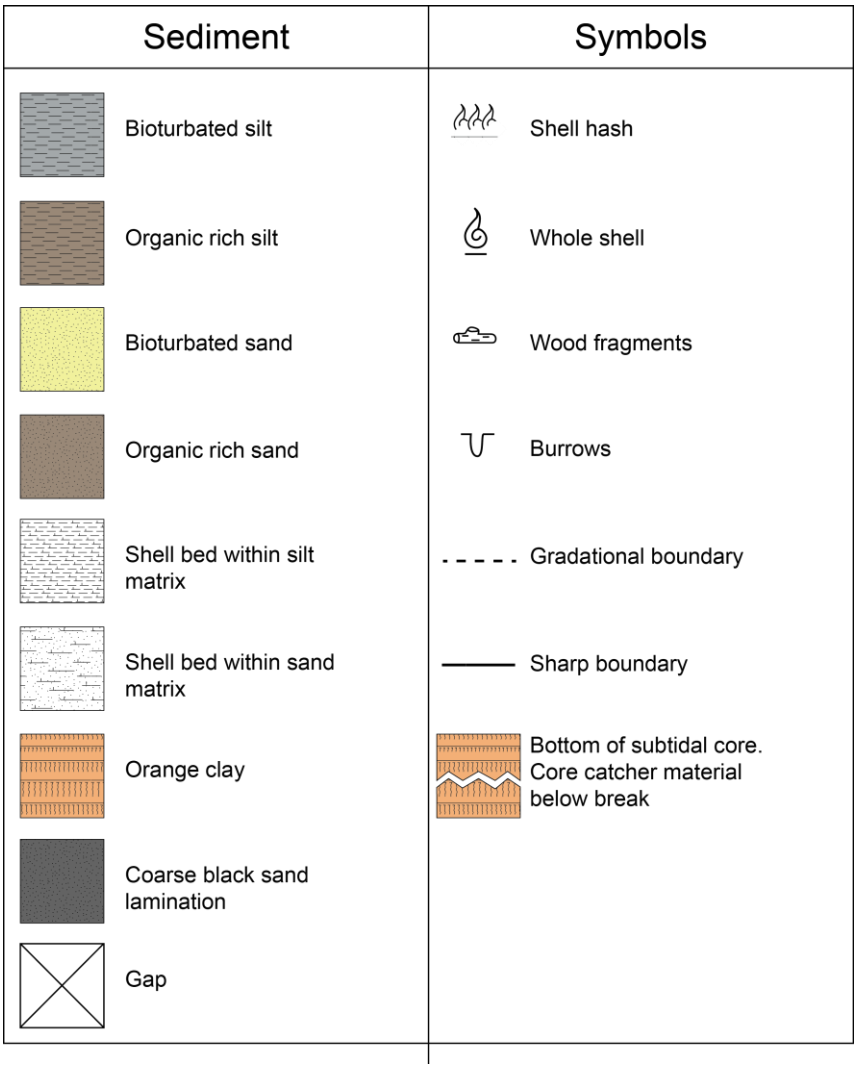

Fig. 4.1 – Legend for presented stratigraphic logs

4.1.2 Intertidal core logs

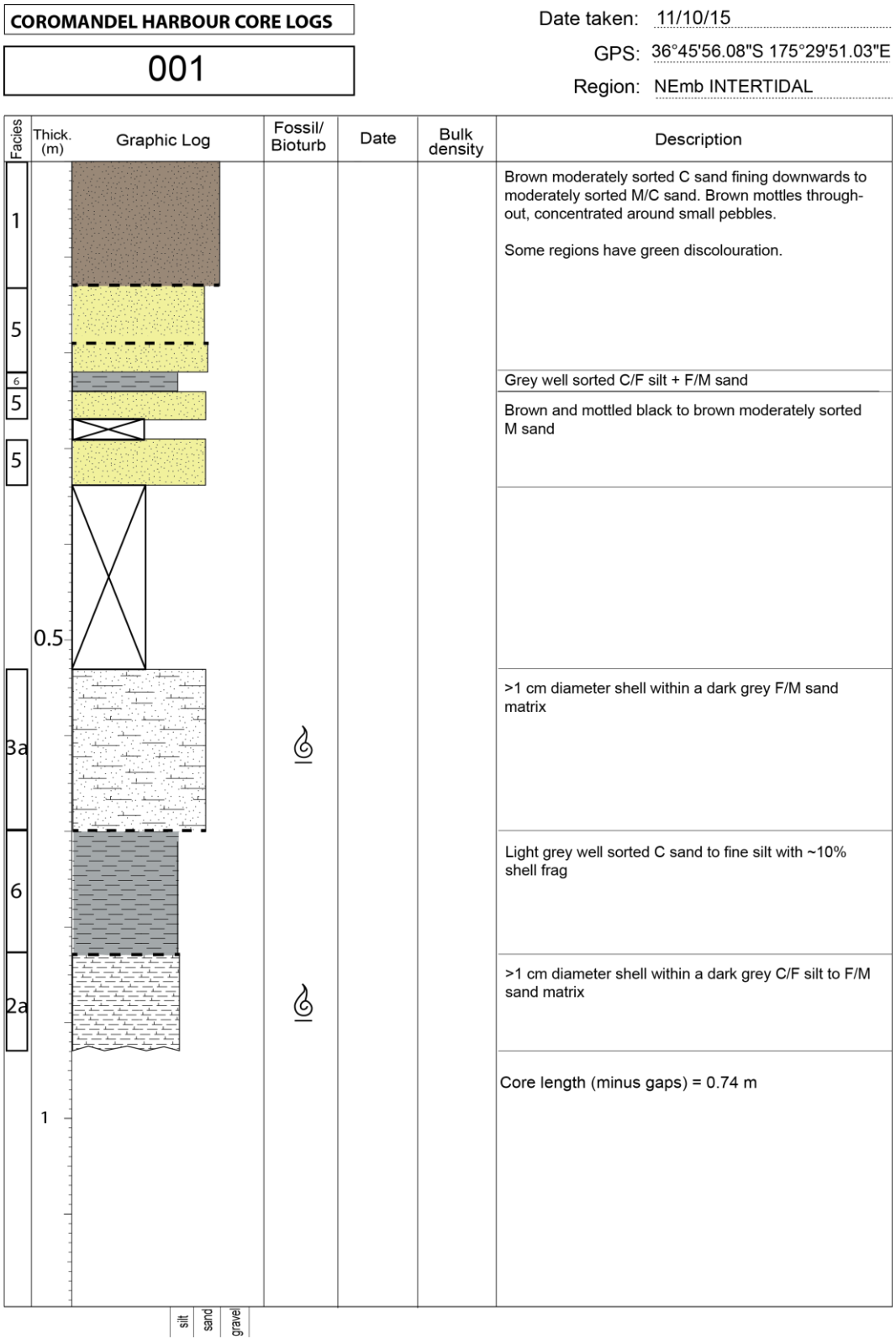

Fig. 4.2 – Stratigraphic log of core 001.

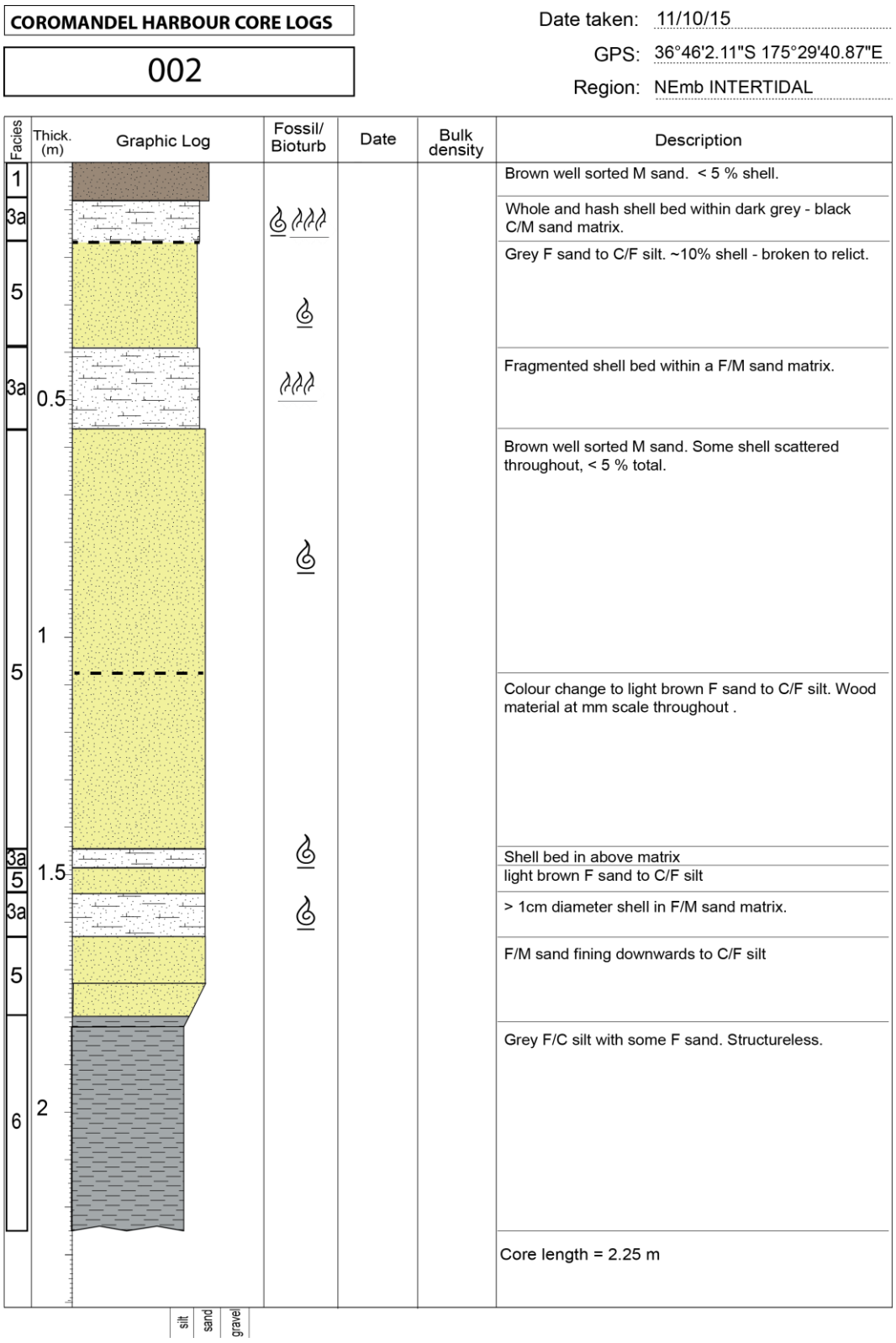

Fig. 4.3– Stratigraphic log of core 002.

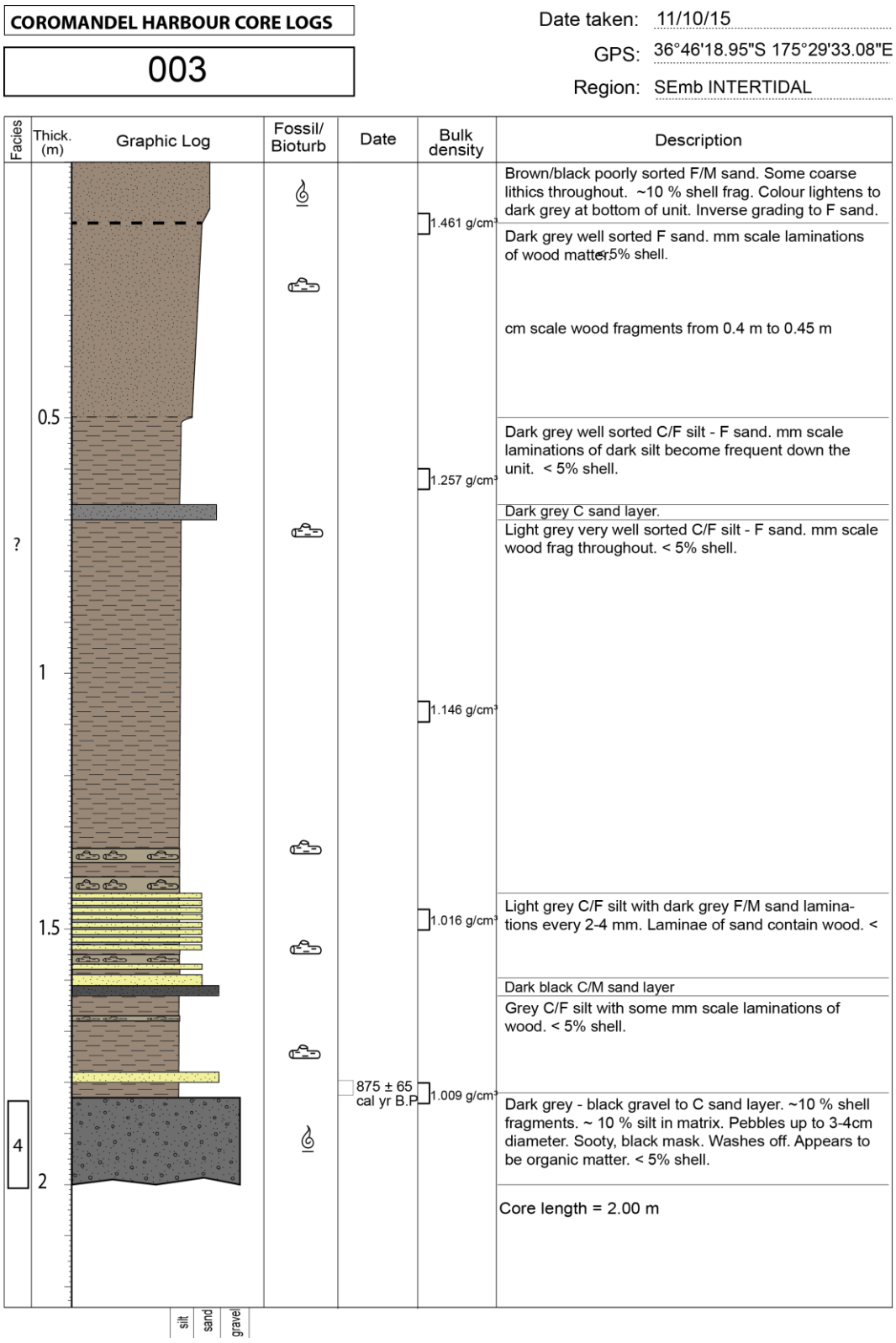

Fig. 4.4– Stratigraphic log of core 003.

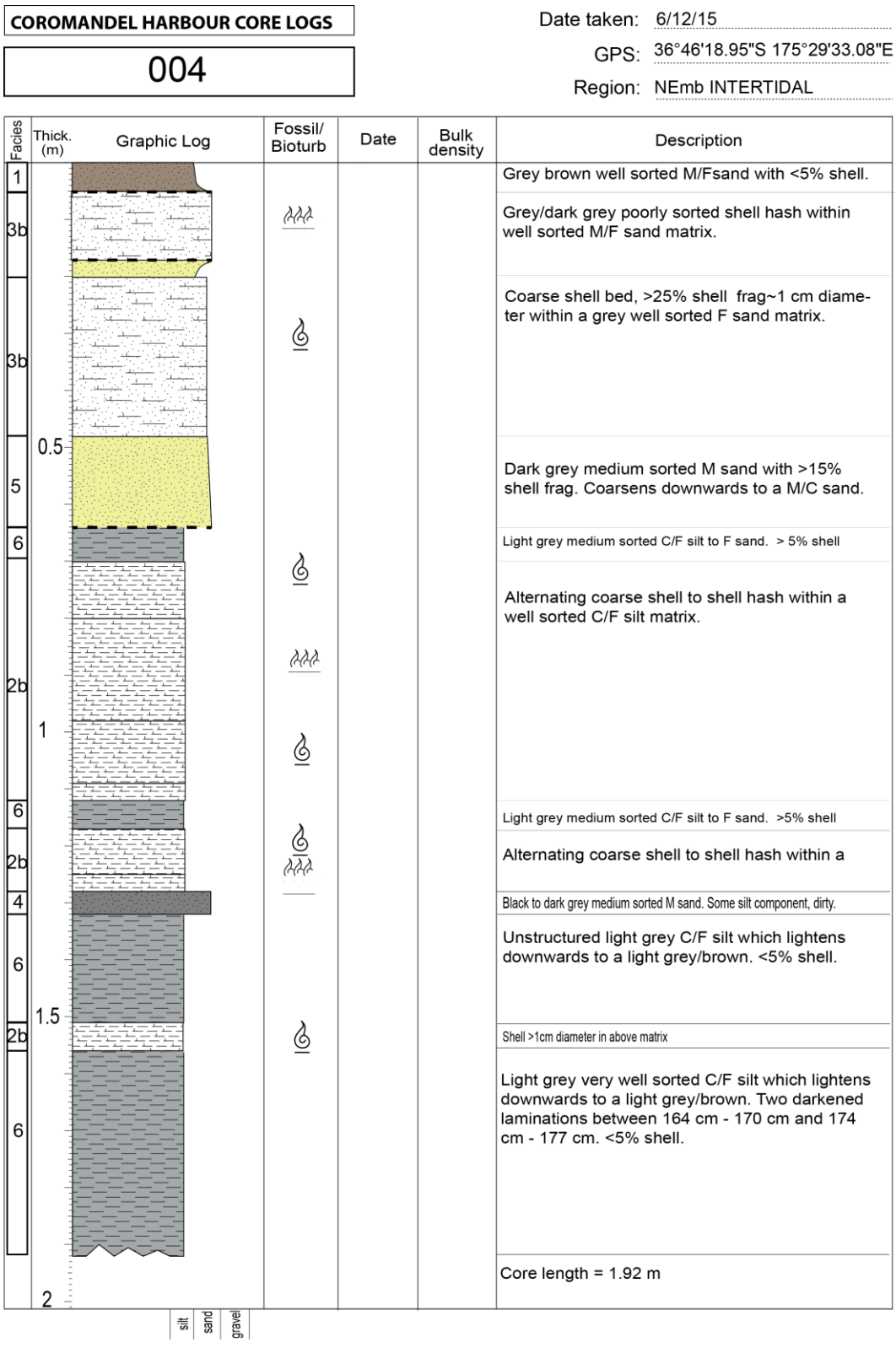

Fig. 4.5– Stratigraphic log of core 004.

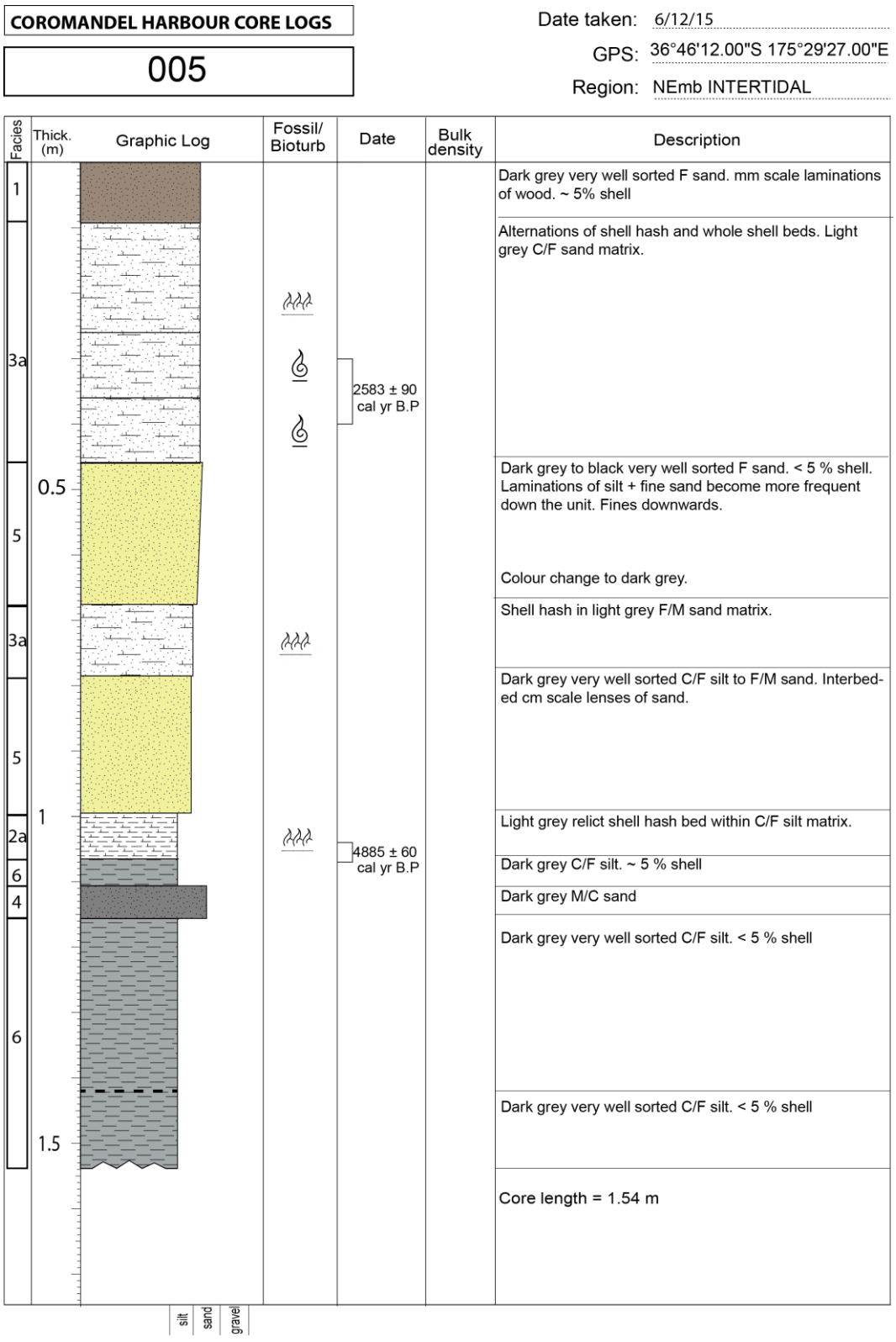

Fig. 4.6– Stratigraphic log of core 005.

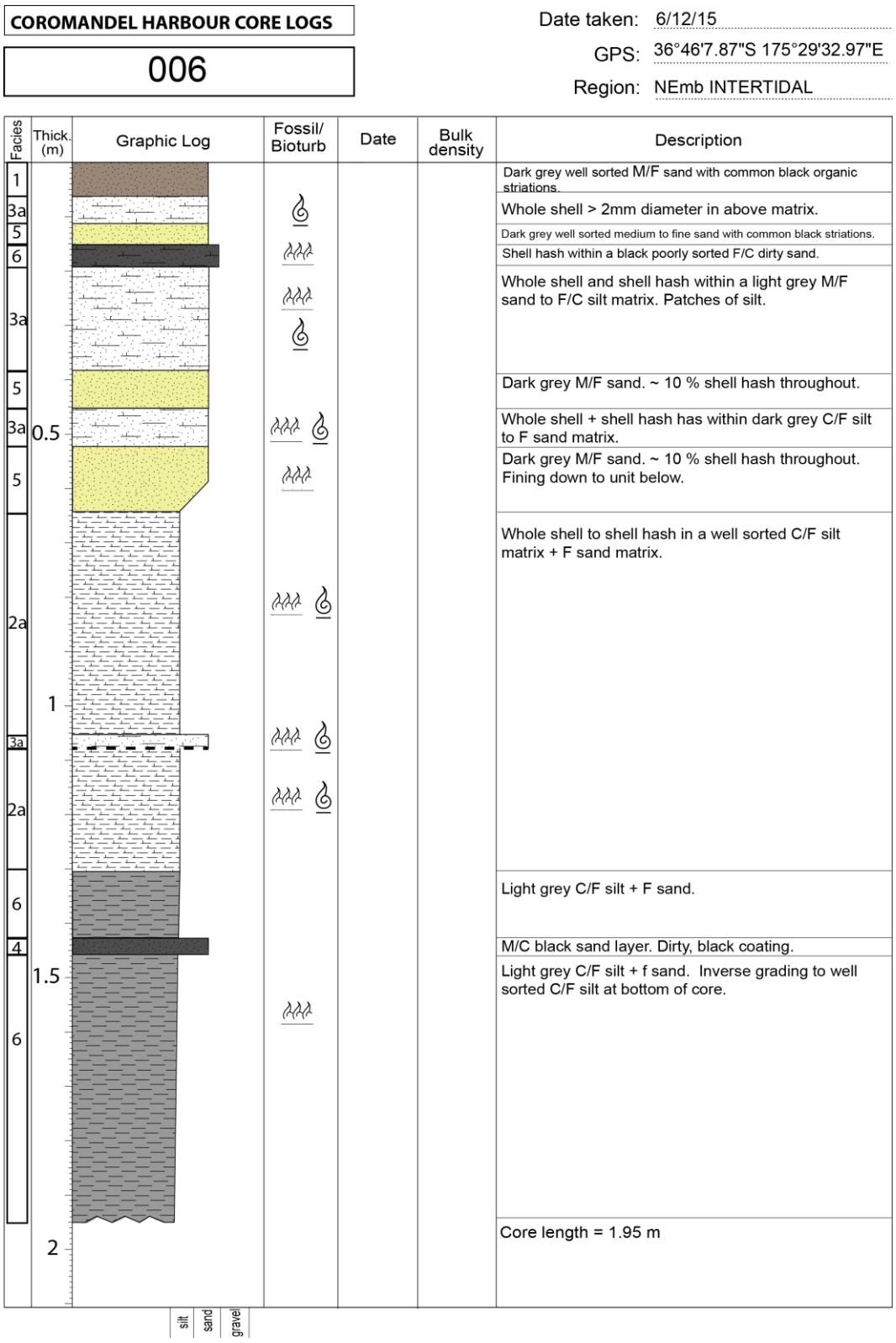

Fig. 4.7– Stratigraphic log of core 006.

4.1.3 Subtidal core logs

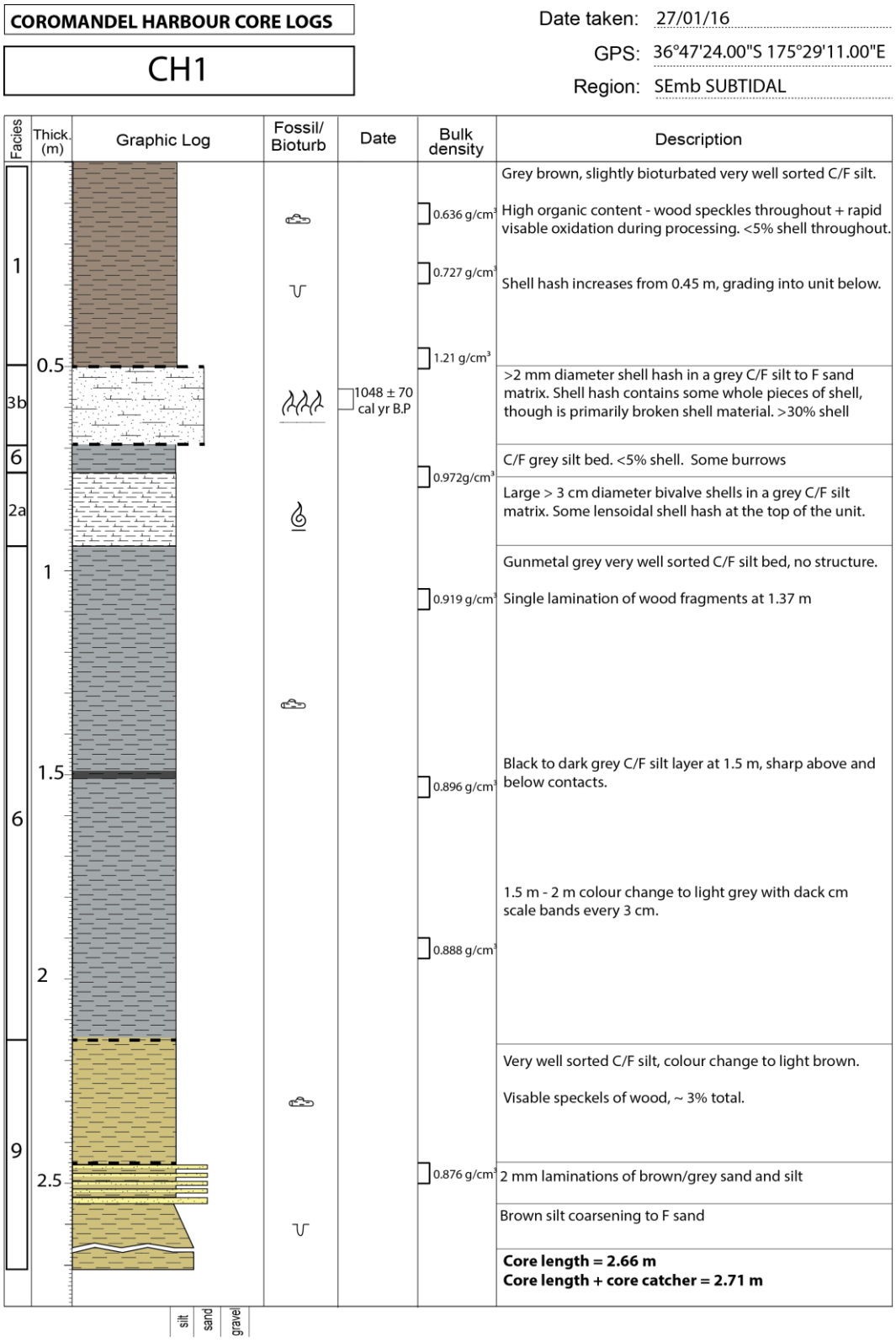

Fig. 4.8– Stratigraphic log of core CH1.

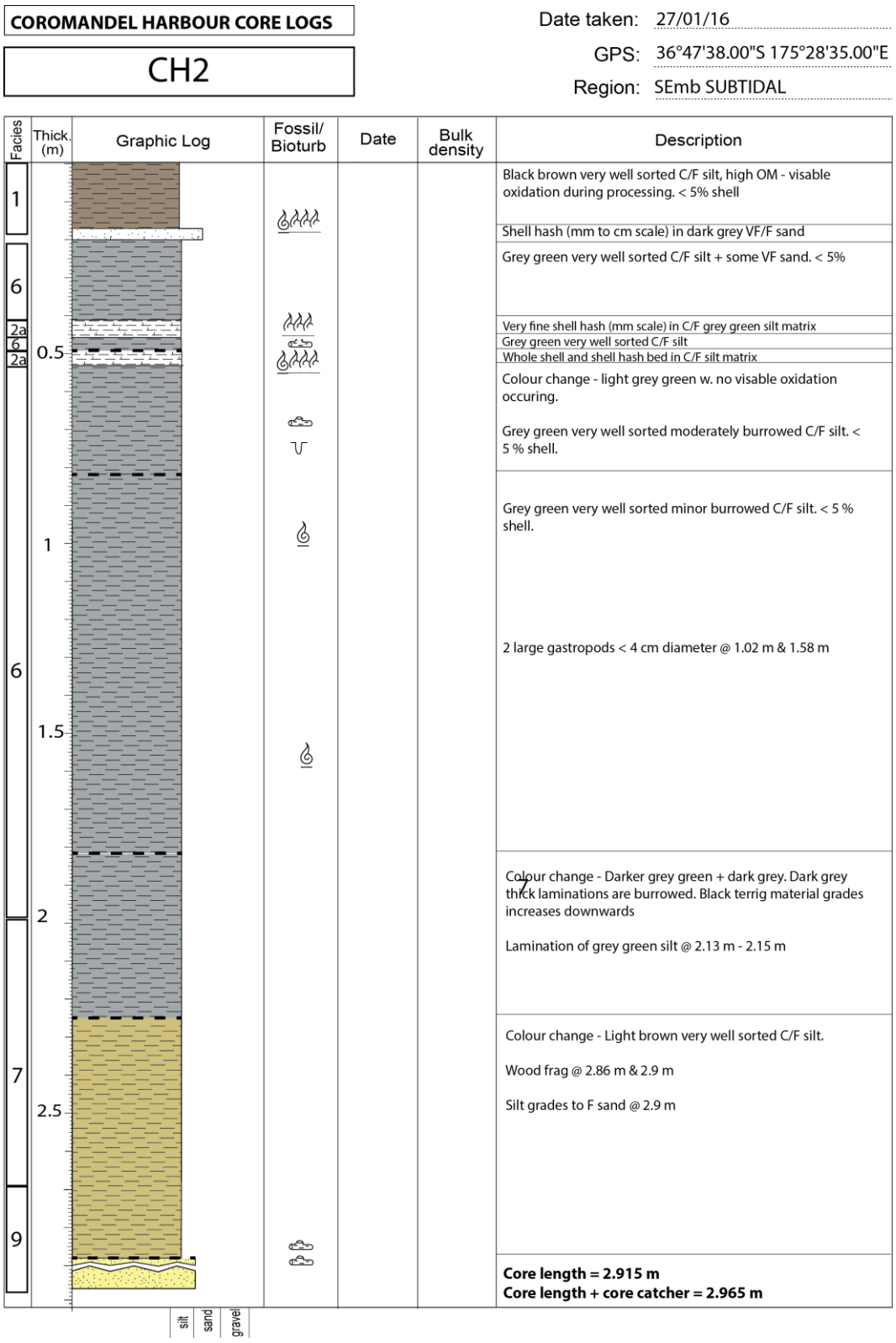

Fig. 4.9– Stratigraphic log of core CH2.

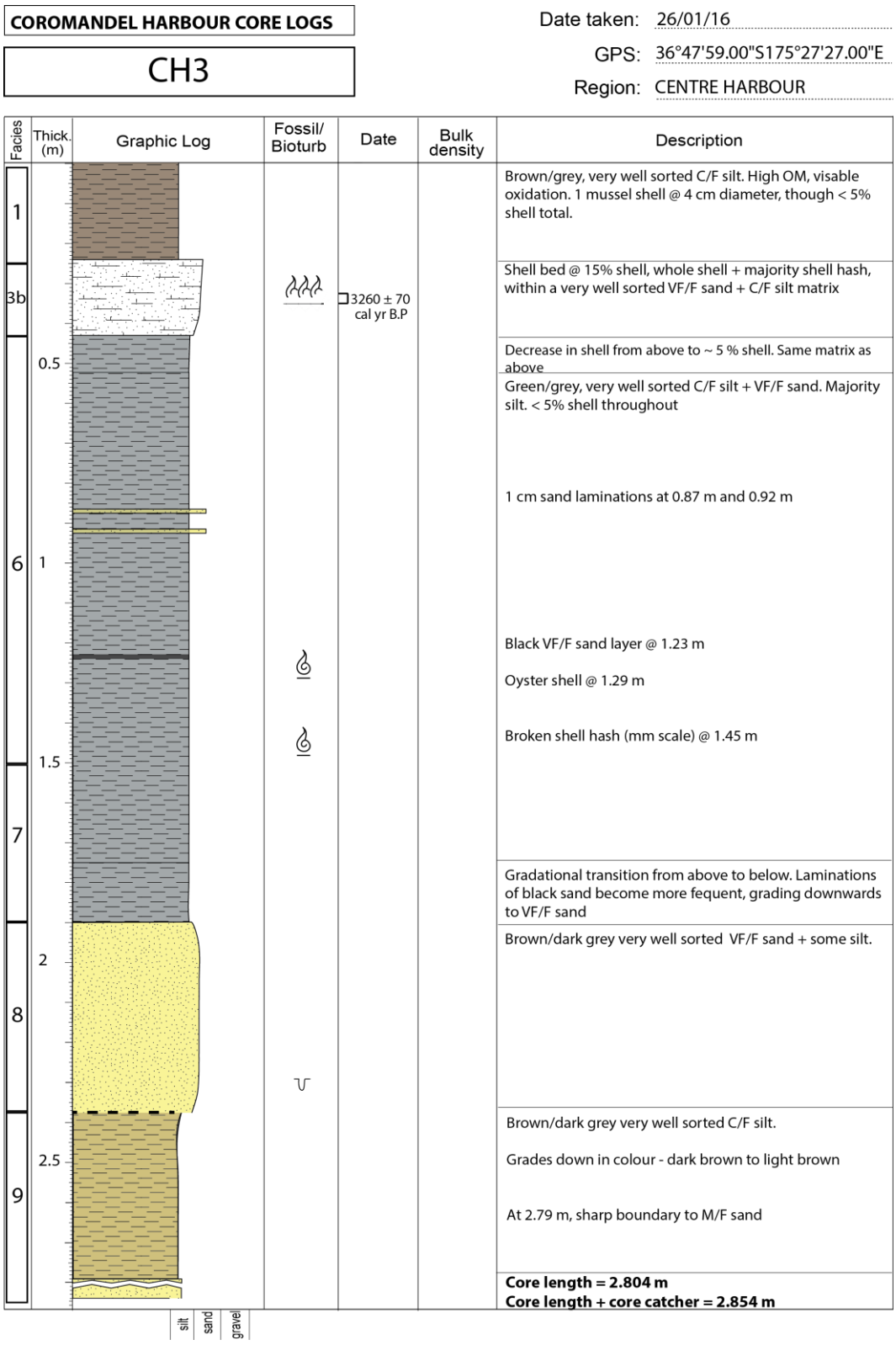

Fig. 4.10– Stratigraphic log of core CH3.

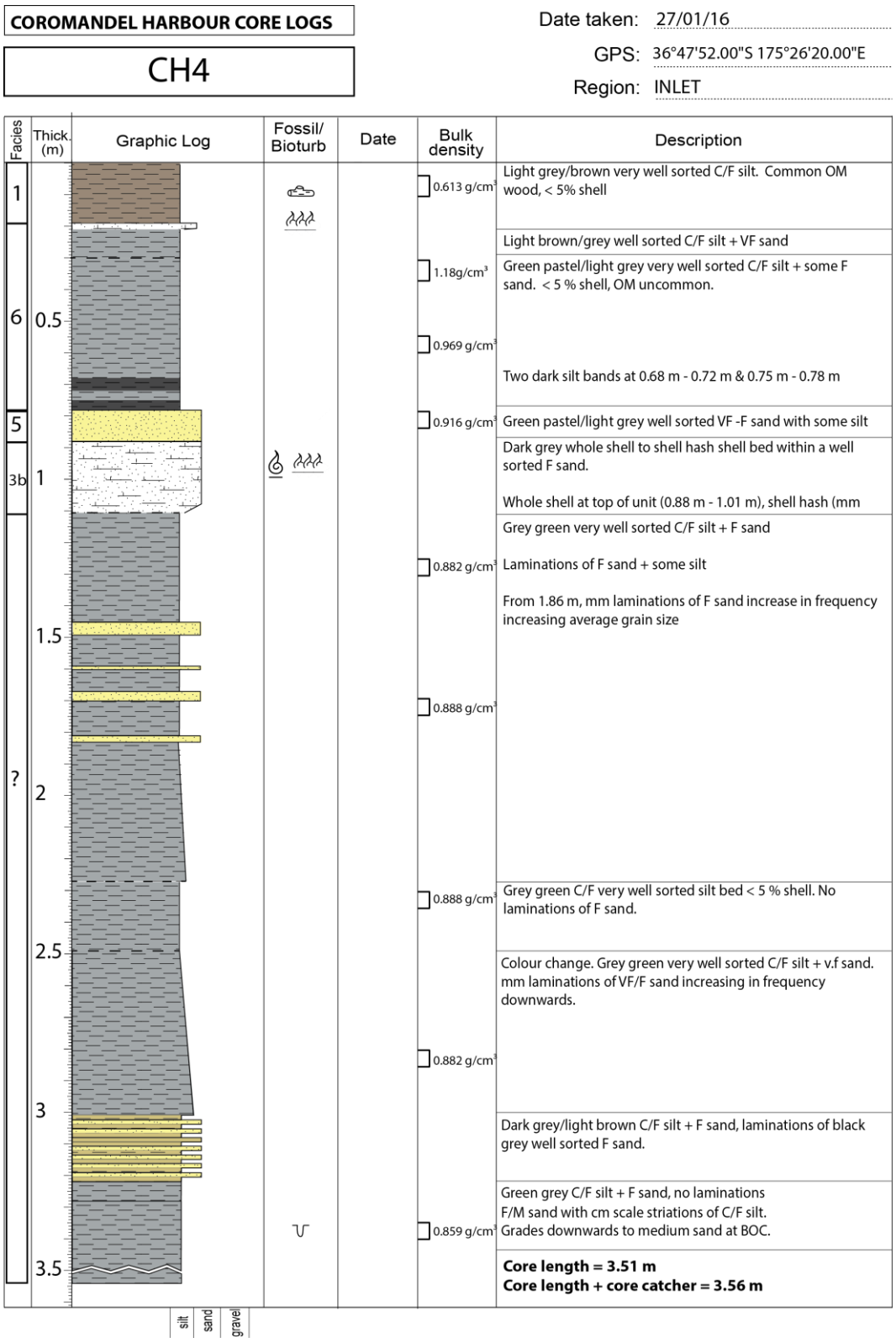

Fig. 4.11– Stratigraphic log of core CH4.

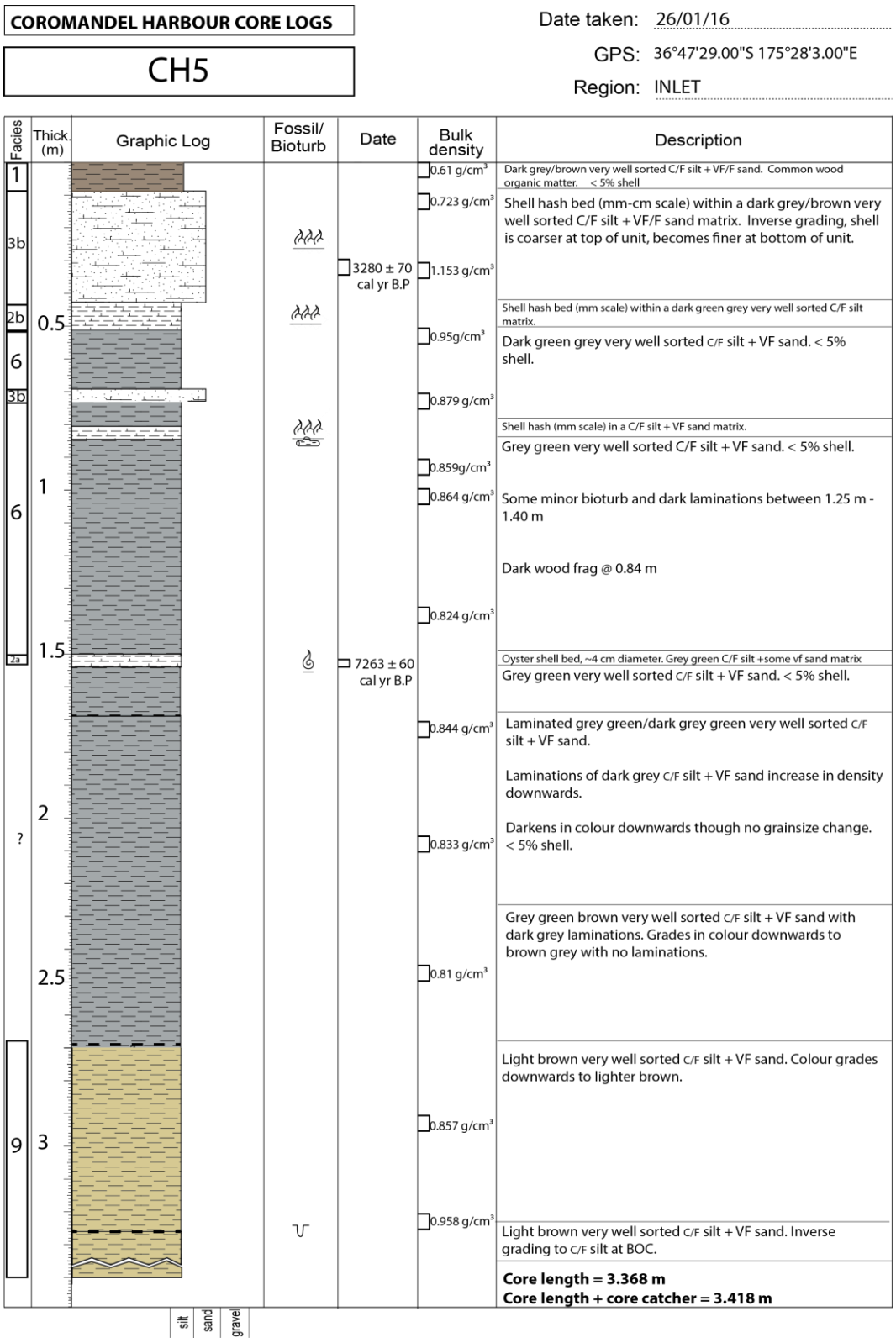

Fig. 4.12 - Stratigraphic log of core CH5.

COROMANDEL HARBOUR CORE LOGS

CH6

Date taken: 26/01/16

GPS: 36°46'54.00"S 175°28'17.00"E

Region: CENTRE HARBOUR

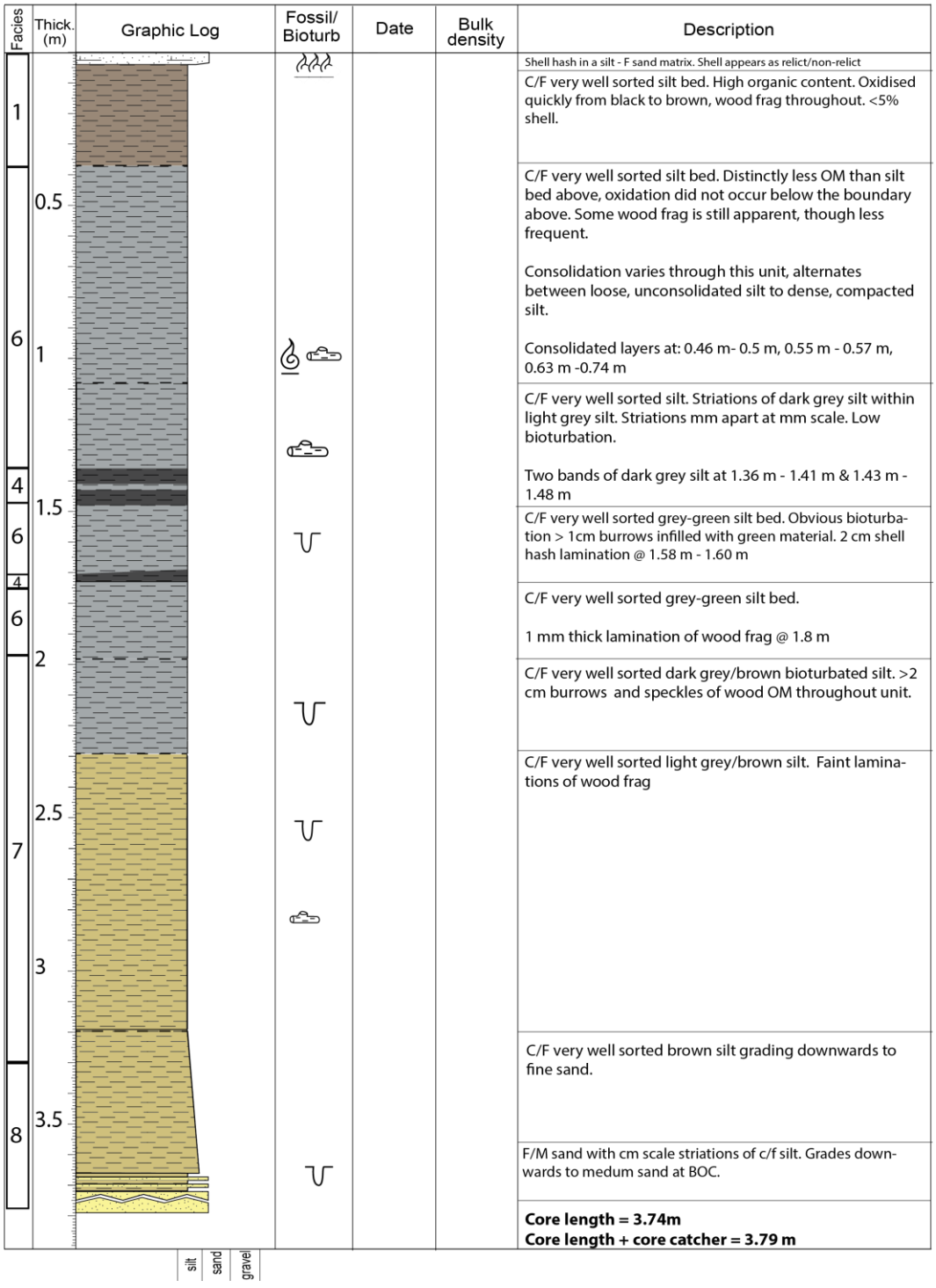

Fig. 4.13– Stratigraphic log of core CH6.

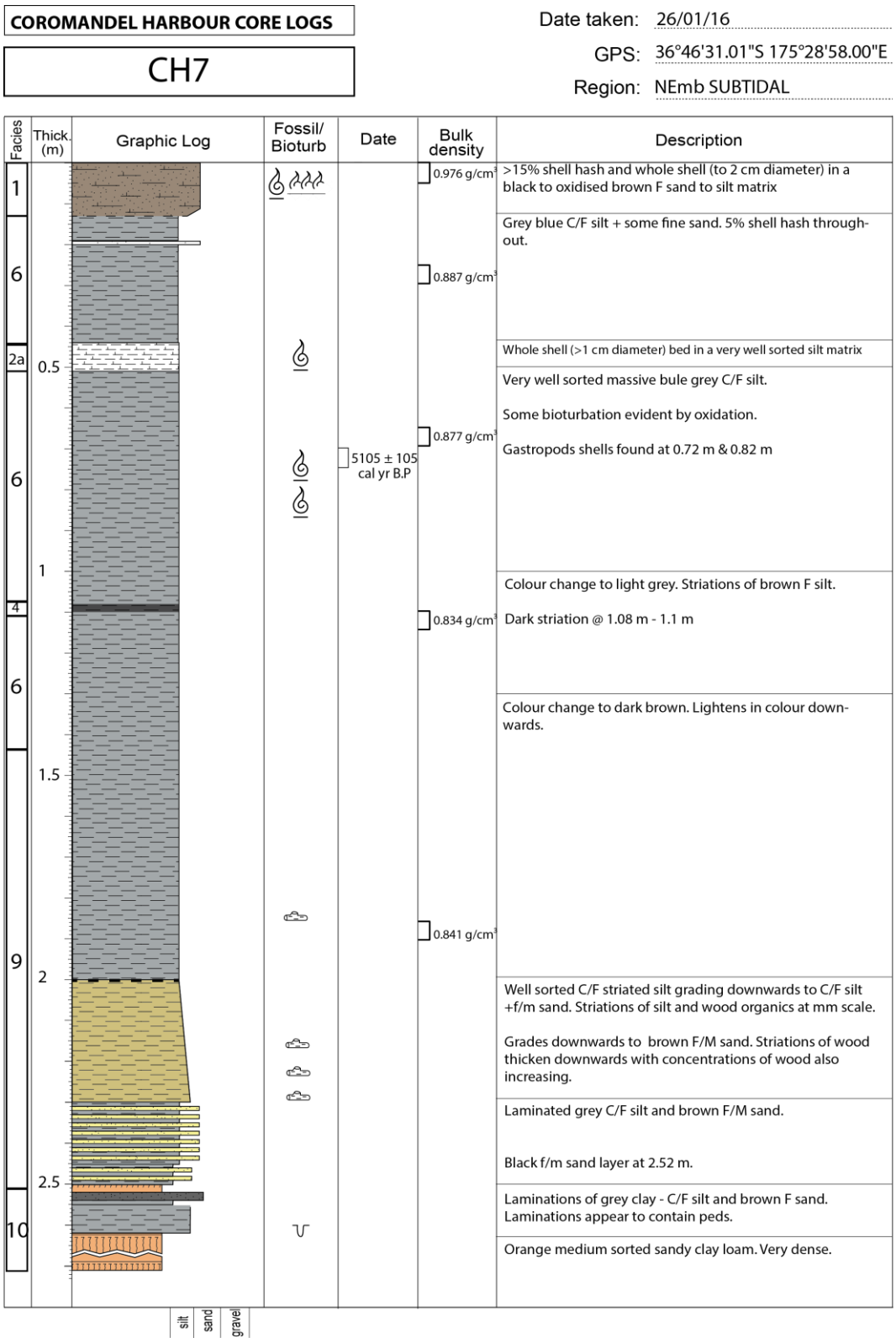

Fig. 4.14– Stratigraphic log of core CH7.

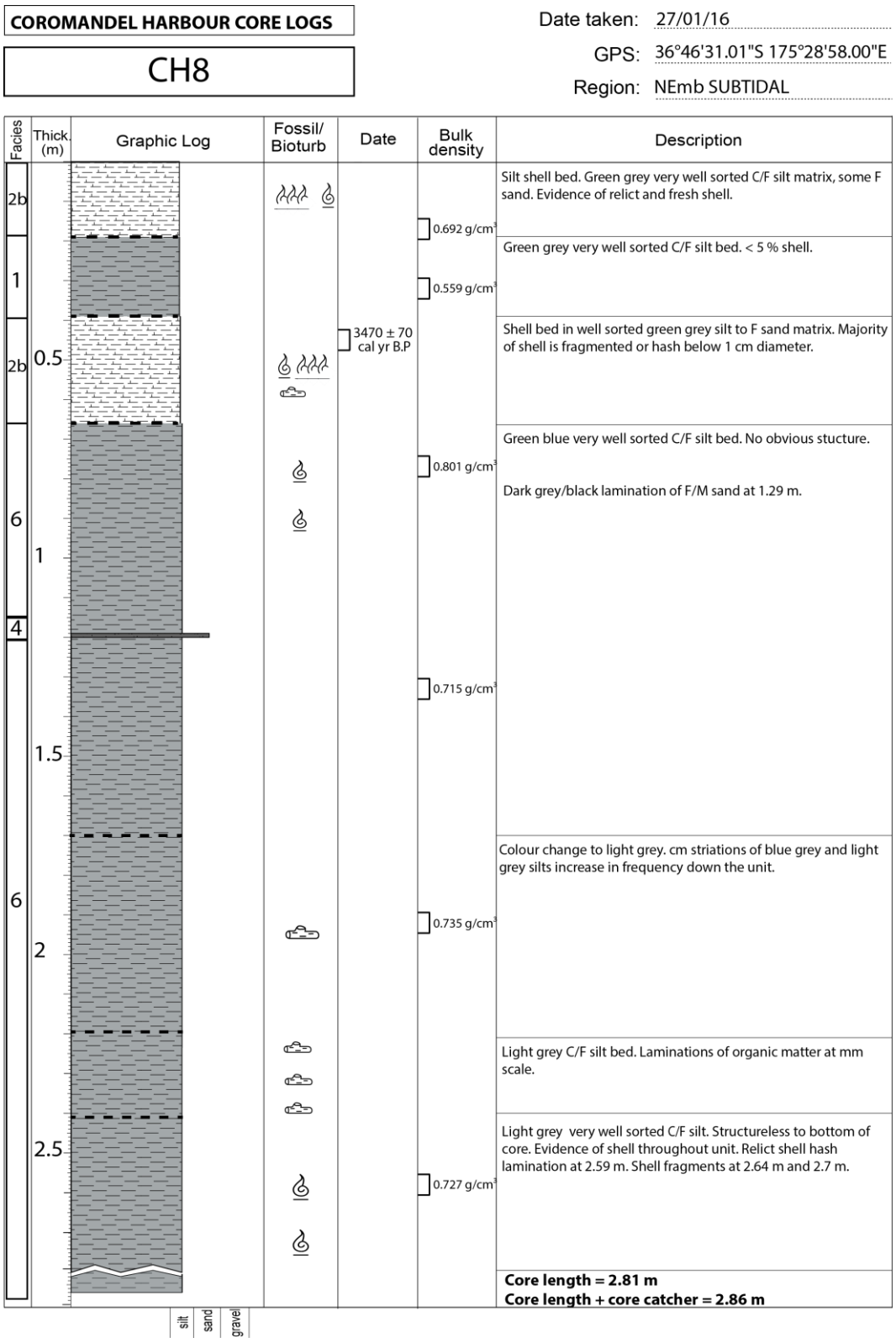

Fig. 4.15– Stratigraphic log of core CH8.

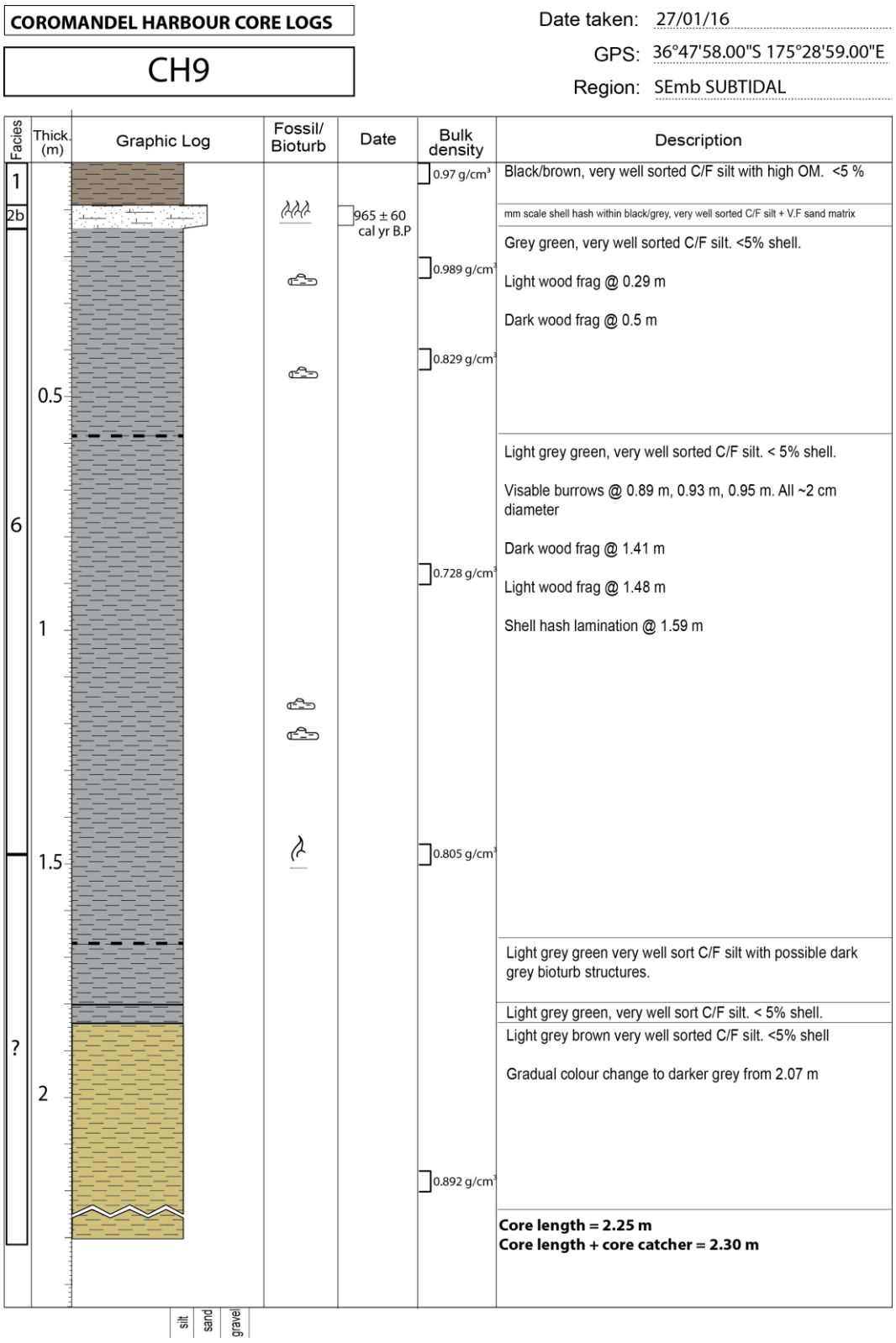

Fig. 4.16– Stratigraphic log of core CH9.

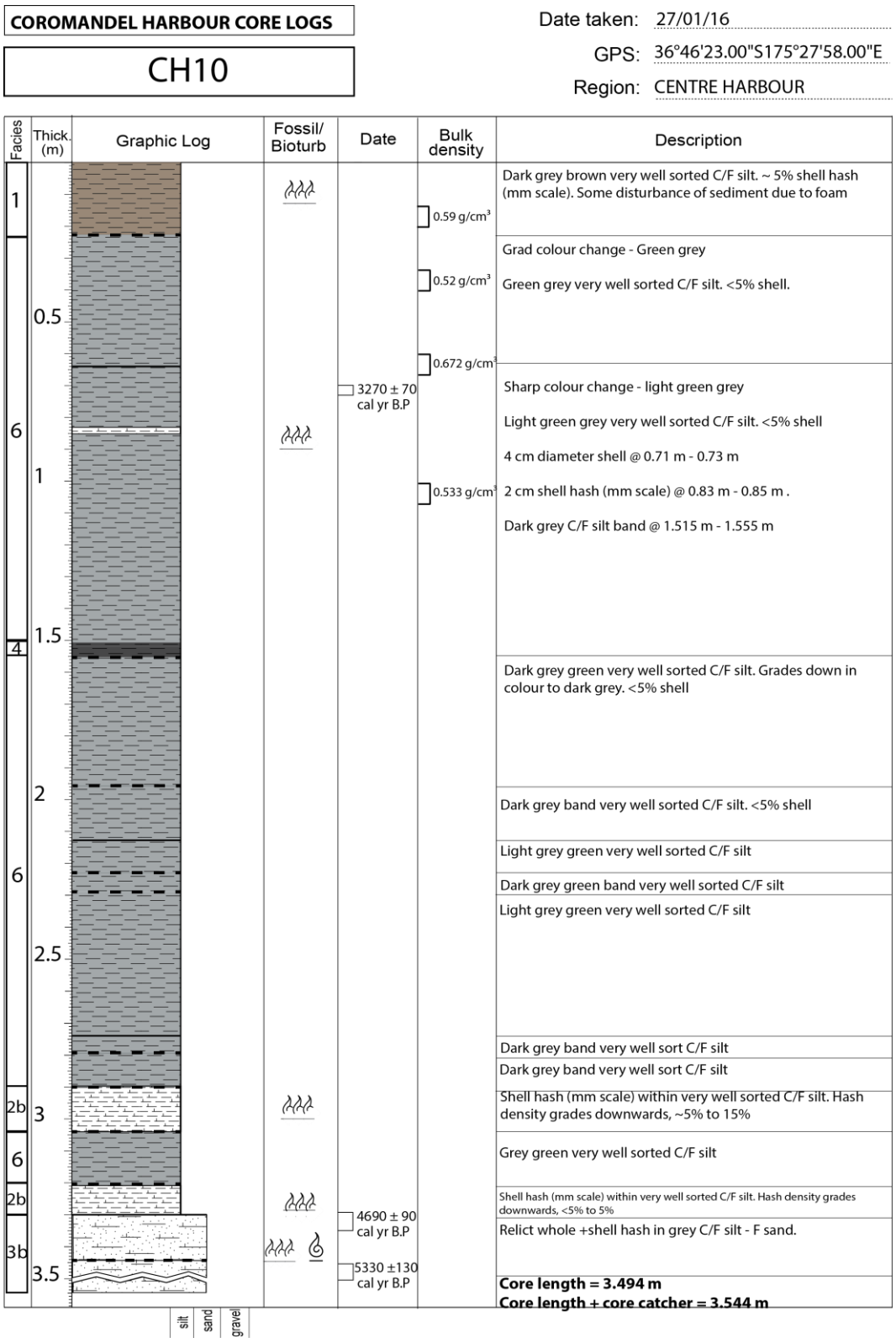

Fig. 4.17– Stratigraphic log of core CH10.

4.2 Down-core MS and Geochemical Data

MS and geochemical is presented for each core analysed. These data are discussed in Chapter 5. Depositional settings have been interpreted from facies analysis and are listed alongside this data. These depositional settings are further developed in Chapter 8. Depositional settings have been interpreted as follows:

1. Palaeosol and fluvial deposits
    - Orange clay loam facies
    - High MS sand facies
    - High MS silt facies
2. Pyritic layer (treated as its own depositional setting)
3. Pre-Polynesian–Polynesian estuarine sediments
    - Bioturbated sand facies
    - Bioturbated silt facies
    - Shelly sand facies
    - Silty shell facies
    - Black sand/silt lamination facies
4. European anthropogenic estuarine sediments
    - Organic rich sand to silt facies

Near shell beds, Ca induced matrix effects generated interference in the geochemical data (see subsection 5.1.6.1.4). Geochemical data within these intervals have been removed where Ca has exceeded 2 wt. %. Note that high resolution versions of these data are presented in Appendix J.

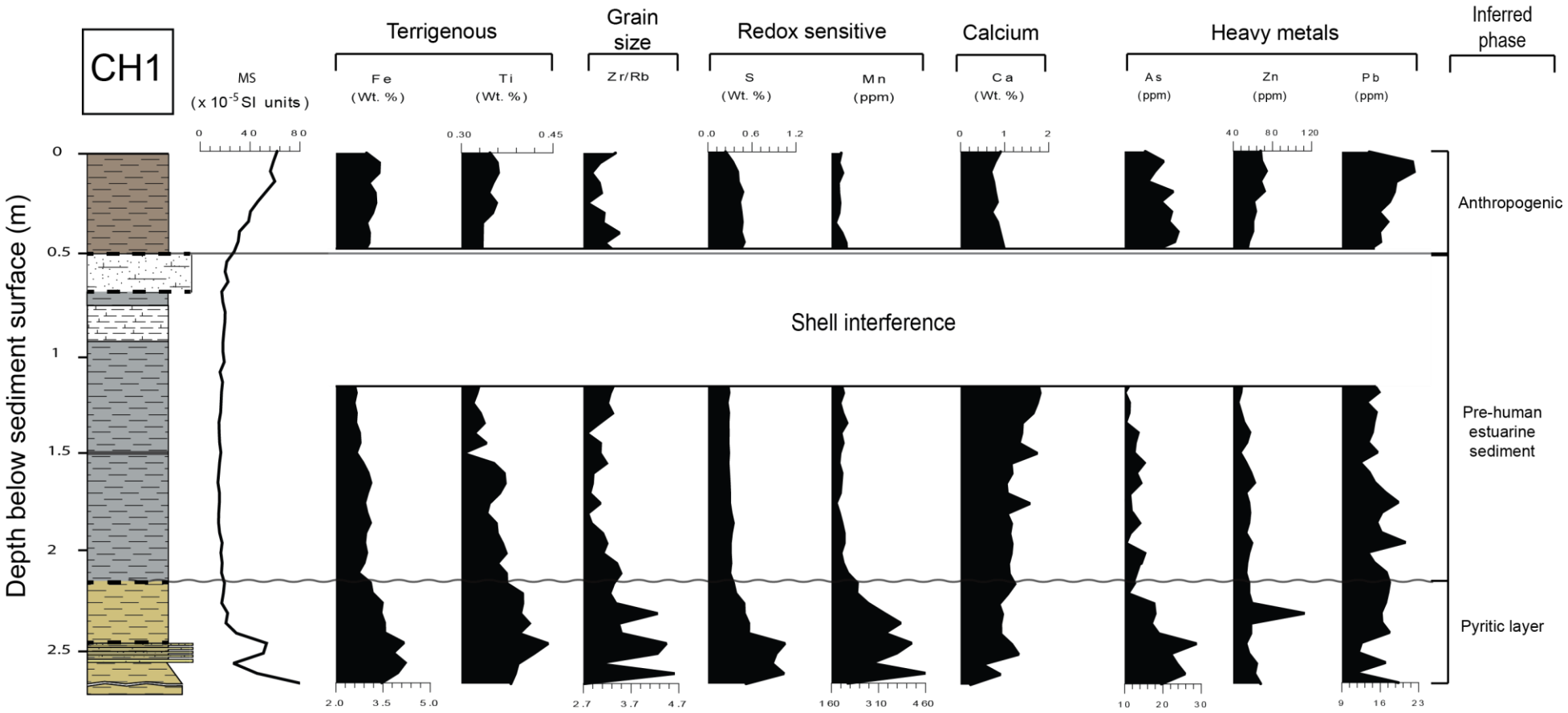

Fig. 4.18 – Down-core MS and geochemical data for core CH1.

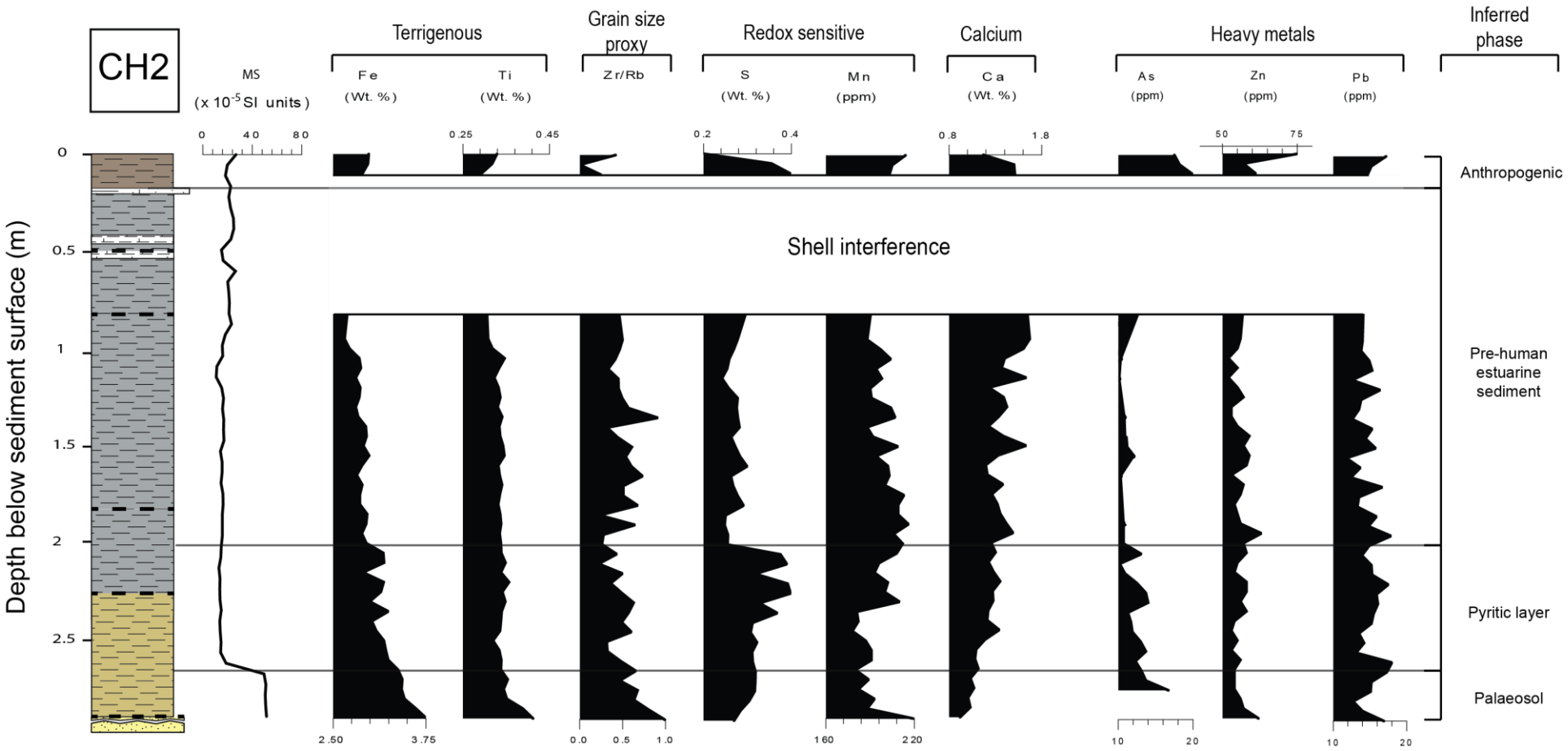

Fig. 4.19 – Down-core MS and geochemical data for core CH2. Elevated As values have been removed from depths > 2.75 m. These values are presented in Fig. 5.26.

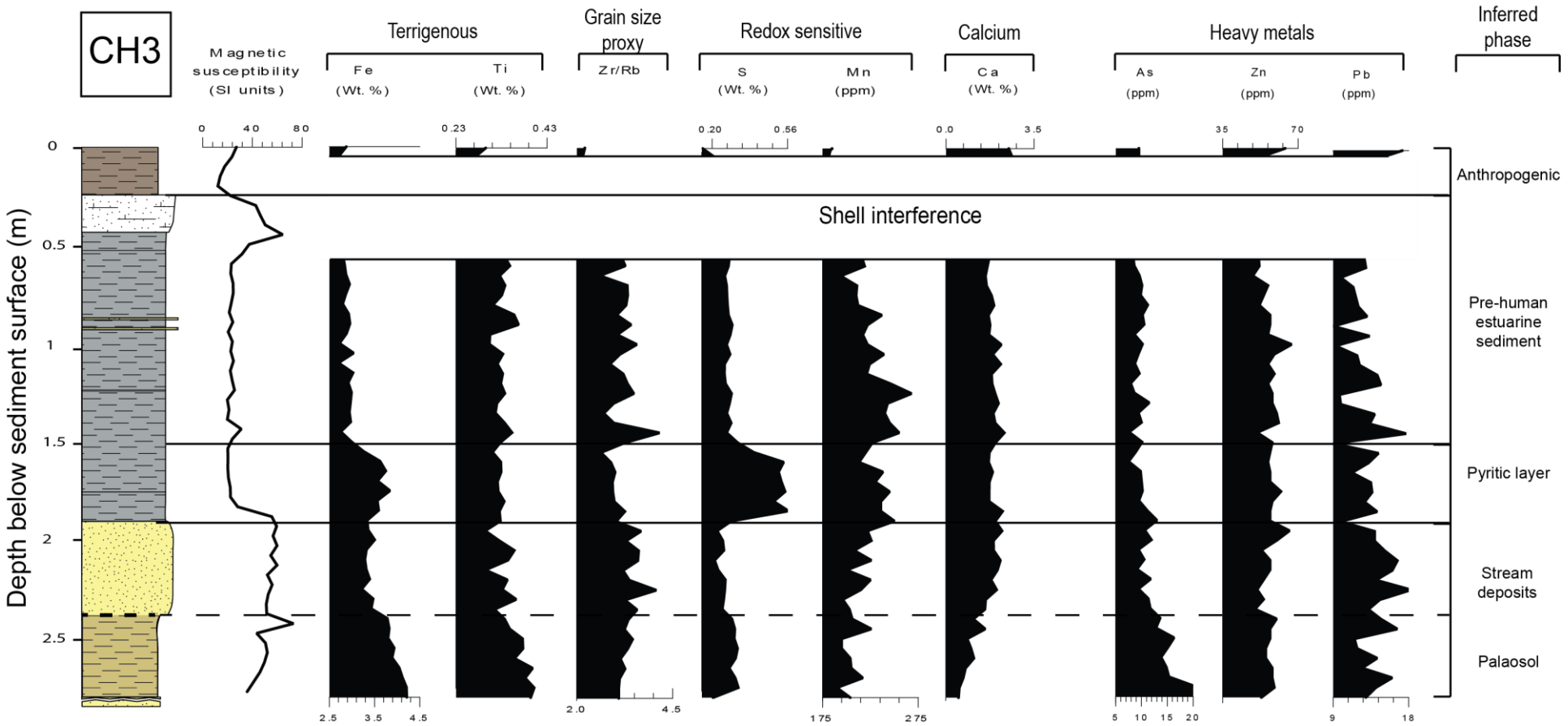

Fig. 4.20 - Down-core MS and geochemical data for core CH3. Dotted line identifies a gradual boundary between the high MS sand and high MS silt facies.

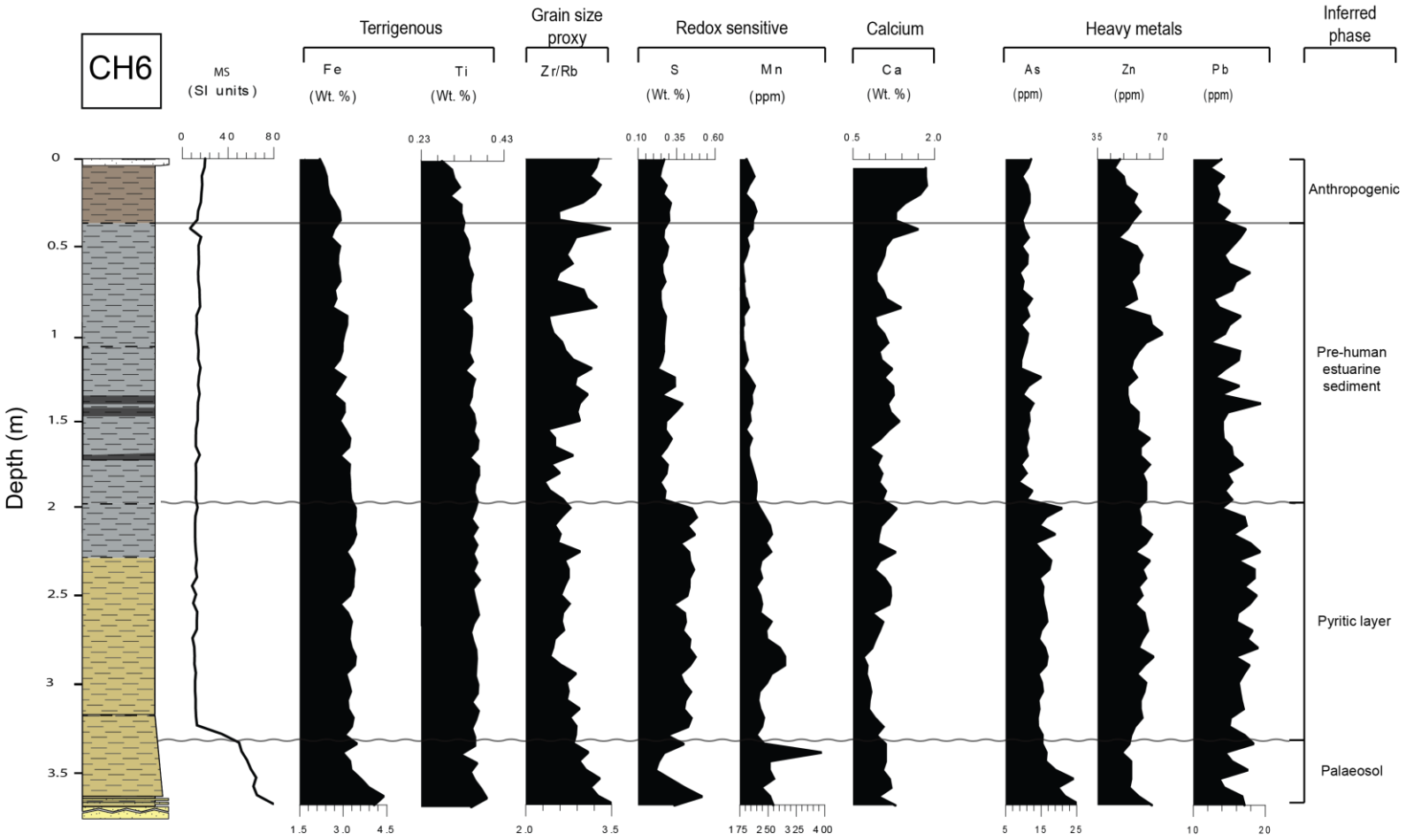

Fig. 4.21 - Down-core MS and geochemical data for core CH6.

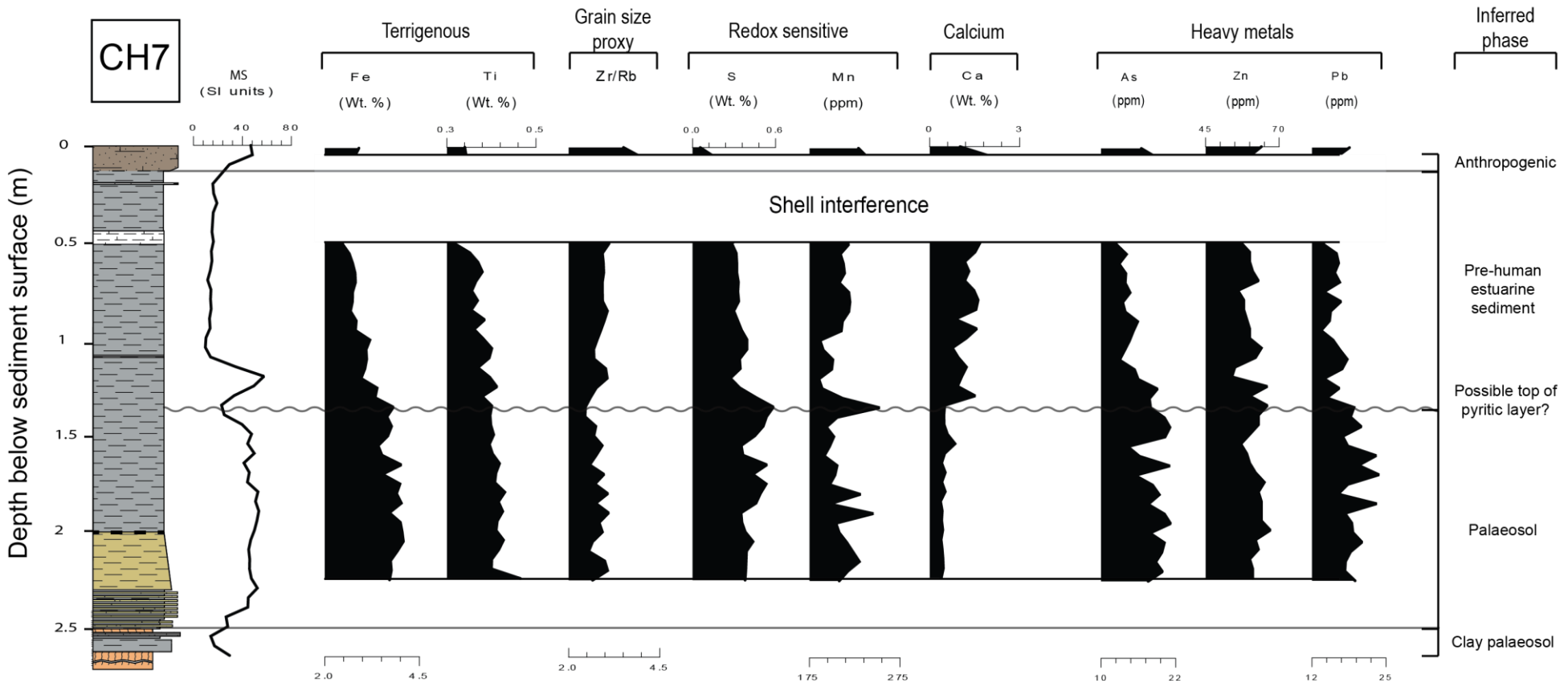

Fig. 4.22 - Down-core MS and geochemical data for core CH7. Geochemical data below ~2.2 m has not been presented here. This data is referred to in subsection 5.2.1

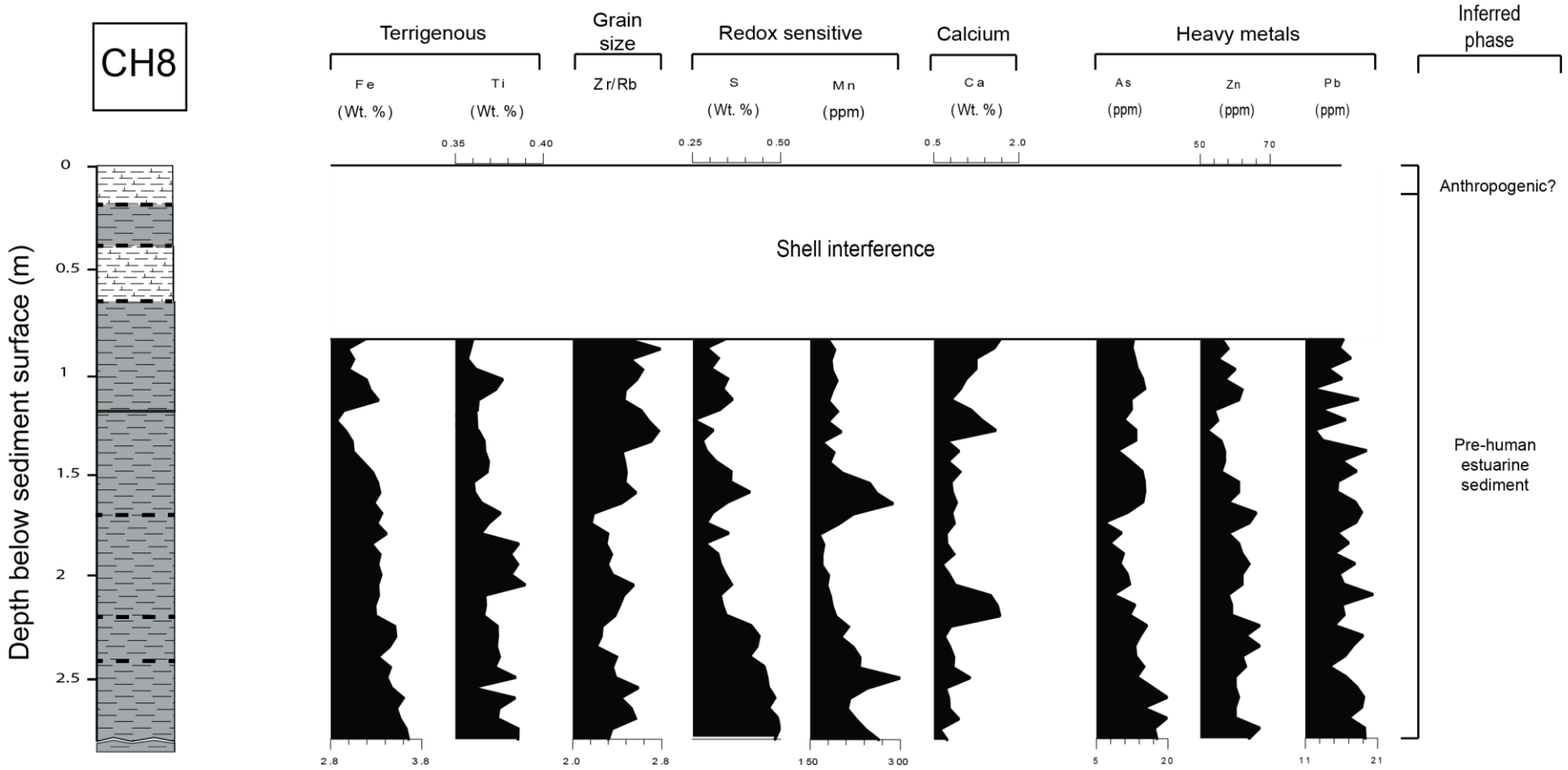

Fig. 4.23 - Down-core geochemical data for core CH8. Possible anthropogenic sedimentation has been inferred from anthropogenic sediment thicknesses from nearby cores.

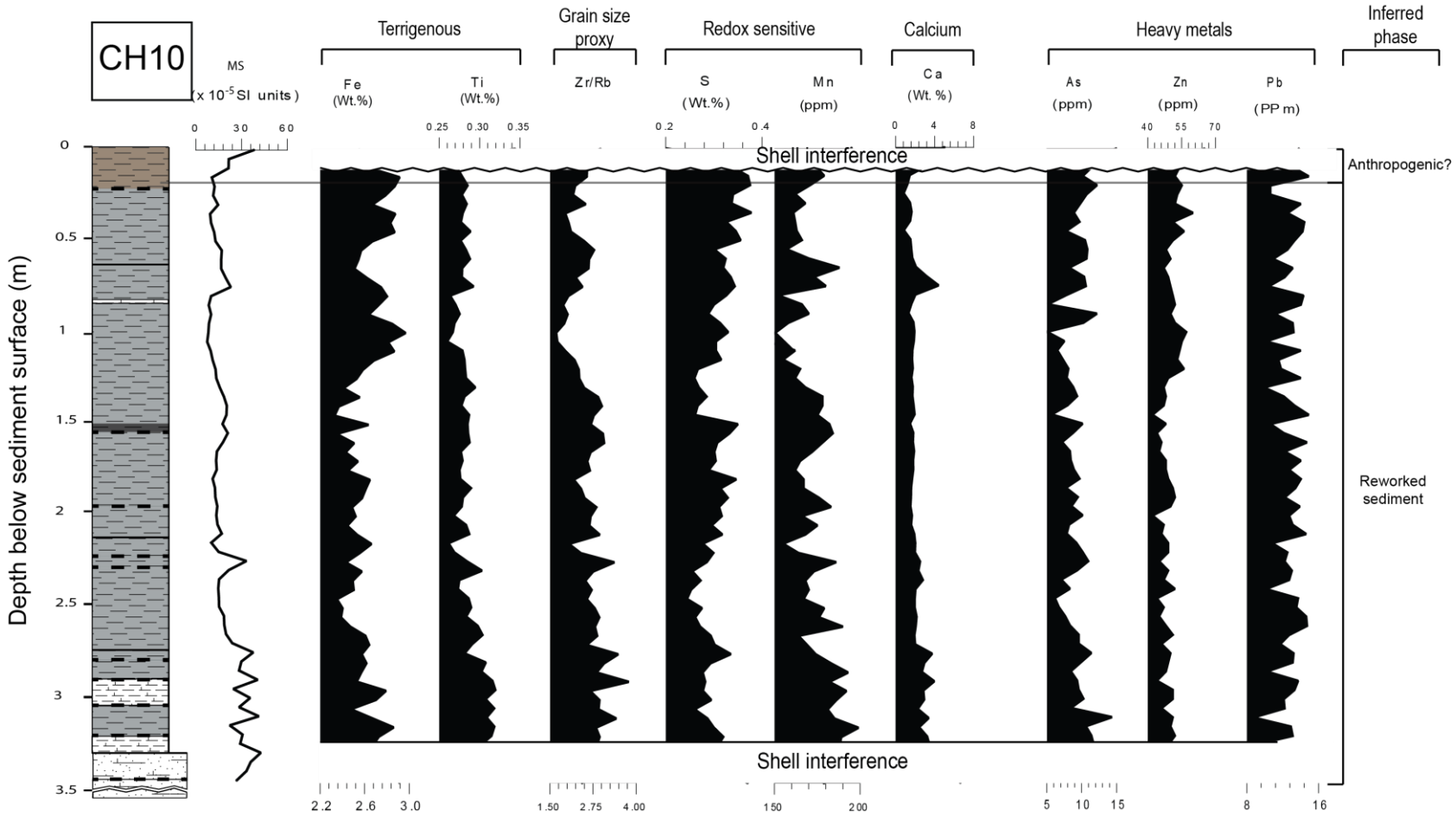

Fig. 4.24 - Down-core MS and geochemical data for core CH10. These sediments have been inferred as reworked in Chapter 6.

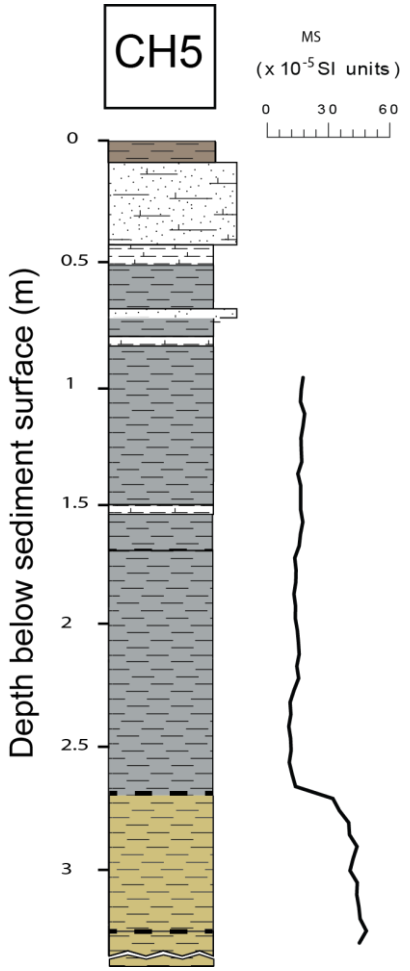

Fig. 4.25 - Down-core MS data for CH5. No geochemical data has been collected from this core and thus phases have not been interpreted for this core.

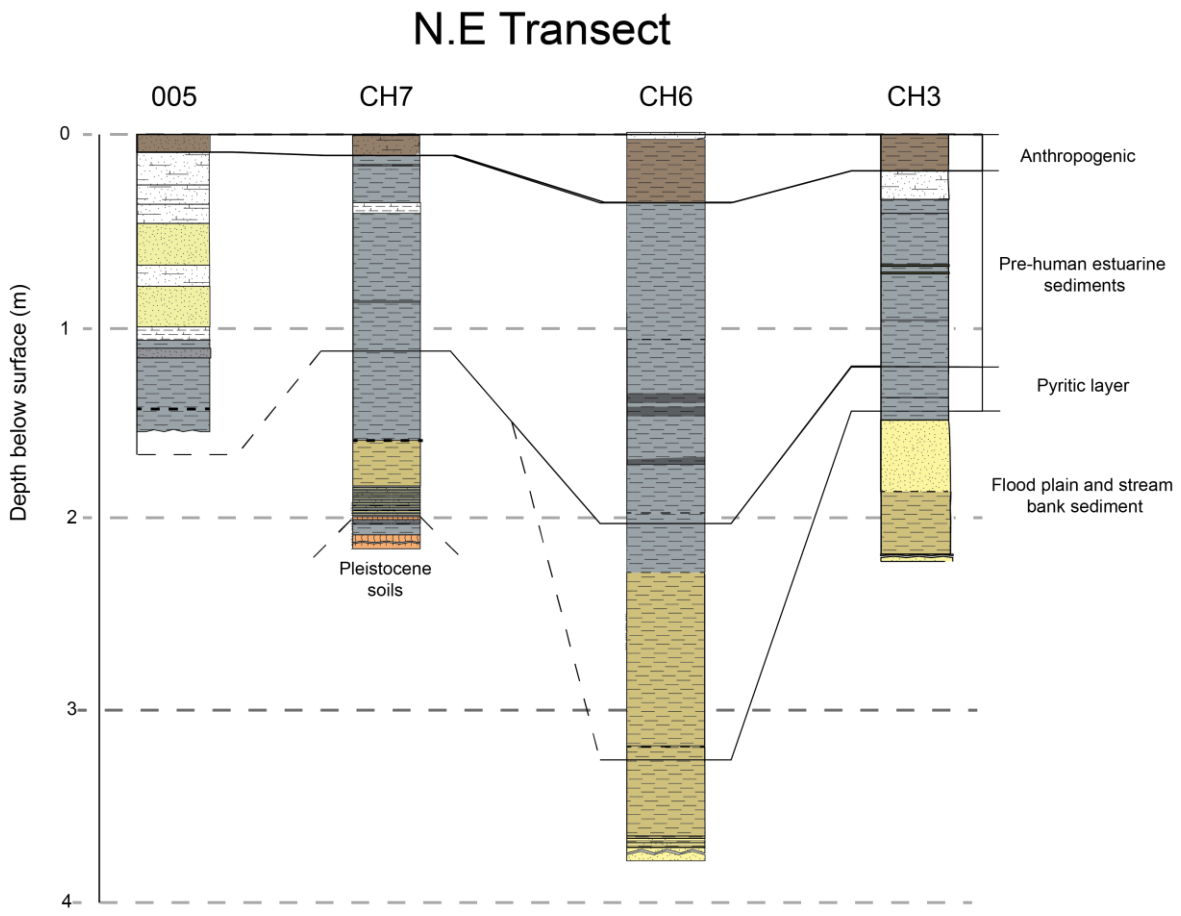

Fig. 4.26 – Spatial distribution of sediments across the NEmb transect. Intertidal regions (005) are on the left. Distance from the Whangarahi Stream increases to the right. Refer to Fig. 3.1 for transect map.

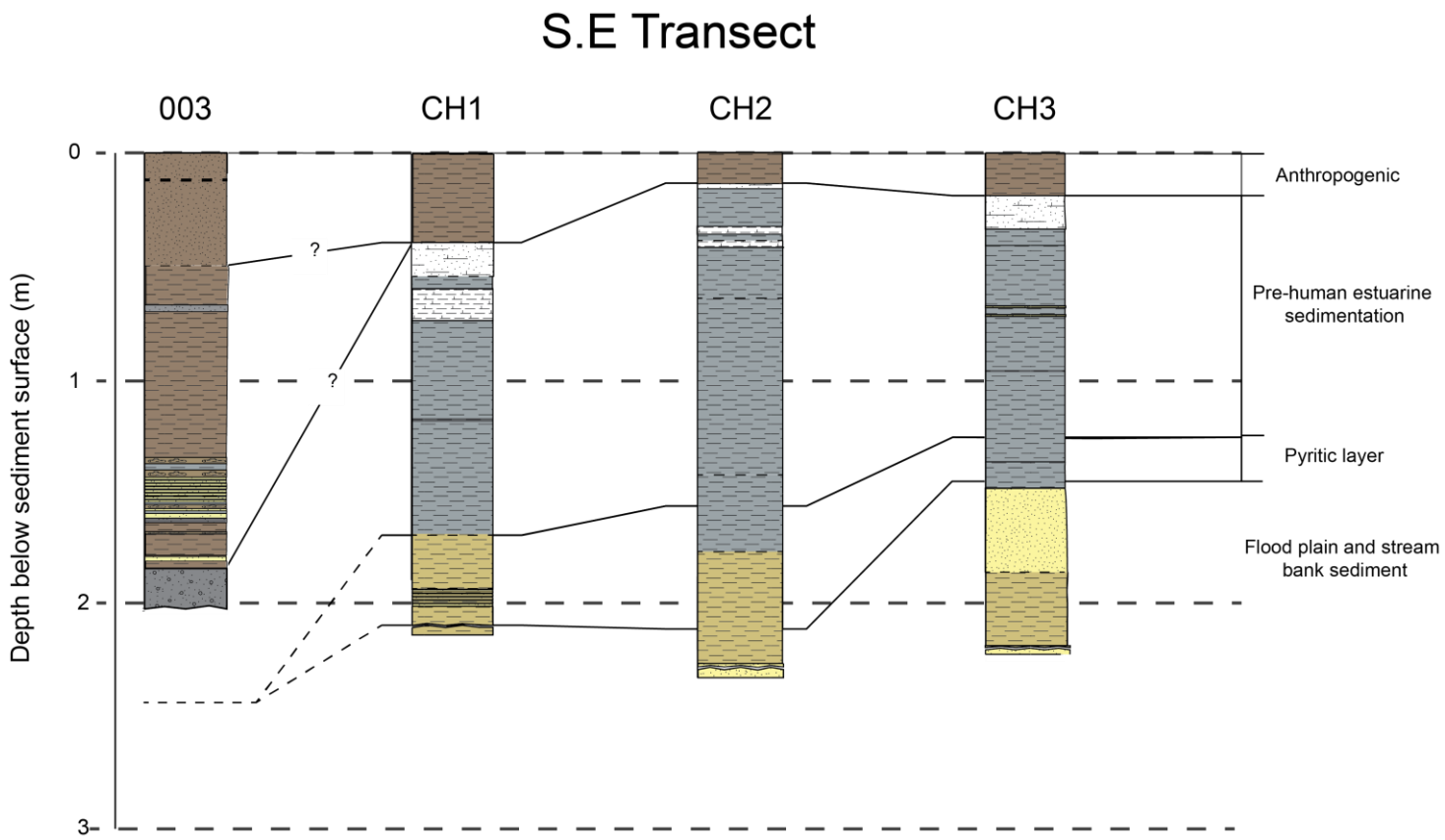

Fig. 4.27 - Spatial distribution of sediments across the SEmb transect. Note that this table includes core 003 which may represent secondary redeposition (see Chapter 6). Thus anthropogenic sediments have been inferred in the core are difficult to identify. Distance from the Waiau Stream increases to the right. Refer to Fig. 3.1 for transect map.

Chapter 5

Coromandel Harbour Facies Analysis

This chapter constructs a facies model for the Coromandel Harbour. First, the methods that are used to infer facies are described. Each facies identified is then described and interpreted in terms of sediment sources, transportation processes and diagenetic processes. A facies table is presented at the end of this chapter to summarise facies analysis interpretations.

Facies analysis is a way to categorise sedimentary rocks into groups based on sets of contrasting characteristics assumed to be related to processes of transport and deposition (Reading, 2000). Facies can be interpreted from observational, physical and chemical data (Reading, 2000). Here, facies analysis has been undertaken to infer changes in depositional setting in the Coromandel Harbour and allow for the distribution of sediments to be assessed. Facies analysis also assists in cross-correlation of sediments throughout the harbour. This, in turn, allows for the spatial and temporal distribution of sediments in the harbour to be interpreted.

5.1 Methods

5.1.1 Grain size analysis

Grain size is a powerful analytical tool that can be used to interpret sediment transport, provenance and weathering processes. Grain size also serves as a correlative measure between cores, as corresponding sedimentary facies that have undergone similar weathering and depositional processes usually share similar textural characteristics.

Samples were sieved to 2 mm and set into individual test pots. The samples were saturated with a water and Calgon solution and placed in an ultrasonic bath for 30 minutes. Disaggregated sediments were measured for grain size distribution with a Malvern 2000 laser sizer (Fig. 5.1).

Fig. 5.1 - Malvern 2000 laser sizer

Grain size distributions were compared to assist in facies analysis. Grain size was also used to infer sediment transport and diagenetic processes in anthropogenic sediments vs. pre-human sediments.

Grain size data were interpreted by plotting the sediment volume (concentration of a grain size) of each grain-size interval against the central point of that interval. This created graphs such as Fig. 5.13. The Malvern instrument reports raw data in 'sizes in-between', where a volume is calculated between two grain size points. Essentially, the instrument measures volume in grain size bins. A narrow bin is present at 10 µm. This bin is typically observed as a marked decrease in the height if the bar plotted at 10 µm compared to bars representing the wider bins on either side. The Malvern instrument software processes the data in such a way as to smooth this marked decrease. Raw data has been used here, and thus the marked decrease is still present. This is an artefact of the measurement system, and is not truly representative of the grain size. The trough that occurs at 10 µm has not therefore been taken into account during facies interpretation.

5.1.2 Mineral analysis

The majority of materials moving into Coromandel estuaries are derived from the catchment sources (Mead & Moores, 2004). Therefore, minerals within Coromandel Harbour sediments can be used to infer catchment erosion processes and sediment sources. The composition of fine-grained sediments is difficult to identify in hand specimen and is therefore best observed using thin sections. Here,

mineralogical analysis is used in conjunction with grain size to define facies and infer sediment provenance and weathering processes.

Dried sediment samples were placed into rectangular aluminium foil reservoirs and mixed with epoxy resin. Set resin blocks were removed from aluminium foil and ground down to expose a flat, clean sediment surface. The sediment surface of each block was glued to a frosted glass slide, labelled and left to set. Mounted blocks were then ground down to 4 microns thick or until the interference colour of quartz reached 1st order white. Each thin section was then petrographically examined using a Nikon microscope. Mineral type, shape, relief and size were noted for each thin section. Mineral assemblages were estimated from the abundance of each mineral viewed under a 20 x magnification.

The characteristics and assemblages of each thin section were subsequently compared across cores to help define sedimentary facies and interpret sediment provenance and weathering processes.

5.1.3 Bulk density

10 cm^3 cylinders were pressed into each core and carefully removed to ensure minimal sediment disturbance (Fig. 5.2). Excess material was removed, ensuring all sediment was held within the cylinder of known volume. Samples were weighed, dried at 50^oC for 48 hours then reweighed. Dry bulk densities were calculated by dividing dry mass by the volume of the cylinder.

Fig. 5.2 - A cleaned 10cm^3 bulk density sediment sample sitting next to its collection location. Gaps throughout the core represent 5 cm spaced subsampling locations.

Shell matter restricted bulk density measurements being made on shell beds. Thus, bulk densities for facies with high shell concentration have not been gathered.

5.1.4 Magnetic susceptibility

In sedimentary geology, magnetic susceptibility (MS) serves two main purposes. First, MS is a quick, non-destructive means of correlating across cores (Dearing, 1994). Sediments that have undergone similar processes of transport, deposition and diagenesis will tend to have similar magnetic characteristics. Applying correlation between the cores allows for sedimentation variability to be interpreted, as well as allowing relative and absolute dates to be interpolated across core samples. Secondly, the method is also a powerful palaeoenvironmental indicator that can be used to infer changes in sedimentary environments (e.g. palaeosol formation, sea level rise) (Richter *et al.*, 2007), where changes in catchment erosion, transport and mineral deposition and alteration can be observed as fluctuations in the magnetic susceptibility record.

5.1.4.1 Background science

All materials, synthetic or organic, exhibit natural magnetism. MS is the quantitative measure of the 'magnetization' of a material when induced by a small magnetic field. Inducing a magnetic field around a material generates a magnetic response within that material, as its magnetic constituents react to the field, either strengthening or weakening it. When the magnetic field is removed, the material reverts to its original non-magnetized state. Measuring the response of the material to the magnetic field gives its magnetic susceptibility, a value that is presented as a dimensionless SI unit, κ.

Sediments are not homogeneous, but rather tend to be a collection of heterogeneous lithics, minerals, organic detrital particles and biogenic materials. All of these constituents contribute to the net MS of a sediment. A sediment's net magnetic susceptibility can therefore be defined as the sum of its various components. The primary influence on sediment MS is the proportion of ferromagnetic (iron) minerals (O'Reilly, 2012). The broad background science of

mineral magnetics is well developed in literature (see Dearing, 1994, O'Reilly, 2012) and is therefore not discussed here.

5.1.4.2 Methods

The natural magnetic properties of minerals can be altered by elevated temperatures (Dearing, 1994; Kletetschka, Hruba, & Nabelek, 2015). To avoid alteration of natural mineral magnetics, samples were dried at a low temperature of 60^{o}C for 24 hours. Dried samples were placed into pre-weighed plastic pots and reweighed to collect sediment specific weight. All magnetic susceptibility measurements were taken from homogenised (refer to 5.1.5.2 for homogenising methods), room temperature samples of >4 g dry weight. Low frequency magnetic susceptibility (χ_{LF}) was measured using a Barrington MS2B device. MS measurements can be affected by background electromagnetic interference and changes in temperature (Dearing, 1994). Measurements were conducted in a Waikato University campus glasshouse away from any significant source of electromagnetic radiation where background magnetism was low. Temperature was measured throughout measurements, with no more than 2^{o}C variation occurring during measurement periods.

Two known magnetic susceptibility standards, 10 cm^3 water and 10 cm^3 $MnCO_3$, were measured before measurement of sample batches to ensure the MS2B device was accurately measuring between batches. Air measurements were taken before and after each sample measurement. A reference sediment sample was measured every 20 samples to identify any device or background magnetic drift through the testing period. At the end of each measurement batch, the susceptibility standards were again measured to further identify magnetic drift and background radiation.

Background air readings for each sample were averaged and subtracted from the sample magnetic susceptibility to correct for background magnetic interference. The MS2B device is calibrated to measure samples with a weight of 10 g. The weights of all measured samples were <10 g, therefore MS measurements were corrected to the calibrated mass as follows:

$$Corrected\ magnetic\ susceptibility = \frac{M_S \times C_M}{S_M}$$

Where M_S is measured low frequency MS in SI units, C_M is the calibrated mass of 10 g, and S_M is the sample mass in grams. Once the corrected mass had been calculated for each subsample, magnetic susceptibility was plotted against depth below surface for each analysed core.

MS was interpreted alongside pXRF data to infer controls on sedimentation and support palaeoenvironmental interpretations. Down-core MS, pXRF and facies analysis data were also applied together to cross correlate sediments observed in core samples. Once cores had been correlated, age constraints could be interpolated across conformable facies in harbour sediments.

5.1.5 X-ray fluorescence (XRF)

XRF was used to identify geochemical variation throughout the Coromandel Harbour. The method was used alongside magnetic susceptibility and facies analysis to interpret the evolution of the harbour from the mid-Holocene to the present day. Heavy metal data from XRF is also used to estimate heavy metal contamination in surficial sediments and compare with pre-human baseline variability.

5.1.5.1 Background science

XRF is a method of analysing the elemental composition of a material through focused, artificial X-ray radiation. As primary beams of X-ray radiation are fired into a material, the electrons of atoms within the material are 'knocked' from their orbitals, generating an instability in the electron order of the specific atom. For the orbital structure to remain stable, an electron must move from somewhere else in the shell into the vacant position (Fig. 5.3) (Margui & Grieken, 2013). Energy will be released outwards during this transition in the form of secondary X-ray radiation (Fig. 5.3). The release of these secondary X-rays is termed *X-ray fluorescence* (Forwick, 2011).

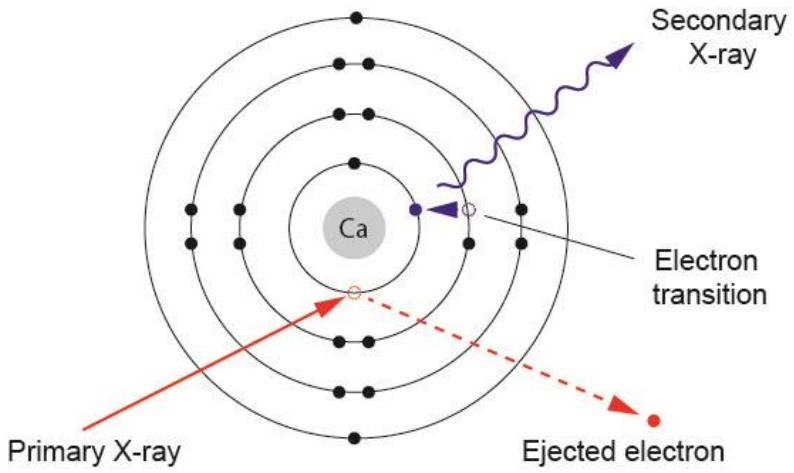

Fig. 5.3 - Simplified illustration of the XRF method being applied on a Calcium atom (Adapted from Forwick, 2011).

As a material is bombarded with primary X-rays, its elemental constituents will fluoresce a spectrum of secondary X-rays. The spectrum of energies released is directly related to the elemental composition in the sample (Rothwell & Croudance, 2015). This energy spectrum can be analysed with advanced computer software to estimate the elemental composition of any specific sample. Commonly, XRF data are presented in parts per million (ppm) or expressed as a percentage of total sample composition (weight percent, or wt.%).

5.1.5.2 Methods

Dried subsamples were homogenised to a semi-uniform grain size in a pestle and mortar and placed into plastic XRF pots (Fig. 5.4). Homogenising decreases analytical error in two ways. Firstly, sediments are thoroughly mixed to form a representative bulk sample. Secondly, average grain size is decreased, reducing inaccuracies derived from particle size limitations (Norrish & Hutton, 1969; Finkelshtein & Brjansky, 2009). Samples were analysed using a 50 KVa Olympus Delta Premium portable XRF (pXRF) mounted in a flexible stand (Fig. 5.4).

Fig. 5.4 - Top left/right - XRF pots filled with sediment. Bottom – A sample batch sitting next to 50kVa Olympus Delta premium pXRF.

The pXRF was calibrated with the Innovex systems calibration disk 316 at the start of each testing period. Four OREAS standards, 620, 621, 622, 623 and 624 were run at the start of each sample batch. A reference standard was run every 20 samples to monitor instrument drift. Measurements were made in soil mode.

5.1.5.3 Selection of paleaoenvironmental proxy elements

The elements iron (Fe), titanium (Ti), calcium (Ca), manganese (Mn), rubidium/zirconium (Rb/Zr) and sulphur (S) were chosen as palaeoenvironmental proxies for this study. These elements have characteristic environment-dependent variabilities that can be used to infer sea level changes, soil formation, changes in sediment delivery and anthropogenic influences in the catchment.

Fe is generally derived from terrigenous sources and often used to identify changes in terrigenous sediment delivery (i.e. erosion and transport) (Rothwell & Croudance, 2015). Fe is redox sensitive, and can be used to infer changes in redox conditions in conjunction with S and Mn (Sluijs *et al.*, 2009; Rothwell &

Croudance, 2015). Changes in redox conditions often occur during sea level change (Rothwell & Croudance, 2015). Changes in these elements may therefore be used to infer mid-Holocene sea level rise following mid-Holocene present mean sea level (PMSL) variability in the Coromandel Harbour. Similarly to Fe, Ti is chiefly associated with catchment sources. Unlike Fe, however, Ti is redox-insensitive, arguably making it a more robust indication of terrigenous-sourced sedimentation in the harbour (Rothwell & Croudance, 2015). A comparison of redox-insensitive Ti with redox-sensitive Fe allows for the degree of Fe reduction to be accessed.

Zr/Rb is commonly applied in palaeoenvironmental investigations as a proxy for grain size. Rb is primarily found in clays while Zr is typically found in coarser grained, erosion-resistant zircon grains (Rothwell & Croudance, 2015). Zr/Rb ratios can identify changes in catchment erosion processes and sediment delivery, where higher Zr/Rb ratios indicate higher-energy sediment delivery. Zr/Rb ratios may also be useful in identifying anthropogenic sediments, which are often coarser grained than pre-human sediments (Hume & Dahm, 1991).

Prior to mid-Holocene sea level rise, Ca inputs into soils are likely to have been primarily sourced from calc-alkaline catchment rocks. Following the onset of mid-Holocene PMSL and the initial formation of the Coromandel Harbour, the sources of Ca shifted to both catchment sources and biogenic Ca (shell) inputs. Ca concentrations are therefore expected to be elevated in estuarine sediments relative to pre-estuarine sediments (Rothwell & Croudance, 2015). Ca may therefore be used to interpret sea level rise and estuarine sediments.

5.1.5.4 Heavy metals

Anthropogenic sediments are typically enriched in heavy metals relative to pre-human sediments. Thus, heavy metals are often used to identify anthropogenic surface sediments in estuarine environments (Hume & Dahm, 1991; Reeve, 2008). The heavy metals arsenic (As), lead (Pb) and zinc (Zn) were of primary focus in this palaeoenvironmental investigation as their concentrations were above the detection limit of the pXRF throughout all harbour sediments.

5.1.6 Accuracy of pXRF measurement

The pXRF method is well known to have limitations that can reduce measurement accuracy (Rothwell & Croudance, 2015). Thus, it is necessary to identify the instrumental accuracy of these elements to ensure interpretations based upon the pXRF results are reliable.

To assess the reproducibility of pXRF analysis, five Ore Research and Exploration Standards (OREAS) with known elemental concentrations were analysed on the pXRF throughout every sample batch. After all sample batches had been run, all OREAS data was collated. The median pXRF measured value for each proxy element was calculated for each OREAS standard. Median values were compared to the certified OREAS lab values. Certified lab values are presented for various methods of identifying elemental concentrations in the standard. In this study, certified OREAS element values were chosen from the 4-acid method.

Linear correlations were plotted for each element and r^2 values used to assess the robustness of the correlation allowing for interpretation of how well the pXRF is reproducing against the certified concentrations. An r^2 value of one is a perfect linear correlation, Hall *et al.* (2014) classifies an r^2 value above 0.9 on the pXRF as excellent.

5.1.6.1 Results

5.1.6.1.1 Palaeoenvironmental proxies

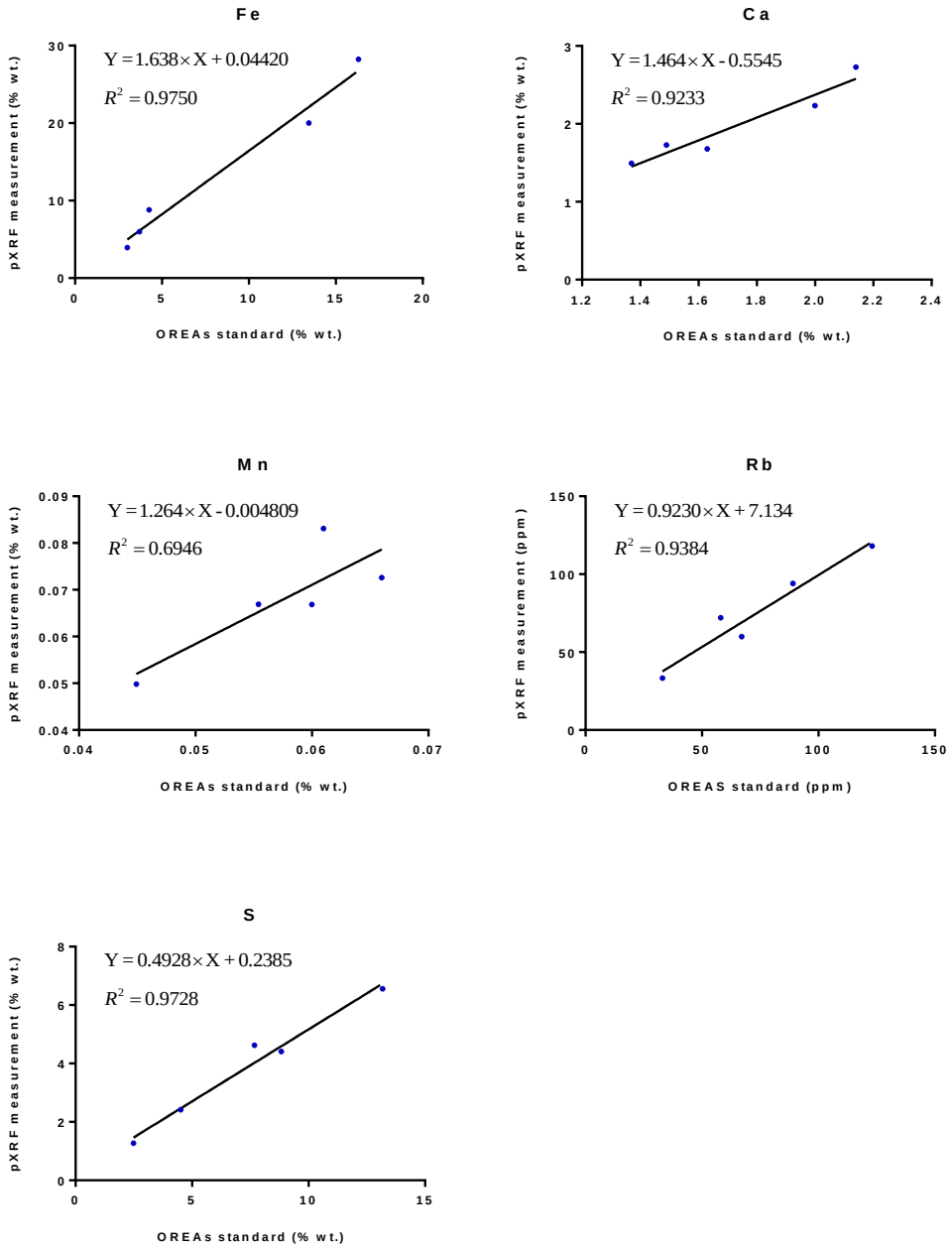

Fig. 5.5 - pXRF measurements vs. OREAS standard concentrations for elements Fe, Ca, Mn, Rb and S. Zr concentrations are not presented in the OREAS dataset and have therefore not presented

pXRF measurements of Fe, Ca, Rb and S compare well against the OREAS standards, having high R2 coefficients >0.92 (Fig. 5.5). Mn compares relatively poorly with a R2 coefficient of 0.69.

5.1.6.1.2 Heavy metals

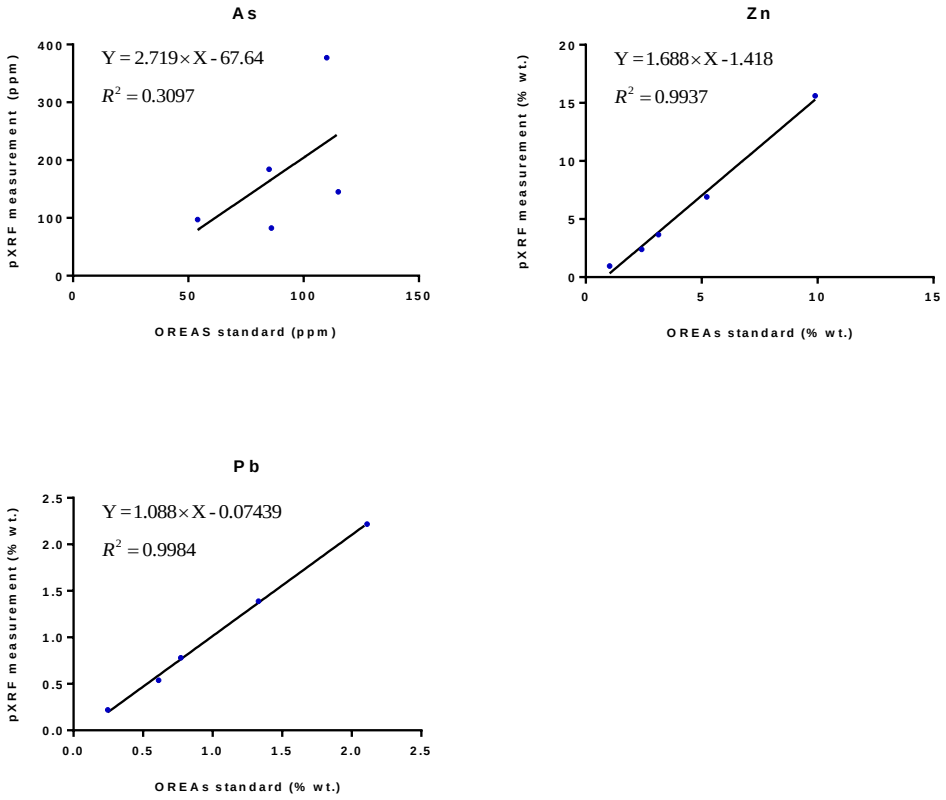

Fig. 5.6 - pXRF measurements vs. OREAS standard concentrations for heavy metals As, Zn and Pb.

Zn and Pb measurements compare very well with the OREAS standards at high concentrations. As measurements compares very poorly to the OREAS standards (Fig. 5.6). This is not unexpected, as the standard concentrations of As are low and likely near pXRF detection limits.

The concentrations of As, Zn and Pb are low (generally <50 ppm) throughout Coromandel Harbour sediments, lower than the concentrations identified in the OREAS measurement accuracy analysis above (see Fig. 4.18 to Fig. 4.24). To estimate the reproducibility of low-concentration heavy metal pXRF analysis, a single sample was re-measured 25 times (Table 5.1). This allowed for the standard deviation of heavy metal measurements to be assessed. pXRF detection limits for each element were calculated by multiplying the standard deviation (S.D) by three (Le Vaillant *et al.*, 2014).

Table 5.1 - Mean, Standard deviation and detection limits of As, Zn and Pb calculated from 25 measurements of a single sample. Values rounded to one decimal place.

Element	Mean (ppm)	Standard deviation (ppm)	Detection limit (ppm)
As	23.3	3.2	9.6
Zn	75.2	10	30
Pb	20	3.1	9.2

Detection limits are around 10 ppm for As and Zn and 30 ppm for Pb. pXRF measurements are well known to become inaccurate near detection limits, thus, we see relatively high standard deviations compared to mean measurements (Le Vaillant *et al.,* 2014; Rothwell & Croudance, 2015). The majority of harbour sediments analysed have similar heavy metal concentrations to this sample (see subsections 4.1.2 and 4.1.3), thus, measurement S.D is likely to remain relatively constant.

5.1.6.1.3 Interpretation

Proxies of Fe, Ti, Ca, Mn, and S are found at relatively high concentrations throughout the harbour and are expected to have consistently high pXRF accuracy. Mn is to be used qualitatively in conjunction with Fe and S. Rb/Zr accuracy is unclear, and is therefore used in conjunction with other terrigenous proxies to infer changes in terrigenous sourced sedimentation. Therefore, slight measurement inaccuracies associated with the element are not a significant issue.

Heavy metals As, Zn and Pb within harbour sediments are near the detection limit of the pXRF and have low measurement accuracies. To account for measurement inaccuracies, a margin of error of 1 S.D. is associated with all heavy metal data presented. Despite relatively high S.D.s, intracore trends of heavy metal elements are likely to be qualitatively reliable. Where heavy metals are used to interpret contamination enrichments in further Chapters, samples will be averaged to remove single measurement variability errors.

5.1.6.1.4 pXRF limitations associated with biogenic shell

Biogenic Ca is abundant around shell beds. High Ca concentrations generate a significant shift in geochemical matrix of analysed sediments. The pXRF device will measure very high concentrations of Ca, however, the signal of other elements will be reduced or diluted relative to the Ca concentration (MacDonald, Harper & Zhu, 2006; Spofforth, Pälike, & Green, 2008). This is termed a "dilution effect" (MacDonald, Harper & Zhu, 2006) and is often highlighted through the subsequent Chapters where pXRF datasets are interpreted. Dilution effects will distort the true non-Ca composition of the analysed sediment, and are not comparable with other sediments that have not had the same dilution effect.

In this study, Ca dilution effects are observed at Ca concentrations >2 wt.% pXRF datasets have been ignored where Ca has exceeded a threshold of 2 wt.% to remove interpretation errors. An exception of this in the case of contamination enrichment in Chapter 7, as dilution does not adversely affect contaminant enrichment interpretation.

5.2 Facies Analysis and Interpretation

A number of depositional facies for the Coromandel Harbour have been inferred from observational, physical and geochemical characteristics. Inferred facies and depositional environments have been supported by absolute and relative age data and literature review.

A significant amount of data has been collected from each facies. Presenting all of this data under analytical sections (e.g. mineralogy or grainsize) would be difficult to interpret. Thus, for simplicity, all data for each facies is presented under specific facies subheadings. Facies are organised in order from the lowermost facies observed to the uppermost facies observed. Some data within this section are presented graphically with some specific values identified in text. All the raw data used to produce the figures and tables in this Chapter can be found in the Appendix.

5.2.1 Laminated sandy clays

Laminated orange and grey sandy clays occur at the bottom of core CH7 (Fig. 5.7). Fine (<1 mm) particulate organic matter is common through this facies. A single interval of black laminated medium sand (similar to the black laminated sand facies, see Section 5.2.8) is found within this facies. These sediments were identified as sandy clay loams in hand specimen. This facies is comprised of predominantly clays and silts with some VF to VC sand (Fig. 5.8). This facies has the highest clay content of any facies in the harbour. These clay loams are often contained within blocky to euhedral peds (i.e. soil clumps).

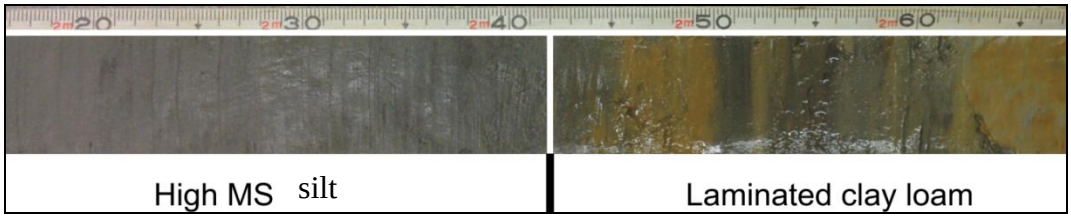

Fig. 5.7 - High MS silt overlying the laminated sandy clays in at the bottom of CH7.

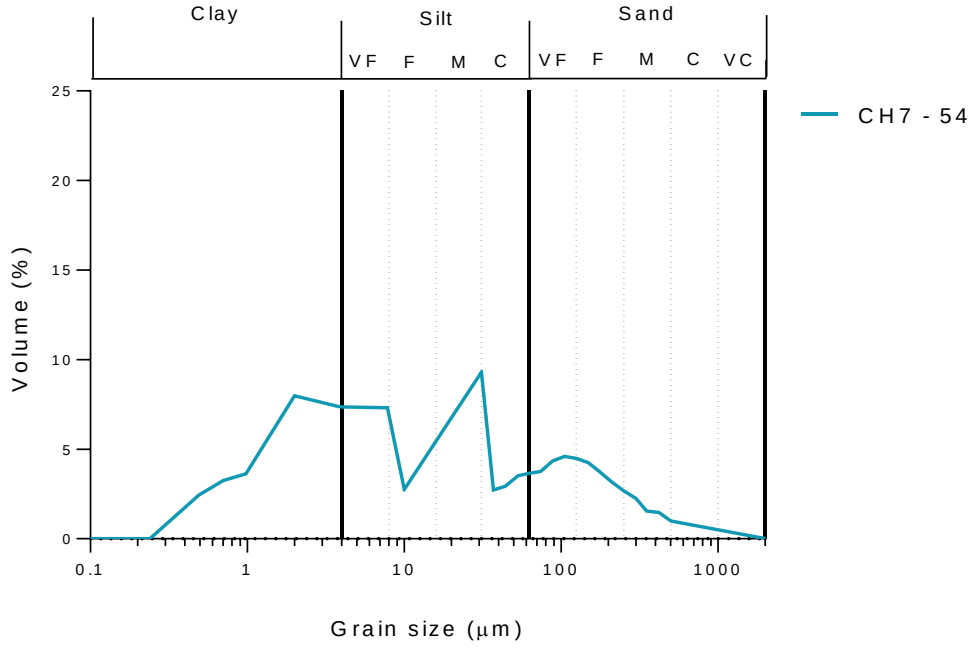

Fig. 5.8 - Grain size distribution for the laminated sandy clay facies.

Greater than 30% of this facies is comprised of extensively weathered, iron stained subangular to rounded mineral grains (Fig. 5.9). Around 30% of the facies is indistinguishable iron stained <2 µm matrix. Observable quartz and feldspar account for ~10% composition and are subangular, often fractured and highly weathered. Mineral opaques are blocky to subangular and account for ~6% composition. Weathered subangular to rounded biotite was noted at ~3% composition (Fig. 5.9).

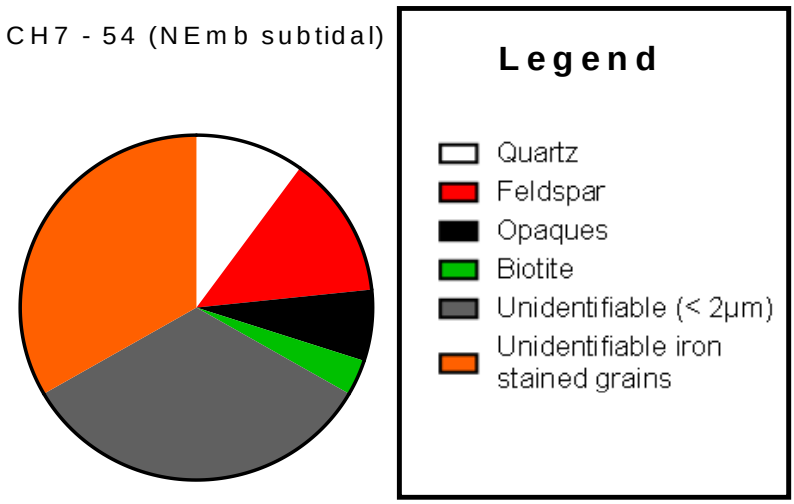

Fig. 5.9 - Estimated mineralogical composition of deeply weathered iron stained clay facies.

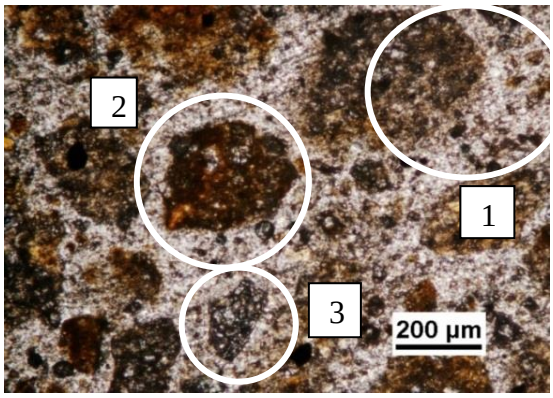

Fig. 5.10 - Thin section photograph of CH7 – 54 taken at 4 x magnification including a feldspar crystal (3), a unidentifiable stained mineral (2) and a highly weathered quartz mineral (1).

This facies has high elemental variability. Concentrations of Fe and Ti are elevated compared with all other facies (Figs. 5.11, 5.24). Concentrations of As and Zn are highest in this facies (Fig. 5.11)

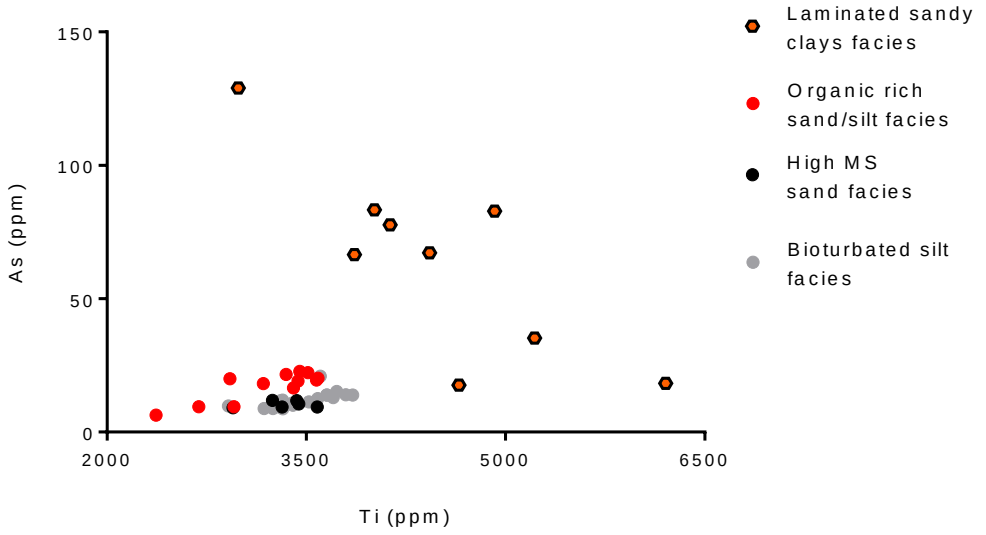

Fig. 5.11 - Concentrations of As against Ti for several facies. Note the high concentrations of As and Ti in the laminated sandy clays facies.

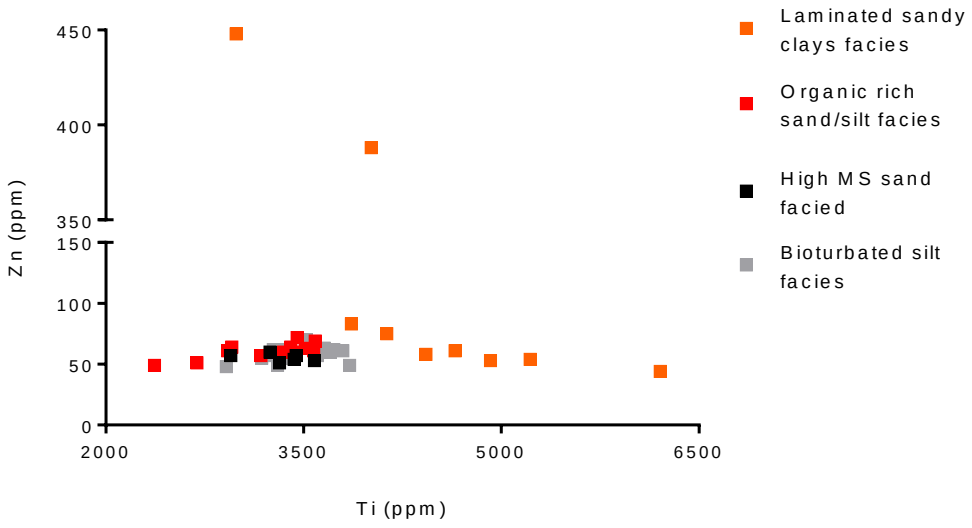

Fig. 5.12 – Concentrations of Zn . Note the high concentrations of Zn and Ti in the laminated sandy clays facies. The two highest Zn concentrations are associated with a grey clay loam lamination in the laminated sandy clay facies.

5.2.1.1 Interpretation

Clays are most typically associated with terrigenous weathering and soil-forming processes (Morgan, 1995). Minerals within this facies are stained with iron oxide. Iron oxide coatings tend to develop during extensive weathering of iron-bearing minerals in aerobic conditions (Cornell & Schwertmann, 2003) Thus, it is likely these sediments developed in a subaerial environment. This conforms with the observation of elevated Ti and Fe which are from terrigenous sources. This is further suggested by the ped structures in these clay loams, which indicate these sediments are likely palaeosols (Morgan, 1995). No dates have been collected from this facies, thus the age of this facies is not known. From the characteristics of the soil, we can, however, infer the possible depositional age of these sediments. Marine sediments that overlie this facies have been dated consistently at < c.7200 cal yr B.P (refer to Chapter 6 for dating). No further evidence of marine sediments older than Holocene age has been identified in this study. These soils must have therefore accumulated between the mid-Holocene advent of present mean sea level (PMSL) and the previous time sea level was at ~PMSL. It is likely that these soils were developed in a warm environment, where weathering and oxidation was rapid. Therefore, these soils have been interpreted as accumulating in the last interglacial period. Further discussion of the formation age of this facies is found in Chapter 8.

This facies has similar mineralogical characteristics to the Kuaotunu Group rocks within the catchment, which are therefore likely to be the parent material of these soils. Manaia Hill Group minerals are not observed in the sample analysed. This may be explained by the fact that this samples was taken from the NEmb catchment where there is little exposure of Manaia Hill Group rocks. The fine-grained nature of terrigenous sediment grains in this facies indicates low energy and/or extensive weathering. It is likely that some parent material is also CVZ and TVZ tephra. This is not developed upon further.

Clays are well known to attenuate heavy metals in sedimentary environments. (Lin, Z., & Puls, 2000; Cadena RizvI & Peters, 1990; Bailey et al, 1999). Fine-grained silicate clay minerals have a net negative charge that captures cations, such as heavy metal cations, from the environment (Lin, Z., & Puls, 2000; Cadena

RizvI & Peters, 1990; Bailey et al, 1999). This explains why the heavy metals As and Zn are markedly elevated in this facies. These heavy metals have likely been sourced from the weathering of mineral grains within the soils. Some water-soluble heavy metals may have also been transported into the sediment through overland flow processes. The processes with which heavy metals have been input into these soils is further discussed in Chapter 8.

5.2.2 High MS sands and silt facies

Sands and silts with high MS values overlie the laminated sandy clay facies in core CH7. High MS sands and silts underlie the high sulphur facies in most other subtidal cores (see core logs in subsection 4.1 in Chapter 4). These sediments are defined as a **high MS silt facies** and **high MS sand facies** due to their varying textural characteristics.

5.2.2.1 High MS silt facies

High MS silts are found in cores CH1, CH2, CH3, CH6, and CH7 (Fig. 4.19 to Fig. 4.22). Values of MS are around two to three times greater in this facies compared to the bioturbated silt facies (Fig. 5.14). Millimetre-scale laminations of organic matter are common lower in the facies.

High MS silts are predominantly clay to silts with some sand component (Fig. 5.13). One sample from this facies (CH3-52) has a coarser grainsize distribution with a VF/M sand component.

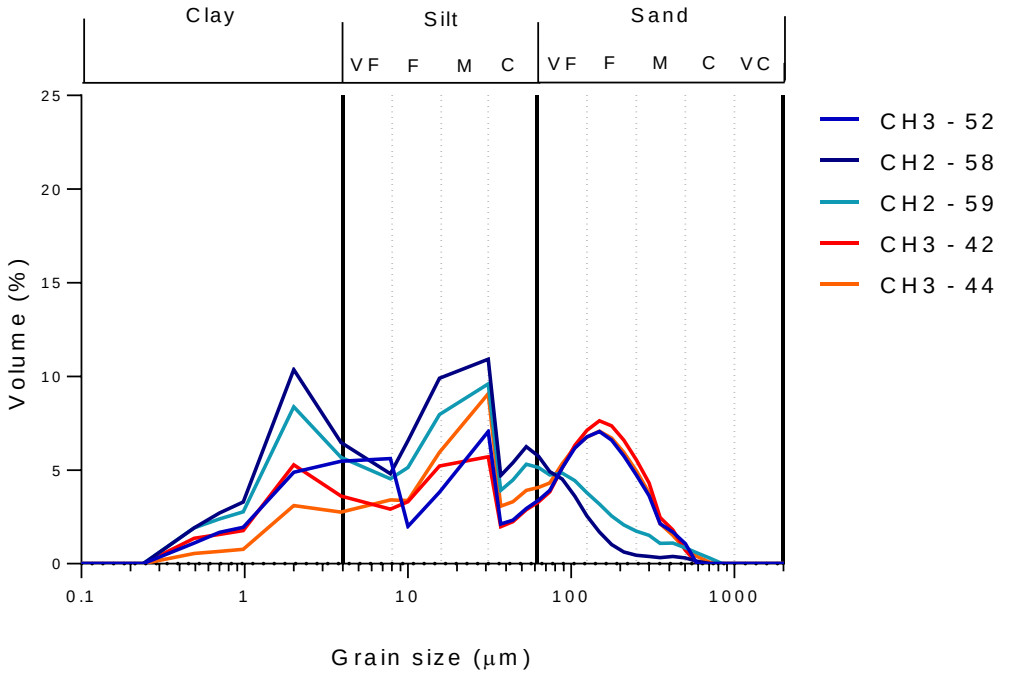

Fig. 5.13 – Grain size distribution for the high MS silt facies (blues) and high MS sand facies (reds).

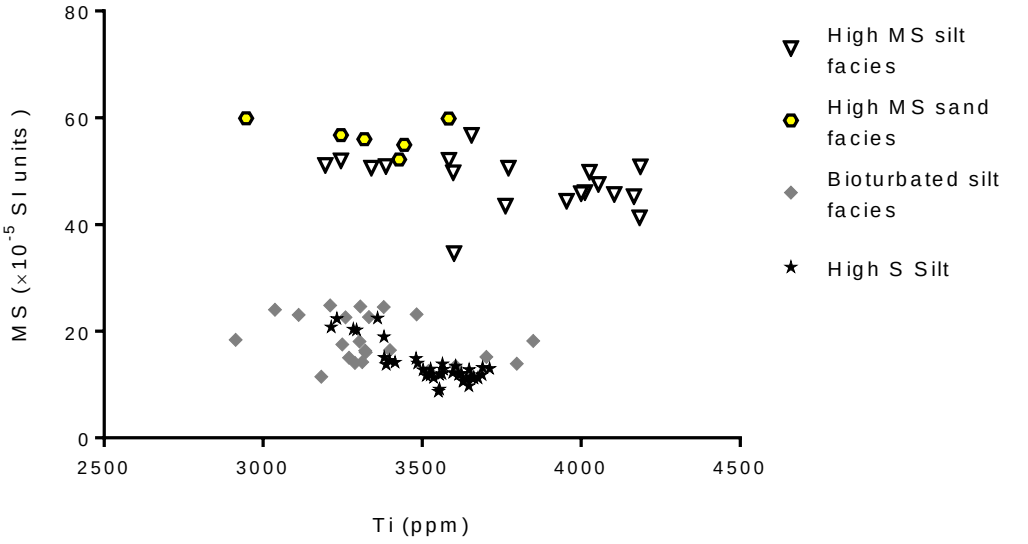

Fig. 5.14 – MS vs. Ti for the high MS sand facies, high MS silt facies, bioturbated silt facies and the high S silt facies.

Calcium concentrations are generally similar to or lower than 10000 ppm (1 wt.%) in this facies. These concentrations are lower than Ca concentrations in the bioturbated silts facies (Fig. 5.15).

This facies has variable Fe and Ti compositions that can exist at elevated concentrations compared to the bioturbated silt facies (Figs. 5.17, 5.19). Heavy metals As and Zn are typically enriched in this facies compared to the bioturbated silt facies (Figs. 5.26**,** 5.27)

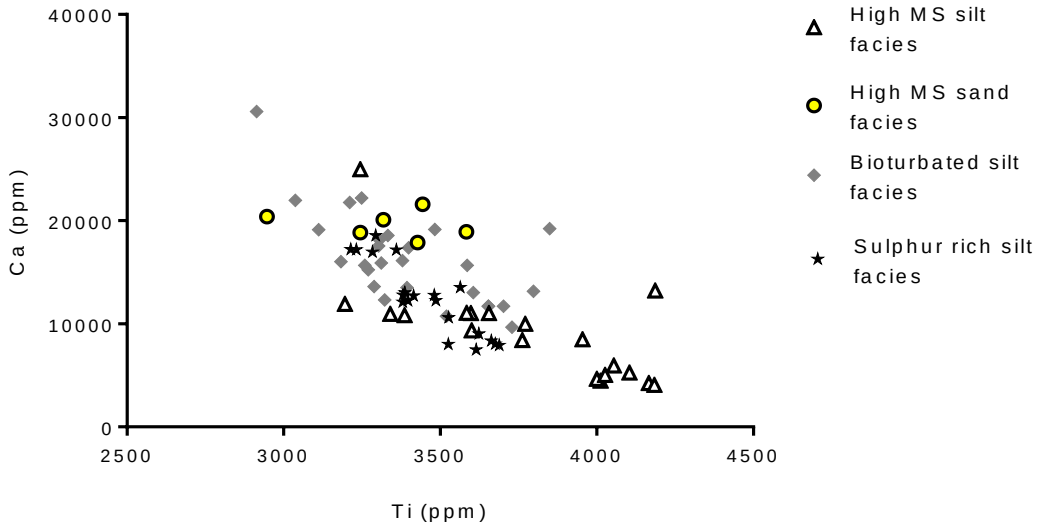

Fig. 5.15 – Ca vs Ti for the high MS sand and silt facies and the bioturbated silt facies. Values of high MS sand have been taken from the outlying occurrence of the facies in CH3.

5.2.2.1.1 Interpretation

Low concentrations of Ca and absence of biogenic shell suggests that these sediments are non-estuarine deposits. These sediments have a noteworthy clay component which is typically associated with soil forming factors, or the redeposition of older soils. High variability in Fe and Ti concentrations suggests a variable terrigenous sedimentation regime. These sediments underlie estuarine sediments that have been dated consistently <7200 cal yr B.P (refer to dating in Chapter 6). Consequently, these silts are interpreted as terrestrial sediments that were deposited prior to the advent of mid-Holocene PMSL in the Coromandel Harbour. Further discussion on the formation (and depositional ages) of these sediments can be found in Chapter 8.

These sediments often have interbedded thin laminations of organic matter and VF to F sand, characteristic of floodplain deposits. Prior to mid-Holocene PMSL in the Coromandel Harbour, the Whangarahi and Waiau Streams (and other smaller streams) most likely ran through their respective embayments and moved through the present-day inlet towards the ocean. These sand and organic lenses have been interpreted as cyclic flood deposits that have been deposited in a

floodplain setting. Sand lenses may have been intermittently deposited overtop of weakly developed soil sediments, and explain the high variability in the grainsize of these sediments and variability in Fe and Ti (i.e. terrigenous sedimentation). A more developed discussion of the formation processes of these sediments is found in Chapter 8.

5.2.2.2 High MS sand facies

Brown, clay to silt to F/M sands with High MS are observed in core CH3 (Fig. 4.20). This facies has a greater VF to M grainsize component compared to the high MS silt facies (Fig. 5.13). MS in this facies are ~60 × 10^{-5} SI units (Fig. 5.14). High MS sand has slightly higher MS values than the high MS silt facies (Fig. 5.14). Unlike the high MS silts, this facies has an elevated Ca concentration (Fig. 5.15).

5.2.2.2.1 Interpretation

Elemental and MS differences between this facies and the high MS silt facies are low which suggests that no significant shift in sedimentary environment has occurred between depositional periods. Ca is elevated in this facies compared to the high MS silt facies, which may suggest a marine influence, input of old shell or increased deposition of Ca rich terrigenous sediments. These sediments underlie estuarine sediments that have been dated consistently <7200 cal yr B.P, thus it is unlikely that these sediments have been influenced by recent marine material. Furthermore, no evidence of shell material was not noted in these sediments. It is most likely that the Ca has been sourced from calc-alkaline rocks in the catchment.

This facies is observed once in CH3 where it overlies the high MS silt facies. A coarsening in sediment size suggests an increase in environmental energy. The transition between inferred soils and this laminated, organic rich coarser sediment is indicative of fluvial processes. This facies has been interpreted as a stream deposit that has accumulated overtop flood plain deposits (high MS silt facies). This stream sediment may have been deposited in a stream channel in the floodplain setting or as a series of coarser flood deposits near a stream channel.

Further discussion of the accumulation of these stream deposits can be found in Chapter 8.

5.2.3 Sulphur-rich silt facies

Clay to silt with elevated concentrations of sulphur overlie the high MS silt and sand facies in CH1, CH2, CH3 and CH6 (Fig. 4.18 to Fig. 4.21). This facies underlies the bioturbated silt facies in these cores. This facies generally has a similar intracore grainsize to the high MS silt facies (Figs. 5.13, 5.16). This facies is predominantly clay to M silt in CH2 and clay to F sand in CH3 (Fig. 5.16). This facies shares similar intracore grainsize distributions with the high MS silt facies. Millimetre scale laminations of organic matter are common throughout this facies. During core splitting of cores containing this facies, a strong H_2S (rotten egg) smell was noted.

MS in this facies is nearly identical to the bioturbated silt facies (Fig. 4.18 to Fig. 4.21). Fe and S in this facies are highly correlated (Fig. 5.18). CH1 is an outlier in this trend (Fig. 5.18). High correlations between Fe and S are not observed in the organic rich sand/silt, bioturbated silt or high MS silt/sand facies (Fig. 5.19). S exists in elevated concentrations compared to intracore MS silt and bioturbated silt facies (Fig. 4.18 to Fig. 4.21). Mn is elevated compared to the high MS silt facies (Fig. 5.17). Ti is elevated in this facies compared with the bioturbated silt facies (Fig. 5.17).

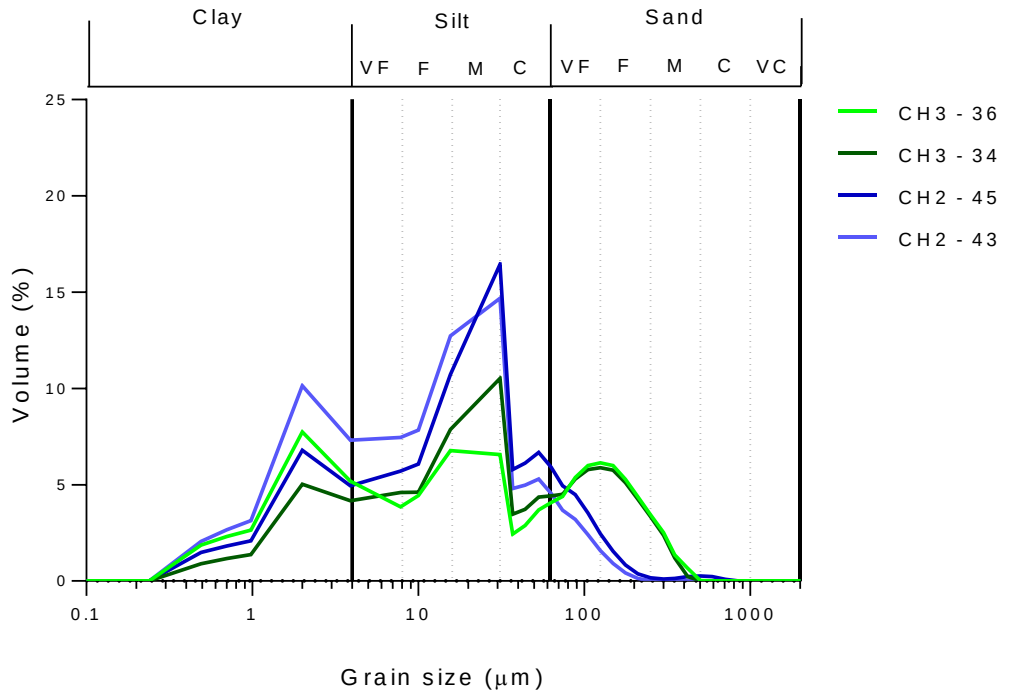

Fig. 5.16 – Grain size distribution for the sulphur -rich silt facies in cores CH2 and CH3.

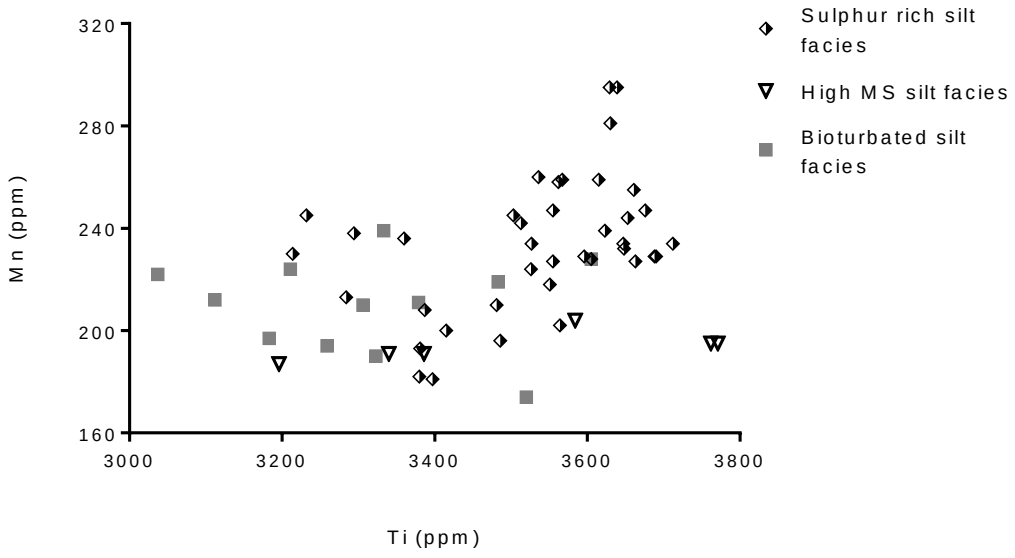

Fig. 5.17 – Mn vs. Ti for the high S silt, high MS silt and bioturbated silt facies.

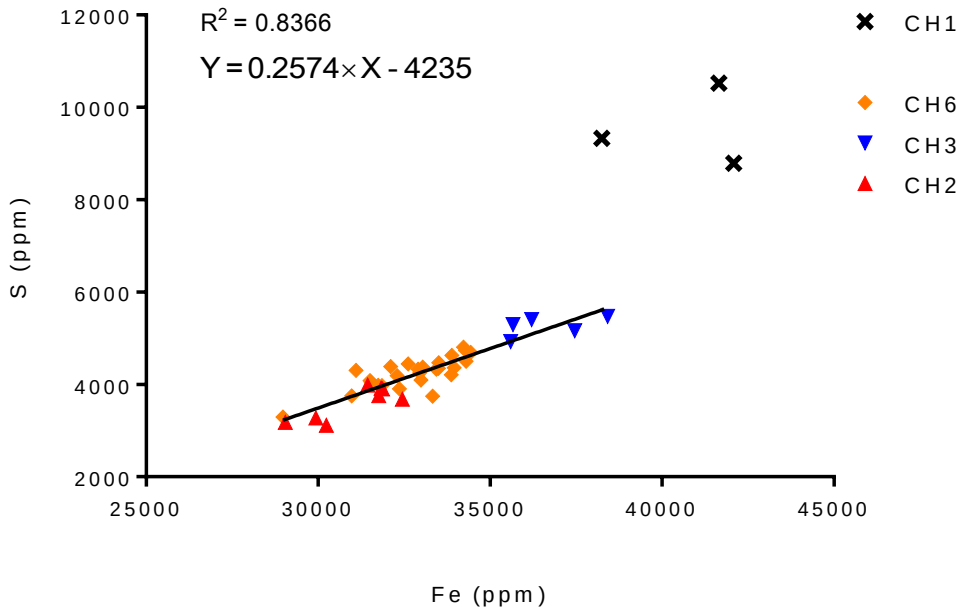

Fig. 5.18 – Intracore S vs. Fe for the high S silt facies. A linear regression for all cores except for CH1 is presented.

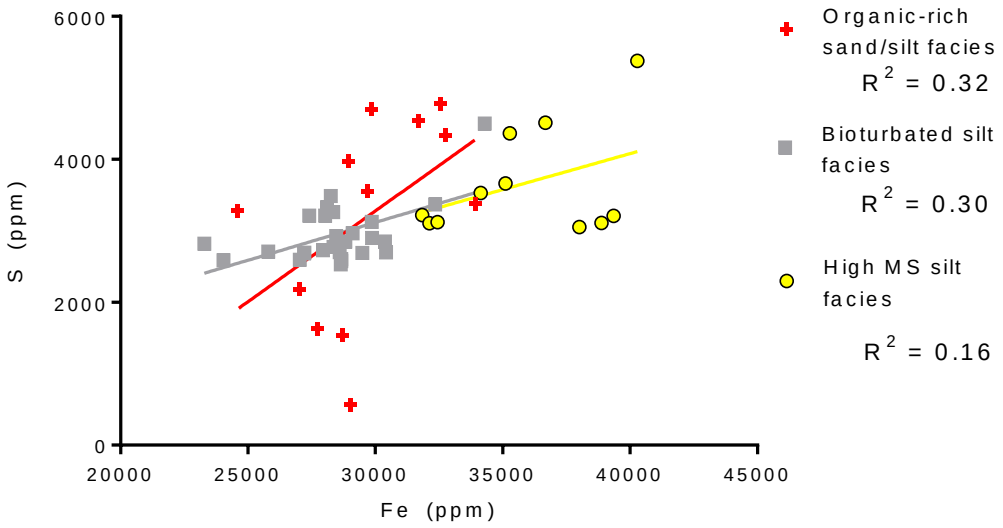

Fig. 5.19 – S vs. Fe for the organic rich sand/silt, bioturbated silt and high MS silt facies.

In CH1, CH2 and CH3, the facies has a thickness of ~0.5 m. In CH6, however, the facies has a thickness of ~1.3 m (Fig. 4.18 to Fig. 4.21).

5.2.3.1 Interpretation

Fe and S are highly correlated in this facies, where these elements are likely intimately related. This facies is well defined by S and Mn enrichment, which suggests a change in redox conditions between this facies and the high MS silt facies (Fig. 4.18 to Fig. 4.21). Oyster shell 30 cm above the top of this facies in CH3 has been measured with an age of c.7100 cal yr B.P (Table 6.1). This shows that these sediments developed prior to c.7100 cal yr B.P, or around the sea level rise in the Coromandel Harbour at c.7500 cal yr B.P.

This facies has been interpreted as a pyritised layer that developed at the onset of PMSL at c.7500 cal yr B.P. Pyritic sediments formed as bacteria in anaerobic tidally inundated sediments converted sulphate from oceanic waters and Fe from sediment to pyrite FeS_2 (DER, 2015). Through pyritisation, S and Fe in these sediments became highly correlated (Fig. 5.18). The change in redox conditions was likely induced by anoxic conditions following marine inundation and creation of a restricted marine environment. This pyritisation likely initially occurred in the inundated high MS silt facies. Thus, apart from redox-sensitive elements, geochemistry between these two facies are similar (Fig. 4.18 to Fig. 4.21). Some pyritisation may have occurred in early estuarine sediments. This is further discussed in Chapter 8.

Under aerobic conditions, pyrite will oxidise and be released as iron sulphate, $FeSO_4$ and sulphuric acid, H_2SO_4, Haematite, Fe_3O_4, sulphur, hydrogen sulphide (rotten egg smell), H_2S and a range of other Fe and S complexes (DER, 2015). This likely explains why a rotten egg smell was noted during core splitting. The boundary between the high MS silt facies and the pyritic layer is marked by a sharp decrease in MS (Fig. 4.18 to Fig. 4.21). This change in MS has likely been induced by pyritisation, where the majority of ferromagnetic iron minerals in the sediment have been reduced to pyrite, which has a lower MS than net iron complexes in the high MS silt facies.

A more developed discussion of the formation processes of this facies can be found in Chapter 8.

5.2.4 Blue/green grey bioturbated silt facies

Blue grey/green grey/grey heavily bioturbated silts were the most commonly observed facies in the Coromandel Harbour (Fig. 5.20). This facies is primarily comprised of VF/C silt with some clay. Coarser grain populations with some F sand component are observed in intertidal areas and near the tidal inlet (Fig. 5.21). Within intertidal regions, this facies has a dry bulk density of 1.083 g/cm^3. Dry bulk densities are less in subtidal regions at 0.559 g/cm^3 to 0.989 g/cm3 (Fig. 5.43).

Fig. 5.20 – Blue/green grey bioturbated silt facies in at depths of 0.6-0.95 m in CH3. Note the absence of any bedding structures.

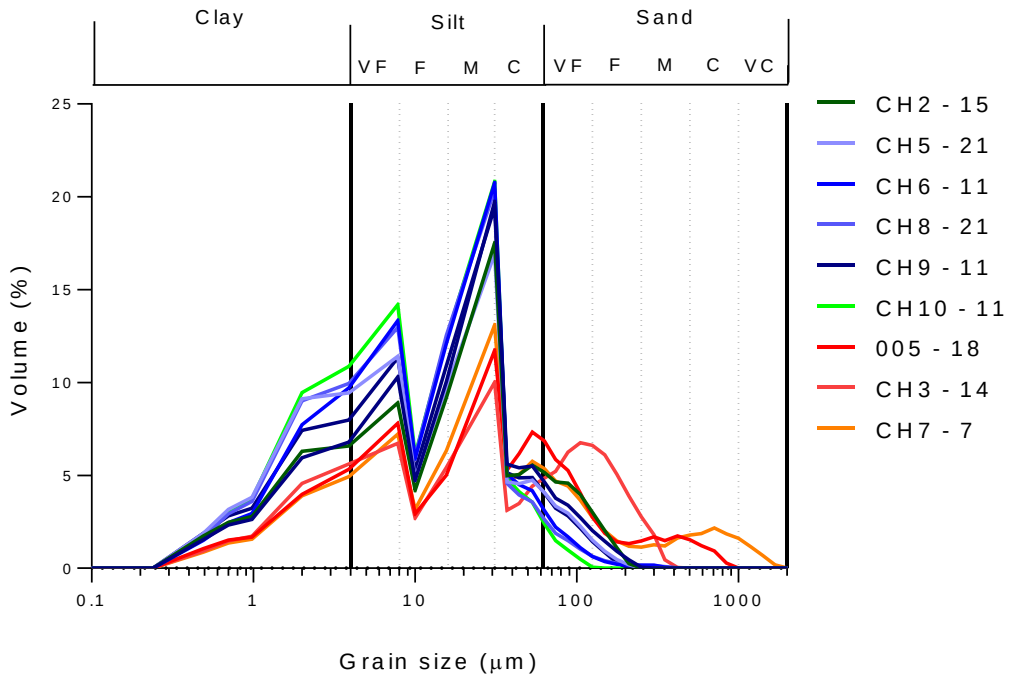

Fig. 5.21 – Grain size distribution of numerous bioturbated silt samples. Distributions in reds and oranges are from intertidal areas or near stream outwash zones. Distributions in blue and green straight lines are from subtidal regions.

In the subtidal regions, around 84–95% of this facies is an undistinguishable fine-grained silt matrix (Figs. 5.22, 5.23). Subangular to subrounded quartz and feldspar account for ~2% composition each. Angular to subangular shell fragments account for ~1% total composition. Opaque minerals account for >5% total assemblage (Fig. 5.22).

In the intertidal areas, 30–65% of the sediment is comprised of an undistinguishable silt grains, 10% each fractured, subangular to subrounded quartz and feldspar,~12% subangular shell fragments and ~5% opaque minerals. Volcanic glass was noted in 002–41. This may be derived from the laminated black sand facies. However, since these grains were not noted elsewhere in this facies, they are not further considered in this thesis. Opaques throughout the facies appear to be comprised of ~70% mineral grains and 30% organic fragments.

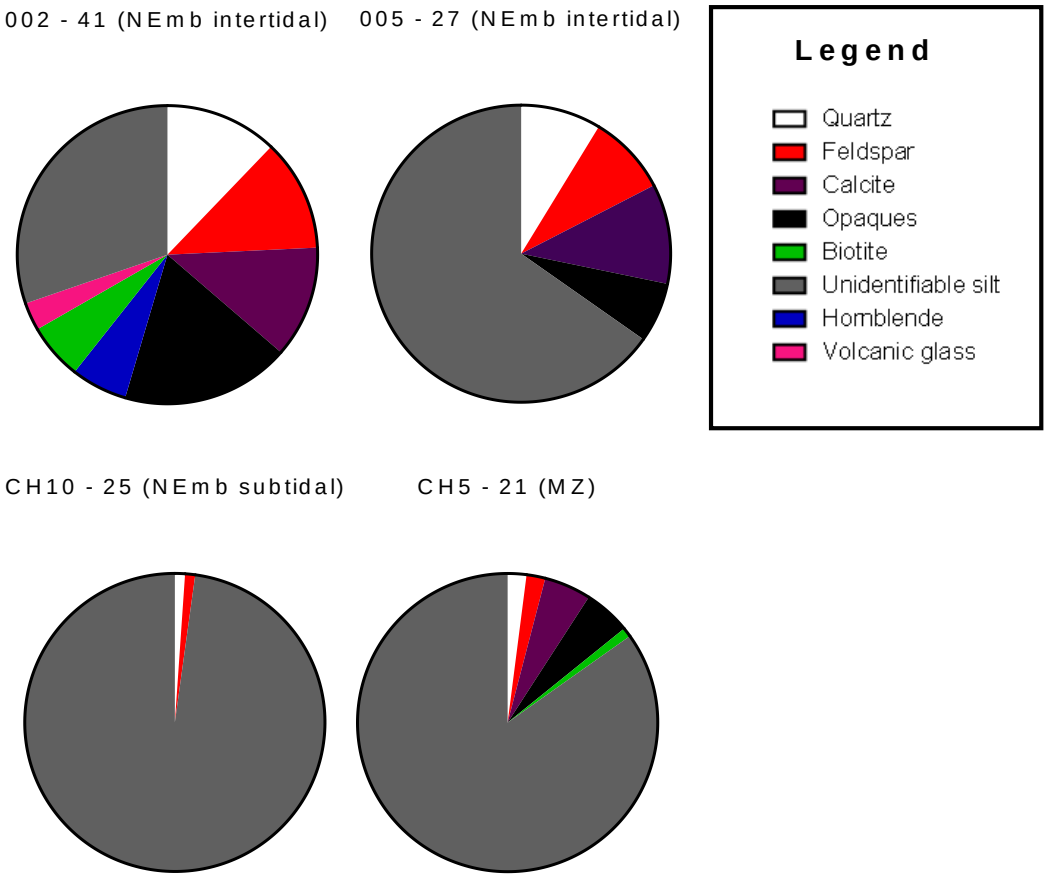

Fig. 5.22 - Estimated mineral assemblage for several samples from the bioturbated silt facies.

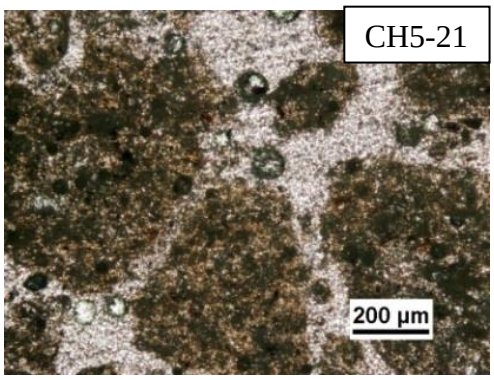

Fig. 5.23 –Thin section photograph of CH5 – 21 taken at 4 x magnification. Note the absence of any grains over ~50 µm.

The lowest harbour-wide MS values occur in this facies. MS has low (<5 x 10^{-5} SI units) intracore variability with MS values typically less than 25 x 10^{-5} SI units (Fig. 5.24).

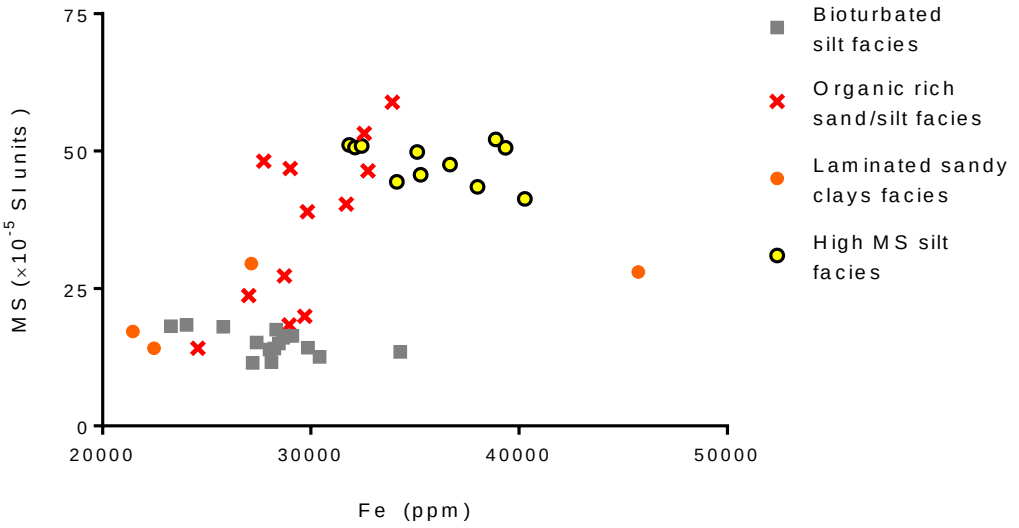

Fig. 5.24 - MS vs. Fe for several facies.

The bioturbated silt facies is characterised by low variability in elemental distribution. Fe and Ti have similar intracore concentrations throughout this facies as do S and Mn (Fig. 4.18 to Fig. 4.24). Ca can be variable, ranging from 1–2 wt.% (Fig. 5.15). This is likely to be primarily related to variability in the proportion of shell fragments throughout the facies. The lowest concentrations of heavy metals in the Coromandel Harbour are observed in this facies. As and Pb

are generally <20 ppm (Figs. 5.25, 5.26). Zn has concentrations range from 40 to 80 ppm (Fig. 5.27).

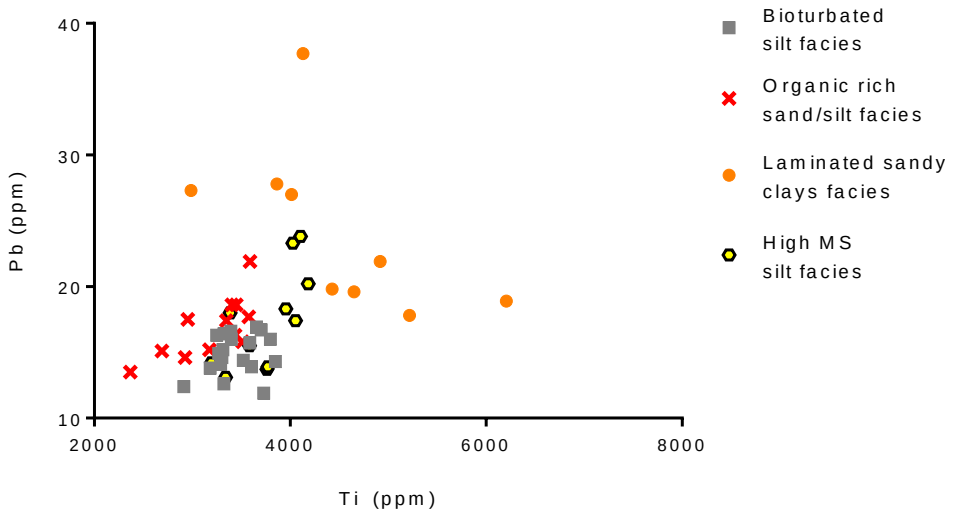

Fig. 5.25 – Pb vs. Ti for serval Coromandel Harbour facies.

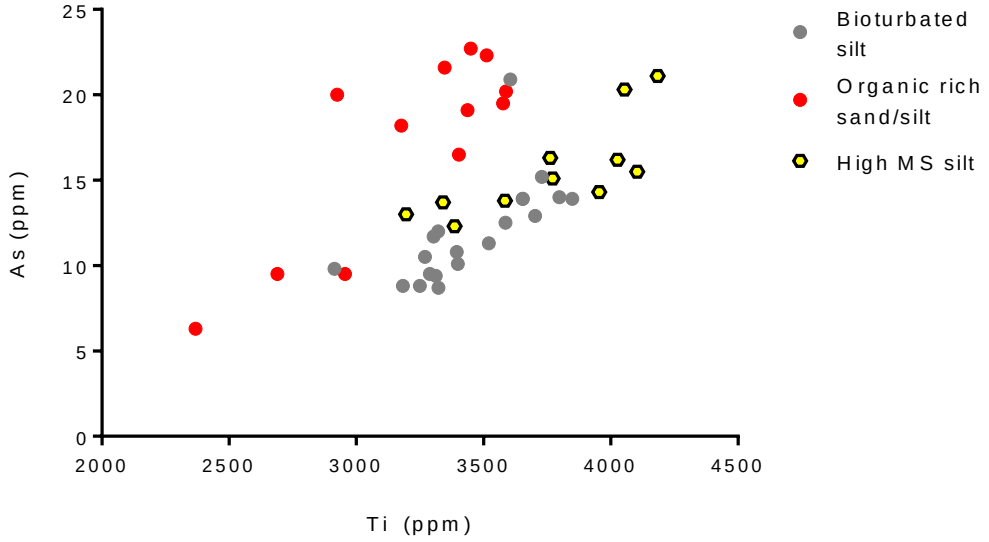

Fig. 5.26 – As vs. Ti for several facies.

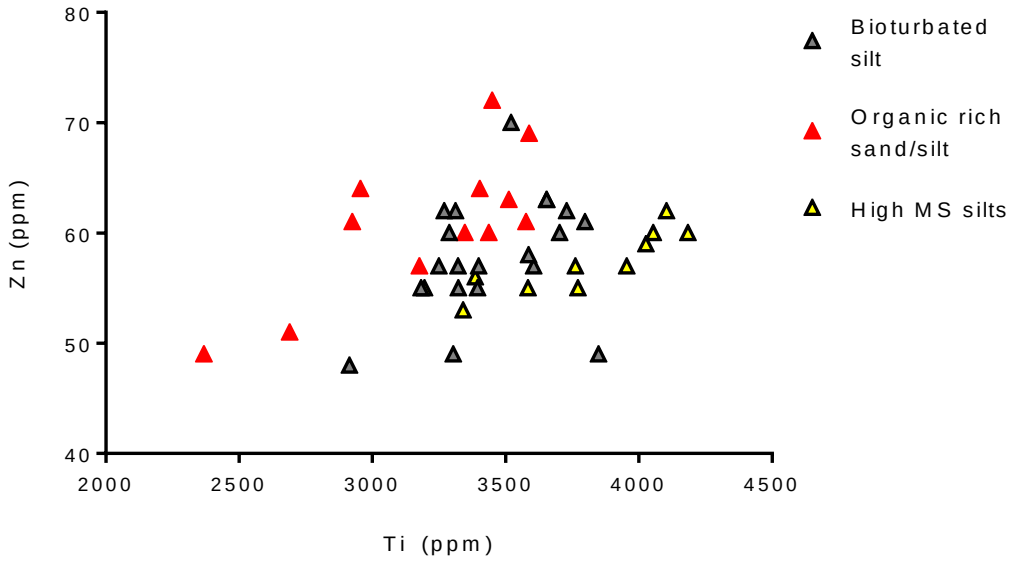

Fig. 5.27 – Zn vs. Ti for several facies.

The base of this facies was not observed in intertidal regions, thus total facies thicknesses in these areas could not be identified. In shallow subtidal cores CH7 and CH1, thicknesses are 1.09 m and 1.65 m respectively (Fig. 5.28). Maximum thicknesses are 1.82 m in CH2 and 1.95 m in CH6. Towards the harbour inlet at CH3, facies thickness is 1.22 m (Fig. 5.28).

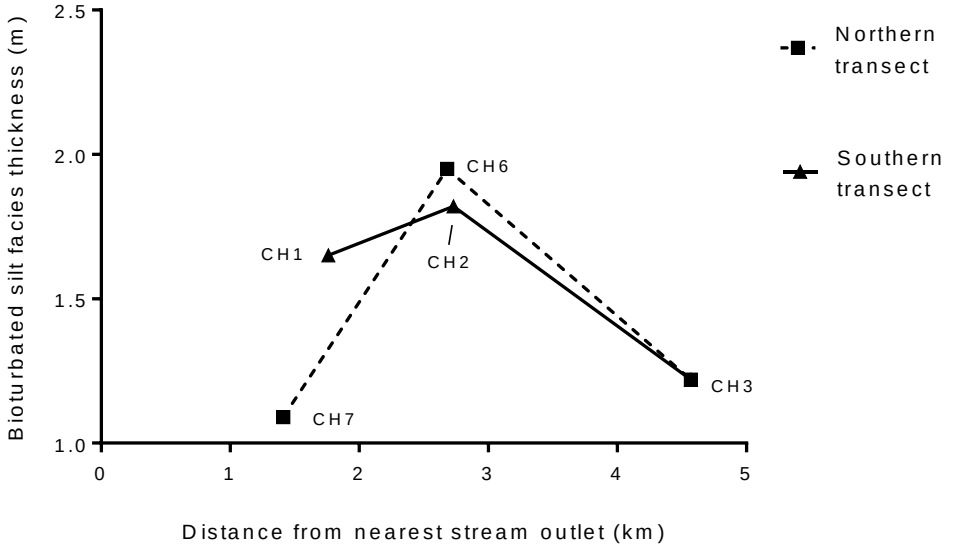

Fig. 5.28 – Thickness of the bioturbated sit facies vs. distance from the nearest (Whangarahi or Waiau) stream outlet.

5.2.4.1 Interpretation

The presence of articulated shells through this facies suggests that these sediments accumulated an estuarine environment. This is validated by numerous radiocarbon dates measured from this facies that range from c.1000 cal yr B.P to 7200 cal yr B.P, where sea level has been at ~PMSL in the Coromandel Harbour (refer to Chapter 6 for dating). Pollen dating in this facies has identified that the uppermost ~20 cm of this facies may be associated with Polynesian phase. Polynesian sediments are expected to be very similar to pre-Polynesian estuarine sediments as catchment erosion processes did not markedly change during their settlement (Hume & Dahm, 1991, Sheffield *et al.*, 1995). Differentiating the Polynesian sediment from the pre-human sediment within this facies is not possible with the limited pollen data in this research. Polynesian sediment thickness is likely to represent a sediment thickness of ~10–20 cm at the surface of this facies Therefore, these sediments are defined as pre-human to Polynesian estuarine sediments.

Sediments and minerals entering the harbour are thought to be derived from the catchment (Hume & Dahm, 1991; Mead & Moores, 2004). This appears to be supported by the mineralogical data collected from this facies. These estuarine silts have similar mineral compositions to the Coromandel Group and Manaia Hill Group rocks in the catchment. This is also suggested by a fining in sediment grainsize moving from the intertidal regions to the deeper harbour. Coarser sediment grains have likely have been deposited in the upper harbour following outwash, while finer silts have been transported (under lower energy conditions) to deeper regions of the harbour. Due to their high densities, opaque minerals are also more likely to be preferentially sequestered in the higher energy upper harbour compared to the subtidal areas of the harbour. The sequestration of denser minerals in the nearshore environment may explain why bulk densities are greater in the upper harbour.

Prior to human habitation and during Polynesian settlement, the catchment had an extensive vegetation cover (Hume & Dahm, 1991). Vegetation cover is well known to reduce overland flow by stabilising soils and catchment geology (Mead & Moores, 2004). This would have resulted in low erosion within the catchment,

and thus low catchment-derived sedimentation in the Coromandel Harbour (Hume & Dahm, 1991). The majority of eroded catchment sediments entering the harbour during this phase are likely to have been extensively weathered silts. Elemental and MS variation through these silts is low. Fe, S and Mn have no large scale variability through the facies, suggesting that the redox conditions within this marine environment remained constant through deposition. Some storm deposits are likely to be present in this facies; however, there is no evidence of coarser event beds. Storm deposits may be masked by extensive bioturbation. This facies appears to have been deposited under stable environmental conditions.

The bioturbated silt facies in subtidal regions is thicker than the bioturbated sand facies in intertidal regions. This suggests that the majority of pre-human estuarine sediments were silts and have been deposited in the subtidal regions of the harbour. Facies thickness is greatest in the centre of the harbour (Fig. 5.28). Thus, the centre of the harbour appears to have been the depositional centre for this facies. This may be an indication of the depositional energies and sediment transport mechanisms in in the harbour. As the F/C silts moved into the harbour from the catchment, the fine-grained silts were transported away from the higher energy intertidal region to the subtidal areas of the harbour. The centre of the harbour is situated away from the inlet, where tidal mixing energies are high, and the nearshore environment, where wind wave mixing is likely high. Thus, total mixing energies are at likely to be low in the centre harbour. F/C silts that are deposited in the centre harbour may not be rapidly resuspended by wind waves and tidal waters, thus accumulating rapidly in these areas.

5.2.5 Bioturbated intertidal sand to silt facies

Extensively bioturbated VF to C sands are found in the nearshore regions of the NEmb (Fig. 5.29). Near the subtidal regions, these sediments fine to have more clay and silt component with less sand component (Fig. 5.29). Bioturbated intertidal sands to silt are poorly sorted and contain on average ~5–20% whole shell and shell fragments. This facies is often difficult to distinguish from the sandy shell facies. Shell in this facies is predominantly fresh, though occurrences of weathered shell fragments are common. The >2 mm grain size fraction varies significantly from 2% total weight to 30% total weight and is composed of shell

fragments and pebbles (see Appendix F). Below 2 mm grain size, this facies is primarily composed of silts and M sands (Fig. 5.29). Grain size populations appear to fine moving from the Whangarahi Stream (002 to 005 in Fig. 5.29). In core 005, this facies has a dry bulk density of 1.26 g/cm3.

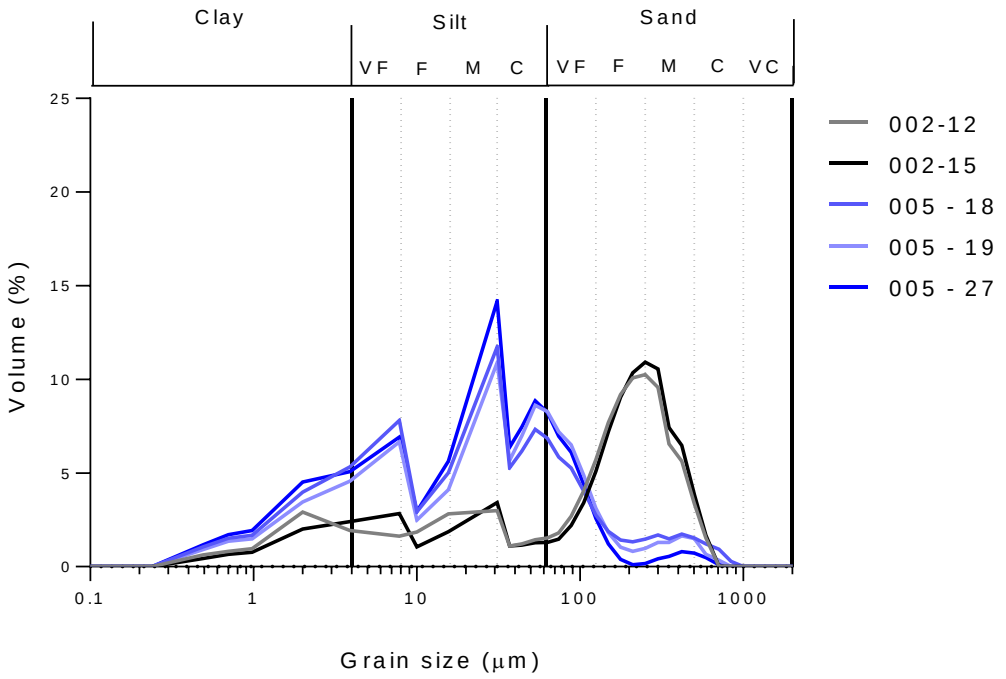

Fig. 5.29 - Grain size distribution of bioturbated intertidal sand and silt facies in cores 002 and 005. Core 002 is in the nearshore, while core 005 is near the subtidal region.

The two samples analysed for mineralogy from this facies have similar mineral characteristics but varying mineral compositions (Fig. 5.30). 002–5 is primarily composed of 30% quartz, 15% biotite, 22% opaque minerals, 15% organic matter, 7% each of feldspar and hornblende and 4% biogenic calcite. 005–12 is predominantly 70% undistinguishable silt, 7% quartz, 7% feldspar, with 4% each of calcite, opaques, hornblende and biotite (Fig. 5.30**)**

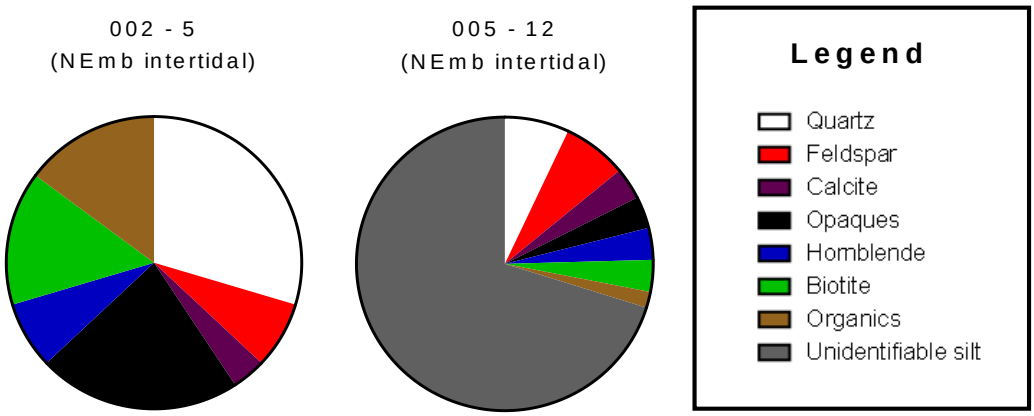

Fig. 5.30 - Estimated mineral assemblage for the bioturbated sand facies.

The bioturbated sand facies is characterised by highly variable elemental trends. MS varies in this facies in 005 from 25–65 × 10^{-5} SI units.

5.2.5.1 Interpretation

As with the bioturbated silt facies, well preserved, articulated shell suggests that this facies accumulated in a marine environment. Radiocarbon dates measured from this facies range from c.2600 cal yr B.P to c.4900 cal yr B.P appear to validate this claim (Table 6.1). These sands have therefore accumulated at generally the same time as the bioturbated silt facies (see bioturbated silt interpretation in 5.2.4). Mineralogical compositions are similar to the bioturbated silt facies. Non-silt mineral concentrations are elevated due to the coarser grained nature of these sediments. Therefore, this facies has been interpreted as pre-human–Polynesian intertidal sediments that have accumulated alongside the bioturbated silt facies. Moving from the nearshore environment to the subtidal environment, this facies will grade into the bioturbated silt facies.

Grain size is coarser in these sediments due to their association with higher energy intertidal environment. Thus, within the energetic nearshore environments (002–5), more mineral grains are observed compared to lower energy regions closer to the subtidal (005-12). This is also the case for grain size populations, where sediments are coarser in the near shore and fine towards the subtidal. High

elemental and MS variability through this facies may be related to the dynamic intertidal environment that the facies has accumulated in. Small scale variation in environmental energy (from stream influences or sea level fluctuations) may be more represented in these sediments compared with the bioturbated silt facies. This variability may also be from the marked shifts in Ca matrix composition through the facies (dilution effect, see 5.1.6.1.4).

Within the NEmb, the bioturbated sand facies overlies the bioturbated silt facies. A radiocarbon date from a shell bed between these two facies in core 005 has a date of c.4900 cal yr B.P. The bioturbated silt facies in the intertidal regions may be a result of elevated sea level in the Coromandel at c.4000 cal yr B.P, where these areas were situated in lower energy environments, where predominantly silt sized sediments accumulated. Further research is required to validate this claim.

5.2.6 Shell bed with sandy matrix (shelly sand) facies

Shell beds within clay to F/M sand matrix are found primarily at sediment depths of <1 m below sea floor (mbsf) throughout the harbour (Fig. 5.31). This facies is generally coarser than intracore bioturbated silt in subtidal regions or sand facies in intertidal regions (Figs. 5.29, 5.32). The sandy shell facies is found directly beneath the highly organic silt/sand facies in most subtidal coring locations and some intertidal areas (Fig. 4.2 to Fig. 4.17). In intertidal regions, the bioclasts primarily consist of predominantly well-preserved, articulated cockle shells and angular to subangular large (>1 cm) shell fragments (Fig. 5.31). In subtidal areas, species are diverse, including various gastropod and bivalve species. The subtidal sandy shell facies consists of varying compositions of shell hash, shell fragments and whole shell mixtures with varying degrees of freshness.

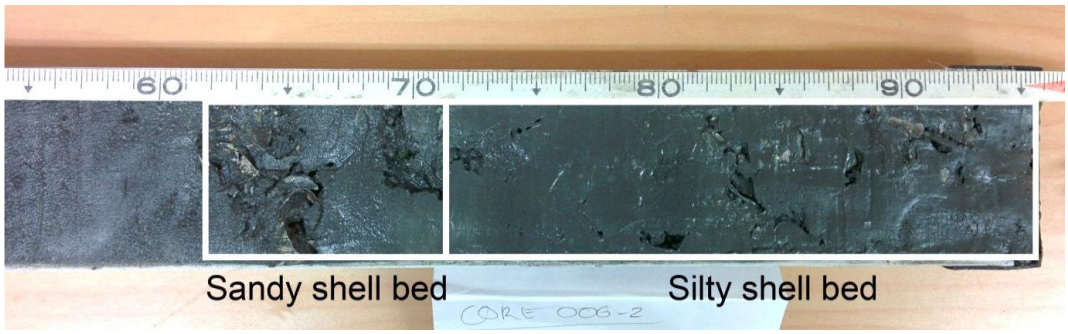

Fig. 5.31 –Shelly sand facies (left) grading into to the silty shell bed facies (right) in core 006.

The sandy shell facies has a clay to F/C silt with a M sand component which distinguishes it from the predominantly clay to F/C silt grained shell in silt matrix facies (Fig. 5.32).

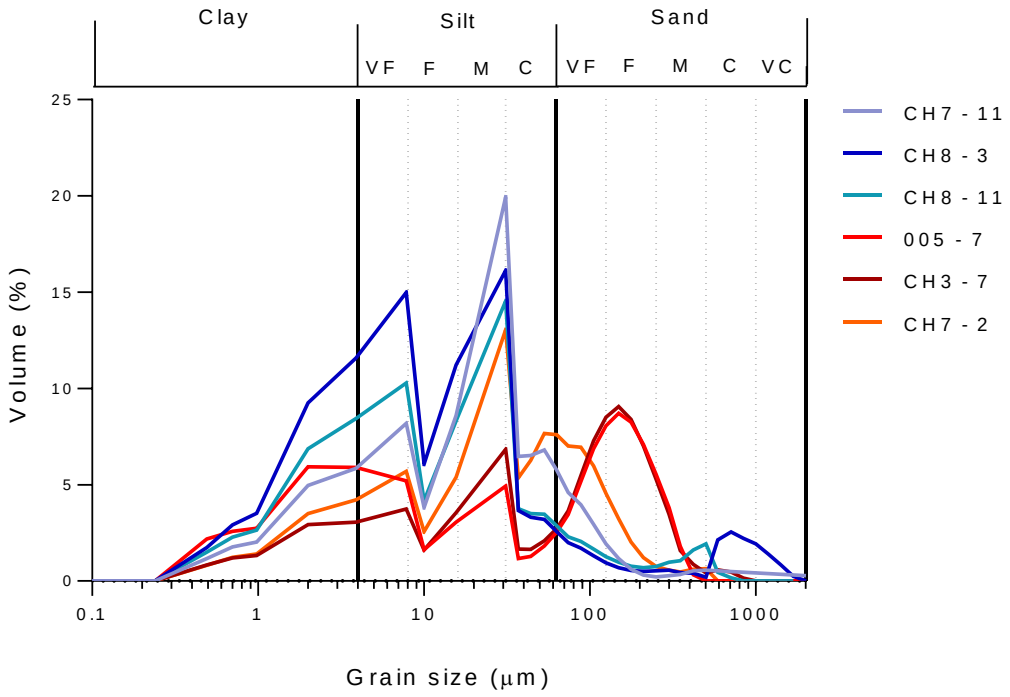

Fig. 5.32 - Grain size distribution of shelly sand (red/orange) and silt shell (blue) facies.

In subtidal regions (CH3–6, CH1–12), around 50% to 80% of this facies is unidentifiable silts (Fig. 5.33). Biogenic shell composition varies significantly, accounting for ~3% to >30% composition. Shell material is both fresh and weathered to relict. Quartz accounts for 2–8% composition. Feldspar accounts for ~2% composition. Opaques and biotite account for ~2% composition each (Fig. 5.33).

In intertidal regions (002–11, 005–7), biogenic shell accounts for >30% composition (Fig. 5.33). Bioclasts appear primarily as subangular fragments. Quartz and feldspar each make up ~10–20%. Hornblende has concentrations of 4–20%. Opaque minerals account for ~8% composition. Biotite is present in 002–11 at 8% (Fig. 5.33).

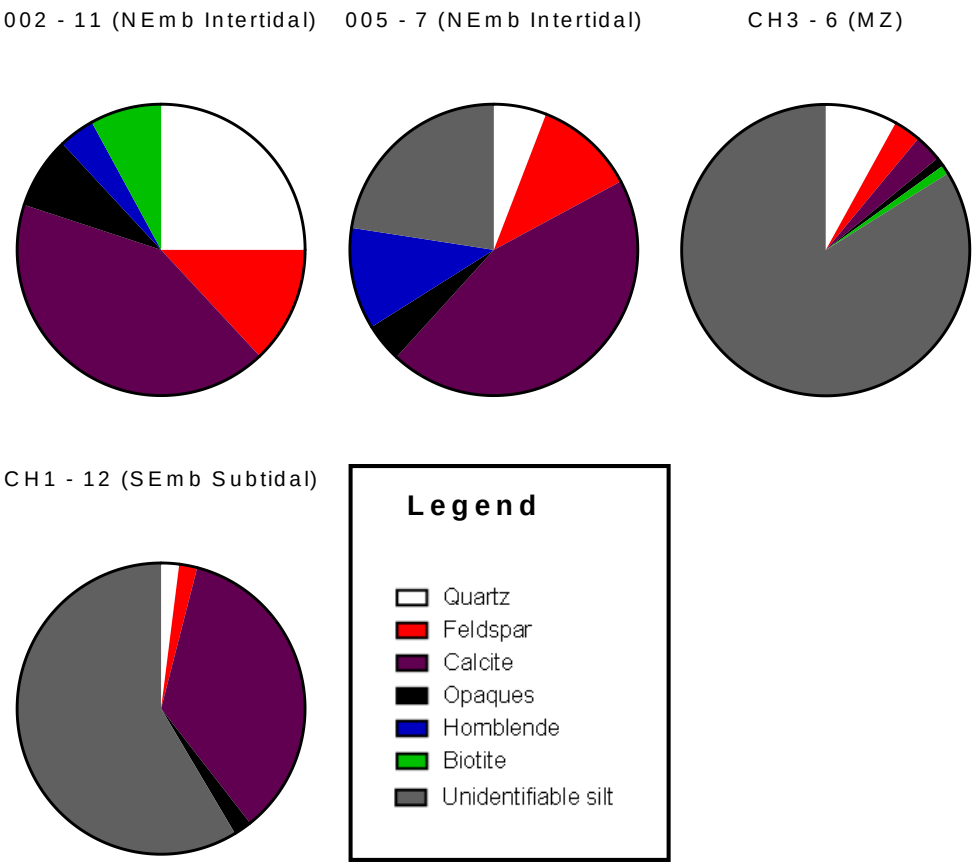

Fig. 5.33 –Estimated mineral assemblage for several samples from the sandy shell bed facies.

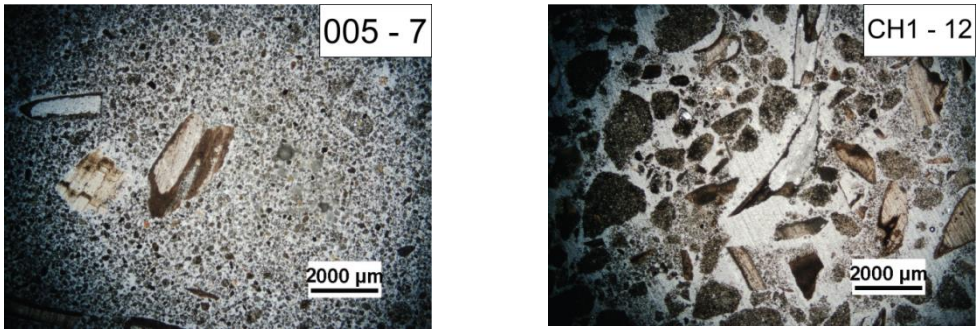

Fig. 5.34 –Thin section photos for 005–7 and CH1-12 at 1 x magnification. Note the abundance of shell fragments.

Due to low sampling resolution, few MS measurements were collected from the sandy shell facies. With the data available, average MS appears to be slightly higher in the sandy shell beds compared to the bioturbated sand and silt facies and

silt shell facies (Table 5.2). In CH5, MS in this facies is ~ two times greater than the intracore bioturbated silt facies (Table 5.2).

Table 5.2 – Average MS for bioturbated silt, sandy shell and silty shell facies across cores 005, CH1 and CH3.

	Average MS ($\times 10^{-5}$ SI units)		
Core no.	Bioturbated silt	Sand shell	Silt shell
005	18.2	28.4	21.1
CH1	18.2	21.3	19.7
CH3	23.7	46.5	NA

Ca in this facies has high concentrations at generally over 2–3%. Concentrations are over the pXRF Ca dilution threshold of 2 wt.%. Therefore, geochemical data for this facies are not presented.

5.2.6.1 Interpretation

This facies appears to have accumulated under different processes in intertidal and subtidal regions. Thus, the facies has been divided into two subfacies:

5.2.6.1.1 Subfacies A: Intertidal Shelly Sand

Within intertidal areas, the majority of this facies contains major component of well-preserved articulated shell and a minor fragmented shell component. Articulated shells suggest that these shell beds have been deposited *in situ*. Fragmented shell is likely a product of redeposition associated with intertidal wind wave mechanisms. Within the intertidal regions, these shell beds have been interpreted as primary shell beds.

5.2.6.1.2 Subfacies B: Subtidal Shelly Sand

In subtidal and some intertidal areas (005), this facies is comprised of shell fragments from various species showing varying degrees of weathering. Shells are also sometimes articulated and fresh, however. These beds occur at similar depths throughout the harbour (see core logs in subsection 4.1 in Chapter 4). On first

observation, this facies appears to be a storm deposit. This is based on a number of observations:

- The sandy shell facies generally has a coarser grain size distribution than the bioturbated silt facies it overlies in subtidal sediments. Therefore, this facies must have been deposited under more energetic conditions than the bioturbated silt facies;

- Marked variation in species diversity, weathering, and shell composition suggests that these beds have not accumulated *in situ* slowly over time, but have rather been sourced (eroded) from a collection of different shell beds;

- MS values are higher in these beds than in surrounding bioturbated sand and silt facies. This suggests reworking of high MS silts or sands under energetic conditions, with dense ferromagnetic grains redeposited from shallower to deeper parts of the harbour.

In certain regions of the harbour, however, these shell beds do not have conformable dates. Rather, these shelly sand facies have been dated in two distinct age suites. In the intertidal regions, these beds have ages of c.1000 cal yr B.P. In the western parts of subtidal regions, these beds have dates of c.3200 cal yr B.P (Table 6.1). Two sets of dates suggest that this facies has not been deposited through a single event. Similarly, if these shells were eroded from multiple other shell beds, some discrepancy between these dates should be observed. This is not the case: within the two groups, dates are very similar and show small standard deviations (Table 6.1).

In the western subtidal region (CH3, CH6, CH8 and CH10), these beds have ages of c.3200 cal yr B.P. This correlates with a time during which mean sea-level is likely to have been ~3 m higher than PMSL (Clement, 2011; Dougherty & Dickson, 2012). These shell beds may represent sediment starvation in the deeper harbour during this period, with low amounts of terrigenous input and condensed shell beds. This facies directly underlies the organic-rich anthropogenic facies in

this region. This would indicate that immediate pre-human (i.e. >700 cal yr B.P) sedimentation in these areas was very low.

The second age suite is observed in the nearshore environment (CH1 and CH9) of the SEmb. These shelly beds are at depths of ~0.2–0.5 m (see core logs in subsection 4.1 in Chapter 4). Here, this facies has several measured radiocarbon dates of ~1000 cal yr B.P (Table 6.1). These dates are generally consistent with the pollen dates gathered from the same facies (refer to Chapter 6 for dating). These beds may represent storm beds that were deposited prior to, or during, Polynesian arrival.

The processes that have led to the formation of these beds are unclear. However, the dates collected from this facies are highly consistent within the two groups. Consequently, these dates have been interpreted as representative of primary deposition and have therefore been applied for SAR estimation.

5.2.7 Shell bed within silt matrix

Shell beds within a predominantly clay to F/C silt occur at depths <2m throughout the harbour (Fig. 5.31). This facies has a very similar non-shell grainsize to the bioturbated silt facies in both intertidal and subtidal regions (Fig. 5.32). Shell matter is primarily comprised of well-preserved articulated cockle and other bivalve shells at >2 cm. Some occurrences of mm scale shell hash laminations do also occur in subtidal areas.

Observable mineralogy in intertidal regions consists of >30% fresh to slightly weathered angular to subangular biogenic calcite (Fig. 5.35). Fractured, subangular quartz generally accounts for 5% composition. Subangular feldspar generally accounts for 9% composition. In subtidal regions, >60% of material is an undistinguishable silt matrix (Figs. 5.35, 5.36). Fresh to slightly weathered, subangular shell accounts for ~10-30%, fractured, subangular quartz for ~2–4%, and subrounded feldspar for ~2–5% (Fig. 5.35). Hornblende and biotite have concentrations of 1–4%. Opaques make up 5–7% of the facies in both subtidal and intertidal regions Opaque are ~50% mineral opaques and ~50% organic matter

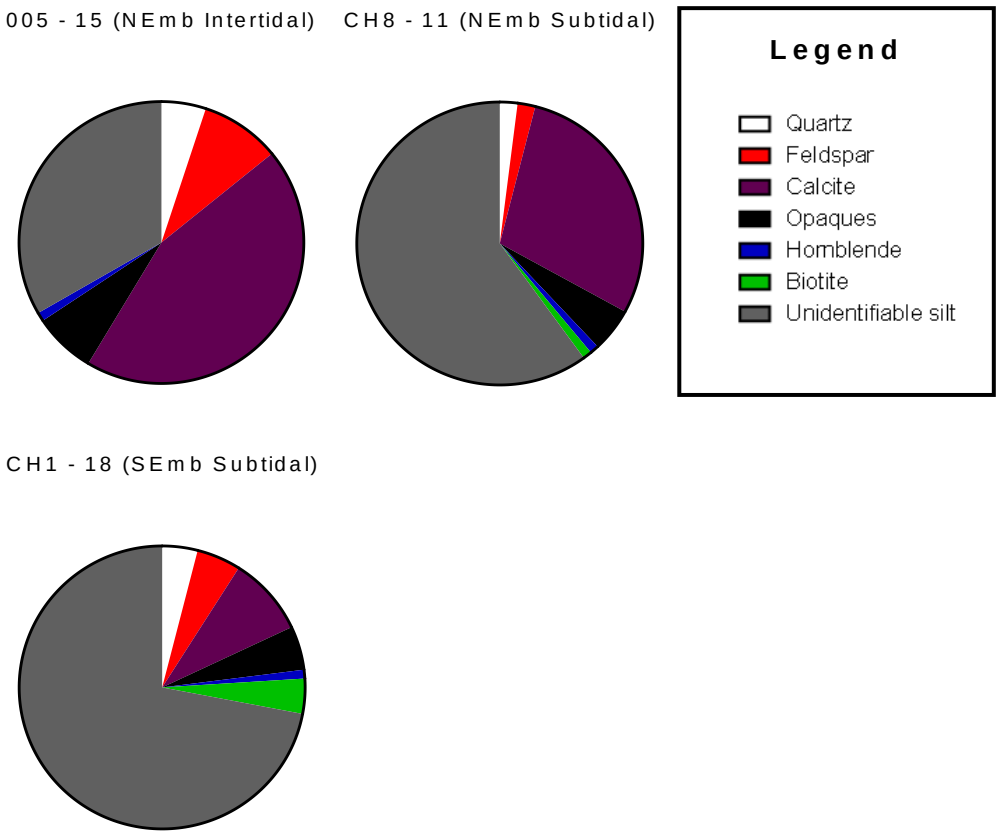

Fig. 5.35 – Estimated mineral assemblage for the silty shell bed facies in intertidal (top left) and subtidal (top right and bottom left) samples.

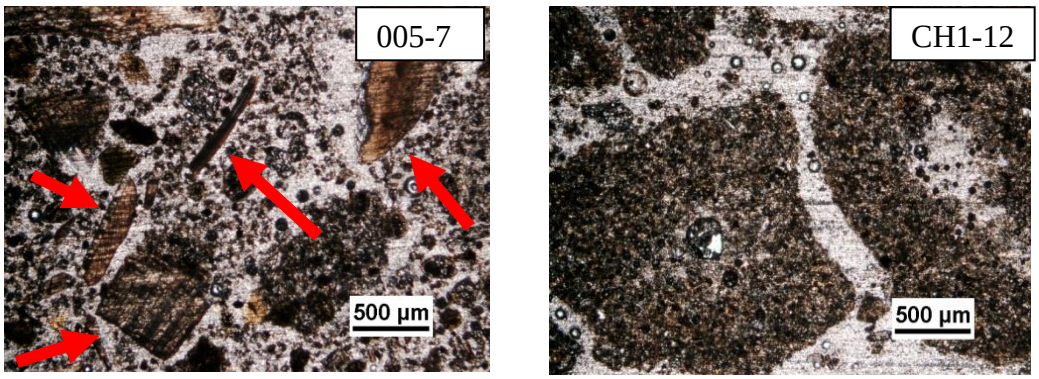

Fig. 5.36 - Thin section photos for 005–7 (left) and CH1-12 (right) at 10 x magnification. Note the elevated shell population in intertidal 005–7 (indicated by red arrows) relative to subtidal CH1-12 which is predominantly silt.

From the few MS measurements that were taken from the facies, MS values are very marginally elevated compared to the bioturbated silt facies (Table 5.2). This

observation may be prone to error as shell bed within silt matrix MS averages were calculated from less than 5 samples.

Ca in this facies has high concentrations at generally over 2–3 wt.% dilution threshold (refer to section 5.1.6.1.4). Therefore, geochemical data for this facies are not presented.

5.2.7.1 Interpretation

This facies has been divided into two subfacies due to variations in sediment texture and shell composition.

5.2.7.1.1 Subfacies A: Whole and Articulated Shells in Silty Matrix

Well preserved, articulated cockle shell beds occur in the bioturbated silt facies in intertidal and subtidal regions. This facies has little MS, sediment texture and mineralogical variation from the bioturbated silt facies. These beds have been interpreted as shell beds that have accumulated *in situ* within the bioturbated silt facies.

5.2.7.1.2 Subfacies B: Shell hash in subtidal silt

Shell hash (<1 mm shell fragments) laminations occur within the bioturbated silt facies in subtidal regions. The shell hash component suggests that fine grained shell matter has been transported in single events. No MS, mineralogical or grainsize data has been gathered from these thin laminations. However, from observational analysis, the matrix of these beds is very similar to the bioturbated silt facies. These beds have been interpreted as storm deposits.

5.2.8 Laminated black sands/silts

Black, well defined laminations occur as gravel to F/C sand in intertidal sediments and as F sand to F/C silt in subtidal sediments (Fig. 5.37). This facies occurs within the bioturbated sand facies in the intertidal regions. In the subtidal regions, this facies occurs within the bioturbated silt facies. This facies has a "sooty" organic matter coating and is visibly enriched in opaque minerals in hand specimen.

In the SEmb intertidal region, the facies is observed once in core 003 with a thickness greater than 10 cm (Fig. 4.4). Within the NEmb intertidal region, this facies is up to 7 cm thick and is observed at consistent depths and thicknesses throughout most NEmb cores (Fig. 4.5 to Fig. 4.7). Moving from nearshore to the centre harbour, this facies fines and thins until it is no longer observable. This facies was not observed in the inlet regions of the harbour.

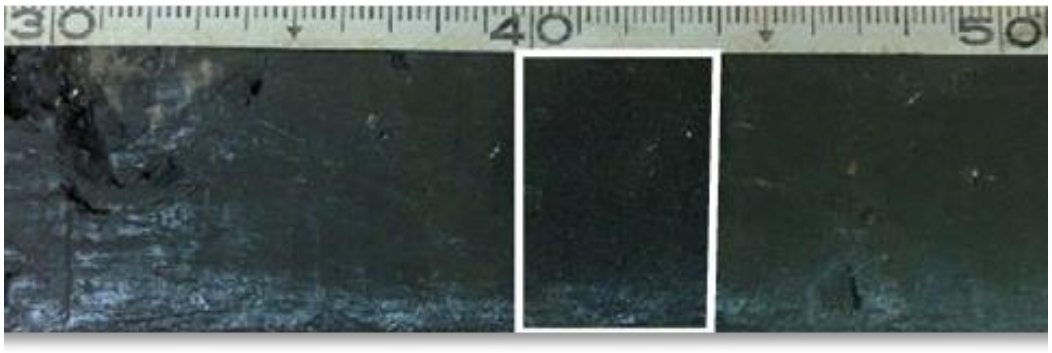

Fig. 5.37 –Laminated black sand/silt facies (outlined in white box) at a depth of 1.4-1.44 m in core 004. NB. 10% saturation has been applied to this photograph.

Sediment sandstone lithics are present in 003 and 005, observed as angular to subangular fragments up to ~0.75 mm. Some sandstone lithics appeared to have some quartz veining. Sandstone lithics comprised around 30% of 003 and 5% of 005 (Fig. 5.38). The facies also includes subangular rhyolitic groundmass fragments with internal phenocrysts of quartz and feldspar. Rhyolitic groundmass accounted for 30% of 003 and 5% of 005. Angular to subangular quartz and feldspar make up ~8–40% of the grains (Fig. 5.38). Sample 004 contained 12% angular volcanic glass shards. Opaque minerals also appear to be enriched relative

to other facies at 8–18%. Biogenic calcite accounts for ~10–20% of the total in 004 and 005. In 003, biogenic calcite accounted for 2% (Fig. 5.38).

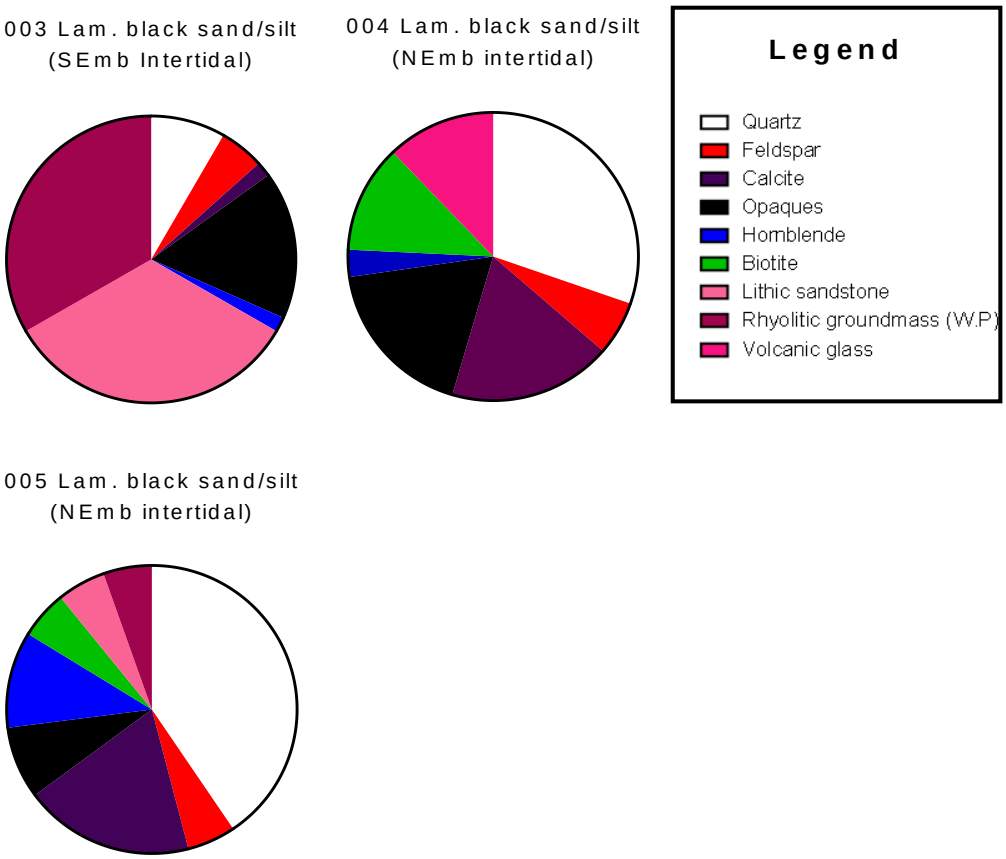

Fig. 5.38 - Estimated mineralogical composition of the laminated black sand facies. Note the elevated concentrations of volcanic materials.

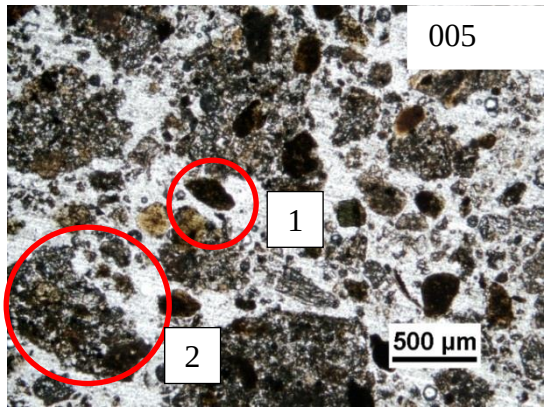

Fig. 5.39 – Thin section photograph of the laminated black sand/silt facies in 005 taken at 10 x magnification. An opaque mineral (1) and quartz grain (2) have been circled.

No XRF or MS data has been collected from this facies.

5.2.8.1 Interpretation

This facies contained high concentrations of volcanic detritus that is not characteristic of the catchment geology and has not been observed in any other facies. Therefore, it is unlikely to have been sourced from the erosion of catchment Kuaotunu Subgroup and Manaia Hill Group rocks. The facies is much coarser than surrounding sediments (i.e. bioturbated sand/silt facies) which suggests it was emplaced under different (likely more energetic) conditions. These are the only lithic sediments throughout the harbour to have a well-defined laminated structure, which suggests they deposited over a relatively short period of time so that they could not be reworked by bioturbation.

This facies is most likely derived from the product of a rhyolitic volcanic eruption in the broader region. A radiocarbon date 5 cm above this facies in core 005 indicate that these sediments were deposited some time prior to c.4900 cal yr B.P. The facies is a M/C sand in the intertidal regions, and a fine sand to silt in the subtidal regions. This suggests that the bulk of this volcanic material was deposited in the catchment reworked from the catchment and transported through stream networks to the harbour. The "sooty" black coating on the sediment in this facies may represent carbon derived from vegetation fire following the eruptive event(s). This facies is not here interpreted as typical estuarine sedimentation and is not further considered in this report.

5.2.9 Organic rich surface sands and silts

Organic sands and silts are the uppermost facies throughout the harbour. This facies typically overlies the sandy shell facies (Fig. 5.40) (also see core logs in subsection 4.1). This facies has a distinctive dark brown colour that is chiefly related to high organic matter concentrations. Organic detritus is present in intertidal regions in the form of mm to cm-scale fragments of wood. Organic detritus in subtidal areas is <mm-scale. The most elevated concentrations of organic matter are found in the SEmb. Cm to mm-scale shell fragments are common throughout the facies. Dry bulk densities in the southern parts of the harbour range from 0.61-0.97 g/cm^3. Dry bulk densities in the NEmb intertidal regions are ~1.4 g/cm^3. Dry bulk density is typically lower in this facies compared to bioturbated sands and silts in the same core (Fig. 5.43).

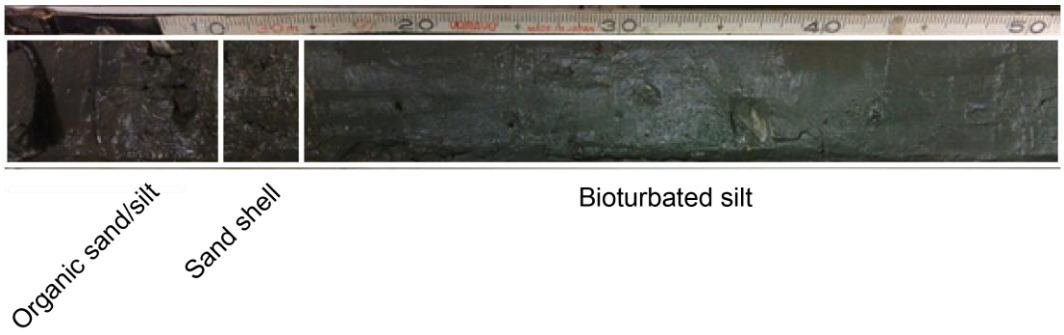

Fig. 5.40 – Organic rich sand/silt observed at the top of core CH9. Note the slight brown discolouration associated with the organic sand/silt facies. Note that the brown discolouration of the shelly sand facies may be due to bioturbation.

These sediments are dominantly silt to VF/F sands in intertidal regions and clays to C silts in subtidal regions (Fig. 5.41). Near the Whangarahi Stream mouth (core 007), this facies is predominantly clay to silt with some VF/M sand (Fig. 5.42). This facies is typically coarser than the intracore bioturbated silt facies in subtidal areas and the bioturbated sand facies in intertidal areas. The >2 mm fraction of this facies was comprised of wooden detritus and shell fragments.

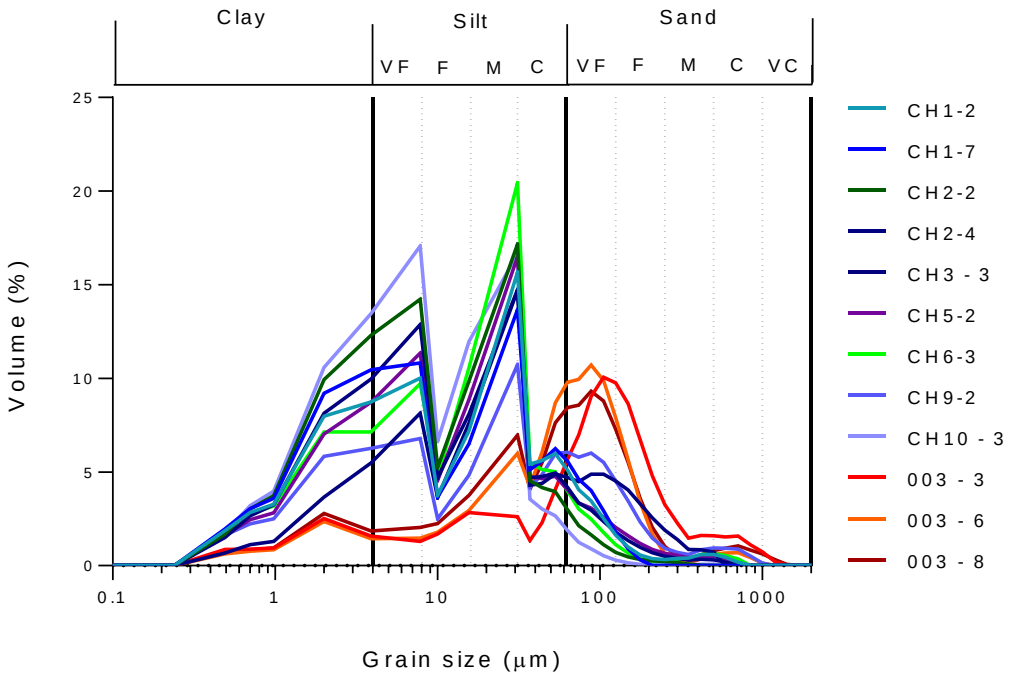

Fig. 5.41 – Grain size distribution for the organic rich sand/silt facies. Distributions depicted in blue and green (straight lines) are from subtidal areas. Distributions in reds and oranges (jagged lines) are from intertidal regions.

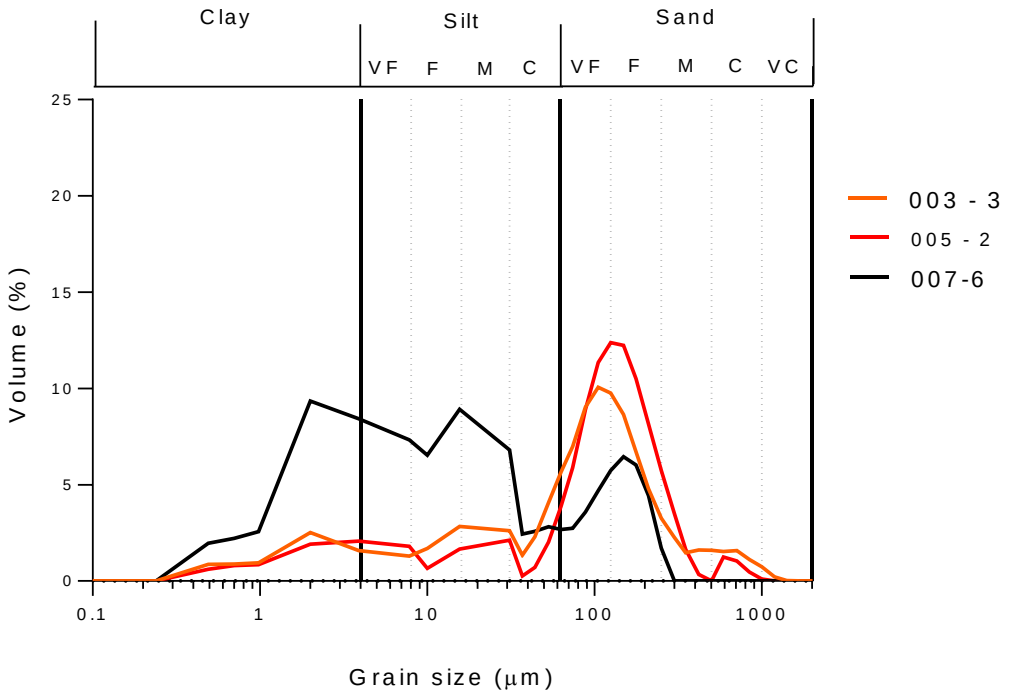

Fig. 5.42 – Grain size distribution for the organic sand/silt facies. This figure has been separated to more clearly depict the distribution of core 007, located near the mouth of the Whangarahi Stream.

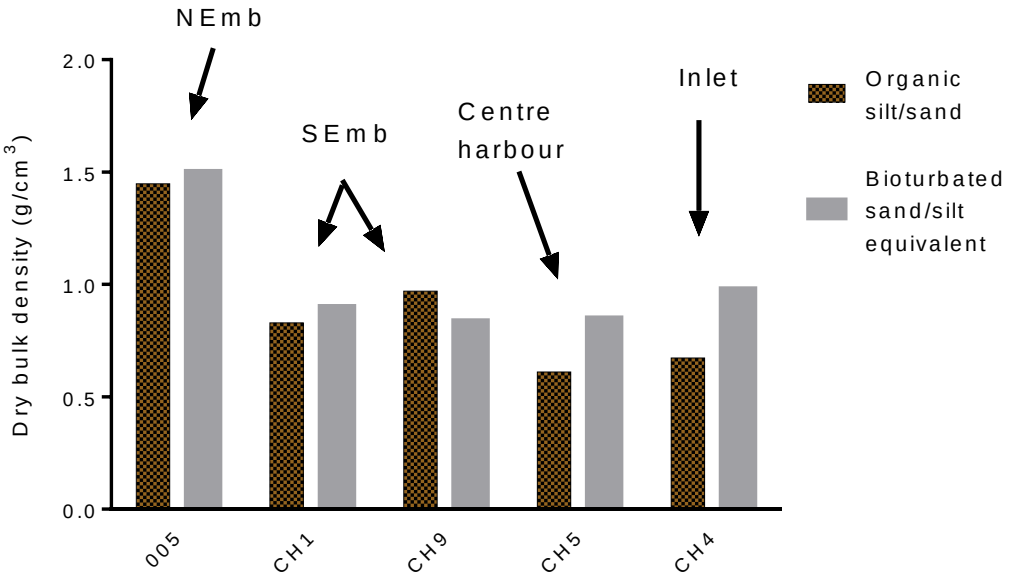

Fig. 5.43 – Average organic sand/silt bulk density vs. Intracore bioturbated sand/silt intracore equivalent for several regions of the harbour.

The majority of materials observed through thin section were undistinguishable silts. Undistinguishable silts had concentrations of >70% in subtidal regions and ~60% in intertidal regions (Fig. 5.44). Accessory minerals biotite and hornblende occur in similar concentrations at around 4% each in intertidal areas and 1% each in subtidal areas. Fresh to relict biogenic calcite accounts for <8% facies composition. Quartz and feldspar make up ~5% composition each in subtidal regions. Quartz makes up 20% composition in intertidal regions (Fig. 5.44). Opaque minerals are difficult to distinguish. Opaque materials appear to be 70% organic matter and 30% opaque minerals.

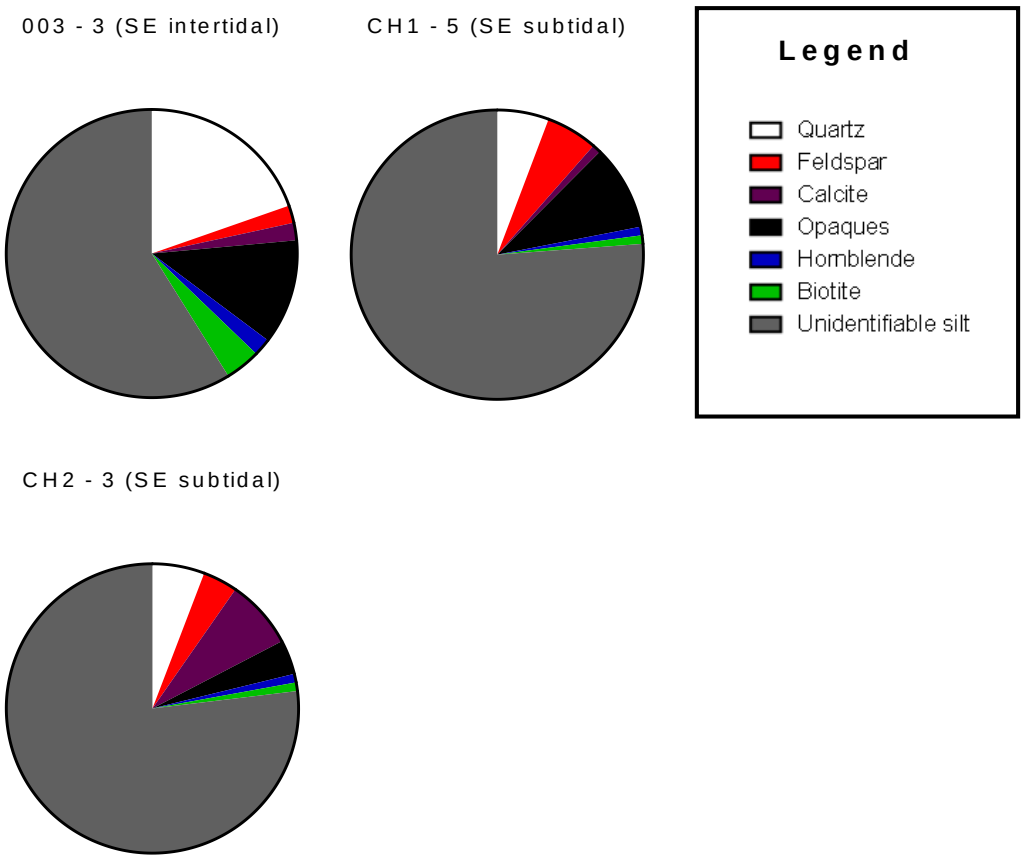

Fig. 5.44 – Estimated mineralogical composition of the organic rich sand/silt facies. A thin section of CH1–5 taken at 4 x magnification.

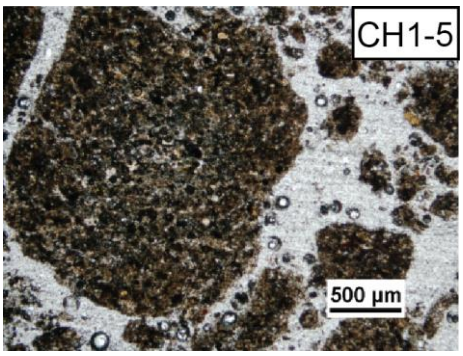

Fig. 5.45 - A thin section photograph of CH1–5 taken at 4 x magnification.

The bottom of this facies often overlies the sandy shell facies (refer to stratigraphic logs in Chapter 4). High biogenic Ca in the sandy shell bed induces a dilution effect that makes pXRF analysis difficult for the lower regions of the facies. This facies is enriched in heavy meals As, Zn and Pb compared with intracore bioturbated sands and silts (Figs. 5.25, 5.26, 5.27).

MS is elevated relative to the bioturbated sand and silt facies in intertidal and shallow subtidal areas (Fig. 4.18 to Fig. 4.24).

Facies thickness is up to 0.5 m in the upper regions of the SEmb. Moving to the inlet along the southern transect, facies thickness declines almost exponentially (Fig. 5.46). Facies thickness is ~0.35 m at the mouth of the Whangarahi Stream, though is less than 0.1 m in other regions of the NEmb (Fig. 5.46). Moving to the inlet along the northern transect, sediment thickness increases markedly at core site CH6 to 0.4 m. Facies thickness then decreases at CH5 and increases where the two transects merge at CH3 (Fig. 5.46).

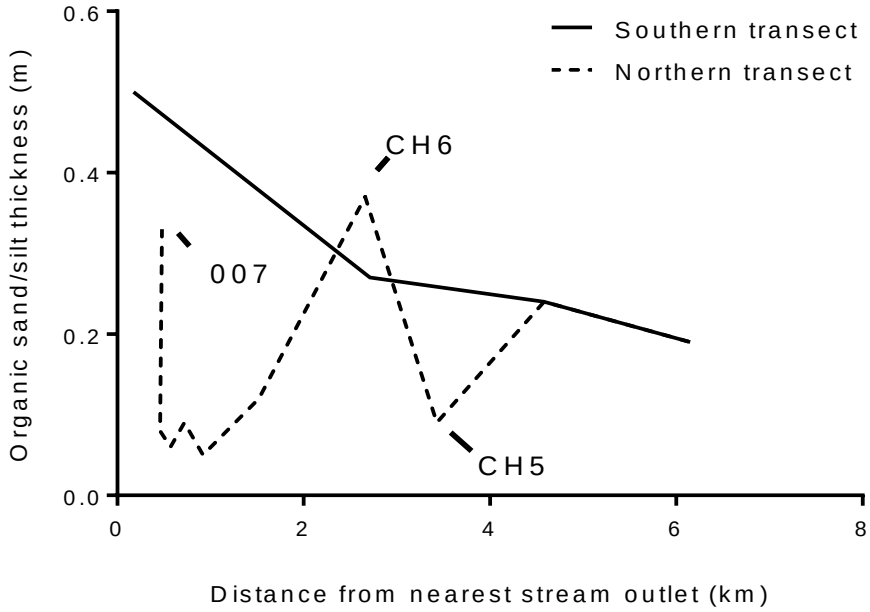

Fig. 5.46 – Thicknesses of the organic rich sand/silt facies plotted against distance from the nearest stream (Whangarahi or Waiau Streams) outlet for the northern and southern transects.

5.2.9.1 Interpretation

This facies is most recent to accumulate in the Coromandel Harbour. The facies has a coarser grain size than the bioturbated sand and silt which have been associated with pre-human sedimentation. This suggests that erosion within the catchment has recently become more energetic (Hume & Dahm, 1991). These sediments are enriched in heavy metals and have significant amounts of organic detritus, suggesting that the catchment vegetation has been significantly altered. These are tell-tale signs of anthropogenic influences in estuarine sedimentation (Hume & Dahm, 1991, Reeve, 2008). Therefore, these sediments have been inferred as anthropogenic. Radiocarbon and pollen dating has identified that these sediments are younger than c.1000 cal yr B.P, supporting this hypothesis.

It has been suggested that European activities led to an increase in the grain size of sediment entering Coromandel Harbour by increasing stream flow and overland flow through removal of forest cover and by inputting coarser material into the stream catchments. (Hume & Dahm, 1991) European activities are also suggested

as greatly increasing the flux of organic matter into Coromandel estuaries (Hume & Dahm, 1991; Sheffield *et al.,* 1995). This facies is also enriched in heavy metals, which is commonly an indication of European catchment land uses (Hume & Dahm, 1991; Mead & Moores, 2004; Reeve, 2008). Polynesian activities in the catchment were not likely to have significantly altered sedimentation processes in the harbour, and are therefore incorporated in the bioturbated silt and sand facies (see subsection 5.2.4.1) (Hume & Dahm, 1991; Sheffield *et al.,* 1995). As a result, these anthropogenic sediments are interpreted as chiefly European related. This has been validated by the observation of pine pollen (associated with European settlement) throughout this facies (refer to subsection 6.2.3.4 for pollen interpretation).

Apart from the Whangarahi Stream mouth, this facies is markedly thicker throughout the SEmb than the NEmb. Assuming sediment is from catchment sources, the majority of anthropogenic sediment that is entering the harbour appears to have been primarily derived from the stream catchments that outflow to the SEmb. The only significant difference in the SEmb catchment use that may be responsible for highly organic sedimentation is kauri milling and recent pine plantations. Pine pollen is abundant throughout this facies in the SEmb, which suggests that the majority of the material in these areas has been sourced from pine plantations (refer to subsection 6.2.3.4 for pollen interpretation). This appears to also be validated by the mineral composition of these sediments. Heavily weathered biotite is observed throughout this facies. Weathered biotite is generally only associated with the Manaia Group rocks in the SEmb catchment (Skinner, 1967). The facies is thick at CH6 along the northern transect. This core shows much thicker deposits of all facies identified (Fig. 4.18 to Fig. 4.24), and may be a depocentre or area with high sediment accommodation space. The anthropogenic sediment in the centre harbour has been interpreted as primarily derived from the SEmb rather than the NEmb.

The geochemistry differences also illustrate the variations in sediment sources between the two embayments. Heavy metals are elevated at the Whangarahi Stream mouth in the NEmb compared with the SEmb (heavy metals further discussed in subsection 7.5). These differences are further discussed in Chapter 7.

The thickness of European sediment decreases markedly moving away from the mouth of the Whangarahi Stream. At the Whangarahi Stream, sediment is primarily clay to silt with some sand and pebble component. Interestingly, moving to areas further away from the stream mouth in the NEmb, grain size increases and the clay content decreases. This is opposite to the SEmb, where coarser grain size populations are observed in the intertidal and fine to the subtidal. This could suggest that the mining activities that took place in the NEmb catchment have generated a large amount of clay which was fluxed into the stream networks and into the harbour. As the clay reached the harbour, it may have been flocculated, where it has been since been sequestered. This possibility is further discussed in Chapter 8.

Within the NEmb, the thickest occurrence of this facies is 0.33 m in in core 007. These sediments are likely related primarily to mining activities. Kauri deforestation did occur in the NEmb, however, the amount of organics is lower in the NEmb than in the SEmb, which suggests the majority of organics in the SEmb sediments are derived from pine plantations.

MS within this facies has a 1:1 relationship with Fe (Fig. 5.14). For this facies, terrigenous Fe sourced from increased erosion of the catchment has been interpreted as the primary influence on MS. The amount of organic detritus in these sediments has been interpreted as the reason why bulk density is lower in this facies than in intracore bioturbated silt facies.

The formation processes of these sediments are further discussed in Chapter 8.

5.3 Summary

The Coromandel Harbour sediments have been categorised into a number of facies based on sediment texture, mineralogical, observational, radiocarbon, pollen, pXRF and MS data. All interpreted facies have been collated in Table 5.3. These facies have been applied to the stratigraphic logs in Chapter 4 and are referred to in subsequent chapters.

Table 5.3 - Summarised facies analysis table. Facies have been assigned numbers that have been applied on the stratigraphic columns in Chapter 4.

Facies no.	Facies	Grain size	Shell compsition	Mineralogy	MS (SI × 10^{-5} units)	Geochem.	Interpretation
10	Laminated clay loam	Clay to silt to F/C sand	None	Weathered iron stained minerals.	~ 15 - 25	Markedly elevated metals (including heavy metals)	Pre-Holocene paleosols
9	High MS silts	Clay to F/C silt, lenses of F sand	< 1%	-	~ 40 - 60	NA	Streambank deposits
8	High MS sands	Clay to F/C silt to F/M sand	< 1%	-	~ 60	NA	Streambank deposits, nearer to a stream than facies 9
7	Sulphur rich silt	Clay to C/F silt. Some F sand	< 5 % shell hash	-	Equal to intracore bioturbated silt	Highly correlated Fe and S	Pyritic layer formed at the advent of mid-Holocene sea level rise
6	Bioturbated silts	Predominantly F/C silt	5 - 10 % shell hash	Mostly undistinguishable < 2 µm silt.	< 25	Non-fluctuating geochemistry. Low heavy metals.	Estuarine silts deposited prior to human arrival
5	Bioturbated sands	F/M sand in nearshore, predominantly silt near subtidal	Whole shell + shell hash	Respective of catchment geology	Highly variable	Highly variable	Intertidal sands deposited prior to human arrival
4	Laminated black sand/silt	Gravel to F sand in intertidal. Silt in subtidal	>5 % Shell hash	Primarily composed of volcanic detritus.	-	-	Volcanic eruptive. Most likley tephra. Source unknown.
3a	Intertidal shelly sand	F/M sand	Articulated and shell hash	Respective of catchment geology	Highly variable	[Dilution effect]	Shell beds that have accumulated in situ
3b	Subtidal shelly sand	F sand to F/C silt	Articulated and shell hash	Respective of catchment geology	Elevated compared to facies 6 and 5	[Dilution effect]	Pre-human shell beds. Origins unclear
2a	Whole and articulated shells in silty matrix	Predominantly clay to F/C silt	Fresh, articulated whole shell	Similar to bioturbated silt	Same as facies 6	[Dilution effect]	Shell beds that have accumulated in situ
2b	Shell hash in subtidal silt	Predominantly clay to F/C silt	Predominantly mm shell hash	Similar to bioturbated silt	Same as facies 6	[Dilution effect]	Storm shell beds
1	Organic rich sand/silt	C silt to M sand in intertidal regions. Clay to M silt in subtidal	< 10 % Shell hash	Elevated organic fragments	>25 in upper harbour. < 25 in subtidal	Elevated heavy metals	Anthropogenic sediments. Primarily associated with European catchment alteration

Chapter 6

Holocene Sedimentation Rates

This chapter identifies sediment accumulation rates throughout the Coromandel Harbour since the mid-Holocene. Firstly, the methods of estimating sedimentation rates are described. Harbour-wide sediment accumulation rate (SAR) estimations are then presented. SAR results are then interpreted to identify natural infilling processes and anthropogenic influences on harbour sedimentation.

High SARs currently threaten harbour-dependent aquaculture farms and boating channels. Preliminary work by Hume & Dahm (1991) has identified that anthropogenic SARs in the Coromandel Harbour are markedly elevated in comparison to pre-Polynesian SARs. This research was based on three cores in the intertidal and shallow subtidal regions of the NEmb and SEmb, and thus relatively little is known of SARs in the deeper subtidal regions of the harbour. Further SAR study in subtidal regions is required in order to provide knowledge necessary for environmental planning regarding proposed harbour developments (TCDC, 2016).

6.1 Methods

6.1.1 Radiocarbon dating

Carbon-14, ^{14}C, is a naturally occurring radioactive isotope of carbon that decays with a half-life of 5730±40 years (Lowe & Walker, 2015). ^{14}C is produced in the upper atmosphere through cosmogenic alteration of nitrogen, and is oxidised over weeks to months to form radioactive carbon dioxide, $^{14}CO_2$. This $^{14}CO_2$ enters the biological carbon cycle where it is incorporated into the tissues of all living organisms (Mead & Moores, 2004). As an organism respires and consumes fresh ^{14}C through its life cycle, the concentration of ^{14}C in the organism remains at a constant concentration relative to atmospheric concentrations. When an organism dies, however, the intake of fresh ^{14}C ceases while stored ^{14}C in the organism's tissues begins to decay. Assuming ^{14}C cycling within the organism has entirely ceased, the death of an organism can be figuratively described as the initiation of a

countdown, with the decay of ^{14}C acting as a ticking clock (Lowe & Walker, 2015).

Selecting appropriate samples for radiocarbon dating is essential for returning accurate and representative dates. Therefore, great care was taken in selecting suitable carbon material for dating. Articulated whole bivalve shells were preferred over disarticulated or fragmented shells. Articulated shells indicate that the organism is likely to have remained *in situ* since death and has likely not been transported. Shell material was not sampled if signs of significant degradation were apparent. Wood, while abundant in some cores, was rejected from radiocarbon analysis. Wood in different parts of a tree (i.e. the outside of a tree vs. the inside of a tree) will have varying ages. Where wood fragments are small, these pieces of wood cannot be easily traced back to their growth position. Thus, dates gathered from these wooden fragments may represent any age that the tree was alive. These are termed in-built age errors (Gavin, 2001). Bottom-feeding taxa such as gastropods were also rejected as they consume and integrate depleted carbon into their tissues, and thus deviate from true atmospheric concentrations.

These guidelines were followed in all but two samples. Weathered shell samples were analysed in CH10.

6.1.1.1 Radiometric Dating

Radiometric dating is a method of counting the β decay events from 14C in a sample through time. This allows for the activity of the sample to be calculated, which can then be used to estimate the age of a carbon based sample (Lowe & Walker, 2015). Radiometric samples were typically retrieved from concentrated occurrences of cockle or oyster shell beds. Samples were taken from 5 cm sampling intervals where the total sample weight exceeded 35 g. Samples were submitted to the University of Waikato Radiocarbon Dating Laboratory and analysed according to their standard operating procedures (SOP).

6.1.1.2 Accelerator mass spectrometry (AMS)

AMS is a method of separating elemental constituents in sample through a particle accelerator. Once elements have been separated, the amount of ^{14}C atoms in a sample can be directly counted and interpreted to collect a date. AMS dates were measured on single specimens of articulated bivalve shells. Cockle and pectin shells were preferred to date shell hashes. Samples were submitted to the University of Waikato Radiocarbon Dating Laboratory and tested according to their SOP. Radiocarbon ages were calibrated to cal yr B.P using the Marine13 calibration curve applying the Southern Hemisphere marine reservoir correction (Remier et al, 2013).

6.1.2 Qualitative Pollen Analysis

Pollen and spore composition through a sedimentary succession reflects the diversity of pollinating species in a region through time (Vandergoes & Cochran, 2015). Species diversity within a region can change significantly due to external influences such as climate and anthropogenic activity, and can therefore be used as a palaeoenvironmental proxy. Here, pollen is primarily used to identify several settlement events and land-use changes within the catchment. The historical dates of these events are well understood, and thus pollen can be used as a relative dating tool in shallow subsurface sediments where other dating proxies are not applicable.

6.1.2.1 Species diversity changes in the Coromandel Harbour catchment

Since the mid-Holocene, the Coromandel Harbour has experienced five main phases with regard to catchment conditions and species diversity (Hume & Dahm, 1991). These phases can be further refined using more recent literature (McGlone et al, 2005).

6.1.2.1.1 Undisturbed forest

Age: >700 cal yr B.P.

Prior to human arrival, the Coromandel was densely vegetated with native forest (McGlone, 1989; Hume & Dahm, 1991; Sheffield *et al.*, 1995; Mead & Moores,

2004). Tall tree forest was comprised of various native podocarp (n. podocarp) species, kauri (*Agathis australis*) and rimu (*Dacrydium cupressinum*). Tree fern species were numerous and abundant. Bracken (*Pteridium esculentum*) was present, but not in elevated concentrations (McGlone et al, 2005). Hutu (*Ascarina lucida),* a species only related to undisturbed native forest, was also present (Hume & Dahm, 1991)

Pollen assemblage characterised by:

- Abundant native podocarp
- Abundant native tree ferns
- Kauri and rimu
- Hutu (*Ascurina luciada*)

6.1.2.1.2 Polynesian settlement

c.700 cal yr B.P. –130 cal yr B.P. (1820 A.D.)

Polynesian settlement in the Coromandel region first occurred at 700 cal yr B.P. (Hume & Dahm, 1991; Wilmshurst & Higham 2004) and was the first instance of anthropogenic influence on regional biota. Coastal areas were cleared with small-scale fires to prepare land for crops, which led to a significant increase in bracken, a highly competitive species that rapidly colonises cleared landscapes (McGlone et al, 2005). In this report, this increase in bracken is termed the bracken spike.

Pollen assemblage characterised by:

- Marked rise in bracken pollen
- Slight decrease in native species

6.1.2.1.3 European settlement

1820 A.D.–Present

Species diversity and land-use changes during European settlement can be differentiated into three sub-phases.

6.1.2.1.4 Early European: deforestation

1820 A.D.–1910 A.D.

Early European deforestation was the most significant anthropogenic change in species diversity to occur within the catchment. The first instance of European deforestation was in 1820 A.D when the H.M.S Coromandel anchored in the Harbour for 12 months before leaving with a load of Kauri Spars. Widespread deforestation had fully developed by ~1830 A.D (Hume & Dahm, 1991). Native deforestation resulted in a significant decrease in the native podocarp and kauri and tree fern species (Hume & Dahm, 1991). As the forests were felled, exotic species such as pine (*Pinus radiata*), dandelion and plantain began to populate the area (Hume & Dahm, 1991, Sheffield *et al.,* 1995).

Pollen assemblage characterised by:

- Marked decline in native podocarp, kauri and rimu
- First appearance of European exotic species
- First appearance of pine pollen

6.1.2.1.5 Late European: farming and native reforestation

1910 A.D.–1975 A.D.

Following the cessation of large-scale deforestation, much of the Coromandel Harbour catchment was converted to farmland. Native species were reintroduced to the area, resulting in the secondary forest that is observed throughout the catchment in the present day (Hume & Dahm, 1991).

Pollen assemblage characterised by:

- Increase in native species
- Presence of exotics

6.1.2.1.6 Recent European

1975 A.D-Present

Recent species diversity change in the catchment is dominated by extensive pine forestry. Pine plantations within the Coromandel Harbour catchment generally post-date 1975 A.D (Hume & Dahm, 1991). Pine plantations are primarily located in the catchment of the southern embayment (Fig. 2.6). Cyclic felling processes and removal of vegetation cover have resulted in a significant flux of pine pollen

and organic matter into the harbour (Hume & Dahm, 1991). As a result, pine pollen is elevated relative to the European farming and reforestation phase. (Hume & Dahm, 1991). Apart from an increase in pine pollen, no new indicator species are associated with this phase. Sediments derived from pine plantations were found to have coarser grain sizes by Hume & Dahm (1991), and to be enriched in organic detritus by Hume & Dahm (1991) and Sheffield et al. (1995).

Pollen assemblage characterised by:

- Increase in native species, especially tree fern
- Presence of exotics
- High concentration of pine pollen

Other characteristics:

- Coarser grain size
- Elevated organic detritus

6.1.3 Palynology Methods

2 cm^3 dried subsamples were placed into 10cc centrifuge tubes. Subsamples were pre-treated with 10% hydrochloric acid (HCl) to remove carbonate material, and then 10% potassium hydroxide (KOH) to de-flocculate sediment constituents. Sodium polytungstate (SPT) with a specific gravity of 1.7 was then added to the samples and thoroughly mixed with a vortex mixer. Samples were left to settle for 10 minutes, and then centrifuged at 2000 rpm for 10 minutes. After centrifuging, the thin pollen/organic film at the surface of the SPT was pipetted and placed into a separate centrifuge tube. The retrieved pollen/organic material was acetolysised with a H_2S0_4 and glacial acetic acid solution at 9:1 to dissolve all non-pollen organics. The pollen concentrate was subsequently water washed several times to remove the acid from the final pollen product.

Pollen concentrates were then mixed with a glycerin jelly and mounted on labelled glass slides. The slides were sealed with a coverslip and analysed for pollen composition using a Nikon microscope. Pollen assemblages were analysed qualitatively, and species diversity in each sample was described but not counted. Pollen assemblage descriptions were compared to the phases of species diversity discussed above to establish a match. Due to possible human errors and

bioturbation effects, a 5 cm margin of vertical error was applied to inferred pollen dates.

Pollen analysis was undertaken on cores CH1, CH7 and 005. Samples were taken from within and just below the organic rich sand/silt facies. Pollen analysis was undertaken on samples from 0.1 m, 0.2 m, 0.4 m, 0.5 m and 0.6 m from core CH1, 0.05 m, 0.15 m, and 0.25 m from core 005, and.0.05 m, 0.1 m, 0.15 m and 0.3 m from CH7.

6.1.4 Dichlorodiphenyltrichloroethane (DDT) dating

DDT is a commercially manufactured organochlorine pesticide that was used in the second half of the 20th century to control grass grub (Hume, Fox, & Wilcock, 1989). The pesticide was applied extensively on agricultural and residential land within New Zealand between 1950 and 1970. The pesticide was banned in 1970 due to adverse effects on the environment (Hume, Fox & Wilcock, 1989; Buckland, Ellis & Salter, 1998). DDT does not occur naturally, therefore its occurrence can be wholly attributed to human use in the middle to late 20th century. Therefore, DDT can be used to interpret ages from anthropogenic sediments deposited between 1950 and 1970 (Hume, Fox & Wilcock, 1989). A more developed discussion of the DDT dating method can be found in Chapter 6.

6.1.4.1 Methods

DDT analysis was undertaken on sediments that had been identified as anthropogenic through pollen and radiocarbon dating methods. These sampling locations can be found in the Appendix I. DDT screening was undertaken by Hills Laboratories using SOP. DDT related compounds of 2,4'-DDT, 4,4'-DDE, 4,4'-DDD and 4,4'-DDT were reported in mg/kg.

6.1.4.2 DDT results

DDT and its breakdown components had undetectable concentrations (i.e. lower than Hills Laboratories DDT detection limits) of <0.005 mg/kg for all 9 samples tested. Thus, no dates could be interpreted from DDT results.

DDT samples were collected from sediments inferred as European sediments through dating and facies analysis methods. Therefore, it is unlikely that the DDT spike and DDT contaminated sediments were missed during sampling. Catchment DDT and its breakdown components are rapidly sorbed to organic particles and detritus, which are rapidly moving into the harbour (Hume & Herdendorf, 1988). Therefore, it is unlikely that the DDT is stored in stream networks. A likely explanation for the absence of detectable DDT is that the application of the organochloride was low in the catchment, so that very little of the pesticide entered the Coromandel Harbour.

6.1.5 Pyritic layer (sea level rise) layer dating

A pyritic layer has been identified through facies analysis as a marker bed for the onset of PMSL in the Coromandel harbour (refer to subsection 5.2.3.1). The top of this layer has been interpreted as a sub-aerial palaeosol to early estuarine sediment that was diagenetically altered to a pyrite layer at the mid-Holocene sea level rise event. Thus, a date of 7500 cal yr B.P has been applied to the top of this layer for the purpose of SAR study. The exact timing and variability of PMSL within the Coromandel Harbour is limited (Clement, 2011). Thus, SARs inferred should be considered with potentially high error.

6.1.6 Wooden floor dating method

Use of the "wooden floor", a layer of milling detritus from deforestation, has been proposed as a possible stratigraphic marker in the Coromandel Harbour in Chapter 2 (Hume & Gibb, 1987). Unfortunately, no such marker bed has been found in the harbour. Thus, this method cannot be used for SAR investigation.

6.1.7 Calculation of sedimentation rates

Sedimentation accumulation rates (SARs) were calculated using absolute or relative dates collected from pollen, radiocarbon, DDT, XRF methods. Rates are presented in mm/yr^{-1}. Due to the low resolution of radiocarbon and pollen dates, SARs calculated from these methods do not give a long-representation of SARs associated with short time scale (i.e. days to years) events such as storms. Where

SARs have been calculated from radiometric dates, the mid-point of the 5 cm sampling band has been applied as the depth occurrence.

6.2 Results

6.2.1 Radiocarbon

15 dates have been collected from shell material from the Coromandel Harbour. These dates range from c.7260 cal yr B.P to c.880 cal yr B.P (Table 1). A majority of these dates correlate well with pollen dates and age inferences made through facies analysis and are likely to be accurate representations of primary sedimentation. Some dates, however, do not match pollen and facies dates and are likely to be reworked. These samples and cores are briefly discussed below. All dates that have not been omitted are interpreted to be reliable representations of the date of sediment deposition.

Table 6.1– Radiocarbon dates measured from shell material from the Coromandel Harbour. Dates highlighted in yellow have been omitted from SAR calculations. 2 σ calibrated ages and calibrated age error margins have been rounded to the nearest 10 years.

Core no.	Depth below surface (m)	Facies	Shell species	Sample type	Method	Code	14C age (B.P)	2 σ age (cal yr B.P)
003	1.80-1.85	Lam. black sands	Cockle	Shell hash	AMS	Wk-43700	1333 ± 20	880 ± 70
005	0.30 - 0.35	Sand shell	Mactra?	Whole, paired shell	RM	Wk-43422	2811 ± 31	2580 ± 90
005	1.06	Silt shell	Cockle	Hash and whole	RM	Wk-43423	4655 ± 24	4890 ± 60
CH1	0.55 -0.60	Sand shell	Cockle	Whole, paired shell	RM	Wk-43424	1492 ± 30	1050 ±70
CH3	0.34	Sand shell	Mussel	Shell hash	AMS	Wk-43695	3383 ± 21	3260 ± 70
CH3	1.29	Bioturbated silt	Oyster	Whole	AMS	Wk-44047	6598 ± 23	7130 ± 70
CH5	0.4	Sand/silt shell	Pecten	Shell hash	AMS	Wk-43696	3400 ± 20	3280 ± 70
CH5	1.50-1.55	Silt shell	Oyster	Whole, paired shell	RM	Wk-43425	6729 ± 32	7260 ± 60
CH7	0.50-0.55	Silt shell	Cockle	Whole, paired shell	RM	Wk-43426	5710 ± 35	6130 ± 80
CH7	0.6	Bioturbated silt	Pecten	Whole, paired shell	AMS	Wk-43697	4294 ± 20	5100 ± 100
CH8	0.40 -0.45	Silt shell	Cockle	Whole, paired shell	RM	Wk-43427	3568 ± 28	3470 ± 70
CH9	0.2	Sand shell	Cockle	Whole, paired shell	RM	Wk-43428	1404 ± 28	970 ± 60
CH10	0.70–0.75	Bioturbated silt	Mussel	Shell hash	AMS	Wk-43698	3389 ± 20	3270 ± 70
CH10	3.30-3.35	Sand shell	Mixed shell	Whole + hash	RM	Wk-44048	4469 ± 32	4690 ± 90
CH10	3.45-3.50	Sand shell	Cockle	Whole + hash	RM	Wk-44049	4960 ± 89	5330 ± 130

6.2.2 Omission of reworked radiocarbon dates

6.2.2.1 Core 003

A date of 880±70 cal yr B.P was measured from shell hash from the laminated black sand (in this case, gravel) facies at a depth of 1.8–1.85 m in core 003. The presence of crushed shell hash in gravel conglomerate suggests these shells have been reworked in an energetic environment. The black laminated sand facies has been dated from whole and paired shell at >c.5000 cal yr B.P in the northern embayment. This date was taken from articulated cockle shell and is interpreted as more reliable than the date from core 003, further suggesting these sediments are products of redeposition.

It is likely that this shell material has been reworked. Reworking is not unexpected in this area due to its proximity to the meandering Waiau stream channel. It may also therefore be possible that this whole core has been subject to ongoing secondary erosion and re-depositional processes. Therefore, this date has been removed for SAR calculations. There is a possibility, however, that this date is accurate and sedimentation rates in this area are very high, sourced from kauri deforestation and milling in the SEmb catchment. Further work is necessary to validate this hypothesis.

6.2.2.2 CH7

Two dates have been collected from CH7. The dates are unconformable, with a date of 6130±80 cal yr B.P overlying a date of 5100±100 cal yr B.P. The younger date was collected from a single articulated well-preserved scallop shell. Scallops do not burrow; therefore, the shell was probably deposited on the sediment surface *in situ* in the bioturbated silt facies. The overlying older shell material is composed of paired scallop and other pecten shell fragments taken from the sandy shell facies. In Chapter 5, the sandy shell beds have been interpreted as sediments that have either accumulated *in situ* or are products of reworking. It is likely that the shells that have the older date have been reworked. The older date has therefore been removed from SAR estimations.

6.2.3 Pollen assemblage analysis

6.2.3.1 CH1 (SEmb subtidal)

Hutu is present to 0.6 m (Fig. 6.1). Kauri pollen has low concentrations up to 0.5 m. Above 0.5 m, kauri pollen is no longer observed. N. podocarp are abundant up to 0.45 m and are largely absent from the pollen record at shallower depths (Fig. 1). Native pollens are found within the sand shell facies and the bioturbated silt facies.

A rise in bracken occurs at 0.55 m (Fig. 6.1). Pine and other European exotics have a distinct advent at 0.5 m and are concentrated upwards to the surface. Wooden organic fragments were abundant throughout this section. Pollen associated with European species correlates with the organic rich sand/silt facies. No rise in native pollens associated with late European land uses was noted in this core.

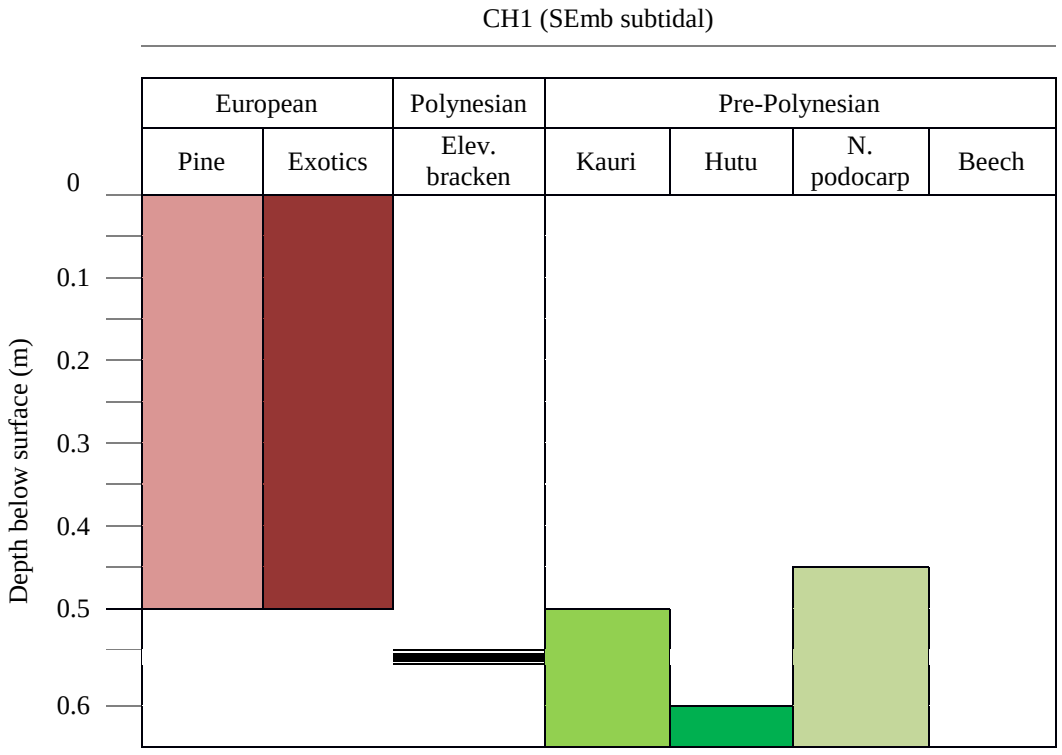

Fig. 6.1 – Pollen assemblage table for CH1. Dark black lines indicate a single occurrence of a specific pollen type or elevated (elev.) bracken.

6.2.3.2 CH7 (NEmb subtidal)

Kauri is present at 0.3 m (Fig. 6.2). Hutu and N. podocarp occur up to 0.2 m and 0.15 m respectively. Beech pollen (*Nothofagus*) is also observed in a single sample at 0.2 m (Fig. 6.2). A rise in bracken is observed at 0.2 m (Fig. 6.2). These native pollens are found within the sand shell and bioturbated silt facies. Similarly to CH1, pine and European exotics occur together (Fig. 6.2). Again, the advent of European pollens correlates with the decrease of native pollens. European pollens occur in the organic rich sand/silt facies. No rise in native pollens associated with late European land uses was noted in this core.

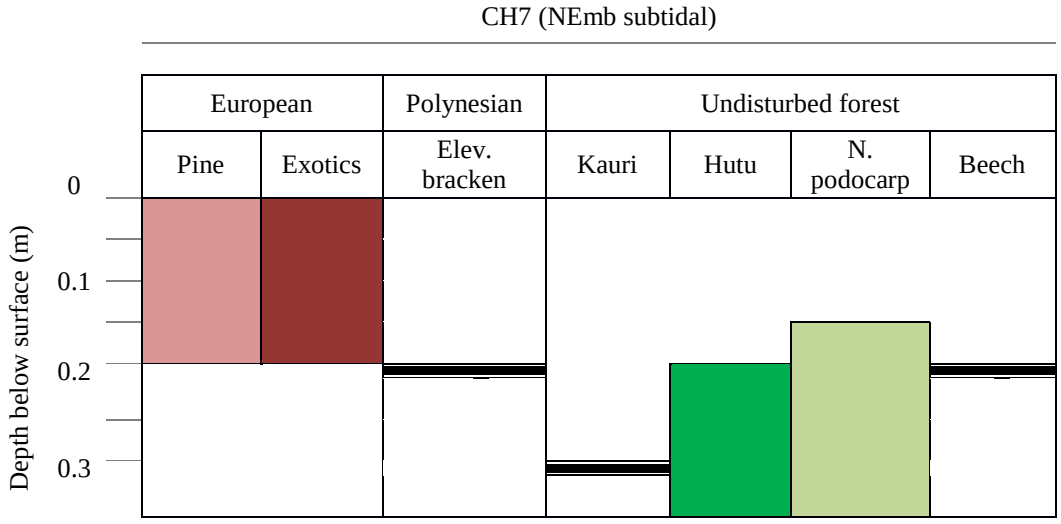

Fig. 6.2 - Pollen assemblage table for CH7. Dark black lines indicate a single occurrence of a specific pollen type or elev. bracken.

6.2.3.3 005 (NEmb intertidal)

Pollen in intertidal core 005 was scarce. This was not unexpected as pollen is typically deposited in lower energy environments. Pollen present was extensively broken and fragmented, likely in response to the higher energy depositional environment. This made pollen assemblage identification in this core difficult. From what could be observed, n. podocarp is present up to 0.2 m (Fig. 6.3). Kauri is present in a single sample at 0.35 m. Native pollens occur in the sand shell facies and bioturbated silt facies. No rise in Bracken was observed in this core. Pine first occurs at 0.1 m and occurs within the organic sand/silt facies (Fig. 6.3).

No other European exotics were identified in this core. No rise in native pollens associated with late European land uses was noted in this core

.

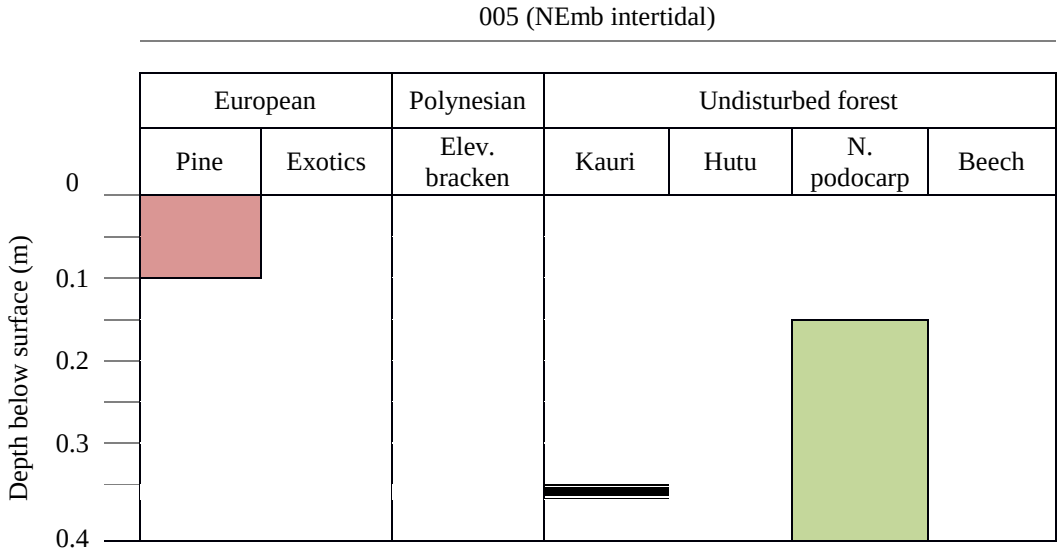

Fig. 6.3 – Pollen assemblage table for 005. Dark black lines indicate a single occurrence of a specific pollen type or elev. bracken.

6.2.3.4 Pollen Assemblage Interpretation

Bracken spikes associated with Polynesian habitation in the catchment occur alongside native forest pollens and generally prior to European pollens. The low sampling resolution of pollen analysis resulted in bracken spikes only being observed in one sample in each core. Thus, the broad increase in bracken associated with Polynesian settlement was not fully observed. This means that sedimentation rates for the Polynesian phase cannot be determined from pollen alone. This also means that where SARs are calculated from pollen, the associated date of 700 cal yr B.P could be expressed anywhere within Polynesian settlement phase.

With European arrival, native species were removed from the catchment (Hume & Dahm, 1991). This appears to be illustrated clearly by both CH1 and CH7, where the advent of European species correlates with the sudden decrease or even total loss of native species pollen. This trend is slightly apparent in 005; however, very low pollen concentrations have made this transition difficult to accurately distinguish. However, elevated pine pollen concentrations in the SEmb relative to

the NEmb suggest that anthropogenic sediments in the SEmb are primarily derived from pine forestry. This appears to validate interpretations made in Chapter 5, where thicker occurrences of SEmb anthropogenic sediments have been interpreted as related to recent (>1975 A.D.) pine plantations in the SEmb catchment.

Throughout the cores analysed, the pollen from the secondary native reforestation associated with the late European was not observed. This may be due to a number of factors. First, in the NEmb, core 005 had very little pollen. It may be possible that the native pollens were observed due to low concentrations. Within CH1 in the SEmb, pine and organic matter was abundant. This could have diluted the concentrations of native pollens in the samples analysed. This may also be the case CH7 in the NEmb.

Anthropogenic sediment in the SEmb and centre of the harbour have therefore been interpreted as primarily deposited after the advent of extensive pine plantations. Thus, an inferred date of ~1975 A.D has been applied to the lower boundary of these sediments in the SEmb to allow for recent European SARs to be estimated. Of course, some of the lower anthropogenic sediment will be early to late European. To account for these sediments, a margin of error has been associated with these SAR calculations. This margin of error has been calculated from the estimated early and late European SAR from Hume & Dahm (1991), multiplied by the length of the early and late European phases (155 years). This generally accounts for 20% of anthropogenic sediment thickness in the shallow subtidal regions. Assuming even sediment dispersal, a margin of error of 20% total anthropogenic sediment thickness above the lower boundary has been applied to these SAR calculations.

In the NEmb, however, sediments could not be distinguished in the same manner. Thus, sedimentation rates in the NEmb have been calculated over the entire span of European settlement in the catchment and not subdivided. Therefore, these SARs provide and average European SAR and do not consider differences in sedimentation between the three phases.

6.3 SARs Results

SARs have been calculated using the dating methods previously described for several core locations throughout the harbour (refer to Fig. 6.1).

Table 6.2 – SARs calculated for various estuarine phases in the Coromandel Harbour with associated dating methods. ASL=pyritic layer dating. 14C=radiocarbon. Recent European SARs have been "inferred" from the thicknesses of the organic rich sand/silt facies (see 6.2.3.4). Refer to Fig. 6.1 for core locations. Centre areas refer to centre harbour areas.

		Early est. sed.		Pre-Polynesian		Polynesian		European		
Core no.	Area	SAR (mm/yr)	Methods	SAR (mm/yr)	Methods	SAR (mm/yr)	Methods	Whole (mm/yr)	Recent (mm/yr)	Methods
005	NEmb	-	-	0.47 ± 0.03	14C	0.13 ± 0.04	Pollen	0.52 ± 0.25	-	Pollen
		-	-	0.25 ± 0.02	14C, pollen	-	-	-	-	-
CH1	SEmb	-	-	0.25 ± 0.01	ASL, pollen	0.05 ± 0.05	Pollen	-	10.37 ± 1.8	Inferred
		-	-	0.22 ± 0.04	ASL,14C	-	-	-	-	-
CH2	Centre	-	-	-	-	-	-	-	3.52 ± 0.62	Inferred
CH3	Centre	0.45 ± 0.08	ASL, 14C	0.23 ± 0.03	14C, ASL	-	-	-	4.98 ± 0.88	Inferred
CH5	Centre	-	-	0.22 ± 0.01	14C	-	-	-	2.2 ± 0.66	Inferred
CH7	NEmb	0.31 ± 0.01	ASL, 14C	0.1 ± 0.02	14C, pollen	0.07 ± 0.07	Pollen	0.77 ± 0.26	-	Pollen
CH9	SEmb	-	-	-	-	-	-	-	3.94 ± 0.7	Inferred
CH10	NEmb	-	-	1.8 ± 0.21	14C	-	-	-	-	-
		-	-	0.22 ± 0.09	14C	-	-	-	-	-

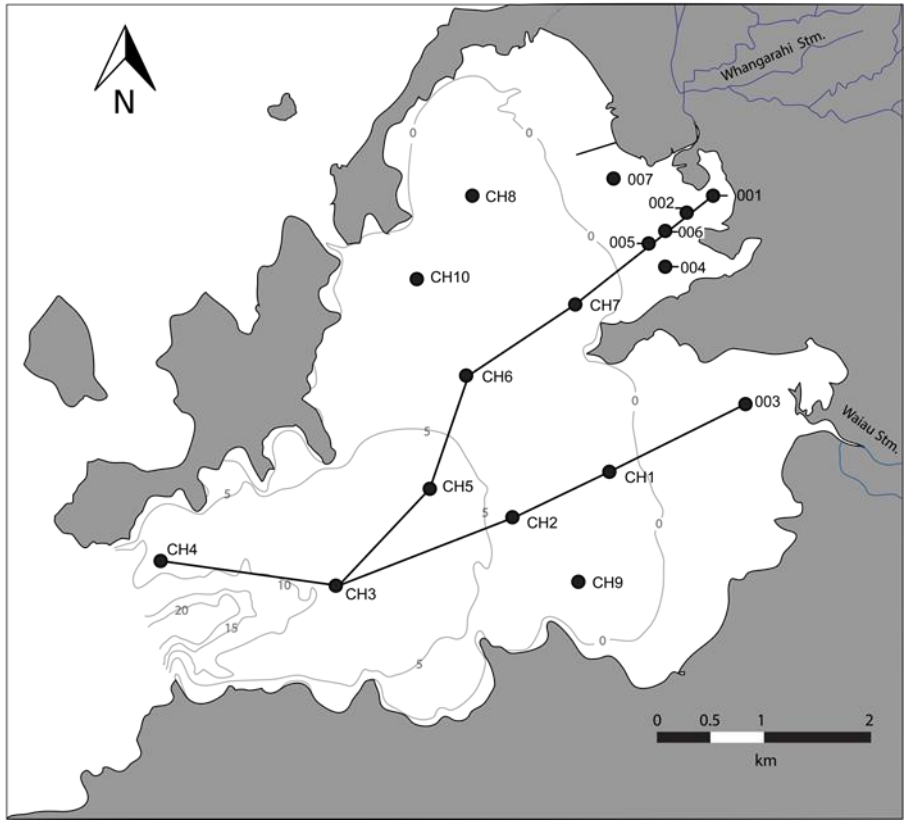

Fig. 6.4:–Coring map for SAR reference. Depths are expressed as depth below mean low water spring (MLWS). Bathymetry and locations of aquaculture farms taken from LINZ (2016) Chart NZ 533.

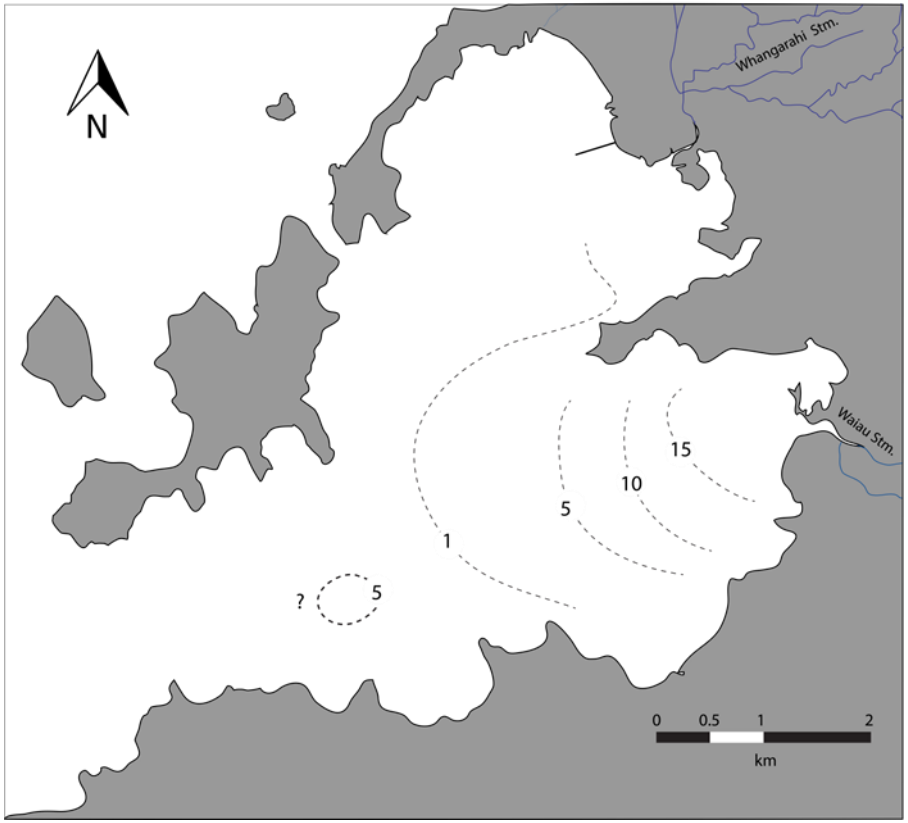

Fig. 6.5:-Recent European SAR iso-rate map created from SAR data from Hume & Dahm (1991) and this study. SAR are presented in mm/yr.

6.4 Interpretation of SARs

6.4.1 Early sedimentation rates

Early estuarine sedimentation rates have been estimated between inferred pyritic layer dates and radiocarbon dates. The early estuarine phase has been interpreted from SARs between dates of c.7500 cal yr B.P to c.7130 cal yr B.P in CH3 and from c.7500 cal yr B.P to c.5000 cal yr B.P in CH7 (Table 6.2). SARs are ~0.41-0.45 mm/yr. SARs for this period are elevated relative to intracore pre-Polynesian phase SARs by factors of 2-3 times, indicating that sedimentation in the harbour was high during the initial stages of estuarine development and have subsequently decreased over time. Hume & Dahm (1991) also noted a similar trend in sedimentation in one of the cores gathered from the Coromandel Harbour in their study. The authors did not discuss this initial high sedimentation in their report.

These rates may relate to initial rapid estuarine sedimentation and stream aggradation following the rise in sea-level to present mean sea level (PMSL) at c.7500 cal yr B.P. As sea level rose to near PMSL, a positive change in stream base level was induced (Schumm, 1993). This resulted in a lower stream gradient at the newly formed estuary, where sediments began to rapidly infill the harbour as the streams began to aggrade in response to the change in base level. Over time, aggradation would have decreased as streams attained a stable stream profile (Schumm, 1993). This shift in sedimentary environment would have correlated with a decrease in environmental energy, observed as a fining-upwards trend in estuarine sediments from the top of the pyritic layer to the bioturbated silt facies.

Early sedimentation rates higher are in CH3 than CH7 (Table 6.2). This may be related to the difference in sedimentary environments between the two core sites during deposition. CH3 is likely to be situated in or near the palaeo-Whangarahi Stream channel. This channel would have been expressed as a depression in the newly formed harbour advent of PSML. Flooded channels may experience rapid sedimentation due to their elevated accommodation space (i.e. more potential for sediment sequestration). In contrast, CH7 is located further away from the Whangarahi Stream near the intertidal regions adjacent to Preece's Point. Here, aggradation processes would have been slower.

6.4.2 Pre-Polynesian sedimentation rates

Pre-Polynesian SARs have been calculated from pXRF, ^{14}C and pollen data. Some of these rates have also been calculated from the pyritic layer marker bed. These rates will incorporate the elevated early estuarine sedimentation phase and may therefore have slightly overestimated SARs.

The highest pre-Polynesian SAR is observed within CH10 at a rate of 1.8 mm/yr (Table 6.2). This core is located 800 m west of the secondary inlet. Review of Google Earth time-lapse photography shows sediment plumes moving through this inlet over tidal cycles. It may be possible that erosion and redepositional processes near this inlet have influenced elevated sedimentation in these areas. This core has highly variable geochemistry which does not correlate well with trends in other subtidal cores (Fig. 4.17). This may be a reflection of the dynamic sedimentation in this area. This core appears to have SARs that are induced by the inlet and not of typical (fluvial sourced) sedimentation in the harbour. The SARs from this core should therefore be considered separately from the other SARs estimated for this phase.

Intertidal SARs of 0.25–0.47 mm/yr have been calculated from core 005 in the NEmb. Intertidal SARs are elevated compared with subtidal SARs (Table 6.2). This is likely to be related to the proximity of fluvial outwash regions, which are the source of the majority of harbour sediments (Mead & Moores, 2004). Subtidal SARs have been calculated using a number of dating methods and are generally conformable and low at ~0.1–0.25 mm/yr (Table 6.2).

The Coromandel Harbour's pre Polynesian SARs are comparatively high compared with other Coromandel Estuaries which have pre-Polynesian SARs typically <0.1 mm/yr (Table 2.1). Relatively elevated pre-Polynesian SARs suggest that the Coromandel Harbour naturally infills more rapidly than its regional counterparts. The Coromandel Harbour catchment shares a similar topography though is as large as many of its regional counterparts (Jones, 2008). Therefore, it is not likely that elevated amounts of catchment sediments were

moved into the harbour are responsible for elevated SARs during this phase. Elevated SARs have been interpreted as induced by the sheltered nature of the harbour, where wind wave mixing and influence from the open ocean are restricted (wind dynamics described in subsection 2.3.4). Despite having a large tidal prism, the harbour may still have a low energy environment and therefore be able to entrain elevated amounts of catchment material through time.

6.4.3 Polynesian sedimentation rates

Polynesian sedimentation rates were calculated from two cores (Table 6.2) exclusively using pollen assemblage analysis. Polynesian SARs are ~0.5–0.13 mm/yr, and are generally around 2 times lower than pre-Polynesian SARs estimated from the same cores (Table 6.2). It is typically the case that Polynesian SARs in Coromandel estuaries are elevated relative to pre-Polynesian SARs, however, this is not observed here (Hume & Dahm, 1991, Sheffield *et al.*, 1995). Polynesian SARs may be underestimated due to pollen dating limitations. Due to the 5 cm of error associated with the bracken spike method, the upper error margin often intercepted the error margin of another pollen date, which made the lower SAR value zero (Table 6.2). These SARs should be treated as potentially underestimated.

6.4.4 European sedimentation rates

European SARs vary significantly across the harbour.

6.4.4.1 NEmb

In the intertidal regions of the NEmb, whole European SARs are on the order of 0.52-0.77 mm/y, or ~2-4 times greater than pre-Polynesian SARs. It is likely that these sediments have primarily been derived from deforestation and mining activities (Hume & Dahm, 1991). It is not clear how much sediment has been derived from either process with this data, however.

6.4.4.2 SEmb

Recent European SARs associated with pine plantations in the SEmb are ~3.94-10.37 mm/yr, around ~20–50 times greater than pre-Polynesian SARs. Recent European SARs are highest near the Waiau Stream outlet, and decrease towards the centre of the harbour (Fig. 6.5). Unfortunately, core 003, which is an intertidal core in the SEmb has been interpreted as a product of secondary redeposition, and thus SARs in the intertidal regions cannot be identified. Early European SARs estimated here are comparable with Hume & Dahm's (1991) SEmb intertidal SAR of 13.2 mm/yr.

These recent European SARs are the highest SARs observed throughout any Holocene estuarine phase.

6.4.4.3 Centre harbour to near inlet

Recent European SARs in the centre harbour have been primarily associated with pine plantation sedimentation (see subsection 5.2.9.1). SARs in the centre harbour range from ~2.2-3.52 mm/yr (Fig. 6.5). SARs appear to decrease moving away from the Waiau Stream mouth (Fig. 6.5). At the near inlet core location CH3, recent European SAR is ~4.98 mm/yr. This SAR is higher than surrounding subtidal areas (Fig. 6.5). It may be possible that the depression near the inlet has a high accommodation space for these sediments and is rapidly infilling as a result. Further coring in these areas may be able to validate this hypothesis.

6.5 Anthropogenic SAR Interpretation

Polynesian SARs estimated here are lower than pre-Polynesian SARs. It is unclear whether this is due to limitations of pollen analysis or if these SARs are correct. A more intensive pollen study Coromandel Harbour would prove useful in accurately identifying Polynesian SARs.

Whole European sedimentation in the NEmb have increased upon pre-Polynesian SARs by 2-3 times. Pine plantation SARs are the highest rates observed throughout the entire estuarine and SARs during anthropogenic phases are up to 20-50 times greater than pre-Polynesian SARs. The most significant

anthropogenic influence on harbour sedimentation appears to be derived from pine plantations in the SEmb catchment. Pine plantation activities are likely to continue in the future, and will therefore continue to infill the southern parts of the harbour at similar rates. Pine plantation sedimentation will primarily affect boating channels and affect marine farms within the SEmb. This poses serious implications for planned harbour development and aquaculture sustainability in these areas.

The only difference in catchment use between the NEmb catchment and SEmb catchment is the presence of mining in the NEmb and pine plantations in the SEmb. SARs in the NEmb are much lower than those observed in the SEmb, which suggests that mining and kauri deforestation activities have not contributed significant amounts of sediment into the harbour compared to pine plantation activities.

6.6 Summary

SARs for various phases of estuarine sedimentation have been estimated using inferred pyritic layer (sea level rise indicator), radiocarbon and qualitative palynology dates. DDT concentrations were lower than detection limits and thus could not be used in SAR studies.

Early estuarine SARs are high, at ~0.31-0.45 mm/yr and may be related to stream aggradation following the onset of PMSL at c.7500 cal yr B.P. Through time, stream profiles became more stable and aggradational sedimentation decreased to give typical, low estuarine sedimentation during the pre-Polynesian phase. SARs through the pre-Polynesian phase are on the order of ~0.1-0.47 mm/yr and are comparatively high relative to other Coromandel estuaries (see Table 2.1). This may be attributed to the sheltered nature of the harbour which allows for high siltation. Pre-Polynesian silt sized sediments sourced from the catchment appear to have been primarily sequestered in the centre of the harbour which has been identified as a possible depocentre for silt sized sediments.

Polynesian SARs estimated here are lower than pre-Polynesian SARs. It is unclear whether this is due to limitations of pollen analysis or if these SARs are correct. Early European, late European and recent European sediments could not be distinguished through pollen analysis in the NEmb. Whole European settlement SARs of ~0.52 –0.77 mm/yr have been calculated for the NEmb. These SARs are ~2-4 times greater than pre-Polynesian SARs. Pine sediments of recent European age were interpreted as representing the majority of anthropogenic sediments in the SEmb and centre harbour areas through facies and pollen analysis. Recent European SARs of up to ~3.94-10 mm/yr are observed in the shallow intertidal areas of the SEmb and decrease towards the centre of the harbour where rates of ~2.2-3.52 mm/yr are observed. The intertidal to shallow subtidal SEmb region of the harbour appears to be the primary depocentre for these sediments. Recent European SARs increase near the inlet to ~4.98 mm/yr. This may suggest that the near inlet areas are acting as a secondary depocentre for these sediments.

SARs relating to pine plantation activity are the fastest in the harbour since the mid-Holocene. Pine plantation sedimentation is likely to continue in the future. Therefore, pine plantations currently pose the greatest threat in terms of harbour infilling and must be carefully considered during the planning phase of proposed harbour development projects.

Chapter 7

Anthropogenic Sediment Contaminant Assessment

This Chapter addresses anthropogenic influences on heavy metal contamination in the Coromandel Harbour. First, heavy metals in human sediments are compared to pre-human sediments to qualitatively identify anthropogenic heavy metal pollution in the harbour. Secondly, heavy metal concentrations in anthropogenic sediments are compared to regional contaminant guidelines to identify the ecological threat surface sediment contaminants currently pose.

7.1 Heavy Metals

Estuaries entrain fluvial sediments and therefore act as sinks for pollutants derived from catchment industry and urbanization (Cundy *et al.,* 2003; Hedge, Knott & Johnston, 2009). Anthropogenic contaminants typically occur at high concentrations and constructively add to natural contaminants derived from the catchment (Hume & Dahm, 1991; Cundy *et al.,* 2003). Thus, anthropogenic sediments are usually enriched in contaminants relative to pre-human sediments (Hume & Dahm, 1991; Reeve, 2008).

Heavy metals, such as As, Zn, Pb, Cr, and Hg are loosely defined as toxic metal elements that can have adverse effects on ecologies or environments (Singh *et al.*, 2011). Elevated concentrations can have significant harmful effects on biota, accumulating within and disrupting vital organ functions and inducing mutagenesis within affected organisms (Yanko *et al.,* 1998; Cundy *et al.*, 2003; Hedge, Knott & Johnston, 2009). Heavy metals are persistent and are not naturally eliminated from estuarine environments (Harding, 2005). As a result, they tend to become entrained in estuarine sediments and bioaccumulate in estuarine food webs. Within the Coromandel Harbour, heavy metal contamination threatens the estuarine ecology, posing threats to both the environment and regional aquaculture.

7.2 Cause for Concern

Heavy metal contamination in the Coromandel Harbour has long been a topic of debate for the Coromandel populace (Hume & Dahm, 1991; Smallman, 2013; Collins, 2015). Many local residents have opposed harbour development projects due to fears that buried, inaccessible heavy metals will be resuspended and reintroduced into the aquatic environment (Hedge, Knott & Johnston, 2009; Smallman, 2013; Collins, 2015).

A number of harbour developments have been proposed as part of the Coromandel Harbour Facilities Project (2016). These developments include dredging the channels of the Coromandel and Te Kouma wharves to accommodate projected increases in tourism, recreational boating and aquaculture in the future. Additionally a proposed pier will extend from the Coromandel Wharf into the subtidal areas of the NEmb. These projects will disturb surfaces sediments that have unknown concentrations of heavy metal contamination. At present, there is little information to base environmental management practices for these developments.

No studies have investigated the spatial distribution of anthropogenic heavy metal contaminants in regions away from the intertidal regions (see subsection 2.7). Therefore, there is a knowledge gap related to the distribution and toxicity of anthropogenic sediments in the subtidal regions of the harbour. This knowledge gap necessitates a study of harbour wide contaminant investigation.

Here, anthropogenic heavy metal contaminants are compared with pre-human baseline conditions to gather enrichment factors (EFs), which are used to interpret anthropogenic influences on heavy metal transport to the harbour. Then, anthropogenic heavy metal contaminants are compared with the Australian and New Zealand Environment and Conservation Council (ANZECC) Interim Sediment Quality Guidelines (ISQG) to identify areas of the harbour with potentially threatening concentrations to estuarine ecologies. All geochemical data presented here has been collected from pXRF analysis (methods discussed in Chapter 5). pXRF heavy metal measurement accuracies for these elements are discussed in Chapter 5.

7.3 Methods

7.3.1 Contaminant enrichment factors (EFs)

Calculating contaminant EFs in sediments is a useful method of quantitatively measuring human influence on sediment chemistry.

When interpreting the contamination of a sediment, contaminated samples must be compared against an uncontaminated reference sediment (Abrahim & Parker, 2008). Pre-human baseline contaminant concentrations of each heavy metal from each core were calculated from sediments that were deposited prior to human habitation in the catchment according to the age model (Abrahim & Parker, 2008; for dating, see Chapter 6). Pre-Human baselines were calculated from intervals with similar textural characteristics to the anthropogenic sediments to reduce errors associated with grain size effects (Abrahim & Parker, 2008). Five measurements for each contaminant were taken from a non-fluctuating pre-human baseline and averaged to provide a reference concentration. EFs were calculated by dividing the concentration of heavy metals in anthropogenic sediments by the pre-human baseline reference concentration:

$$Enrichment factor = \frac{Heavy\ metal\ concentration}{Pre\text{-}human\ Baseline\ average}$$

Heavy metals arsenic (As), lead (Pb) zinc (Zn) and chromium (Cr) were of primary focus as they have concentrations above the pXRFs detectable thresholds throughout all cores. Other heavy metals, such as mercury (Hg), cadmium (Cd) and copper (Cu), often had baseline concentrations lower than pXRF detection limits; therefore EFs for these elements could not be calculated.

Contaminant enrichment analysis was undertaken on cores CH1, CH2, CH3 and CH7. Other cores have either not been analysed through pXRF or have had biogenic Ca induced dilution effects (Ca dilution discussed subsection 5.1.6.1.4) in the anthropogenic sediments.

Differences in grain size will influence heavy metal distribution and concentration (Hume & Dahm, 1991; Abrahim & Parker, 2008). Heavy metals are typically

associated with finer grained sediments (i.e. silts and clays) in estuarine environments, where heavy metals readily sorb into the large surface area of these sediments (Hume & Dahm, 1991; Singh *et al.,* 1999; Lin & Puls, 2000; Maslennikova, Larina & Larin, 2012). To account for variations in grainsize, heavy metal contaminants are typically normalised against a grain size proxy, usually Fe or Al, (Abrahim & Parker, 2008; Karageorgis *et al.*, 2009) however, in this setting, both are likely to be released alongside heavy metals, thus, normalisation was not undertaken.

7.3.2 Contaminant comparisons with ANZECC ISQG

Anthropogenic heavy metals concentrations measured through pXRF have been compared with the ISQG classifications for core sites 005, 007, and CH7 in the NEmb and CH1, CH2, in the SEmb, and CH3 in the centre harbour. ISQG-Low and High values for heavy metals discussed in this Chapter can be found in Table 2.2.

7.4 Results

7.4.1 Anthropogenic heavy metal EFs

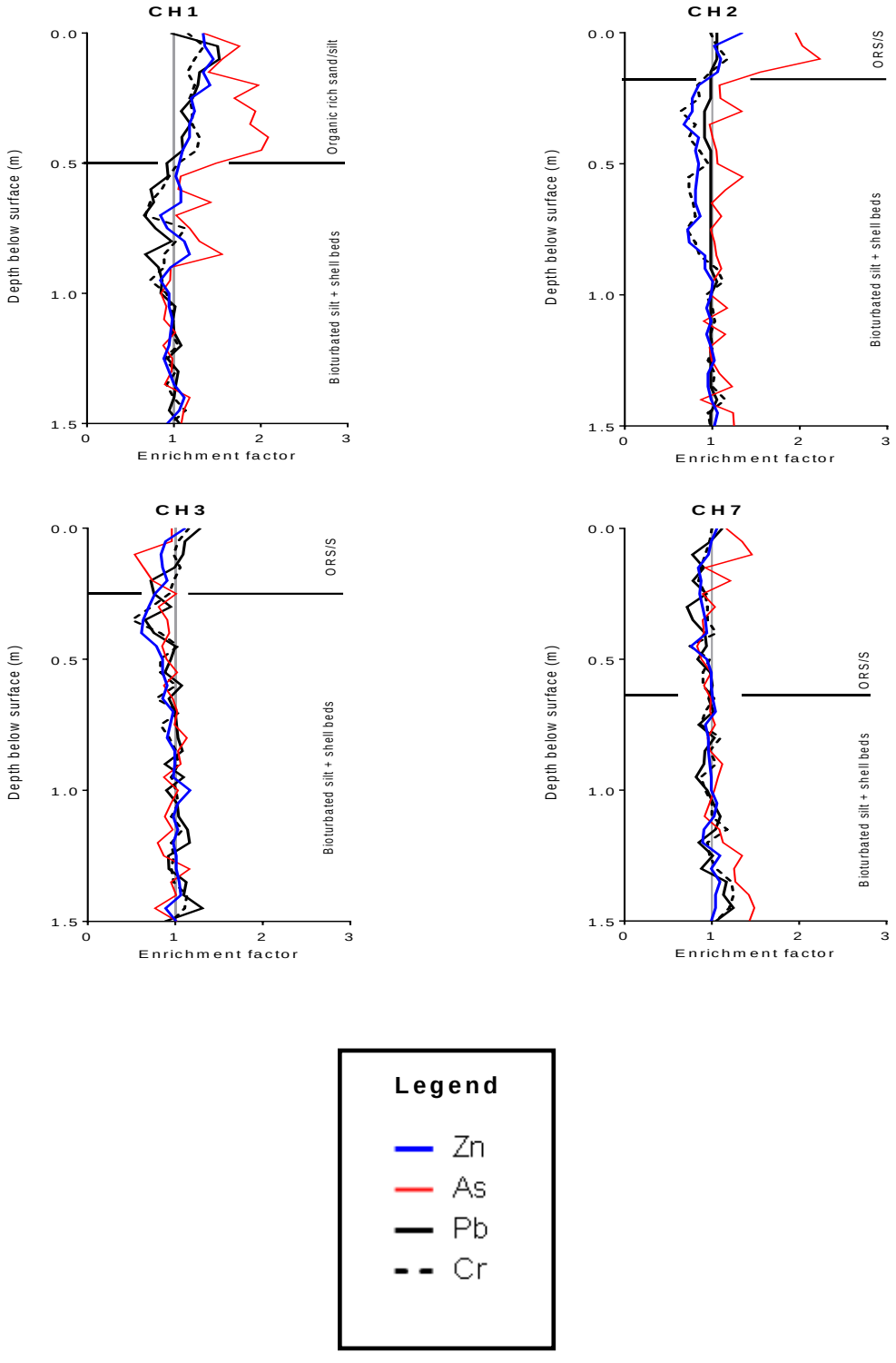

Fig. 7.1 – Contaminant enrichment factors for each core plotted against depth. Horizontal lines on graphs indicate the boundary between the organic rich facies and bioturbated silt and sandy/silty shell facies.

Table 7.1 - Average contaminant enrichment factors for the organic rich sand/silt facies in the cores analysed.

	Average contaminant enrichment factor			
Core no.	As	Zn	Pb	Cr
CH1	1.73	1.28	1.14	1.2
CH2	2.07	1.16	1.05	1.07
CH3	0.96	1	1.2	1.1
CH7	1.32	1	0.96	0.97

CH1, CH2 and CH3 show average enrichments of Zn, Pb and Cr of <1.3. CH7 shows no enrichment in these elements. Arsenic in CH1, CH2 and CH7 have average enrichments of 1.73, 2.07 and 1.32 respectively (Table 7.1). Arsenic in CH3 is not enriched above pre-human baseline (Table 7.1). Enrichment of heavy metals in these cores correlates with the organic rich sand/silt facies (Fig. 7.1). Depletion in heavy metals (i.e. values below baseline values) are observed below the organic rich facies in these cores. This may be related to the dilution effect induced by the shelly sand facies that underlies the organic rich facies (Fig. 7.1, see stratigraphic logs in Chapter 4).

7.4.2 Concentrations of anthropogenic contaminants

Heavy metals Zn, Pb, Cr, Cd and Cu are all below ISQG-Low values for all anthropogenic sediments identified in this study (see all heavy metal data in Appendix E) (Table 7.2). Only As and Hg exist above ISQG-Low values in sediments analysed.

The highest levels of As, Zn and Pb are found in core site 007 which is located at the mouth of the Whangarahi stream (Table 7.2). All anthropogenic samples analysed from core 007 have As concentrations greater than ISQG-Low value of 20 mg/kg. Harbour-wide maximum As concentrations of 33.5 mg/kg are observed at the surface of core 007. Several values of As in subtidal cores CH1, CH2 and CH7 exceed ISQG-Low values (Table 2.2). As has a maximum value of 23.1 mg/kg in CH1, 20 mg/kg in CH2 and 20.7 mg/kg in CH7 (Table 7.2). Hg in both anthropogenic and pre-human sediments throughout the harbour often have

concentrations of ~3–6 mg/kg compared with the ISQG-Low value of 0.15 mg/kg and high value of 1 mg/kg (Appendix E, Table 7.2). Intertidal cores 003 in the SEmb and 005 in the NEmb have the lowest anthropogenic heavy metal contaminants observed across all cores.

7.4.3 Dichlorodiphenyltrichloroethane (DDT) contamination

Dichlorodiphenyltrichloroethane (DDT) concentrations were measured for surface sediments in cores 005, CH1 and CH7 (DDT sampling described in subsection 6.1.4). All concentrations were below the detection limit of 0.005 mg/kg. Organic compounds must be normalised to 1% organic carbon, which was not measured in this study. Thus DDT contamination cannot be further discussed with regard to ISQG guidelines.

7.4.3.1 Grain size of anthropogenic sediments

Grain size of the anthropogenic surface sediment varies throughout the harbour. Core 003 in the intertidal region of the SEmb has a VF to M sand distribution, similar to that of core 005 in the intertidal region of the SEmb (Fig. 7.2). Core 007 has a predominantly clay to C silt grain size distribution, and is finer grained than core 005. Grain size distributions in the subtidal SEmb are clay to C silt (Fig. 7.2, *CH1-2* and *CH2-2*). CH3 in the centre harbour has a coarser distribution than the SEmb, predominantly comprised of VF to C silt.

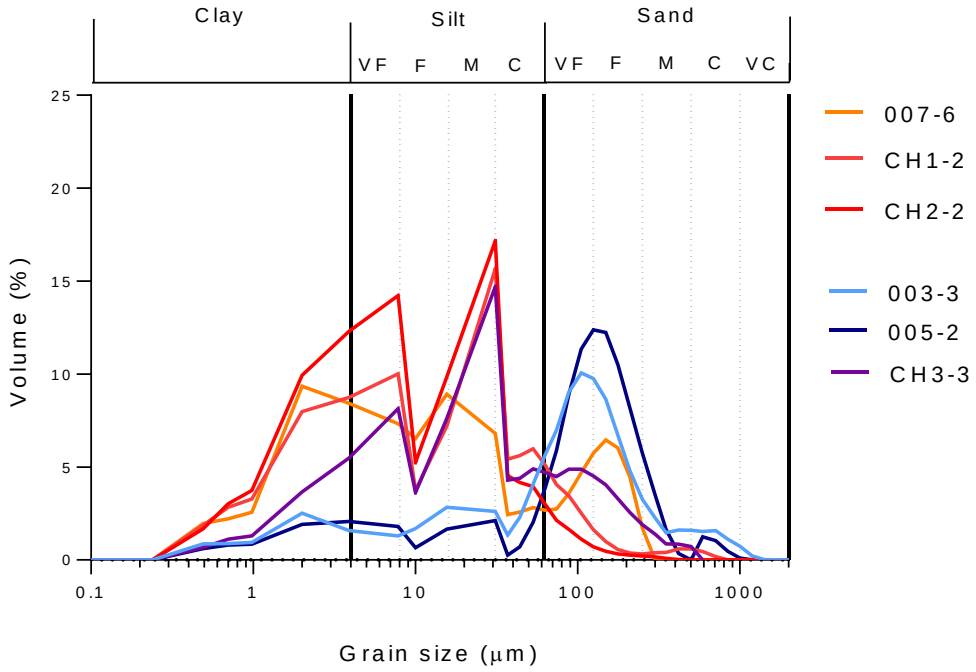

Fig. 7.2 – Grain size distributions for anthropogenic sediment across the harbour. Distributions in blue are from anthropogenic sediments with highest concentrations of heavy metals (refer to Table 7.2). Distributions in blue are from anthropogenic sediments with low concentrations of heavy metals.

Table 7.2– As, Zn, Pb and Hg concentrations within anthropogenic sediment for several cores. Cores not included here either have not been analysed through pXRF or were influenced by Ca dilution. LOD = Lower than pXRF detection limits.

As (mg/kg)

Depth (m)	003	005	007	CH1	CH2	CH3	CH7
0	12.3	11	33.5	15.4	17.5	9.5	16.5
0.05	11.9	11.2	24.3	20.2	18.2	9.5	19.1
0.1	11.2	13.2	29.6	17.9	20	5.3	20.7
0.15	11.6	12.5	26.1	16.1	13.9	6.3	
0.2	5.8		31	22.7	9.7	7.3	
0.25	7.1		27	19.5		10	
0.3	12.3		28.5	22.3			
0.35	10.3		31	21.6			
0.4	7.8			24			
0.45	8.2			23.1			
0.5	6.5			17.1			

Zn (mg/kg)

Depth (m)	003	005	007	CH1	CH2	CH3	CH7
0	47	63	93	68	75	64	64
0.05	40.7	60	82	69	57	51	60
0.1	42.2	57	94	74	61	48	58
0.15	45	47	98	68	59	49	
0.2	43.8		95	72	47	52	
0.25	40.3		95	61			
0.3	42		105	63			
0.35	49		81	60			
0.4	46			60			
0.45	45			56			
0.5	48			54			

Pb (mg/kg)

Depth (m)	003	005	007	CH1	CH2	CH3	CH7
0	9.5	12.4	29.5	14	17.2	17.5	18.6
0.05	8.7	16.3	39	21.9	15.2	15.1	16.3
0.1	8.7	16.1	30	22.2	14.6	14.8	12.9
0.15	9.7	11.9	38.8	18.9	10.5	13.5	
0.2	12.8		31.2	18.6	11.9	9.8	
0.25	8.6		38	17.7			
0.3	10		44	15.8			
0.35	11		23.3	17.4			
0.4	13			15.9			
0.45	11.2			16.1			
0.5	11.7			13.4			

Hg (mg/kg)

Depth (m)	003	005	007	CH1	CH2	CH3	CH7
0	3.4	<LOD	4	3.8	<LOD	3.9	3.6
0.05	3.7	3.1	<LOD	<LOD	<LOD	3.8	<LOD
0.1	<LOD	3.5	<LOD	5	<LOD	3.4	5.1
0.15	4.1	3.6	4	4.6	4.9	3.8	
0.2	3.6		3.5	5.7	<LOD	<LOD	
0.25	2.9		4	3.1			
0.3	<LOD		5.2	3.2			
0.35	<LOD		5.5	4.4			
0.4	4.6			4.9			
0.45	<LOD			5.9			
0.5	4.1			3.5			

7.5 Anthropogenic Contamination Interpretation

Mercury has concentrations of ~3–6 mg/kg in a significant proportion of anthropogenic and pre-human sediment samples (Table 7.2, Appendix E). This places a significant volume of harbour sediments well over the ISQG-High value of 1 mg/kg. Previous studies have found elevated levels of Hg in Coromandel Harbour sediments (Coffee, 1992; PDP, 2012; Aurecon, 2013). However, of all studies that were focused at the Whangarahi Stream mouth, a maximum value of 3.1 mg/kg has been identified. Concentrations of 3–6 mg/kg appear to be close to detection limits of the pXRF used, where many values are presented as lower than detection (<LOD). It may be possible that Hg concentrations are overestimated by the pXRF. With the data available, it is unclear if the concentrations of Hg are representative or misinterpreted. Further geochemical analysis (perhaps by lab XRF, not pXRF) is required to identify whether these measurements are accurate.

Throughout the sediments analysed, arsenic is the only other heavy metal that exceeds ISQG-Low values. Arsenic has elevated enrichments compared to other heavy metals analysed (Fig. 7.1, Table 7.2). This may be because As in iron hydroxides is soluble in the typically neutral pH conditions of Coromandel stream networks, while other base metals such as Zn, Cu and Pb are not readily leached from mine wastes and catchment rocks under the same conditions. (Craw & Chappell, 2000). Arsenic may therefore be moving through stream networks and entering the harbour at a greater rate than other heavy metals.

A maximum arsenic concentration of 33.5 mg/kg occurs in surface sediments near the Whangarahi Stream mouth, and is most likely related to mine waste outwash which is well known to have fluxed heavy metals into stream networks (Hume & Dahm, 1991, Craw & Chappell, 2000). The sediment which this maximum arsenic concentration was measured in is a chiefly clay to silt sediment (Fig. 7.2, *007-6*). It is not unexpected to find high concentrations of heavy metals in clays, where soluble heavy metals readily adsorb to negatively charged clay surfaces (Cadena Rizvi & Peters, 1990; Bailey et al, 1999). Moving away from the Whangarahi Stream mouth to distal regions of the NEmb at core sites 005 and CH7, grain size increases and heavy metal concentrations decreases (Table 7.2, Fig. 7.2). It is likely that the heavy metals derived from mining in the NEmb are associated with

clays and silts. Interestingly, the clay component in the NEmb appears to be confined to the Whangarahi Stream mouth, and has not been transported throughout the high energy intertidal environment to site 005. This may suggest these clays, and elevated mining heavy metals, are sequestered in the outwash of this river, possibly by flocculation processes. This hypothesis is further discussed in Chapter 8.

The clay component within anthropogenic sediments at the Whangarahi Stream mouth is much higher than in the intertidal region of the SEmb (Fig. 7.2). This suggests that mining activities have fluxed a large volume of clays to this region of the harbour. This may be related to extensive working and physical weathering of catchment rocks during mining activities. This hypothesis discussed in Chapter 8.

Anthropogenic sediments in the SEmb and centre harbour have been interpreted as predominantly pine plantation sediments (see subsections 5.2.9.1 and 6.1.2.1.6). Arsenic enrichments in pine plantation sediments against pre-human baselines are pronounced throughout the subtidal SEmb at cores CH1 and CH2, enriched by factors of up to 2 times. The highest arsenic concentrations occur at <23 mg/kg, and only marginally exceed ISQG-Low value of 20 mg/kg. Note that these measurements have an error of ±3 mg/kg (pXRF errors defined in subsection 5.1.6.1.3). Heavy metal concentrations are higher in the subtidal SEmb than in the intertidal region of the SEmb at core 003. Within cores CH1 and CH2, anthropogenic sediments have a higher clay and silt component than 003. It is likely that heavy metals are associated with clays to silts in the SEmb. In contrast to the NEmb, these clays and silts appear to be transported away from the intertidal regions and into the subtidal SEmb. It may also be possible that as heavy metals are liberated by pine plantation activities, they can readily sorb to fine organic detritus. Organic matter particles are low in density and readily transported to, and dispersed throughout the subtidal regions of the SEmb. Heavy metal concentrations are low in the intertidal regions and at core CH3 near the inlet. Thus, the primary depocentre for pine plantation heavy metals in the SEmb appears to be in the subtidal region of the SEmb.

7.6 Summary

Heavy metals Zn, Pb, Cu, Cr, Cd analysed in this study do not exist over ISQG-Low values, and do not pose a significant threat to estuarine ecologies Arsenic and mercury are the only contaminants in the sediments analysed that pose threats to estuarine ecologies, rising above the ISQG-Low guidelines. Hg values of ~3–6 mg/kg occur throughout pre-human and anthropogenic sediments. It is not known whether these values are accurate or a result of pXRF measurement limitations. The maximum measured arsenic concentration of 33.5 mg/kg occurs in surface sediments near the outwash of the Whangarahi Stream., and appears to be related to heavy-metal-rich clay sediments sourced from mining activities. Mining-related clays appear to be sequestered as the Whangarahi Stream mouth, and thus anthropogenic sediments further from the stream mouth in the NEmb have low heavy metal concentration and enrichments against pre-human levels. Heavy metals Pb, Zn and Cr are not enriched in these areas. Only arsenic is enriched by 1.3 times greater than baseline levels in these areas.

Throughout the other regions of the harbour, elevated arsenic concentrations in anthropogenic sediments only slightly exceed ISQG-Low ratings with values of <23 mg/kg. Pine plantation heavy metals appear to be related to clay and silt sediment composition. Heavy metals may also be adsorbing to readily available organic detritus. The main depocentre for pine plantation heavy metals appears to be the subtidal SEmb. In these areas, arsenic is enriched against baseline levels by up to 2 times.

Chapter 8

Sedimentary Evolution of the Coromandel Harbour

This chapter collates all data presented in previous chapters to outline the sedimentary evolution of the Coromandel Harbour.

The evolution of the harbour has been arranged into depositional phases. These phases are the subaerial phase (oldest), pre-human estuarine phase and anthropogenic phase (most recent). These phases are specifically used to define harbour evolution in this Chapter, and are distinct from other time phases defined in this report.

8.1 Subaerial Phase

Prior to mid-Holocene sea level rise at c.7500 cal yr B.P, the Coromandel Harbour area was a subaerial environment (Hume & Dahm, 1991; Mead & Moores, 2004; Clement 2011). Soils developed from eroded catchment Kuaotunu Group and Manaia Hill group rocks alongside terrigenous organic inputs (see subsection 5.2.1.1).

8.1.1 Pleistocene subaerial weathered soils

Laminated orange, heavily weathered sandy clay loams are the lowermost sediments observed in this study (Fig. 4.22). No dates have been measured from these soils, thus their formation ages are unclear. Some inferences of the soil ages can be made from their characteristics, however.

Marine sediments that overlie this facies have been dated consistently at <c.7200 cal yr B.P (Table 6.1). No further evidence of marine sediments older than Holocene age has been identified in this study. These soils must have therefore accumulated before the mid-Holocene advent of present mean sea level (PMSL), and after the previous time sea level was at ~PMSL. The last time sea level was

near its present day level in the harbour most likely somewhere near the last interglacial at c.120 ka, where sea level eustacy was near its present day level (Fig. 8.1) (Pillans *et al.*, 1998; Nichol, 2011). Limited information on relative sea level rise through the Pleistocene in the eastern Coromandel region restricts fine scale interpretation of when this may have occurred. These sediments have therefore been interpreted as developing somewhere between c.120 ka to c.7.5 ka (c.7500 cal yr B.P). The development of clays suggests extensive weathering, which is more likely to occur during warmer and more temperate climates (interpreted in subsection 5.2.1) (Morgan, 1995). This is further suggested by the substantial iron weathering and staining of these soils (iron staining described in 5.2.1.1). Therefore, these soils have been interpreted as forming during the warmer interglacial period prior to the extended last glacial maximum (eLGM) at c.29 ka (also see subsection 8.1.2 for further explanation).

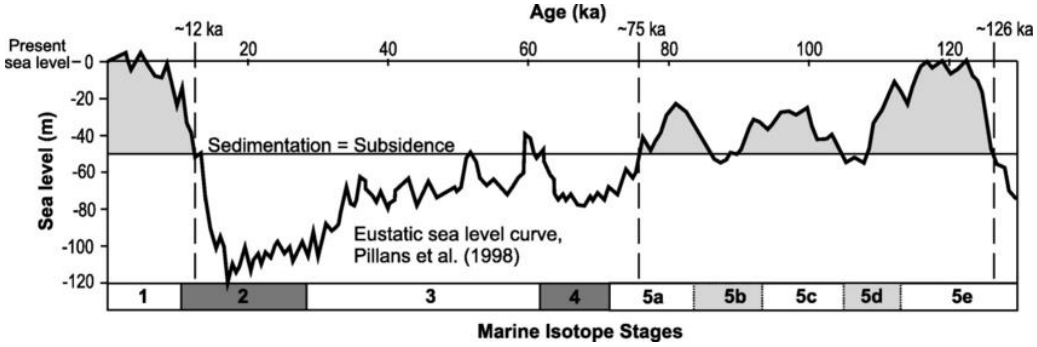

Fig. 8.1 – Sea level eustacy curve since 130 ka. From Nichol (2011), adapted from Pillans et al. (1998).

The extensive chemical weathering of these sediments suggests that these soils may have formed over extensive periods of time (thousands of years) in a temperate subaerial environment, where minerals in the soil were chemically weathered to form fine grained clay components (Fig. 5.8). The same weathering liberated iron out of mineral grains where it was then oxidised to give these clays a distinctive orange iron oxide colour (Fig. 5.7) (Morgan, 1995; Cornell & Schwertmann, 2003).

Heavy metals As and Zn are markedly enriched compared with other Coromandel Harbour sediments (Figs. 5.11, 5.12). These soils have a high clay content (Fig.

5.8). Clays have large surface areas with net negative charge and are well known to attenuate heavy metal cations from the environment (Lin, Z., & Puls, 2000; Cadena Rizvi & Peters, 1990; Bailey et al, 1999). Extensive weathering of Kuaotunu Group minerals likely released soluble heavy metal cations into the soil. Heavy metal cations were also likely eroded from the catchment and introduced to the soil during runoff events. Some heavy metal cations were adsorbed to negatively-charged clay mineral surfaces within the soils during these processes. As a result, these soils have high heavy metal concentrations, and are enriched in heavy metals compared with other Coromandel Harbour facies (see subsection 5.2.1.1).

These soils were only observed in core CH7, where soils were at relatively shallow depths that could be penetrated by coring procedures (see subsection 5.2.1.1). It is likely that these soils underlie the entire area of the harbour, but were not observed in other cores due to coring depth limitations. Subtidal regions appear to have thicker Holocene sedimentation compared to CH7, and the techniques used for intertidal coring led to limited depth of penetration. Personal communications with crew that obtained engineering-related drill cores from the harbour suggests that these soils commonly occur at depths of ~2-4 m throughout the harbour (Pers. Comm. Ian Boyce).

8.1.2 Soils and stream deposits

Light grey to brown, clay to VF sand sediments overlie the laminated orange clay soils in CH7 (high MS silt and High MS sand facies in Chapter 5). Similarly to the clays discussed above, these sediments underlie estuarine sediments of <7200 cal yr B.P and must have been deposited prior to the mid-Holocene and after the last interglacial at c.120 ka. These sediments have therefore been interpreted as terrigenous sediments (further discussed in subsection 5.2.2.1.1).

These sediments are not as oxidised or as chemically weathered as the orange clay soils which have been inferred as developing over extensive periods of time, suggesting that the sedimentary environment and weathering regime has changed between the depositions of these two sets of terrigenous sediments. Less extensive

chemical weathering and oxidation of iron in these sediments suggests that the climate may have become cooler, leading to lower rates of weathering have decreased. This may be related to cooling during the extended last glacial maximum (eLGM) in the Southern Hemisphere at 29-19 k cal yr. B.P (Newnham *et al.*, 2007). A transition from highly weathered clays may also suggest a shift in vegetation cover, where a dense forest cover that sheltered soils and allowed for deep weathering has been removed. This also appears to support the eLGM hypothesis: as temperatures decreased in the eLGM, vegetation shifted from tall trees to shrub and grass species, exposing the catchment to increased erosional processes (Newnham *et al.*, 2007). The lower sections of these sediments have therefore been interpreted as eLGM sediments. With the data available, it is not possible to distinguish sediments that were deposited immediately after the eLGM to the mid-Holocene sea level rise event. Post eLGM to >c.7500 cal yr B.P sediments will sit on top of the eLGM sediments, though their extent is not clear.

These sediments are interbedded with mm scale laminations of VF sand and organic matter. The soils also have markedly variable Fe and Ti, which suggests shifts in terrigenous sedimentation (Rothwell and Croudance, 2015). These traits are characteristic of floodplain deposits, with low-energy background sedimentation interbedded with coarser sandy lenses representing episodic flooding events. This gives these sediments a clay-silt to silt-sand interbedded structure (see subsection 5.2.2 and stratigraphic logs in Chapter 4). Prior to the Holocene, the palaeostream channels of the Whangarahi and Waiau Streams and their stream networks would have run through the catchment floodplain to the primary inlet and consequently out to sea (Fig. 8.2). During the eLGM, the amount of vegetation cover was reduced, which may have destabilised the river banks and exposed the catchment to flooding and overland flow erosion and redeposition. These sediments (high MS silt facies in Chapter 5) have been interpreted as eLGM to >c.7500 cal yr B.P floodplain deposits.

The proximity to the stream channel would have likely influenced the degree of flood sedimentation and coarser grained sedimentation. Within core CH3, a ~0.5 m thick sandy silt deposit (high MS sand facies in Chapter 5) has been identified

(discussed in subsection 5.2.2.2). This may represent a region nearer to the stream channel or a stream channel deposit.

The exact formation processes of these sediments do not fit within the scope of this project and are not further considered.

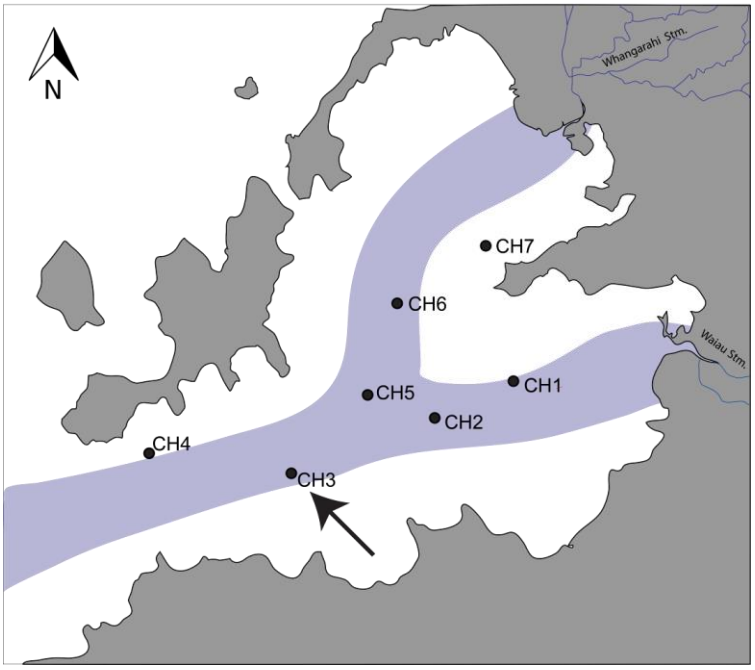

Fig. 8.2 - Map of possible palaeostream channels (blue) in the Coromandel Harbour with core locations where inferred flood plain and river deposits (high MS silt and sand) have been found. Core CH3 (marked with an arrow) is the only core to have inferred stream deposits.

8.2 Pre-human Estuarine Phase

8.2.1 Pyrite layer formation

Age: c.7500 cal yr B.P

A pyritised sediment layer has been identified below estuarine sediments in several areas of the harbour (see subsection 5.2.3). Pyritisation is commonly associated with mid-Holocene sea level rise (Dent, 1995; Powell & Martens, 2005; DER, 2015).

As sea level rose to its PMSL at c.7500 cal yr B.P, organic-rich subaerial soils and river deposits (high MS silts and high MS sands in Chapter 5) were inundated with sulphate-rich tidal waters (Dent, 1995; Powell & Martens, 2005; DER, 2015). Under anaerobic conditions, bacteria in these sediments reduced sulphate from sulphate-rich tidal water to produce hydrogen sulphide, H_2S. This H_2S reacted with dissolved iron in the sediment to form FeS_2, most commonly pyrite (DER, 2015).

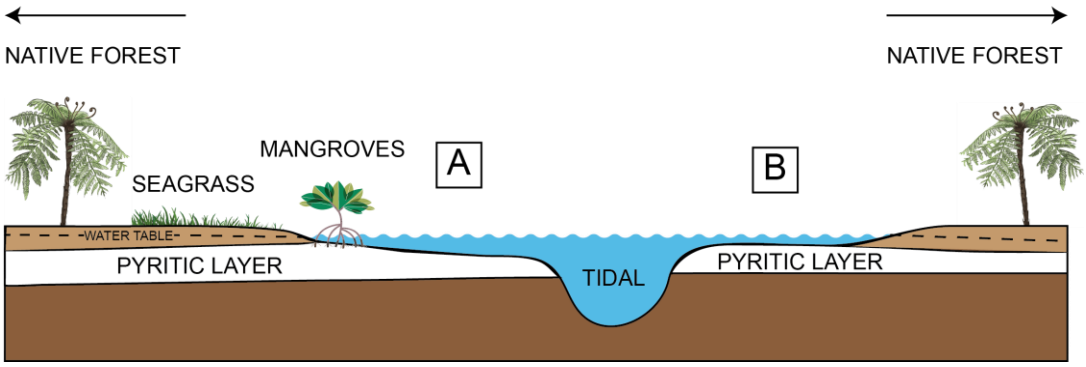

Fig. 8.3 – Pyritisation following the advent of mid-Holocene PMSL in the Coromandel Harbour. Two pyritisation scenarios, "A" and "B" are described in text. Adapted from Sammut & Lines-Kelly (2004).

Pyrite formation in these settings requires anaerobic waterlogged conditions and (Van Breemen, & Buurman, 2002) It is unlikely that pyritisation developed in a anaerobic swamp setting, as the concentration of organic matter is uncharacteristically low for this scenario. It is more likely that pyritisation occurred in a restricted marine setting, where tidal waters were stratified due to limited tidal flushing through a constricted tidal inlet. Stratification of tidal waters would have induced anoxia in bottom waters, and thus the submarine sediment surface. Assuming sea level rose slowly, pyrite would have would have initially formed under a restricted marine marginal sea setting, with the harbour both undergoing land pyritisation (i.e. pyritisation seen under the native forest in Fig. 8.3 *A*) and submarine pyritisation (i.e. pyritisation occurring beneath tidal waters). Marginal marine vegetation (such as mangroves and seagrass) was likely present to varying degrees, depositing organic matter at the sediment surface (Fig. 8.4, *A*).

Under these conditions, the pyritisation initially diagenitically altered in the top of the eLGM to >c.7500 cal yr B.P terrigenous sediments. Thus, apart from redox-sensitive elements, no marked changes in geochemistry are apparent between the pyrite layer and the eLGM to >c.7500 cal yr B.P sediments (high MS silt facies in Chapter 5). As early estuarine sedimentation occurred, fresh Fe and organic matter would have been moved into the restricted basin. Pyritisation would have continued to occur in these early estuarine sediments (such as in Fig. 8.4). Organic and Fe input may have been higher near the outwash of streams, which may explain why the pyritised layer is thickest in CH6 (associated with possible palaeostream channels) (Fig. 4.21). This would explain why, in terms of texture and colour, the pyritised sediments grade from sharing the characteristics of the underlying eLGM to >c.7500 cal yr B.P high MS silt facies to sharing the characteristics of the overlying Holocene estuarine sediments of the bioturbated silt facies (see stratigraphic logs in Fig. 4.18 to Fig. 4.21).

Over time and as sea level rose to PMSL, the stratification of the estuary was destroyed as the tidal inlet area increased and allowed for increased tidal mixing. As estuarine waters transitioned to a well-mixed aerobic setting pyrite formation likely stopped. Bottom waters became oxygenated, and organisms began to dwell at the sediment surface, where they bioturbated sediments, further exposing sediments to aerobic conditions. Thereafter, non-pyritised estuarine sediments began to accumulate on top of these pyritic layers.

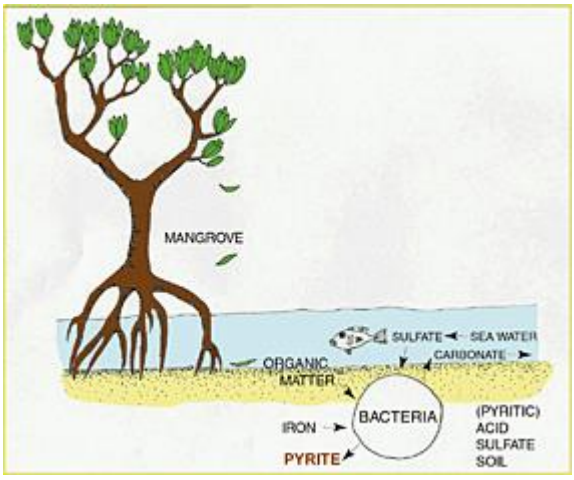

Fig. 8.4 - Formation of pyrite in an estuarine environment (from Queensland Government, 2013). Note, an acid sulphate soil is a pyritic layer that has been introduced to an aerobic environment (DER, 2015).

Under aerobic conditions, pyrite will oxidise to H_2SO_4 and a suite of iron and sulphur complexes (see subsection 5.2.3). As pyritic sediments such as these are exposed Pyritic sediments in the nearshore (i.e. intertidal) regions of the harbour may have been exposed to aerobic conditions through groundwater interaction or fluctuations in sea level. This is here interpreted as the reason why CH1 (shallow subtidal SEmb) does not share a similar Fe/S correlation as observed in other cores (Fig. 5.19). Oxidation processes do not appear to have occurred in the deeper subtidal regions of the harbour, where Fe/S correlation is strong (Fig. 5.19). This is unsurprising as sea level has remained above or about its present mean level since the mid-Holocene PMSL advent (Clement, 2011).

8.2.2 Early estuarine stream aggradation

Age: c.7500 cal yr B.P-c.5000 cal yr B.P

As sea level reached ~PMSL, a positive change in base level was induced to the Coromandel Harbour's stream networks (Fig. 8.5) (Schumm, 1993, Waugh, 2000). The newly formed estuary became the base level to these streams, and organic-rich catchment sand and silts materials rapidly aggraded in the present day subtidal regions of the harbour at rates of ~0.31–0.4 mm/yr, burying the pyritic layer. These sedimentation rates are greater than intracore rates during the subsequent pre-human sedimentation phases (Table 6.2) (sedimentation rates

described in subsection 6.4.1). SARs have been calculated between c.7500 cal yr B.P to c.5200 cal yr B.P. The exact extent and dynamics of this sedimentation has been averaged, and timing of aggradation and sedimentation variability is unknown (refer to subsection 6.4.1 for further discussion). Over time, the graded profiles of the stream networks began to reach an equilibrium, and aggradation in the nearshore areas of the harbour decreased until sedimentation transitioned to stable estuarine sedimentation (see 8.2.3). This broad transition is expressed as a fining in sedimentation into the bioturbated silt facies/steady estuarine sedimentation in the following section.

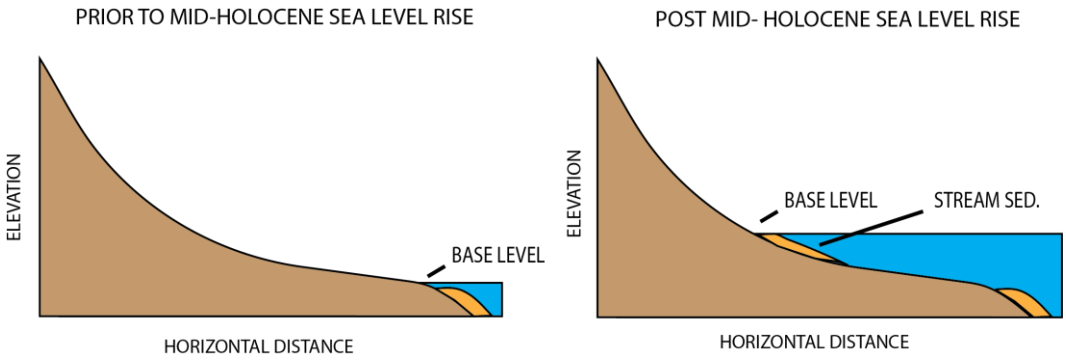

Fig. 8.5 – Stream aggradation following an increase in base level with mid-Holocene sea level rise in the Coromandel Harbour. Not to scale.

8.2.3 Steady estuarine sedimentation

Age: c.7500–700 cal yr B.P

Once streams had reached a relatively stable graded profile, harbour sedimentation rates appear to have decreased and become more stable to ~0.47 mm/yr in intertidal regions and ~0.1–0.25 mm/yr in subtidal regions (Table 6.1). It is difficult to identify when this transition to steady estuarine sedimentation happened exactly. As steady European SARs have also used the pyritic layer dating method, SARs calculated for this phase do overlap with the early estuarine phase.

An extensive forest cover likely reduced catchment erosion and sediment runoff into the harbour. Sediment delivery to the harbour did not change significantly through this phase, with physical and geochemical measurements remaining

generally constant and consistent between subtidal areas (refer to down-core geochemical data in subsection 4.2). Low levels of erosion of Kuaotunu Subgroup rocks resulted in low volumes of heavy metals transported into the harbour (refer to subsection 2.6.1 for further explanation). As a result, these sediments have the lowest heavy-metal concentrations of all estuarine sediments (Fig. 5.25, Fig. 5.26, Fig. 5.27).

Shell beds accumulated both *in situ* and through erosion and redeposition, likely associated with storm events (see core logs in subsection 4.1). Some near surface shell beds within the subtidal regions have been dated at c.3200 cal yr B.P (Table 6.1). This may suggest that the subtidal harbour has been sediment starved up until European settlement (see subsection 5.2.6.1 for further discussion).

The subtidal regions of the harbour have greater pre-human estuarine sediment thicknesses compared with the intertidal regions (Fig. 5.28). The centre of the harbour appears to be the depocentre for these chiefly silt-sized sediments (Fig. 5.28). This suggests that the majority of sediments moving into the harbour during pre-human estuarine times were silts. This also appears to show that the centre of the harbour naturally infills with clays to silt sized sediments at rates greater than those observed in other Coromandel estuaries (Table 2.1).

8.3 Anthropogenic Phase

8.3.1 Polynesian

Age: 700 cal yr B.P–130 cal yr B.P (1820 A.D)

Polynesian settlers arrived in the Coromandel at c.700 cal yr B.P (Hume & Dahm, 1991, Wilmshurst & Higham, 2004; McGlone et al, 2005). Upon arrival, settlers used small fires to clear coastal lands for crops (Hume & Dahm, 1991, Sheffield et al, 1995). Polynesian SARs are observed as lower than pre-Polynesian SARs in the two core sites analysed in this study (see Chapter 6 for dating). SARs range from ~0.05-0.13 mm/yr. These SARs may associated with errors derived from low sampling resolution, and have been interpreted as likely underestimated (Polynesian SAR limitations further discussed in subsection 6.4.3). Geochemical characteristics of Polynesian-age sediments are also uncertain, as Polynesian sediments typically coincided with shell hash that induced dilution errors in pXRF measurement (dilution errors described in subsection 7.4.1). The influences of Polynesian land-use changes on the evolution of the harbour are unclear.

8.3.2 European

8.3.2.1 Early European

Age: 130 cal yr B.P – 40 cal yr B.P (1820 A.D – 1910 A.D)

European kauri deforestation and kauri damming began in ~1820 A.D and continued through to ~1910 A.D. Kauri was felled in significant volumes and transported through the Coromandel Harbour's stream networks (refer to subsection 2.4.2.3.1) (Hume & Dahm, 1991). Organic rich sediments entered the harbour from soil erosion and as milling outwash. Gold was mined extensively though the Kuaotunu Group rocks in the catchment from 1860 A.D to around 1910 A.D (Hume & Dahm, 1991; Moore & Ritchie, 1996). Vast volumes of mine tailings were deposited in stream channels in the NEmb catchment (Hume & Dahm, 1991; Moore & Ritchie, 1996). These practises have likely contributed the majority of whole European (i.e. 1820 A.D-present) sedimentation in the NEmb which have contributed to whole European SARs are ~0.52-0.77 mm/yr in the NEmb (Table 6.2). Based on the interpretation of mining-related sediments in cores 007, 004, 005 and CH7, the mouth of the Whangarahi Stream appears to be

the depocentre for these sediments in the NEmb (Fig. 5.46). Early European sediments were difficult to identify in the SEmb, and thus distributions in these areas are not presented (refer to Chapter 6 for further SAR discussion).

At the Whangarahi Stream mouth, anthropogenic sediments have been noted with high clay and silt grain size distributions (Fig. 7.2). Clay sediments do not occur at high concentrations in the SEmb (Fig. 7.2). The only significant difference in NEmb catchment use has been gold mining. This suggests that mining activities generated a significant volume of clay sediment. This may be related to extensive crushing and working of mining ore during mining periods. Kuaotunu Group rocks were mined from the catchment and crushed in stampers, with tailings deposited in Whangarahi Stream channels. Some clay sediments may have been generated from these practices. Coarser fine grained sands to silts may have also been readily exposed to chemical weathering processes in the catchment, which may have eroded to clay sized sediments through time.

Coarser silt to sand distributions with less clay and more coarse sand are noted ~0.75-1.25 km to the south in cores 005 and CH7 (Fig. 7.2). This may suggest that these clays are sequestered in near the outwash of the Whangarahi Stream. It may be possible that once mining clays enter the harbour, they are flocculated and sequestered in higher energy environments along with sand-sized sediment (Fig. 7.2). Flocculated clays require higher energies to erode than unflocculated clays. It may be possible that the energies in this area are below the threshold necessary to erode the clays, and so these clays have remained *in situ* since deposition and have not been transported to further reaches of the NEmb.

The clay component in the NEmb has been associated with elevated heavy metals, where heavy metals have likely adsorbed to clay surfaces (see subsection 7.5). A coarsening in anthropogenic sediments away from the Whangarahi Stream mouth coincides with a decrease in anthropogenic heavy metal concentrations (heavy metal variability discussed in subsection 7.5). Thus, elevated concentrations of mining-related heavy metals As and Hg appear to be associated with silts and clays which are primarily located at the mouth of the Whangarahi Stream mouth (heavy metal concentrations for these sediments can be found in subsection 7.4.2).

8.3.2.2 Late European

Age: 1910 A.D–1975 A.D

Late European sedimentation was not identified in this study. This was likely resultant of pollen dilution and low native pollen concentrations in the sample analysed for pollen assemblage (refer to subsection 6.4 for pollen interpretation). SARs from these sediments have been included in the whole European SARs calculated in core 005 and CH7 (SARs presented in subsection 8.3.2.1). The impacts of late European sedimentation in the harbour are not clear.

8.3.2.3 Recent European

Age: 1975 A.D–Present

Pine plantations have been situated in the SEmb catchment since 1975 A.D (Hume & Dahm, 1991). Cyclic harvesting processes have exposed organic rich pine soils (usually on steep slopes) to energetic weather systems in the region (Hume & Dahm, 1991, Marden, Rowan, & Phillips, 2006). As a result, significant volumes of sediment have been transported into the harbour during runoff events (Hume & Dahm, 1991).

As pine plantation sediments enter the harbour, they appear to be primarily deposited at the intertidal Waiau Stream mouth and in the subtidal regions of the SEmb (Fig. 5.46). SARs calculated for this region are as high as ~10.37 mm/yr (all recent European SARs presented in Table 6.2). Pine plantation sediments have low density, which is probably due to their high organic matter content (Fig. 5.43). Organic matter and terrigenous clays to silts may be transported through the harbour under relatively low energy conditions. In the centre of the harbour, pine-plantation-related SARs are ~2.2-4.98 mm/yr (Fig. 6.5). At the harbour inlet, centre harbour pine-plantation-related SARs are at their highest at ~4.98 mm/yr (Fig. 6.5). The bathymetric depression of the inlet may be acting as a secondary depocentre for these sediments (further interpretation in subsection 6.5).

These SARs are much higher than European SARs in the NEmb, and suggest that the influences of kauri deforestation and mining processes generated lower sediment fluxes than recent pine plantation activity (Table 6.2). Pine plantation

SARs are the highest SARs observed throughout all sedimentation phases identified in this study (Table 6.2).

Pine plantation erosion has liberated As, Zn, Pb and Cr from catchment Kuaotunu Group rocks. Heavy metals appear to sorb to readily available organic detritus which are easily dispersed throughout the subtidal regions of the harbour (refer to subsection 7.5). At present, the only heavy metal in these sediments to occur with concentrations greater than ISGQ-Low value of 20 mg/kg is arsenic with maximum concentrations of 23 mg/kg. The pine plantation sediment with the highest heavy metal concentrations are located in the subtidal region of the SEmb (Fig. 7.1). Heavy metals Pb, Zn and Cr are not enriched more than 1.3 times pre-human concentrations in these sediments. Arsenic can exist at concentrations 2 times greater than pre-human baselines (Fig. 7.1). Arsenic may be at higher concentrations as it is soluble under the neutral conditions in the Coromandel stream networks, while other heavy metals are not (refer to subsection 7.5 for further discussion).

8.4 Summary

During the Lower Pleistocene to mid-Holocene (c.120-7.5 ka), the Coromandel Harbour was a subaerial environment. Soils initially developed over broad time periods through the Pleistocene, experiencing extensive chemical weathering. These soils were later buried by coarser, more organic-rich floodplain and stream deposits that may have accumulated between the advent of the eLGM at 29 ka to >c.7500 cal yr B.P.

At c.7500 cal yr B.P, sea level rose to near PMSL. In a restricted marginal marine setting, anaerobic bacteria in organic-rich soils began to convert Fe from the sediment (within eLGM to >c.7500 cal yr B.P and early estuarine sediments) and sulphate from tidal waters to pyrite, forming a pyritic layer throughout the harbour. Streams began to aggrade as their base levels changed with sea level rise, and buried the pyritic layer with early estuary silt and sands. Through time, aggradation processes decreased and stable estuarine sedimentation developed.

Pre-human estuarine sedimentation continued up until c.700 cal yr B.P, when Polynesians settled in the catchment.

European deforestation and mining in the NEmb are likely chiefly responsible for European sedimentation in the NEmb .Whole European SARs in the NEmb are ~0.52-0.77 mm/yr. Elevated concentrations of mining-related heavy metals appear to be confined to the Whangarahi Stream mouth where they are associated with clay minerals that have flocculated and been sequestered in these higher-energy regions. The extent of early and late European sedimentation is unclear in the SEmb. SARs associated with Recent European pine plantation are the highest SARs observed throughout all sedimentation phases. Pine plantation SARs are at up to ~3.94-10.37 mm/yr in the SEmb, which has been interpreted as the primary depocentre for these sediments. Pine plantation sediments are typically silts to clays, have high organic contents and low densities and appear to be transported throughout the harbour. The inlet appears to be a secondary depocentre for these sediments, where SARs of up to ~4.98 mm/yr are observed. Pine plantation sediments are enriched in heavy metals, which are likely sourced from erosion of Kuaotunu Group rocks in the SEmb catchment.

Chapter 9

Conclusion

This chapter summarises all of the findings of this study and proposes areas of future research.

9.1 Research summary

Prior to the mid-Holocene sea level rise, sediments in the Coromandel Harbour area developed as soils in a subaerial environment. Deeply weathered soils formed somewhere between the last Pleistocene interglacial at c.120 ka and the extended last glacial maximum (eLGM) at 29 ka. These soils were overtopped by interbedded flood deposits during the extended last glacial maximum (eLGM) through to the mid-Holocene sea level rise at c.7500 cal yr B.P. At c.7500 cal yr B.P, sea level rose to arounds its present level. Pyritic layers formed within eLGM to c.7500 cal yr B.P sediments and early estuarine sediments in a stratified, restricted marine setting. As sea level rose to its ~PMSL, the inlet became unrestricted and tidal flushing began to remove stratification in the harbour. Anoxic conditions required for pyrite formation were removed, and pyritisation ceased. Pyritic sediments were overtopped relatively quickly as streams aggraded as the harbour became their new base level. Stream aggradation appears to have induced elevated SARs in the subtidal regions in the early estuarine phase (c.7500-5000 cal yr B.P) of ~0.31-0.45 mm/yr. Through time (likely hundreds to thousands of years), streams aggraded to stable stream profiles. Sedimentation consequently decreased to generally conformable rates of 0.25-0.47 mm/yr in the intertidal regions and ~0.1-0.25 mm/yr in the subtidal regions during the pre-Polynesian phase (c.7500-700 cal yr B.P).

Polynesian SARs (700-130 cal yr B.P) are lower than pre-Polynesian SARs at ~0.05-0.13 mm/yr. These rates may be associated with potential SAR calculation error, and have been interpreted as possibly underestimated. European sediments in the NEmb appear to be predominantly from mining and deforestation practices. Whole European SARs (1820 A.D-present) in the NEmb are ~0.52-0.77 mm/yr.

Pine plantation and associated intensive erosion processes appear to be the primary influence on European SARs in the SEmb and subtidal harbour areas of the harbour. Recent European SARs (1975 A.D-present) are ~3.94-10.37 mm/yr in the SEmb. The SEmb appears to be the primary depocentre for these sediments. A secondary depocentre appears to be at the near inlet regions of the harbour, where SARs of ~4.98 mm/yr are observed. Pine plantation activities are likely to continue in the future and will inevitably continue to rapidly further infill these areas. Consideration of this sedimentation will be required in future harbour development projects.

Heavy metals Zn, Pb, Cu, Cr, Cd exist below ISQG-Low values throughout the harbour. Heavy metal contaminants have their highest concentrations at the Whangarahi Stream mouth in the NEmb, and are chiefly related to gold mining outwash. Mining heavy metals in the harbour are chiefly confined to intertidal areas near the Whangarahi Stream mouth. Here, arsenic often has concentrations greater than the ISQG-Low value of 20 mg/kg, with a maximum measured harbour-wide value of 33.5 mg/kg identified at the surface of core 007. Mercury throughout the harbour appears to be ~3-6 mg/kg throughout pre-human/anthropogenic sediments in the harbour, and are elevated compared with the ISQG-High value of 1 mg/kg. Measurements of mercury may be overestimated due to pXRF limitations. Pine plantation sediments in the SEmb are enriched in arsenic by ~1.5-2 times pre-human baseline concentrations with maximum As concentrations of 22.3 mg/kg. Arsenic may be readily adsorbing to readily available organic matter as it is leached from the amplified erosion of Kuaotunu Group rocks under neutral pH in the catchment.

9.2 Potential for Future Research

Ecologically threatening concentrations of mining related heavy metals are generally confined to the Whangarahi Stream mouth. These metals may be stored within the Whangarahi Stream networks, where they may be transported to the harbour during storm (high energy) events. An interesting topic to investigate is the heavy metal transport mechanisms active in the stream networks of the NEmb.

Studying stream concentrations of mining wastes and transport processes through these streams would be useful in understanding how heavy metals contamination of the harbour might change in the future. Such studies may also identify potential for remediation of these mine wastes, restricting their movement into the harbour.

It may be useful to conduct further research on the pyritic layer in the harbour. Dredging may intercept this layer and induce oxidation of the pyrite. Sulphuric acid is a resultant by-product of pyrite oxidation, which will be fluxed into the harbour where it will undoubtedly generate adverse effects on the estuarine environment. The extent of these effects are unknown and warrant further investigation.

References

Abrahim, G. M. S., & Parker, R. J. (2008). Assessment of heavy metal enrichment factors and the degree of contamination in marine sediments from Tamaki Estuary, Auckland, New Zealand. *Environmental monitoring and assessment*, *136*(1-3), 227-238.

Adams, C. J., Graham, I. J., Seward, D., Skinner, D. N. B., Adams, C. J., Skinner, D. N. B., & Moore, P. R. (1994). Geochronological and geochemical evolution of late Cenozoic volcanism in the Coromandel Peninsula, New Zealand. *New Zealand Journal of Geology and Geophysics*, *37*(3), 359–379. https://doi.org/10.1080/00288306.1994.9514626

Aurecon (2013) *Coromandel Wharf Upgrade; Preliminary Sediment Quality Assessment*. Retrieved from 1/09/14 from http://www.tcdc.govt.nz/Global/AureconreportandPDPreport.pdf

Australian and New Zealand Environment and Conservation Council [ANZECC] (2000). *Australian and New Zealand guidelines for fresh and marine water quality.* Australian and New Zealand Environment and Conservation Council and Agriculture and Resource Management Council of Australia and New Zealand, Canberra, 1-103.

Bailey, S. E., Olin, T. J., Bricka, R. M., & Adrian, D. D. (1999). A review of potentially low-cost sorbents for heavy metals. *Water Research*, *33*(11), 2469–2479. https://doi.org/10.1016/S0043-1354(98)00475-8

Booden, M. A., Smith, I. E. M., & Mauk, J. L. (2009). Petrogenesis of basalts, andesites and dacites in the Coromandel Volcanic Zone – Implications for the genesis of epithermal Au mineralisation. *Proceedings of the AusIMM New Zealand Branch Annual Conference, Queenstown, 2009*, 21–30.

Booden, M. A., Smith, I. E. M., Mauk, J. L., & Black, P. M. (2012). Geochemical and isotopic development of the Coromandel Volcanic Zone, northern New Zealand, since 18Ma. *Journal of Volcanology and Geothermal Research*, *219–220*, 15–32. https://doi.org/10.1016/j.jvolgeores.2012.01.005

Bradshaw, B. E. (1991). *Nearshore and inner shelf sedimentation on the East Coromandel coast*, New Zealand. Unpublished PhD thesis, University of Waikato, Waikato, New Zealand.

Cadena, F., Rizvi, R., & Peters, R. W. (1990). Feasibility studies for the removal of heavy metals from solution using tailored bentonite. In *Hazardous and Industrial Wastes- Proceedings of the Mid-Atlantic Industrial Waste Conference* (pp. 77-94).

Chappell, P. R. (n.d). *The Climate and Weather of the Waikato Region* (2nd ed.). Niwa Science and Technology Series Number 61. Retrieved from https://www.niwa.co.nz/static/Waikato%20ClimateWEB.pdf

Christie, A. B., & Brathwaite, R. L. (2005). *Regional targeting of epithermal Au-Ag deposits in a Miocene-Pliocene volcanic terrane*: Hauraki goldfield, New Zealand. In Mineral Deposit Research: Meeting the Global Challenge (pp. 1457-1460). Springer Berlin Heidelberg.

Christie, A. B., Simpson, M. P., Brathwaite, R. L., Mauk, J. F., & Simmons, S. F. (2007). Epithermal Au-Ag and related deposits of the Hauraki Goldfield, Coromandel Volcanic Zone, New Zealand. *Economic Geology*, *102*, 785–816. https://doi.org/10.2113/gsecongeo.102.5.785

Clement, A. J. H., Sloss, C. R., & Fuller, I. C. (2010). Late Quaternary geomorphology of the Manawatu coastal plain, North Island, New Zealand. *Quaternary International*, *221*, 36–45. https://doi.org/10.1016/j.quaint.2009.07.005

Clement, A. J. H. (2011). *Holocene sea-level change in the New Zealand archipelago and the geomorphic evolution of a Holocene coastal plain incised-valley system: the lower Manawatu valley, North Island, New Zealand*. Unpublished Ph.D thesis, Massey University, Palmerston North, New Zealand.

Coffee, B. T (1992). *A Revised Assessment of Biological and Selected Chemical Effects relating to proposed channel improvements: Furey's Creek, Coromandel Harbour*. A report written for the Thames Coromandel District Council.

Collins, K. (2015). *Development plans for Coromandel Harbour stirring up resistance.* Forest and Bird. Retrieved from http://blog.forestandbird.org.nz/development-plans-for-coromandel-harbour-stirring-up-resistance/

Cornell, R. M., & Schwertmann, U. (2003). *The iron oxides: structure, properties, reactions, occurrences and uses* (2nd ed.). John Wiley & Sons.

Craw, D., & Chappell, D. A. (2000). Metal redistribution in historic mine wastes, Coromandel Peninsula, New Zealand. *New Zealand Journal of Geology and Geophysics*, *43*(2), 187-198. https://doi.org/10.1080/00288306.2000.9514880

Cundy, A. B., Croudace, I. W., Cearreta, A., & Irabien, J. (2003). Reconstructing historical trends in metal input in heavily-disturbed, contaminated estuaries: studies from Bilbao, Southampton Water and Sicily. *Applied Geochemistry*, *18*(2), 311-325.

Dent, D. L., & Pons, L. J. (1995). A world perspective on acid sulphate soils. *Geoderma*, *67*, 263–276. https://doi.org/10.1016/0016-7061(95)00013-E

Department of Conservation [DOC], (n.d). *Coromandel Town and the Whangarahi Catchment*. Retrieved from http://www.waikatoregion.govt.nz/PageFiles/1167/sec2e.pdf

Department of Environment Regulation [DER] (2015). *Identification and investigation of acid sulphate soils and acidic landscapes*. Retrieved from https://www.der.wa.gov.au/images/documents/your-environment/acid-sulfate-soils/guidelines/Identification_and_investigation_of_acid_ss_and_acidic_landscapes.pdf

Dougherty, A. J., & Dickson, M. E. (2012). Sea level and storm control on the evolution of a chenier plain, Firth of Thames, New Zealand. *Marine Geology*, *307–310*, 58–72. https://doi.org/10.1016/j.margeo.2012.03.003

Edbrooke, S.W. (compiler) 2001: *Geology of the Coromandel Harbour area: scale 1:50,000*. Lower Hutt: Institute of Geological & Nuclear Sciences Limited. Institute of Geological & Nuclear Sciences 1:50,000 geological map 4. 44 p. + 1 folded map

Forwick, M. (2011). *X-ray fluorescence*. University of Tromsø. Retrieved from http://naturweb.uit.no/ig/xrf/AboutXRF.html

Gavin, D. G. (2001). Estimation of inbuilt age in radiocarbon ages of soil charcoal for fire history studies. *Radiocarbon*, *43*(1), 27-44.

Gibb, J. G. (1986). *A New Zealand regional Holocene eustatic sea-level curve and its application to determination of vertical tectonic movements*. Royal Society of New Zealand Bulletin, 24, 377-395.

Harding, J. S. (2005). Impacts of metals and mining on stream communities. *Moore, TA, Black, A., Centeno, JA, Harding, JS and Trumm, DA (Eds.)*, 343-357.

Hedge, L. H., Knott, N. A., & Johnston, E. L. (2009). Dredging related metal bioaccumulation in oysters. *Marine Pollution Bulletin*, *58*(6), 832-840.

Hochstein, M. P., Tearney, K., Rawson, S., Davey, F. J., Davidge, S., Henrys, S., & Backshall, D. (1986). *Structure of the Hauraki Rift (New Zealand).* Royal Society of New Zealand Bulletin, 24, 333-348.

Hume, T. M & Dahm, J. (1991). *An Investigation into the Effects of Polynesian and European Land Use on Sedimentation in Coromandel Estuaries*. DSIR Marine and Freshwater Consultancy Report No. 6104.

Hume, T. M., & Gibb, J. G. (1987). The " Wooden-Floor " marker bed — A new method of determining historical sedimentation rates in some New Zealand estuaries. *Journal Of The Royal Society Of New Zealand*, *17*(1), 1–7. https://doi.org/10.1080/03036758.1987.10421703

Hume, T. M., & Herdendorf, C. E. (1988). A geomorphic classification of estuaries and its application to coastal resource management-A New Zealand example. *Ocean and Shoreline Management*, *11*(3), 249–274. https://doi.org/10.1016/0951-8312(88)90022-7

Hume, T. M., Fox, M. E., & Wilcock, R. J. (1989). Use of organochlorine contaminants to measure sedimentation rates in estuaries: a case study from the Manukau Harbour. *Journal of the Royal Society of New Zealand*, 19(3), 305-317.

Jones, H. F. E. (2008). *Coastal sedimentation: what we know and the information gaps.* Environment Waikato. Report: TR 2008/12

Karageorgis, A. P., Katsanevakis, S., & Kaberi, H. (2009). Use of Enrichment Factors for the Assessment of Heavy Metal Contamination in the Sediments of Koumoundourou Lake, Greece. *Water, Air, and Soil Pollution*, *204*(1–4), 243–258. https://doi.org/10.1007/s11270-009-0041-9

Kletetschka, G., Hruba, J., & Nabelek, L. (2015, December). *Magnetic Susceptibility of Wet vs. Dry Sediment and Mass Normalized vs. Volume Normalized Magnetic Susceptibility*. In AGU Fall Meeting Abstracts.

Land Information New Zealand [LINZ]. (2016). *Chart NZ 533 Firth of Thames*. Retrieved from https://data.linz.govt.nz/layer/1278-chart-nz-533-firth-of-thames/

Land, Air, Water (2016). *Waiau River*. Retrieved from https://www.lawa.org.nz/explore-data/waikato-region/river-quality/waiau-river/

Le Vaillant, M., Barnes, S. J., Fisher, L., Fiorentini, M. L., & Caruso, S. (2014). Use and calibration of portable X-Ray fluorescence analysers : application to lithogeochemical exploration for komatiite-hosted nickel sulphide deposits. *Geochemistry: Exploration, Environment, Analysis*, *14*(3), 199–209. https://doi.org/10.1144/geochem2012-166

Lin, Z., & Puls, R. W. (2000). Adsorption, desorption and oxidation of arsenic affected by clay minerals and aging process. *Environmental Geology*, *39*(7), 753–759. https://doi.org/10.1007/s002540050490

MacDonald, J. H. J., Harper, G. D., & Zhu, B. (2006). Petrology, geochemistry, and provenance of the Galice Formation, Klamath Mountains, Oregon and California. *Geological Society of America Special Papers*, *410*, 77–101. https://doi.org/10.1130/2006.2410(04).

Marden, M., Rowan, D., & Phillips, C. (2006). Sediment sources and delivery following plantation harvesting in a weathered volcanic terrain, Coromandel Peninsula, North Island, New Zealand. *Soil Research*, 44(3), 219-232.

Margui, E., & Grieken, R. (2013). *X-ray fluorescence spectrometry and related techniques: an introduction.* Momentum Press.

Maslennikova, S., Larina, N., & Larin, S. (2012). The effect of sediment grain size on heavy metal content. *Lakes reservoirs and ponds*, *6*(1), 43-54.

McSaveney, M. J., & Beetham, R. D. (2006). *The Potential for Debris Flows from Karaka Stream at Thames, Coromandel*. Environment Waikato Regional Council.

Mead, S. T., Moores, A., & Waikato (N.Z.). Regional Council. (2004). *Estuary sedimentation: A review of estuarine sedimentation in the Waikato region*. (No. 2005/13; 2005/13.). Hamilton [N.Z.]: Environment Waikato.

Ministry for the Environment. (2012). *LUCAS New Zealand Land Use Map 1990 2008 2012 (v016).* Map retrieved from https://data.mfe.govt.nz/layer/2375-lucas-nz-land-use-map-1990-2008-2012-v016/

Moore, P. R., & Ritchie, N. A. (1996). *Coromandel Gold*: A Guide to the Historic Goldfields of Coromandel Peninsula. Dunmore Press.

Morgan, R.P.C. 1995. *Soil Erosion and Conservation*. (2nd ed.). Longman Group Limited, Essex, England.

Newnham, R. M., Lowe, D. J., Giles, T., & Alloway, B. V. (2007). Vegetation and climate of Auckland, New Zealand, since ca. 32 000 cal. yr ago: support for an extended LGM. *Journal of Quaternary Science*, *22*(8), 801–815. https://doi.org/10.1002/jqs

Nicol, A. (2011). Landscape history of the Marlborough Sounds, New Zealand. *New Zealand Journal of Geology and Geophysics*, *54*(2), 195-208.

O'reilly, W. (2012). *Rock and mineral magnetism*. Springer Science & Business Media.

Otago Daily Times 10-6-1920. *Mining*. Alexander Turnbull Library, Wellington, New Zealand. Retrieved from http://natlib.govt.nz/records/32948178

PDP. (2012). *Sediment Quality Assessment at Coromandel Wharf.* March 2012. Ref A02435106

Pillans, B. (1986). A late Quaternary uplift map for North Island, New Zealand. *Royal Society of New Zealand Bulletin*, 24, 409-417.

Pillans, B., Chappell, J., & Naish, T. R. (1998). A review of the Milankovitch climatic beat: Template for Plio-Pleistocene sea-level changes and sequence stratigraphy. *Sedimentary Geology*, *122*(1–4), 5–21. https://doi.org/10.1016/S0037-0738(98)00095-5

Powell, B., & Martens, M. (2005). A review of acid sulfate soil impacts, actions and policies that impact on water quality in Great Barrier Reef catchments, including a case study on remediation at East Trinity. *Marine Pollution Bulletin*, *51*(1–4), 149–164. https://doi.org/10.1016/j.marpolbul.2004.10.047

Queensland Government. (2013). *Acid sulfate soils explained*. Retrieved from https://www.qld.gov.au/environment/land/soil/acid-sulfate/explained/

Reading, H. G. (Ed.). (2009). *Sedimentary environments: processes, facies and stratigraphy*. John Wiley & Sons.

Reeve, G. (2008). *Sedimentation and hydrodynamics of Whitianga Estuary*. Unpublished M.S.c thesis, University of Waikato, Waikato, New Zealand.

Rothwell, R. G, Croudance I. W. (2015). *Twenty years of XRF core scanning marine sediments: What do geochemical proxies tell us?.* In Micro-XRF Studies of Sediment Cores (pp. 25-102). Springer Netherlands.

Sammut, J, Lines-Kelly, R. (2004). *An introduction to acid sulphate soils*. New South Wales. Retrieved from http://www.dpi.nsw.gov.au/content/agriculture/resources/soils/ass/general/introduction

Schumm, S. A. (1993). River Response to Baselevel Change: Implications for Sequence Stratigraphy. *The Journal of Geology*, *101*(2), 279–294. https://doi.org/10.1086/648221

Sheffieldt, A. T., Healy, T. R., & McGlone, M. S. (1995). Infilling rates of a steepland catchment estuary, Whangamata, New Zealand. *Journal of Coastal Research*, 1294-1308.

Singh, A. K., Hasnain, S. I., & Banerjee, D. K. (1999). Grain size and geochemical partitioning of heavy metals in sediments of the Damodar River - a tributary of the lower Ganga, India. *Environmental Geology*, *39*(1), 90–98. https://doi.org/10.1007/s002540050439

Skinner, D. N. B (1967). *Geology of the Coromandel region with emphasis on some economic aspects*. Unpublished Ph.D thesis, Auckland University, Auckland, New Zealand.

Skinner, D. N. B. (1986). Neogene volcanism of the Hauraki volcanic region. *Royal Society of New Zealand Bulletin*, 23, 21-47.

Sluijs, A., Schouten, S., Donders, T. H., Schoon, P. L., Röhl, U., Reichart, G., … Damsté, J. S. S. (2009). Warm and wet conditions in the Arctic region during Eocene Thermal Maximum 2. *Nature Geoscience, 2* (November), 777–780. https://doi.org/10.1038/NGEO668

Smallman, E. (2013). Council slated for plan to take tailings from Coromandel Harbour. *The Waikato Times*. Retrieved from http://www.stuff.co.nz/waikato-times/8574839

Spofforth, D. J. A., Pälike, H., & Green, D. (2008). Paleogene record of elemental concentrations in sediments from the Arctic Ocean obtained by XRF analyses. *Paleoceanography*, *23*(1), 1–13. https://doi.org/10.1029/2007PA001489

Swales, A., Ovendeen, R., Budd, R., Hawken, J., McGlone, M. S., & Hermanspahn, N. (2005). *Whaingaroa (Raglan) Harbour: Sedimentation and the effects of historical catchment landcover changes*. Environment Waikato (New Zealand) Technical Report, 36.

Thames-Coromandel District Council [TCDC]. (2010). *Coromandel Peninsula Peak Population Study, 2009/2010*. Retrieved from http://www.tcdc.govt.nz/Visiting-or-moving-to-the-Coromandel/Our-Peninsula/Peak-Population-Study/

Thames-Coromandel District Council [TCDC]. (2016). *Council Projects: Coromandel Harbour Facilities Project.* Retrieved from http://www.tcdc.govt.nz/Your-Council/Council-Projects/Current-Projects/Coromandel-Harbour-Facilities-Project-/

Van Breemen, N., & Buurman, P. (2002). *Soil formation*. Springer Science & Business Media.

Waikato Regional Council (WRC) (n.d). *Pollutants in sediments: technical information.* Retrieved from http://www.waikatoregion.govt.nz/Environment/Environmental-information/Environmental-indicators/Coasts/Coastal-water-quality/pollutants-in-sediments-techinfo/

Waugh, D. (2000). *Geography: An integrated approach*. Nelson Thornes.

Wentworth, C. K. (1922). A scale of grade and class terms for clastic sediments. *The Journal of Geology*, *30*(5), 377-392.

Wilmshurst, J. M., & Higham, T. F. G. (2004). Using rat-gnawed seeds to independently date the arrival of Pacific rats and humans in New Zealand. *The Holocene*, *14*(6), 801–806. https://doi.org/10.1191/0959683604hl760ft

Yanko, V., Ahmad, M., & Kaminski, M. (1998). Morphological deformities of benthic foraminiferal tests in response to pollution by heavy metals: implications for pollution monitoring. *Journal of Foraminiferal Research*, *28*, 177-200.

Appendix

Appendix material is presented in an attached CD-ROM.